Roles of the Coronavirus 3'-to-5' Exoribonuclease and N7-Methyltransferase in Counteracting Innate Immunity

By

James Brett Case

Dissertation

Submitted to the Faculty of the

Graduate School of Vanderbilt University

in partial fulfillment of the requirements

for the degree of

DOCTOR OF PHILOSOPHY

in

Microbiology and Immunology

May 11, 2018

Nashville, Tennessee

Approved:

Eric P. Skaar, Ph.D.

Manuel Ascano Jr., Ph.D.

James W. Thomas, M.D.

Kristen M. Ogden, Ph.D.

Mark R. Denison, M.D.

To my mom and dad, for their endless sacrifices to make my life better and

to my wife, Kayla, infinitely loving and supportive

ACKNOWLEDGEMENTS

I believe one the biggest misconceptions regarding biomedical graduate school is that it exclusively consists of prescribed coursework and the teaching of prior knowledge that is to be mastered to an acceptable level in a predetermined amount of time. While I understand this disconnect may be attributable to preconceived notions of traditional undergraduate courses and other professional programs, I have learned that obtaining a Ph.D. is anything but predetermined and straightforward. Graduate school is a demanding experience, even for the most well prepared and hardest working. The awarding of the degree of Doctor of Philosophy, almost by definition, means that you have become an expert in the existing knowledge of your particular area of study and subsequently contributed novel findings that surpass all prior human understanding. The skills that you develop and the amount of time in which it takes you to accomplish these goals are purely up to how fast you can make the natural world reveal its secrets. Undoubtedly, graduate school challenges you to go beyond what you believed you could achieve mentally and at times, physically. While I am proud of my accomplishments and the skills I have developed over the past five years, it would be remiss of me if I told you I did it all on my own. The following are just a few of a very long list that have helped me along the way:

Affiliated Departments and Funding Sources

Thank you to the Department of Pathology, Microbiology, and Immunology, the Vanderbilt University Medical Center Department of Pediatrics, Division of Pediatric Infectious Diseases, and the Elizabeth B. Lamb Center for Pediatric Research for administrative, educational, and financial support during my graduate career. Additionally, thank you to Dr. Paul Bock and the Mechanisms of Vascular Disease training grant T32HL07751 (J.B.C.) funded by the National

Institutes of Health, National Heart, Lung, and Blood Institute and to R01 AI108197 (M.R.D.) funded by the National Institutes of Health, National Institute of Allergy and Infectious Diseases for educational and financial support.

Denison Lab

Even though my graduate training only lasted four and a half years in the lab, I have overlapped and had the pleasure of working with a large number of people. Thank you to all present and past members of the Denison lab. Each one of you has helped me in one way or another. From guidance regarding the qualifying exam to the passing along of lab knowledge that cannot be found in a methods section, I am grateful to have worked in a lab that helped one another without hesitation. Dr. Chris Stobart, Dr. Megan Culler-Freeman, and Dr. Dia Beachboard, thank you for answering all of my many questions during my first couple of years in the lab. Lindsay, thank you for your friendship and camaraderie during our second year course-work. Dr. Michelle Becker, thank you for coordinating and managing our lab and for training me in the BSL-3. Dr. Clint Smith, thank you for setting an excellent example of what a great scientist should be. Without your input and developments in the lab, my work would have suffered. Erica Andres, thank you for being a genuinely nice person and spreading your optimism throughout your time in the lab. Selene, Litton, and Laura thank you for all of our laughs while you were here. Dr. Nicole Sexton, thank you for your friendship and for listening to many of my questions and complaints, both professional and personal, over the years. I am grateful that you were a year ahead of me and never hesitated to help me navigate graduate school. Kevin and Maria, my rotation students, thank you for your friendship, helpful conversations, and making the lab a fun place to work. Dr. Jim Chappell, thank you for being such a kind and helpful person. You make

our lab better each day. Xiaotao Lu, thank you for sharing all of your expertise in the lab and for our casual garden conversations. Without your help, I undoubtedly would be still trying to clone something or recover a difficult virus. You selflessly help everyone in the lab on a moments notice, and as many of the graduate students from our lab have stated over the years, I could not have done it without you. To my mentor, Dr. Mark Denison, thank you for all of your guidance over the years. You have a unique enthusiasm and positive outlook on science, and life in general, that sometimes I needed. Thank you for giving me the resources, the freedom, and your trust to pursue hypotheses outside of the lab's traditional expertise.

Kendall and Thomas Labs

To the Kendall and Thomas Labs, thank you for allowing me to be a part of your labs. Peggy, thank you for the opportunity to work in your lab and for having the patience to more or less allow me to operate as a graduate student. Under your guidance, I amassed a wealth of scientific knowledge and realized how amazing the immune system really is. Working in your lab not only solidified my decision to go to graduate school but also gave me the experiences and knowledge I needed to be successful. Tom, thank you for being a great second mentor. You are incredibly kind, knowledgeable, and always provide helpful advice. Allison Sullivan, NP, Dr. Jon Williams, Dr. Rachel Henry-Bonami, Amita Rachakonda, Chrys Hulbert, and Dr. Zak Kistka, thank you for your friendship and helpful interactions with regard to science and life in general.

Binder Lab

Dr. Brad Binder, thank you for taking a chance on me. Within ten minutes of contacting you, we met to discuss potential undergraduate research projects. Your lab environment and enthusiasm

for research sparked a love for science and learning in me that have led me to where I am today. Brad and Beth Shieh, thank you for your patience and for taking time to explain the science behind things. Sadly, I have realized this type of instruction is often a rarity in the science world.

Thesis Committee

Dr. Eric Skaar, Dr. Manny Ascano, Dr. Tom Thomas, Dr. Kristen Ogden and previously, Dr. Terry Dermody and Dr. John Williams, thank you for your time and commitment to my graduate training. I appreciate all of your questions, support, and helpful suggestions throughout my graduate career. I have tremendous respect for each of you and I know that I am a better scientist having trained under your guidance.

Dermody Lab

To the Dermody Lab, while you may be far away now, I benefitted greatly from each and every interaction with you while you were at Vanderbilt. Specifically, thank you to Dr. Andrea Pruijssers and Dr. Laurie Silva. On many occasions, our lunch conversations provided necessary comic relief from otherwise stressful days. Dr. Alison Ashbrook, thank you for sharing your wealth of knowledge. From methods, reagents, or simply casual conversation, you greatly enriched both my science and work environment. Dr. Terry Dermody, thank you for your genuine interest and guidance in my both my scientific research and career. Without exception, you provided a smile every time we encountered one another and thoughtful questions about my research at every opportunity. You are an exceptional example for all scientists in every regard and I am better for having worked with you.

Weiss Lab

Dr. Susan Weiss, when I first joined the Denison lab, I found myself constantly reading publications from your lab. I was and still am very interested in how coronaviruses, and viruses in general, antagonize the innate immune response. The work from you and your lab provided an excellent foundation from which some of the questions I asked and the methods I used were developed. I am grateful to be able to call you a collaborator. Thank you for being so kind, supportive, and genuinely interested in my work. Thank you and Henry Li for allowing me to visit your lab to learn and to perform necessary experiments.

Family

To all of my family members, both given and chosen, thank you for your constant support and curious questions about my research. Although "When will you be finished?" and "What will you do then?" are by far the two hardest and most stressful questions I have been asked as graduate student, I never had the heart to ask you to stop because it let me know that you were interested in my career. To my little brother, Ryan, I am proud of you. I know pharmacy school has its own challenges and I admire how hard you study and strive for perfection. I enjoy our conversations in the areas where our subject matters overlap. To my mom and dad, thank you for your endless love and support. To my mom, thank you for ensuring school and homework came first. Thank you for being a second teacher out of the classroom, checking my homework, and providing extra help if needed. I honestly believe my education and life would be drastically different if it were not for your input in this regard. Thank you for your constant words of encouragement. To my dad, thank you for teaching me how to work hard and for always believing in me. Over the years, you have blindly said many times, "well, if anyone can do it or

figure it out, I know you will". While this may or may not be true, your support inspires me to be determined to accomplish any goal I set. To my wife, Kayla, you are an amazing person. Thank you for always being there for me on good science days and bad science days alike. Even if a complaint was entirely in science jargon that you did not understand, you always offered a solution or words of encouragement. Thank you for your constant love and for supporting my career.

TABLE OF CONTENTS

LIST OF TABLES

Table Page

LIST OF FIGURES

CHAPTER I

BACKGROUND AND LITERATURE REVIEW

Introduction

Coronaviruses are positive-sense, single-stranded RNA viruses that are important pathogens of both humans and animals. Coronaviruses belong to the *Coronaviridae* family of viruses and were first classified as a distinct virus family as a result of human respiratory pathogen research during the 1960s (Masters, 2006). In negative-stained electron micrographs, early investigators noted the enveloped virion was surrounded by a "fringe of crown-like projections" (Figure 1) (Masters, 2006). Ultimately, their fundamental observations reminded them of the solar corona and led them to propose the name coronaviruses (Almeida et al., 1968). Since their initial discovery, coronaviruses have been shown to infect a wide range of mammalian and avian species and are notoriously capable of transmission to new hosts (de Wit et al., 2016; Perlman and Netland, 2009). Primarily, coronaviruses cause respiratory or enteric disease in their hosts and are spread by respiratory droplet and fecal-oral routes (Masters, 2006). In humans, approximately 15% of all cases of the common cold each year are caused by coronaviruses (Wei et al., 1975; Züst et al., 2011). In addition, coronaviruses are capable of causing severe and lethal human disease as demonstrated by severe acute respiratory syndrome coronavirus (SARS-CoV) and Middle East respiratory syndrome coronavirus (MERS-CoV), which have emerged into the human population in this century. Currently, no specific antiviral therapies or vaccines exist for human coronaviruses, highlighting the need for an increased understanding of coronavirus biology. In

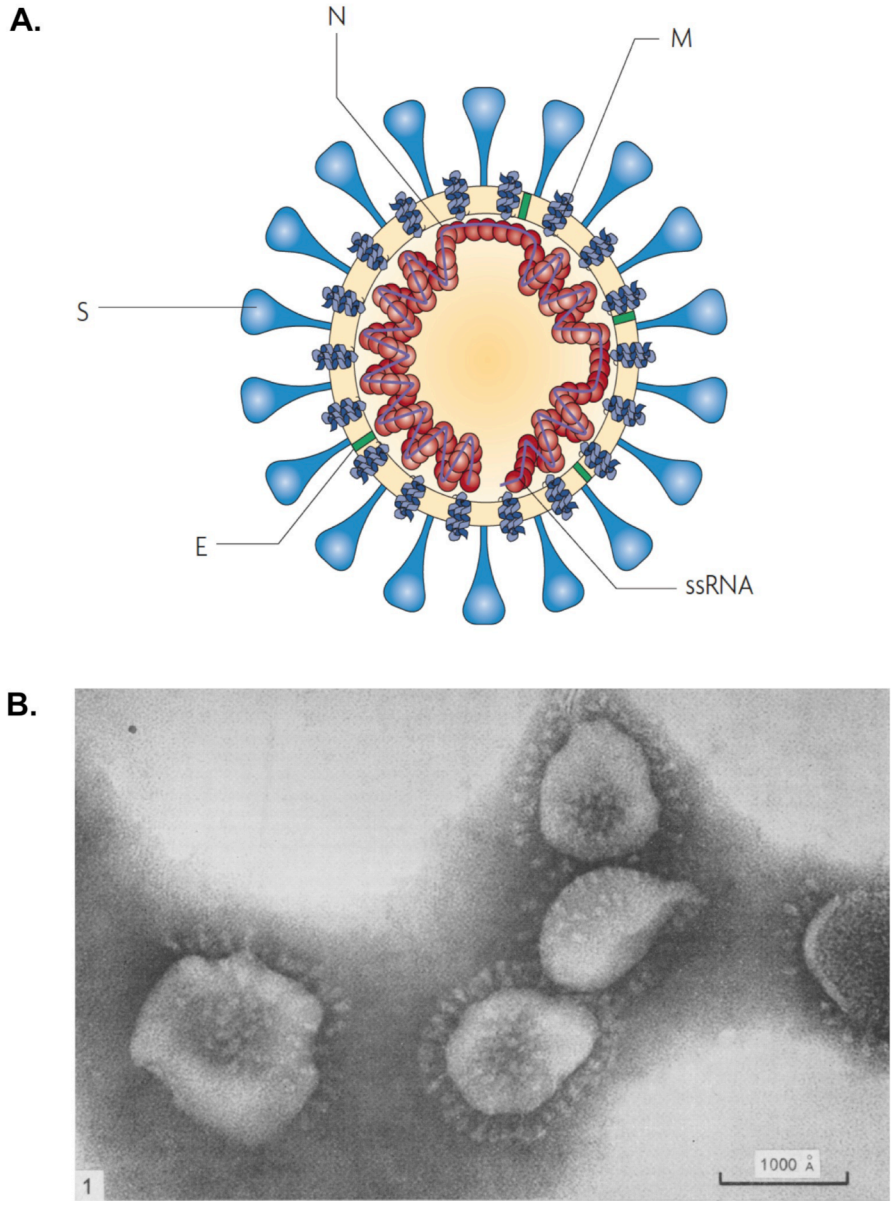

Figure 1. Coronavirus virion structure and EM

(A) Schematic representation of a coronavirus virion. Spike (S), nucleocapsid (N), membrane (M), and envelope (E) structural proteins are indicated. (B) Negatively stained electron micrograph of avian infectious bronchitis virus particles with notable spike protein projections visible. This figure is derived from Perlman and Netland, 2009 and Berry and Almeida, 1968 with permission.

this dissertation research, I advance our knowledge of coronavirus replication requirements and how coronaviruses overcome host defenses.

Coronavirus disease and emergence

Coronaviruses are widely distributed throughout mammals and birds. Coronavirus infections have been observed in humans, mice, dogs, cats, pigs, hedgehogs, cattle, turkeys, chickens, bats, whales, and numerous other animals (Leibowitz et al., 2011). Notably, coronaviruses cause several veterinary diseases of economic importance (Acheson, 2011). In pigs, transmissible gastroenteritis virus (TGEV) and porcine epidemic diarrhea virus (PEDV), as their names imply, cause severe diarrhea and dehydration resulting in significant morbidity and mortality. It is estimated that PEDV alone causes $900 million to $1.8 billion in economic losses in the United States each year (Annamalai et al., 2015). One of the first identified and most studied coronaviruses, infectious bronchitis virus, causes respiratory disease in meat-type and egg-laying chickens and is one of the foremost causes of economic loss within these industries (Cavanagh, 2007). Bovine coronavirus causes respiratory and enteric infections in newborn calves and other wild ruminants. Further, bovine coronavirus infection can result in clinical syndromes known as winter dysentery with hemorrhagic diarrhea and shipping fever in adult cattle (Saif, 2010). In all of these examples, mortality rates can approach 100% in newborn animals (Acheson, 2011).

Currently, four coronaviruses are endemic in the human population: human coronaviruses 229E, OC43, HKU1, and NL63. All human coronaviruses are proposed to have emerged into the human population through zoonotic events. Human coronaviruses 229E and OC43 were discovered during the previously mentioned search for the common cold of the 1960s (Garbino

et al., 2006; Masters, 2006; Perlman and Netland, 2009). Using molecular clock analysis, researchers propose that human coronavirus 229E emerged into the human population between approximately 1686-1880 A.D. and is most closely related to coronaviruses isolated from alpacas, which may represent intermediate hosts from bats (Crossley et al., 2012; Pfefferle et al., 2009). Using similar methods, researchers propose human coronavirus OC43 emerged into the human population somewhere between 1866-1918 A.D. from cattle (Vijgen et al., 2005). Primarily, human coronaviruses 229E and OC43 cause mild upper respiratory tract infections and occasionally more severe disease in elderly, infant, and immunocompromised populations (Perlman and Netland, 2009).

In November 2002, the first reported case of severe acute respiratory syndrome (SARS) occurred in China (de Wit et al., 2016). By February 2003, more than 300 new cases had been reported in China, many of which were health care providers. Thereafter, the contagion spread to Hong Kong, Vietnam, Canada and several other countries through air travel of infected individuals. In March 2003, the World Health Organization established a network to identify the causative agent of SARS (de Wit et al., 2016). By April 2003, a novel coronavirus was identified as the etiological agent of SARS (Drosten et al., 2003; Ksiazek et al., 2003). Interestingly, the characteristic virion morphology observed by researchers in the 1960s, among several other identifiers, helped demonstrate that the new human respiratory pathogen was a coronavirus (Masters, 2006). By July 2003, SARS-CoV had spread to 27 countries, resulting in more than 8,000 reported cases and 774 deaths. Subsequent studies demonstrated that SARS-CoV spread primarily via respiratory droplets, direct contact, and airborne routes; although, virus was isolated from some fecal and urinary samples, which may represent additional routes of

transmission (Chan et al., 2004; Gu and Korteweg, 2007; Peiris et al., 2003). Contrary to human coronavirus 229E and human coronavirus OC43, SARS-CoV caused severe lower respiratory tract infections (Figure 2) (Gu and Korteweg, 2007; Perlman and Netland, 2009). In addition, SARS-CoV demonstrated a capacity to cause systemic disease, with evidence of viral pathology present in the gastrointestinal tract, liver, kidney, and brain of some cases (Perlman and Netland, 2009). SARS-CoV patients presented with influenza-like symptoms such as fever, chills, and cough (Gu and Korteweg, 2007). Additional common symptoms included malaise, headache, and shortness of breath, and less common symptoms included diarrhea and nausea (de Wit et al., 2016; Gu and Korteweg, 2007). Due to the fact that virus shedding did not occur until after the onset of symptoms, the SARS-CoV epidemic was ultimately controlled by quarantine of suspected cases and is likely why viral spread was predominately nosocomial in nature (de Wit et al., 2016). Fortunately, SARS-CoV is no longer circulating in the human population, and numerous studies have sought to determine from where SARS-CoV emerged. An initial study demonstrated SARS-CoV could be isolated from palm civets and raccoon dogs. Moreover, antibodies against SARS-CoV were detected in Chinese ferret badgers. Interestingly, all of these animals are sold in live-animal markets in China, and several animal handlers were also seropositive for SARS-CoV, suggesting that these markets may have facilitated the cross-species transmission events that led to the SARS-CoV epidemic (de Wit et al., 2016; Guan et al., 2003; Perlman and Netland, 2009). Yet, there was no indication that SARS-CoV was circulating in these animals in the wild and thus, were likely incidental hosts rather than the primary animal reservoirs (de Wit et al., 2016; Wang et al., 2006). Additional studies identified viruses that were closely related to SARS-CoV in fecal samples of Chinese horseshoe bats (Lau et al., 2005; Li, 2005). However, these viruses did not use the bat homolog of angiotensin converting enzyme 2

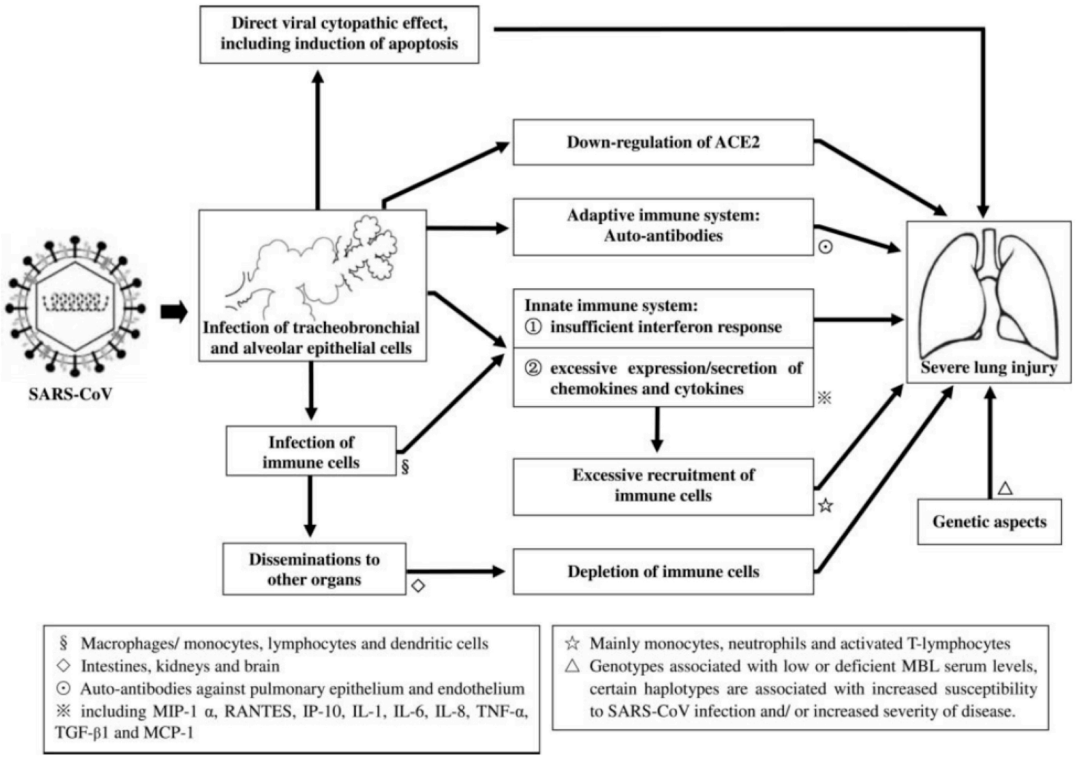

Figure 2. SARS-Coronavirus Pathogenesis

The major mechanisms of SARS-CoV pathogenesis are indicated. SARS-CoV infection of tracheobronchial and alveolar epithelial cells in the lung results in a cascade of changes that result in the clinical symptoms and pathological findings observed. Ultimately, direct viral cytopathic effect, infection of immune cells, and an insufficient innate immune response result in severe lung injury, dissemination, and disease. This figure is from Gu and Korteweg, 2007 and used with permission.

(ACE2), which is the SARS-CoV viral receptor in humans, to infect cells (Becker et al., 2008; Ren et al., 2008). In 2013, two novel bat coronaviruses were discovered that are capable of infecting humans, civets, and Chinese horseshoe bats using the respective ACE2 receptor from each animal to gain cell entry (Ge et al., 2013). These data are the strongest to date that Chinese horseshoe bats are the natural reservoir for SARS-CoV and that intermediate animal hosts may not be required for direct human transmission. Further, these data indicate that SARS-CoV-like viruses are still circulating in bats and could re-emerge into the human population (de Wit et al., 2016).

After the SARS-CoV epidemic of 2002-2003, increased viral surveillance led to the discovery of numerous bat coronaviruses and the identification of two previously unrecognized human coronaviruses, human coronavirus NL63 and human coronavirus HKU1. Human coronaviruses NL63 and HKU1 were isolated from hospitalized young children with respiratory disease and elderly patients with other co-morbidities, respectively (Fouchier et al., 2004; Perlman and Netland, 2009; van der Hoek et al., 2004; Woo et al., 2004). Human coronavirus NL63 is associated with bronchiolitis, colds, pneumonia, and in children less than three years of age, croup. Human coronavirus HKU1 is primarily responsible for colds and pneumonia of varying severity.

More recently, in June 2012, another novel coronavirus emerged into the human population. MERS-CoV was isolated from a sputum sample of a 60-year-old man that died from acute pneumonia and renal failure in Saudi Arabia (Zaki and van Boheemen, 2012). Since that time, MERS-CoV has spread by travel of infected persons to more than 27 countries including a

cluster in the United Kingdom and a large outbreak in South Korea involving 186 patients and 16 hospitals in 2015 (Figure 3) (de Wit et al., 2016; 2017a). As of this publication, 2,143 laboratory-confirmed cases of MERS-CoV, including at least 750 related deaths, have been reported to the World Health Organization (2017b). MERS-CoV infections share many common symptoms with SARS-CoV infections. However, MERS-CoV infected patients are more likely to have abnormal chest x-rays and to require intensive care. Further, MERS-CoV infection results in a higher incidence of acute respiratory distress syndrome, which is likely reflected in the higher mortality rate (~35%), compared to SARS-CoV infection (~10%) (de Wit et al., 2016). While MERS-CoV-like viruses have been isolated in bats, serological studies point to dromedary camels as the likely reservoir of MERS-CoV (Drexler et al., 2014; Reusken et al., 2013). MERS-CoV-neutralizing antibodies have been isolated from dromedary camels in Oman and the Canary Islands. However, no viral RNA was recovered from these animals (Reusken et al., 2013). In one specific outbreak on a farm in Qatar, MERS-CoV RNA was isolated from three camels that were linked to two human cases of MERS-CoV; thus, demonstrating that humans in close contact with MERS-CoV infected camels can become infected by the same strain (Figure 3) (Azhar et al., 2014; Haagmans et al., 2014). In two other studies, infectious MERS-CoVs were isolated from dromedary camels in Saudi Arabia and Qatar (Hemida et al., 2014; Raj et al., 2014). In addition, there is serological evidence that MERS-CoV or a MERS-CoV-like virus has existed in dromedary camel populations of the Middle East, Eastern Africa, and Northern Africa since as early as 1983 (Figure 3) (de Wit et al., 2016; Müller et al., 2014). Collectively, these studies provide strong evidence for dromedary camels as the reservoir of MERS-CoV. Further, close contact between dromedary camels and humans due to cultural practices in these regions constitutes a possible explanation for the continued circulation of MERS-CoV. In contrast,

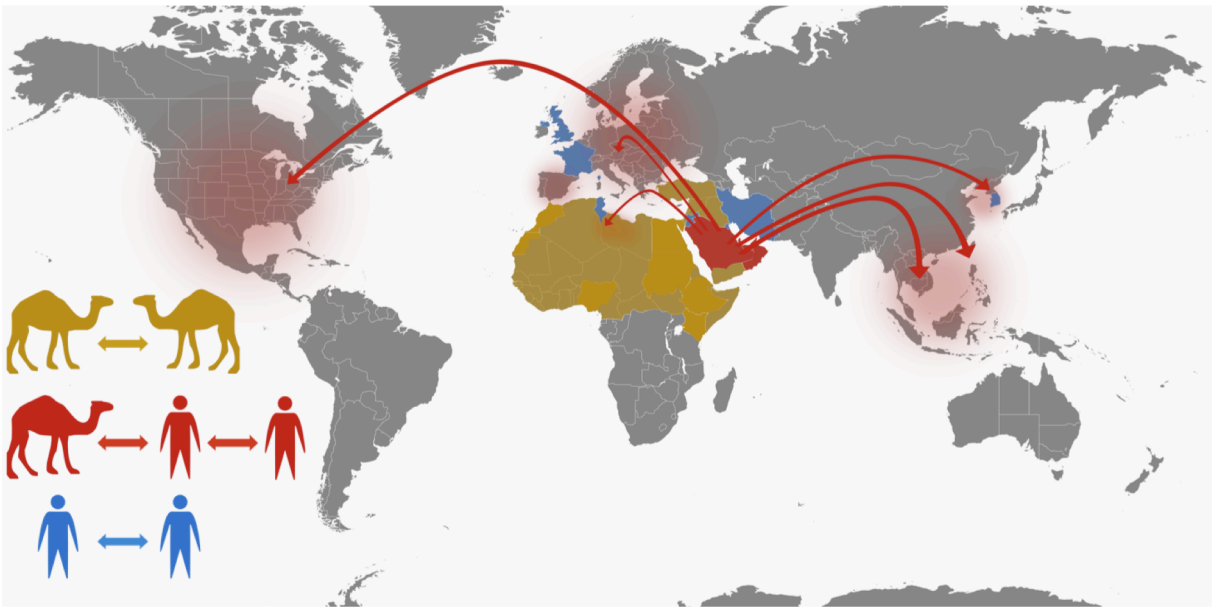

Figure 3. MERS-Coronavirus transmission and spread

Serological studies suggest MERS-CoV or a MERS-CoV-like virus have been circulating in dromedary camels in the Middle East, Northern Africa, and Eastern Africa since at least 1983 (Gold). In Qatar and Saudi Arabia, transmission events between camels and humans have been reported. These findings suggest that humans in close contact with MERS-CoV infected camels can become infected by the same strain (Red). MERS-CoV has spread to at least 27 countries due to travel of infected persons from the Middle East (Red arrows). In some cases, this has resulted in local outbreaks in traveler destination countries (Blue). This map is adapted from www.who.int/emergencies/mers-cov/en/.

SARS-CoV, without a sustained intermediate host, was more rapidly contained (de Wit et al., 2016).

Bat species represent greater than a fifth of the 5,000 known species of mammals and are known reservoirs of many human viruses such as Marburg, Hendra, Nipah, and rabies (Calisher et al., 2006; Huynh et al., 2012). To date, at least 60 novel bat coronaviruses have been identified in North America, Europe, Africa, and China by surveillance studies (Dominguez et al., 2007; Gloza-Rausch et al., 2008; Perlman and Netland, 2009; Tong et al., 2009; Woo et al., 2007). Therefore, it is not surprising that all human coronaviruses are believed to have originated in bats with the exception of human coronavirus OC43, which emerged from cattle (Huynh et al., 2012). Despite persistent infection with many viruses, bats rarely display clinical symptoms of disease (Baker et al., 2013). In fact, as high as 84% of individuals in some Chinese horseshoe bats populations have antibodies against SARS-CoV-like viruses. However, SARS-CoV-like virus-infected bats exhibit no observed pathology (Calisher et al., 2006). Some studies attribute the ability of bats to coexist with many viruses in the absence of disease to constitutive expression of interferon-alpha (IFN-α) and indirect consequences of flight on the innate immune system (Baker et al., 2013; Zhang et al., 2013; Zhou et al., 2016). Regardless, bats are a reservoir for a large number of coronaviruses, including SARS-CoV-like and MERS-CoV-like viruses, and will continue to pose a threat for the zoonotic spillover of novel coronaviruses into the human population (de Wit et al., 2016; Drexler et al., 2014). Moreover, this threat will continue to escalate as the human population expands into previously uninhabited or sparely inhabited regions of the world.

Coronavirus genome organization and replication strategy

The order *Nidovirales* consists of four virus families: *Arteriviridae*, *Coronaviridae*, *Mesoniviridae*, and *Roniviridae*. The *Coronaviridae* family is divided into two subfamilies: *Torovirinae* and *Coronavirinae*. The subfamily *Coronavirinae* contains four genera of coronaviruses: *Alphacoronaviruses*, *Betacoronaviruses*, *Gammacoronaviruses*, and *Deltacoronaviruses*. Currently, viruses in the *Coronavirinae* subfamily, which are positive-sense, single-stranded RNA viruses, contain the largest known genomes for RNA viruses (26-32kb) (Gorbalenya et al., 2006; Smith et al., 2014). Coronavirus genomes are structurally similar to cellular mRNAs since they consist of a 5'-capped RNA molecule with a 3' poly-(A) tail (Lai and Stohlman, 1981; Lai et al., 1982; Masters, 2006). Coronaviruses encode at least 6 open reading frames (ORFs) (Perlman and Netland, 2009). The first, ORF1, comprises the first two-thirds of the coronavirus genome. ORF1 is translated as one of two possible large polyproteins (pps), pp1a or pp1ab. Each translation initiation event begins at the 5' end of pp1a. Due to a -1 ribosomal frameshift, which is recognized approximately 40% of the time, translation continues resulting in pp1ab (Brierley et al., 1987; Plant et al., 2005). Pp1ab encodes 16 non-structural proteins (nsps) that are involved in RNA synthesis and RNA modification (Figure 4 and Table 1). The remaining one-third of the coronavirus genome encodes several accessory proteins that are coronavirus species-dependent and four structural proteins: the spike glycoprotein, the membrane glycoprotein, the envelope protein, and the nucleocapsid protein (Figure 4 and Table 1).

A single coronavirus replication cycle begins when the spike glycoprotein on the surface of a coronavirus virion binds to the cellular receptor utilized by that particular coronavirus strain

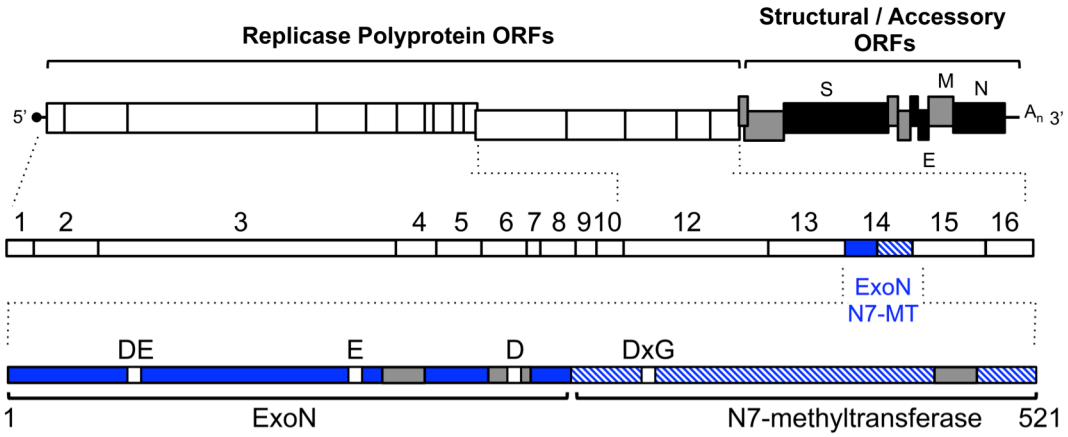

Figure 4. Coronavirus genome and nsp14 organization

Coronaviruses encode 16 non-structural proteins within polyprotein 1ab, which comprises approximately two-thirds of the coronavirus genome. Nsp14 is a multifunctional protein that encodes 3'-to-5' exoribonuclease and N7-methyltransferase activities. The ExoN domain (blue) is located in the N-terminal half of the protein whereas the N7-methyltransferase domain (blue hatched) is located in the C-terminal half. Nsp14 ExoN activity is conferred by four, invariant active site residues (DE-E-D). A conserved DxG motif in the N7-methyltransferase domain confers SAM binding and N7-methyltransferase activity. Three zinc fingers are encoded in CoV nsp14 (gray boxes).

Protein	Function(s)
nsp1	Host mRNA degradation; cell cycle arrest; IFN antagonist
nsp2	Unknown; dispensable for viral replication *in vitro*
nsp3	Papain-like proteases; cleavage of nsp1-nsp3; poly(ADP-ribose) binding; IFN antagonist; deubiquitinase activity; DMV formation
nsp4	Transmembrane protein; DMV formation
nsp5	Main protease; nsp4-nsp16 polyprotein cleavage
nsp6	Transmembrane protein; DMV formation
nsp7	ssRNA binding protein; may form a hexadecameric complex with nsp8
nsp8	Primase; may form a hexadecameric complex with nsp7
nsp9	ssRNA binding protein; part of replicase complex
nsp10	Stimulates nsp14 ExoN activity; required for SARS nsp16 2'O-MTase
nsp11	13 amino acid peptide; contains ribosomal frameshift signal; unknown
nsp12	RNA-dependent RNA polymerase
nsp13	RNA 5'-triphosphatase; helicase
nsp14	3'-to-5' ExoN activity; proofreading; N7-MTase activity; RNA capping
nsp15	Endonuclease; may degrade dsRNA
nsp16	2'O-MTase activity; RNA capping
S	Virion structural protein; receptor binding; membrane fusion
E	Virion structural protein; envelope formation; transmembrane protein
M	Virion structural protein; transmembrane protein; virion formation
N	RNA binding protein; forms helical nucleocapsid; IFN antagonist

Table 1. Coronavirus protein functions

Coronavirus non-structural and structural protein functions are described.

(Figure 5). Murine hepatitis virus (MHV), SARS-CoV, and MERS-CoV, the coronaviruses studied in our lab, use murine carcinoembryonic antigen-related cell adhesion molecule 1a (CEACAM1a), angiotensin-converting enzyme 2 (ACE2), and dipeptidyl peptidase 4 (DPP4), respectively, to enter cells (Hemmila et al., 2004; Li et al., 2003; Raj et al., 2013). Upon entry by receptor-mediated endocytosis or direct membrane fusion, viral RNA uncoating occurs in the cytoplasm (Masters, 2006). The capped 5' ends of coronavirus genome RNAs are recognized by ribosomes and are translated into pp1a and pp1ab (de Wit et al., 2016; Perlman and Netland, 2009). These polyproteins are proteolytically processed by papain-like proteases 1 and 2 encoded in nsp3 and the main protease in nsp5 to generate 16 individual nsps. Data suggest during coronavirus replication, nsps 3, 4, and 6 function to modify intracellular membranes derived from the rough endoplasmic reticulum to form double membrane vesicles (Kanjanahaluethai et al., 2007; Knoops et al., 2008; Oostra et al., 2007; Snijder et al., 2006). Inside double-membrane vesicles, coronavirus replication complexes assemble and coronavirus RNA replication occurs through two distinct phases: genome replication and subgenomic mRNA synthesis (Masters, 2006; Smith et al., 2014). The coronavirus replication-transcription complex, which is responsible for replicating all viral RNAs, is an intricate, multi-subunit complex comprised of several nsps (Smith and Denison, 2013; Smith et al., 2014). Nsp7 and nsp8 form an RNA-binding, hexadecameric supercomplex that resembles a sliding clamp, which functions to increase polymerase processivity (Smith and Denison, 2013; Smith et al., 2014; Subissi et al., 2014; Zhai et al., 2005). In addition, nsp8 encodes a noncanonical RNA dependent-RNA polymerase activity that acts as a primase (Smith and Denison, 2012; Smith et al., 2014; Velthuis et al., 2011). Other coronavirus replication-transcription components include nsp9, which binds single-stranded RNA; nsp12, the RNA-dependent RNA polymerase; nsp13, which encodes

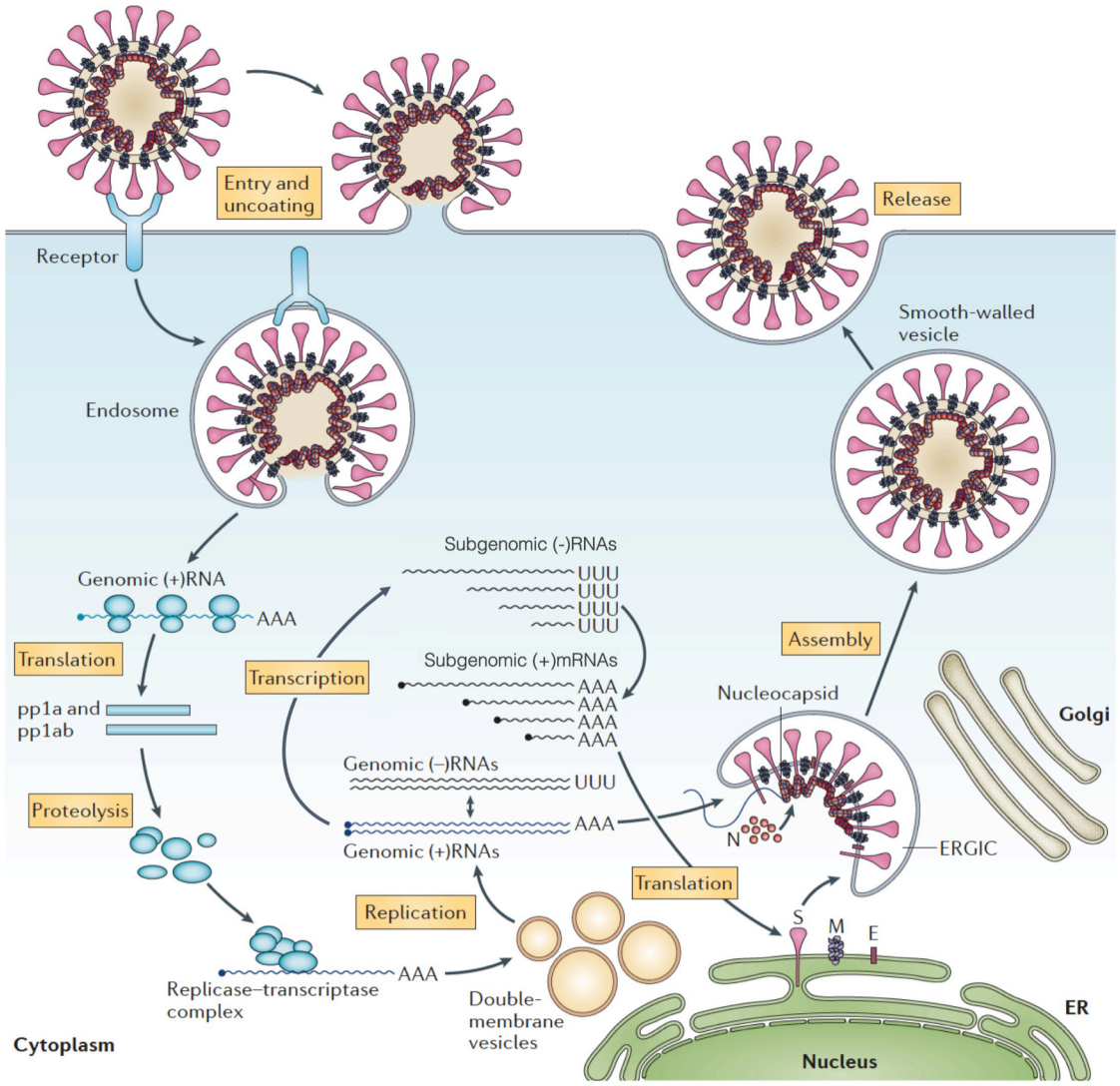

Figure 5. Coronavirus replication cycle

Following receptor-mediated endocytosis, coronavirus spike proteins facilitate membrane fusion and viral uncoating. In the cytoplasm of the cell, the positive-sense coronavirus genome is recognized and translated by ribosomes. Viral proteases encoded by nsp3 and nsp5 cleave translated polyproteins in individual, mature proteins. Coronavirus replication-transcription complexes form on virus-induced double-membrane vesicles and coronavirus genomic and subgenomic RNAs are replicated. Viral particles are assembled at the ER-Golgi intermediate compartment (ERGIC). Assembled virions are released from infected cells through a non-lytic, exocytosis pathway. This figure is adapted from de Wit et al., 2016 and is used with permission.

nucleotide triphosphatase and helicase activities; and nsp15, which encodes endonuclease activity (Adedeji et al., 2012; Egloff et al., 2004; Ivanov et al., 2004a; Smith et al., 2014). Nsp10 is a non-enzymatic co-factor that has been demonstrated to interact with nsp14 and nsp16 (Bouvet et al., 2012; 2010; Decroly et al., 2011a). Coronavirus nsp14 encodes 3'-to-5' exoribonuclease activity (ExoN) and N7-methyltransferase activity (N7-MTase) (Chen et al., 2009; Minskaia et al., 2006). All data to date support the hypothesis that nsp14 ExoN performs a novel proofreading function during replication and may be responsible for expansion of the coronavirus genome to such a large size (Gorbalenya et al., 2006; Lauber et al., 2013). Moreover, coronavirus nsp14 N7-MTase activity and nsp10-nsp16 complexes are involved in 5' capping of viral RNA (Bouvet et al., 2010; Chen et al., 2009; 2013; Decroly et al., 2008).

From the positive-sense genome RNA, the coronavirus replication-transcription complex generates a full-length, negative-sense anti-genome RNA, which is used as a template for subsequent positive-sense genome RNA amplification (Figure 6A). In addition, coronavirus structural and accessory proteins are expressed as a nested set of subgenomic mRNAs through a discontinuous transcription mechanism (Masters, 2006; Sawicki and Sawicki, 1998; 2005; Smith et al., 2014)(Figure 6 B-D). First, the coronavirus replication-transcription complex generates negative-sense subgenomic RNAs from the 3' end of the positive-sense genome RNA (Figure 5B). Each negative-sense subgenomic RNA contains a common 3' end sequence known as the transcriptional regulatory sequence. Upon recognizing the transcriptional regulatory sequence, the replication-transcription complex will either read-through the regulatory sequence and continue into another subgenomic ORF or dissociate the negative-sense subgenomic RNA from the positive-sense RNA genome. This process generates negative-sense subgenomic RNAs of

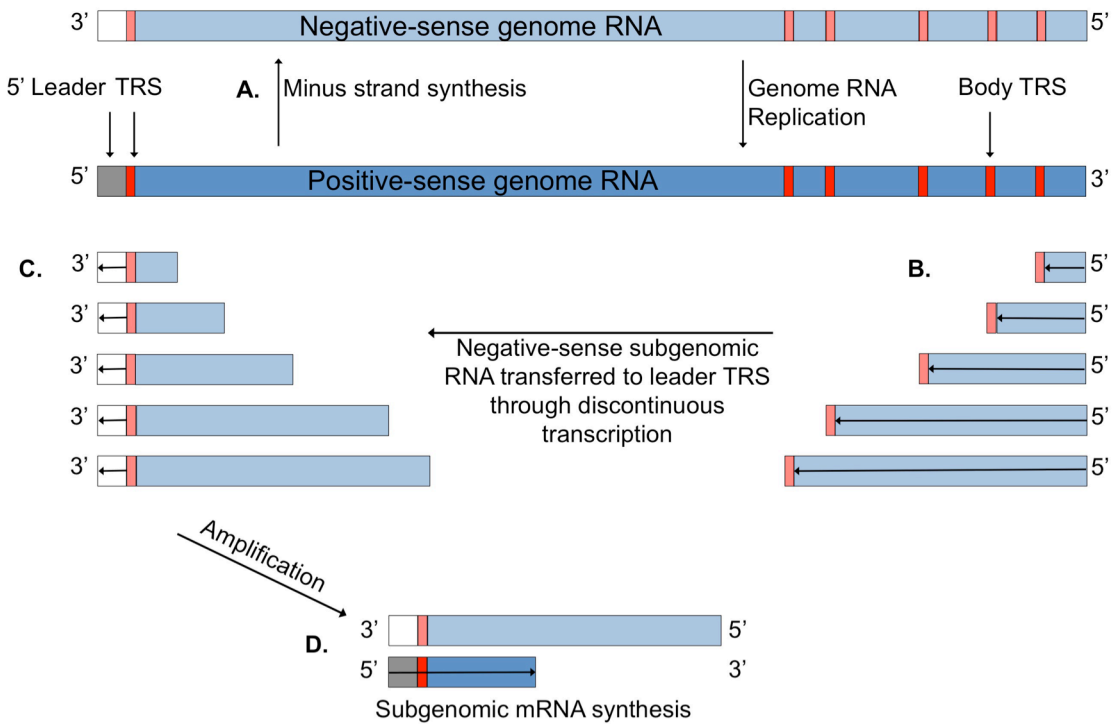

Figure 6. Coronavirus genomic and subgenomic RNA replication

(A) Coronavirus replication-transcription complexes generate a negative-sense genome RNA from a positive-sense genome RNA. Negative-sense genome RNAs serve a templates for generating progeny positive-sense genome RNAs. **(**B) Coronavirus replication-transcription complexes generate negative-sense subgenomic RNAs of varying lengths from positive-sense genome RNAs. (C) Through a discontinuous transcription mechanism, negative-sense subgenomic RNAs dissociate from the 3'-end of the positive-sense RNA genomes and reassociate through base-pairing interactions at the 5' leader transcription regulatory sequence (TRS) of the positive-sense genome RNA. (D) Negative-sense subgenomic RNAs serve as templates for subgenomic positive-sense RNA amplification.

varying lengths and thus, varying numbers of subgenomic ORFs. Upon dissociation from the positive-sense genome RNA, the replication-transcription complex reassociates with the 5' leader transcriptional regulatory sequence through base pairing interactions at the 5' end of the positive-sense genome RNA and negative-sense subgenomic RNA transcription continues through the 5' end of the genome (Figure 6C). Finally, these negative-sense subgenomic RNAs serve as templates for positive-sense subgenomic mRNA production (Figure 6D). Although subgenomic mRNAs may contain more than one ORF, only the 5' most subgenomic ORF is translated. Subgenomic accessory protein ORFs are interspersed between the four structural ORFs. The number and function of encoded accessory proteins is dependent on the coronavirus strain. Often, coronavirus accessory proteins are not required for viral replication in cell culture and many have been described that have innate antagonism roles. Therefore, it is likely that coronavirus accessory proteins serve important roles in viral replication in natural host settings (Perlman and Netland, 2009). Upon translation of the coronavirus membrane and envelope structural proteins, which are transmembrane glycoproteins, they are incorporated into assembling virions (de Wit et al., 2016; Masters, 2006; Perlman and Netland, 2009). The membrane protein is responsible for giving virions their shape, and the envelope protein is important for virion release (Masters, 2006; Perlman and Netland, 2009) Further, the spike glycoproteins, which protrude from virions and mediate viral attachment to the host cell and membrane fusion, are inserted into the endoplasmic reticulum and are subsequently incorporated into assembling virions (de Wit et al., 2016; Masters, 2006). The coronavirus nucleocapsid structural protein is an RNA binding protein and interferon antagonist. By encapsidating viral RNA, nucleocapsid proteins prevent viral RNA degradation and detection by the host (Perlman and Netland, 2009). Virion assembly and genome RNA packaging occur on membranes that bud

into the endoplasmic reticulum-Golgi intermediate compartment. Next, vesicles containing newly assembled virions migrate and fuse with the plasma membrane to release virus progeny (de Wit et al., 2016).

The multiple functions of coronavirus nsp14

Coronavirus nsp14 is a multifunctional protein that encodes 3'-5' exoribonuclease (ExoN) and N7-methyltransferase (N7-MTase) activities (Figure 4) (Chen et al., 2009; Minskaia et al., 2006). The coronavirus nsp14 ExoN and N7-MTase domains are located in the N-terminal and C-terminal halves of the protein, respectively. Further, two of the three zinc-finger motifs encoded by coronavirus nsp14 are located in the ExoN domain and are likely important for binding RNA (Ma et al., 2015). Initial biochemical studies of nsp14 ExoN activity demonstrated that ExoN has a preference for double-stranded RNA (dsRNA) and the capacity to excise 3' end misincorporated nucleotides (Minskaia et al., 2006). The coronavirus nsp14 ExoN is a member of the DE-D-Dh superfamily of DNA and RNA exonucleases, so named for the three motifs of four active site residues (Minskaia et al., 2006). SARS-CoV and MHV expressing engineered, ExoN-inactivating substitutions at active site residues in Motif I (DE→AA) [ExoN(-)] demonstrate an approximately 15-20-fold increase in mutation frequency during viral replication (Eckerle et al., 2007; 2010). In addition, ExoN(-) viruses are profoundly sensitive to inhibition by RNA mutagens (Case et al., 2017; Eckerle et al., 2007; Graepel et al., 2017; Sexton et al., 2016; Smith et al., 2013). Thus, coronavirus nsp14 ExoN is the first description of an RNA virus encoded proofreading enzyme and nsp14 ExoN activity is required for high-fidelity replication(Smith and Denison, 2012; 2013; Smith et al., 2014). Furthermore, a mouse

pathogenesis study demonstrated that SARS-CoV ExoN(-) virus is attenuated *in vivo* but protects mice from lethal challenge with WT SARS-CoV (Graham et al., 2012).

Current models place nsp14 as a key component in a multi-subunit coronavirus replication complex that includes the nsp12 RNA-dependent-RNA polymerase and nsp10, a non-enzymatic co-factor, among several other proteins (Smith and Denison, 2013; Smith et al., 2014). Coronavirus nsp10 binds nsp14 and stimulates ExoN activity up to 35-fold (Bouvet et al., 2012). In addition, mutations in nsp10 that disrupt binding to nsp14 decrease virus replication fidelity (Smith et al., 2015). Relative to DNA-based organisms, RNA viruses have high mutation rates and are thought to be limited in genome size due to the lack of proofreading mechanisms (Bradwell et al., 2013; Eigen, 1971; Sanjuan et al., 2010; Smith et al., 2014). Thus, the acquisition of nsp14 ExoN is thought to be a contributing factor in the expansion of the coronavirus genome to allow such a large RNA genome to be faithfully replicated and maintained (Gorbalenya et al., 2006; Lauber et al., 2013; Smith and Denison, 2013; Smith et al., 2014).

Interestingly, outside of the order *Nidovirales*, the only other known RNA virus-encoded 3'-to-5' exoribonucleases are found in the *Arenaviridae* family of viruses. Lassa fever virus nucleoprotein ExoN is not thought to participate in fidelity regulation, but rather it participates in immune evasion by degrading dsRNA and thereby prevents antigen-presenting cell-mediated natural killer (NK) cell activation (Hastie et al., 2011; Qi et al., 2010; Russier et al., 2014). Recently, in the *Alphacoronavirus* transmissible gastroenteritis virus (TGEV), an nsp14 ExoN zinc finger mutant was shown to generate lower levels of dsRNA compared to wild-type (WT)

TGEV. However, in that study viruses with mutations in ExoN active site motifs were non-viable and therefore, could not be directly tested for effects on innate immunity (Becares et al., 2016). In work described in Chapter III of this dissertation research, I explore my original interests and test the hypothesis that coronavirus nsp14 ExoN also functions to antagonize the innate immune response.

The coronavirus nsp14 N7-MTase was initially identified in a functional screen, wherein SARS-CoV nsp14 was capable of complementing N7-MTase deficient yeast (Chen et al., 2009). Strikingly, these data also presented evidence than an enzyme encoded by an RNA-based virus was capable of complementing the corresponding function of a DNA-based organism (Chen et al., 2009). Since the initial discovery, structure-function studies have demonstrated that SARS-CoV nsp14 N7-MTase activity is mediated by a conserved DxG motif within the MTase domain *in vitro* (Chen et al., 2013; Ma et al., 2015). In addition, all three DxG motif residues were required for complete binding of S-adenosyl-L-methionine, the methyl donor for the reaction, and full N7-MTase activity *in vitro* (Bouvet et al., 2010; Chen et al., 2013). Alanine substitution of SARS-CoV nsp14 at position D90/E92 in the ExoN domain or at position D331 in the N7-MTase domain did not affect N7-MTase or ExoN activities *in vitro*, respectively (Chen et al., 2009; 2013). However, truncation of as few as 17 residues of the nsp14 C-terminal end of the protein ablates ExoN activity. Further, truncation beyond residue 61 from the N-terminal end of the protein ablates N7-MTase activity (Chen et al., 2013). Therefore, these data suggest the ExoN and N7-MTase domains, but not the respective domain activities of nsp14, are interdependent. The nsp10/nsp14 crystal structure further supports these data as the ExoN and N7-MTase domains were demonstrated to interact using hydrophobic interactions. Additionally,

the nsp10/nsp14 crystal structure suggests that S-adenosyl-L-methionine, and the methyl acceptor, guanosine-triphosphate RNA, are held in a highly constricted, hydrophobic pocket where conditions are favorable for methyl transfer to occur (Ma et al., 2015). Coronavirus nsp14-mediated N7-methylation of guanosine triphosphate-RNA to form a cap-0 structure is a prerequisite for nsp10/16-mediated 2'O-methylation *in vitro* (Bouvet et al., 2010). However, the requirements of the coronavirus nsp14 N7-MTase during viral replication were not known at the beginning of this dissertation. In studies described in Chapter II, I demonstrate that viruses with altered N7-MTase activity are attenuated in replication and translation, and that they are detected by and sensitive to the innate immune response.

5' capping of viral and cellular RNA

Eukaryotic mRNAs possess a methylated 5' guanosine cap linked to the penultimate nucleotide by a 5'-5' triphosphate bridge (Figure 7) (Shatkin, 1976). The 5' cap of a cellular mRNA functions in RNA stability, pre-mRNA splicing, mRNA export from the nucleus, translation, and protection against cellular antiviral defenses (Darnell, 1979). The canonical cellular capping process involves three enzymes: 1) an RNA triphosphatase, which is responsible for cleaving the γ-phosphate of the nascent transcript, 2) a guanylyltransferase, which transfers a guanosine monophosphate moiety to the 5' diphosphate RNA, and 3) an N7-methyltransferase, which is responsible for transferring a methyl group from the methyl donor, S-adenosyl-L-methionine, to the N7 position of the guanosine base (Furuichi and Shatkin, 2000). These sequential reactions lead to formation of a cap-0 (7-methyl-Gppp) structure, which is thought to be the minimal cap determinant required for eukaryotic translation initiation factor E (eIF4E) recognition and efficient translation (Figure 7B) (Filipowicz et al., 1976; Marcotrigiano et al., 1997; Schibler and

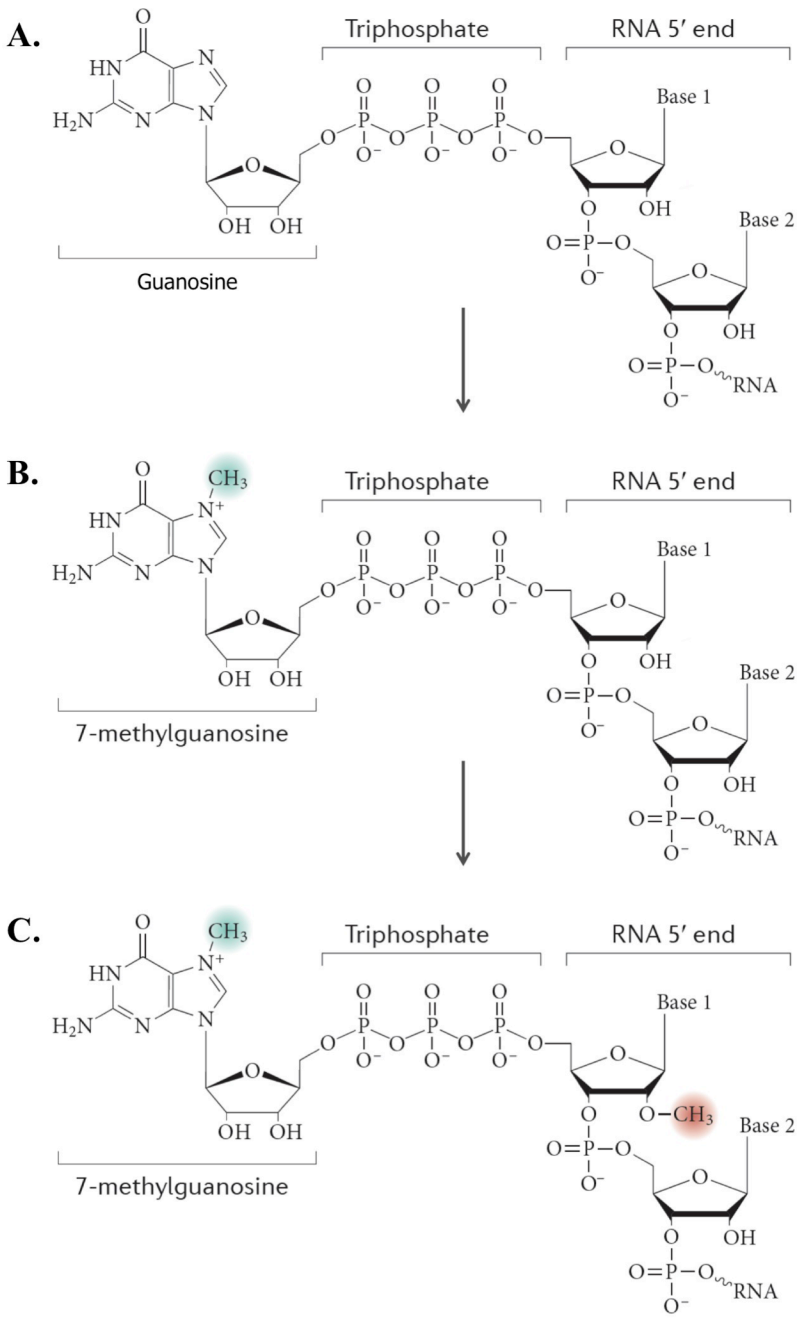

Figure 7. RNA 5' cap structure and formation

The canonical eukaryotic cell and the hypothesized CoV mRNA capping pathway begins with removal of the γ-phosphate of the nascent transcript by an RNA triphosphatase. Next, a guanylytransferase transfers a guanosine monophosphate moiety to the 5'-diphosphate-RNA to form a guanosine-triphosphate-RNA structure (A). Then, the N7-methyltransferase transfers a methyl group from the methyl donor, S-adenosyl-L-methionine, to the N7 position of the guanosine base to form a cap-0 structure (B). In CoVs, nsp14 encodes N7-methyltransferase activity in the C-terminal half of the protein. Finally, a 2'O-methyltransferase adds a methyl group to the 2'O position of the ribose sugar of the penultimate nucleotide to form a cap-1 structure (C). CoV nsp16, when bound by nsp10, functions as a 2'O-methyltransferase. This figure is adapted from Decroly et al., 2012 and is used with permission.

Perry, 1977). Higher eukaryotes express 2'O-methyltransferases (2'O-MTase) that add a methyl group to the ribose 2'O position of the penultimate nucleotide of the cap-0 RNA. This reaction results in formation of a cap-1 structure that allows cells to differentiate self from non-self RNAs in the cytoplasm (Figure 7C) (Wei et al., 1975; Züst et al., 2011).

Viruses are obligate intracellular parasites, meaning they need host cell machinery and resources in order to replicate. Many viruses encode capping enzymes to disguise viral RNAs from the cell. Cap structures can be added to viral RNAs by one of the following three mechanisms: 1) use of cellular capping machinery, 2) cap snatching, or 3) use of virus encoded capping enzymes. The first capping mechanism is utilized by viruses that use cellular RNA polymerase II to synthesize their mRNA. Examples include DNA viruses such as those in the *Herpesviridae* and *Hepadnaviridae* families and by RNA viruses of the *Retroviridae* family. Viruses of the *Orthomyxoviridae, Arenaviridae,* and *Bunyaviridae* families utilize the second mechanism, which involves stealing 5' caps from cellular mRNAs via endonucleolytic cleavage. Lastly, many viruses encode their own capping enzymes, which can be categorized as either conventional, meaning the capping pathway follows that of cellular mRNAs, or unconventional. Overall, the diversity of enzymes and mechanisms used by viruses to synthesize capped RNA products suggests that there is a strong selective pressure on viruses to cap their RNAs (Decroly et al., 2011b).

Coronaviruses encode several enzymes within their large, positive-sense RNA genomes (26-32 kb) that are implicated in viral RNA capping. The coronavirus genome possesses a 5' terminal cap and 3' poly-A tail (Lai and Stohlman, 1981; Lai et al., 1982; Masters, 2006). All data to date

support the hypothesis that coronavirus genomes are capped using the canonical mRNA capping pathway (Bouvet et al., 2010). SARS-CoV nsp13 displays RNA triphosphatase activity *in vitro* (Ivanov et al., 2004b). The coronavirus guanylyltransferase has not been identified but, according to the current model, would function to add a guanosine monophosphate to the diphosphate RNA product of nsp13. The RNA-dependent RNA polymerase of equine arteritis virus and SARS-CoV displays nucleotidylation activity (Lehmann et al., 2015). While further study is required to define the function of this activity in viral replication, it is possible that the RNA-dependent-RNA-polymerase participates in coronavirus RNA capping. Nsp16 of feline coronavirus functions independently as a 2'O-MTase, but SARS-CoV nsp16 requires nsp10 as a co-factor for 2'O-MTase activity (Decroly et al., 2008; Grotthuss et al., 2003; Snijder et al., 2003). SARS-CoVs lacking 2'O-MTase activity are recognized and sequestered by interferon-induced protein with tetratricopeptide repeats 1 (IFIT1) due to the lack of a cap-1 structure (Bouvet et al., 2010; Chen et al., 2011; Daffis et al., 2010; Decroly et al., 2011a; Habjan et al., 2013; Menachery et al., 2014). In work described in Chapter II of this dissertation, I determine the requirements of the MHV nsp14 N7-MTase for viral RNA capping and efficient translation during the course of viral infection. In addition, I characterize the innate immune response to viruses with ablated nsp14 N7-MTase activity.

Innate immune response to pathogens

The innate immune response within a mammalian cell is hardwired into the genome and provides the first line of defense against an invading pathogen. The capacity of a cell to distinguish 'self' from 'non-self' is essential for mounting an effective innate immune response. Cells accomplish this task in the context of RNA virus infection through the use of pattern recognition receptors,

namely retinoic acid-inducible gene like receptors, such as RIG-I and MDA5, and toll-like receptors (TLRs), such as TLR3, TLR7, and TLR8 (Brubaker et al., 2015). Pattern recognition receptors have evolved to recognize pathogen associated molecular patterns (PAMPs), which are conserved features of pathogens. Therefore, while the innate immune response does not afford memory to previous infections, it does provide a broadly applicable and robust response to infection and initiates the adaptive immune response. In most cases, single- or double-stranded RNAs act as the primary PAMPs that are sensed by a cell during RNA virus infection, often resulting in the induction of type I interferon (IFN) gene expression and other pro-inflammatory antiviral responses (Baum and García-Sastre, 2009). Upon secretion from a cell, IFNs bind to cell surface-expressed IFN-α/β receptors (IFNARs) in an autocrine and paracrine manner (Figure 8). Subsequently, an IFN signaling cascade utilizing the Janus kinase (Jak) and signal transducer and activator of transcription (STAT) pathway leads to the induction and expression of hundreds of interferon stimulated genes (ISGs) that act to limit or prevent viral replication and spread to neighboring cells and tissues. In fact, ISGs targeting every stage of virus replication have been described: entry (Mx, TRIM, and IFITM proteins), viral translation and replication (IFIT, OAS/RNAse L, and PKR proteins), and viral egress (viperin and tetherin proteins). Further, ISGs may act broadly against numerous viruses or may have evolved specifically to counteract a single virus family (Schneider et al., 2014).

The 5’ end of an mRNA present in the cytoplasm is assessed by several ISGs as one potential mechanism to distinguish self from non-self. RIG-I specifically recognizes 5’ triphosphate-RNAs, which in the absence of infection, should not be present within the cytoplasm of a cell (Decroly et al., 2011a; Hornung et al., 2006). Further, MDA5 recognizes RNA that only

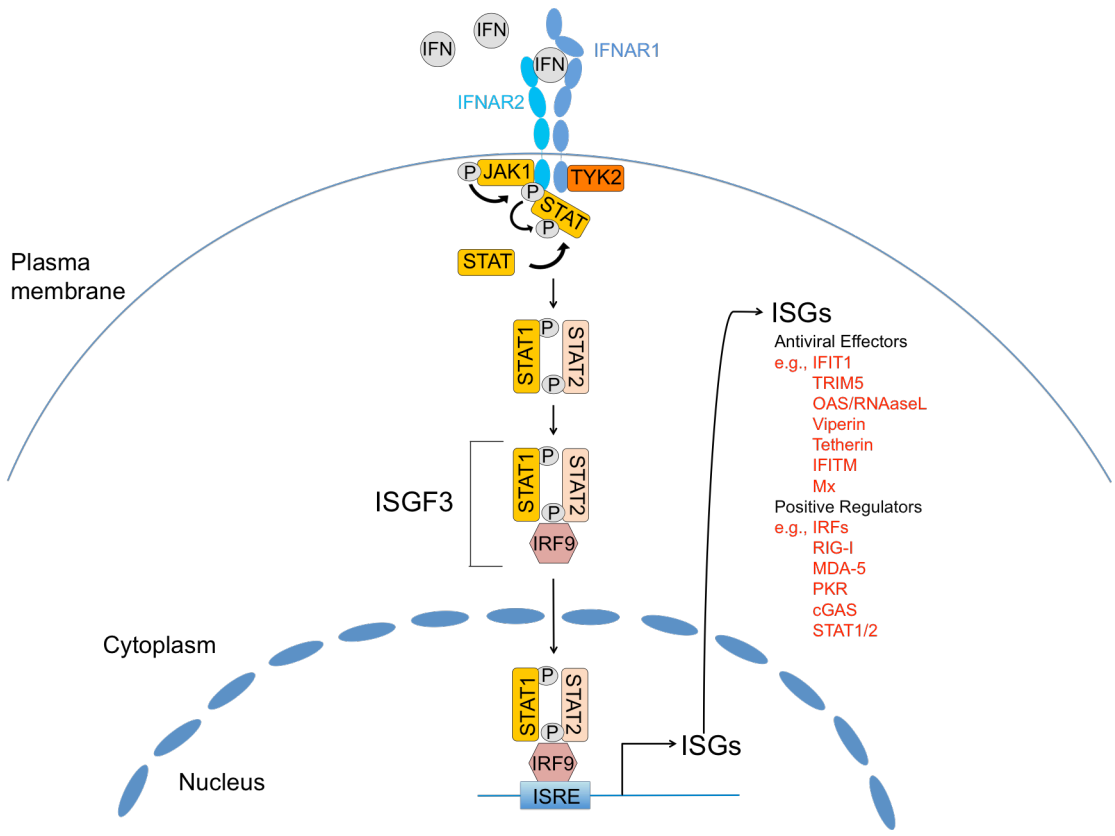

Figure 8. Type I interferon signaling pathway

Upon binding of type I interferon to the interferon alpha/beta receptor (IFNAR 1 and 2 heterodimers), Janus kinase 1 (JAK1) and tyrosine kinase 2 (TYK2) undergo transphosphorylation and activation. Once activated, Jaks phosphorylate IFN receptor chains, leading to the recruitment of STAT proteins. Next, STAT proteins become phosphorylated and disassociate from IFN receptors. Phosphorylated STAT1 and STAT2 proteins form a heterodimer and interact with interferon regulatory factor 9 (IRF9), forming what is known collectively as the interferon stimulated gene factor 3 (ISGF3) complex. ISGF3 translocates to the nucleus and functions as a transcription factor by binding interferon stimulated response elements (ISREs) in the promoter regions of ISGs, resulting in transcription of hundreds of genes. This figure is adapted from Schneider et al., 2014.

possesses a cap-0 structure or is linked to a protein. In addition, IFIT1 and IFIT2 specialize in binding and sequestering 5' triphosphate-RNA and cap-0 RNA (Decroly et al., 2011a; Züst et al., 2011). In Chapter II of this dissertation, I determine the requirements of MHV nsp14 N7-MTase for viral capping in the context of viral infection and report the ensuing innate immune response to viruses with defective capping mechanisms. In Chapter III, I demonstrate that coronaviruses lacking ExoN activity are restricted by the IFN-β-mediated innate immune response. In Chapter IV, I describe the development of assays and reagents to determine the ISG or ISGs responsible for mediating ExoN(-) virus restriction.

Coronavirus innate immune antagonists

As obligate intracellular parasites, viruses have evolved numerous mechanisms to prevent and antagonize innate detection by host cells (Decroly et al., 2011a; Katze et al., 2002). Coronaviruses, like many other successful viruses, have evolved numerous mechanisms to counter the innate immune response (Perlman and Netland, 2009). Coronaviruses encode many IFN antagonists that prevent the induction of IFN. In addition, coronaviruses are also known to exhibit a relatively high level of resistance to the effects of IFN pretreatment of cells (Roth-Cross et al., 2007). Coronavirus nsp1 antagonizes the innate immune response by degrading host mRNAs and suppressing IFN-β expression (Kamitani et al., 2006; Zhang et al., 2015). The nsp3 of SARS-CoV prevents interferon regulatory factor 3 phosphorylation and NF-κB signaling (Devaraj et al., 2007). In addition, SARS-CoV nsp3 encodes deubiquitinating and deISGylating activities (Barretto et al., 2005; Rose and Weiss, 2009). Coronavirus viral RNA evades innate detection by MDA5 and IFIT1 due to the formation of a 5' cap-1 structure by encoding N7- and 2'O-methyltransferases (Case et al., 2016; Chen et al., 2009; Decroly et al., 2008; Menachery et

al., 2014; Züst et al., 2011). MHV and MERS-CoV encode 2'-5' phosphodiesterases that degrade 2'-5' oligoadenylates. 2'-5' oligoadenylates are key signaling molecules generated by oligoadenylate synthetase (OAS) in response to innate detection of dsRNA that subsequently activate RNase L (Zhao et al., 2012b). Most recently, a coronavirus nsp15 endonuclease (EndoU) activity mutant virus was shown to have increased dsRNA levels, suggesting that nsp15 EndoU functions to reduce dsRNA levels during infection (Kindler et al., 2017). SARS-CoV ORF3b and ORF6 accessory proteins prevent IFN induction (Kopecky-Bromberg et al., 2006; Perlman and Netland, 2009). In addition, the nucleocapsid protein of SARS-CoV and MHV inhibits NF-κB activation and activator protein 1 signaling and PKR function, respectively (He et al., 2003; Kopecky-Bromberg et al., 2006; Ye et al., 2007). In work described in Chapter III of this dissertation, I present evidence in support of coronavirus nsp14 ExoN activity as an innate immune antagonist.

Summary

Coronavirus genomes are the largest known among single-stranded RNA viruses. The extreme size of the coronavirus genome results in a need to reliably replicate the genome without accumulating a lethal level of mutations. Coronaviruses have likely solved this issue by devoting a considerable portion of their coding space to a large, multi-protein replication complex that includes a novel 3'-to-5' exoribonuclease activity encoded within nsp14. In addition to 3'-to-5' exoribonuclease activity, coronavirus nsp14 encodes an N7-methyltransferase activity that participates in viral RNA capping. In this dissertation research, I determine the residues of nsp14 that are required for N7-MTase activity in replicating virus and that N7-MTase activity is required for evading detection by and mediating resistance to the innate immune response. In

addition, I investigate the hypothesis that nsp14 ExoN activity is involved in mediating resistance to the innate immune response by a potentially novel mechanism. Two highly lethal human coronaviruses have emerged into the human population in this century and virus-specific therapeutics or vaccines currently do not exist for the treatment of human coronavirus infection. Therefore, the development of strategies to attenuate viral replication is critical. This dissertation research provides evidence for two potential targets within coronavirus nsp14.

Chapter II

MUTAGENESIS OF S-ADENOSYL-L-METHIONINE-BINDING RESIDUES IN CORONAVIRUS NSP14 N7-METHYLTRANSFERASE DEMONSTRATES DIFFERING REQUIREMENTS FOR GENOME TRANSLATION AND RESISTANCE TO INNATE IMMUNITY

Introduction

At the beginning of this dissertation research, the coronavirus (CoV) non-structural protein 14 (nsp14) N7-methyltransferase (N7-MTase) had been studied using only recombinantly expressed proteins in an *in vitro* setting. CoV nsp14 N7-MTase activity was originally identified using a functional screen in N7-MTase defective yeast and utilized S-adenosyl-L-methionine (SAM) as a methyl donor (Chen et al., 2009). Further, a study had demonstrated that nsp14 N7-MTase-mediated cap-0 formation necessarily preceded nsp10/nsp16 2'O-methyltransferase (2'O-MTase)-mediated cap-1 formation *in vitro*. A conserved DxG motif in the nsp14 N7-MTase domain was demonstrated to be required for nps14 N7-MTase activity and SAM binding. However, the requirement for and the consequences of altered coronavirus N7-MTase activity during viral replication were unknown. I hypothesized that coronavirus nsp14 N7-MTase activity would be an excellent target for viral attenuation due to the known functions and importance of cellular and other viral 5' caps in translation and viral immune evasion. In this chapter, I used site-directed mutagenesis to assess the effect of mutations in the DxG motif of murine hepatitis virus (MHV) nsp14 N7-MTase on viral replication. I show that alanine substitution of nsp14 D330 does not alter viral replication kinetics or increase sensitivity to interferon-β (IFN-β)

treatment relative to wild-type (WT) MHV. However, alanine substitution of nsp14 G332 impaired virus replication, resulting in delayed replication kinetics and decreased peak titer, relative to WT MHV. In addition, nsp14 G332A virus displayed increased sensitivity to treatment of cells with IFN-β, and nsp14 G332A genomes were translated less efficiently *in vitro* and during infection. These data suggest that residue G332, but not residue D330, is required for MHV nsp14 N7-MTase activity, and collectively, that the regulation of coronavirus capping is likely more complex in the context of replicating virus than during *in vitro* biochemical studies with isolated proteins. Further, these data demonstrate the requirement for CoV nsp14 N7-MTase activity for efficient viral RNA translation and resistance to the innate immune response. I performed all experiments and final analysis for the data presented in this chapter. The coauthors provided the following contributions: Alison Ashbrook generated bone marrow-derived dendritic cells (BMDCs) for some replicates of the figure involving BMDCs and assisted me in generating BMDCs for the remaining replicates.

Recovery and replication kinetics of MHV nsp14 N7-MTase mutants

The DxG SAM-binding motif is conserved among the nsp14 N7-MTase domains of alpha-, beta-, and gammacoronaviruses (Figure 9A). Mutations in this motif of SARS-CoV nsp14 ablate N7-MTase activity of purified proteins *in vitro* (Bouvet et al., 2010; Chen et al., 2009; 2013). To determine whether this motif is required for viral replication, I engineered alanine substitutions at the DxG SAM-binding motif in the MHV nsp14 N7-MTase domain. Virus containing either a D330A or G332A substitution in nsp14 was recovered and sequence confirmed across the nsp14 coding region. Following infection of DBT cells at an MOI of 1 PFU/cell, nsp14 D330A virus replicated with kinetics comparable to WT MHV (Figure 9B). Nsp14 D330A plaque morphology

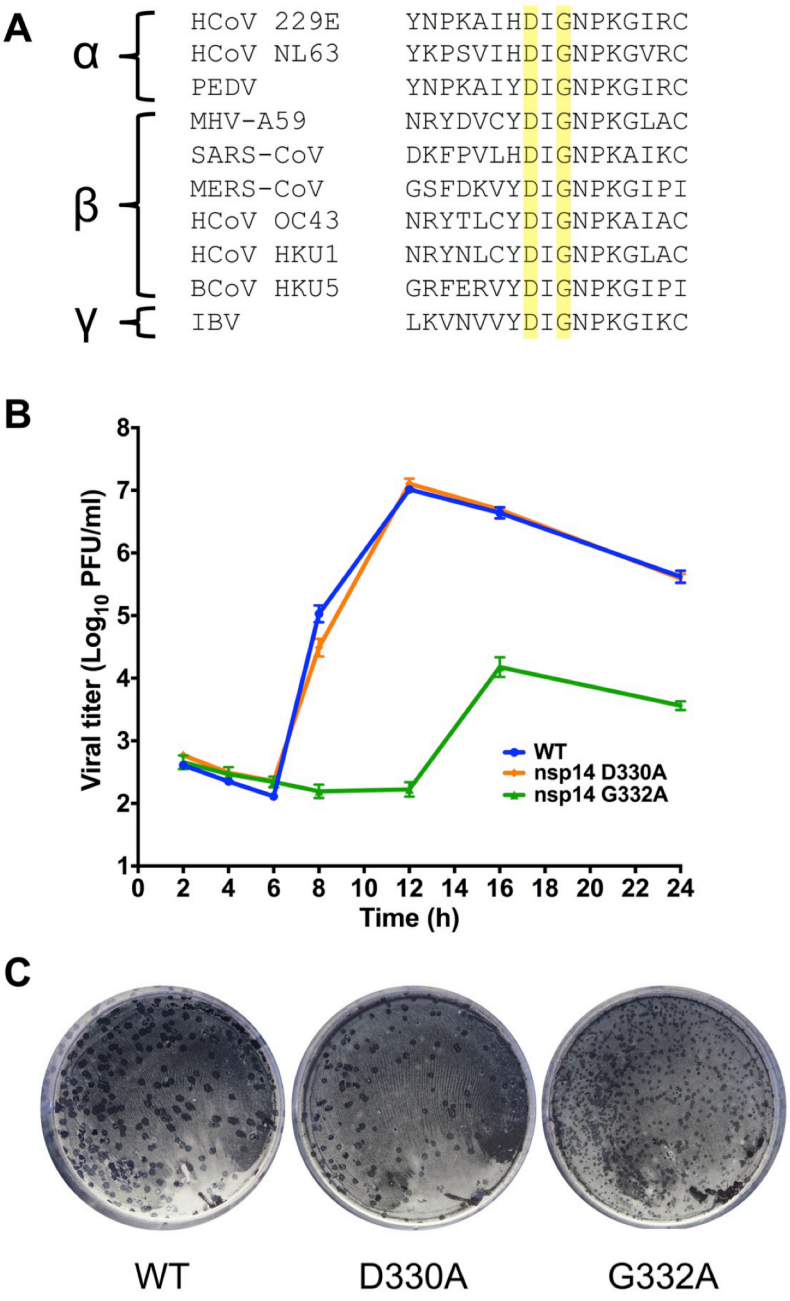

Figure 9. Replication kinetics of viruses with altered N7-MTase SAM-binding residues.

(A) Alignment of GenBank ORF1b sequences of the α-, β-, and γ-CoVs shown demonstrates that SAM-binding residues (shaded) are highly conserved. (B) DBT cells were infected with the viruses shown at an MOI of 1 PFU/cell. Cell culture supernatants were collected at the indicated times post-infection, and viral titers were determined by plaque assay. Error bars indicate SEM (n = 6). (C) Plaque morphology of the viruses shown following agarose overlay plaque assay and fixation with 3.7% paraformaldehyde 24 h post-infection.

also was similar to that of WT MHV (Figure 9C). In contrast, the nsp14 G332A virus began exponential replication 4-6 h later than WT MHV and reached a lower peak titer (1.5×10^4 PFU/ml) relative to WT MHV (10^7 PFU/ml) (Figure 9B). The nsp14 G332A virus plaque size was also decreased relative to WT MHV (Figure 9C). Thus, despite the requirement of D330 for nsp14 N7-MTase activity *in vitro* (Bouvet et al., 2010; Chen et al., 2009; 2013; Ma et al., 2015), my data indicate that the D330A mutation has no detectable effect on MHV replication kinetics in cell culture.

Nsp14 D330A or G332A mutations do not significantly influence nsp14 ExoN activity

Coronavirus nsp14 is a multifunctional protein with two known enzymatic activities, a proofreading 3'-5' exoribonuclease activity (ExoN) and N7-MTase activity (Chen et al., 2009; Minskaia et al., 2006). Based on *in vitro* studies, the ExoN and N7-MTase domains of CoV nsp14 are interdependent (Chen et al., 2013). This conclusion is supported by the crystal structure of nsp14, demonstrating that the ExoN and N7-MTase domains interact through a large hydrophobic interface (Ma et al., 2015). In addition, disruption of ExoN (ExoN-) via mutations at two active-site residues decreases replication fidelity of MHV and SARS-CoV and renders the viruses sensitive to the RNA mutagen 5-fluorouracil (5-FU) (Eckerle et al., 2007; 2010; Smith et al., 2013). Thus, 5-FU sensitivity has been shown to be an *in vitro* indicator of ExoN activity. Therefore, I tested whether the D330A or G332A mutations affect ExoN activity by treating cells with increasing concentrations of 5-FU or vehicle (DMSO) prior to infection with either nsp14 D330A or nsp14 G332A virus at an MOI of 0.01 PFU/cell (Figure 10). The nsp14 D330A and nsp14 G332A viruses were not significantly altered in 5-FU sensitivity compared with WT MHV

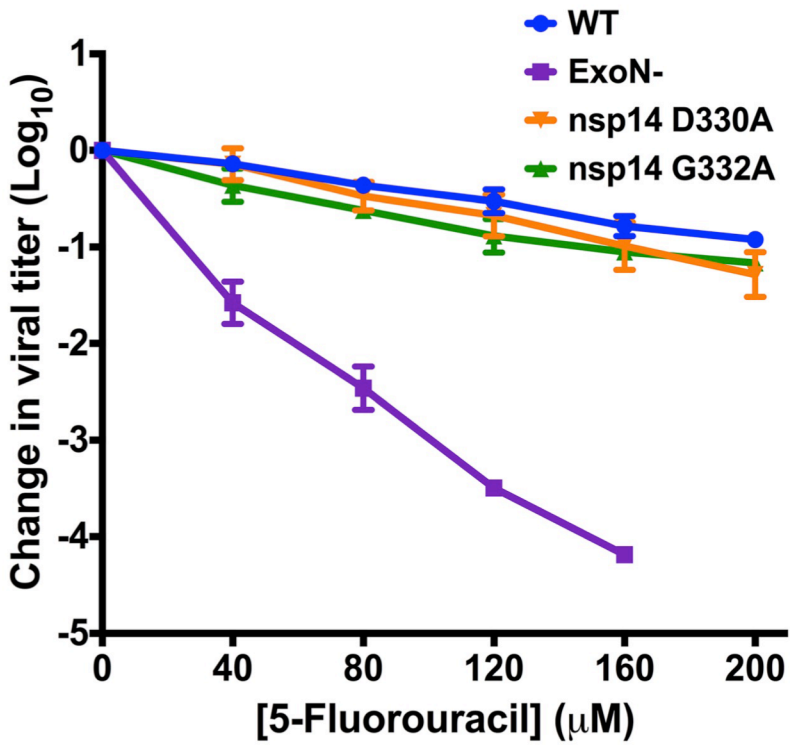

Figure 10. N7-MTase mutants display WT-like sensitivity to the RNA mutagen 5-FU.

DBT cells were treated with the indicated concentrations of 5-FU for 30 min prior to infection with the viruses shown at an MOI of 0.01 PFU/cell. Medium containing 5-FU or vehicle was added 30 min post-infection. After 24 h, cell culture supernatants were collected, and viral titers were determined by plaque assay. For each virus, titers were normalized to those following infection of DMSO-treated controls. Change in viral titer for nsp14 D330A and nsp14 G332A viruses were not statistically significant relative to WT MHV by one-way ANOVA. Error bars indicate SEM (n = 4).

(N.S. by One-way ANOVA). In contrast, the ExoN- virus displayed a concentration-dependent increase in 5-FU sensitivity. These results indicate that neither D330A nor G332A significantly alter ExoN activity during virus replication.

MHV nsp14 G332A is detected by and sensitive to the type I interferon-mediated innate immune response

Coronavirus RNA capping likely follows the conventional capping pathway, with nsp14 N7-methylation being a prerequisite for 2'O-methylation *in vitro* (Bouvet et al., 2010). Therefore, decreased nsp14 N7-MTase activity should reduce overall 2'O-methylation, thereby increasing virus sensitivity to exogenous type I IFN due to recognition by IFIT1 and MDA5 (Habjan et al., 2013; Menachery et al., 2014). To test this hypothesis, I pretreated DBT cells with murine IFN-β prior to infection with WT MHV, nsp16 D130A, an IFN-sensitive positive control due to ablated 2'O-MTase activity (Daffis et al., 2010; Habjan et al., 2013; Menachery et al., 2014; Smith et al., 2015), or nsp14 D330A or nsp14 G332A N7-MTase mutant viruses at an MOI of 1 PFU/cell. Cell culture supernatants were collected at either 12 or 24 h post-infection, and viral titers were determined by plaque assay. As expected, the nsp16 D130A virus was sensitive to IFN-β pretreatment (Figure 11A). The nsp14 G332A virus demonstrated a dose-dependent increase in IFN-β sensitivity, which became undetectable by plaque assay at IFN-β concentrations greater than 75 U/ml (Figure 11A). In contrast, nsp14 D330A virus displayed sensitivity to IFN-β comparable to WT MHV (Figure 11B). Because nsp14 D330A displayed replication kinetics and resistance to IFN-β pretreatment indistinguishable from WT MHV, it is likely that the D330A substitution does not significantly affect N7-MTase activity. Therefore, I focused solely on the nsp14 G332A mutant for the remainder of the experiments in this study.

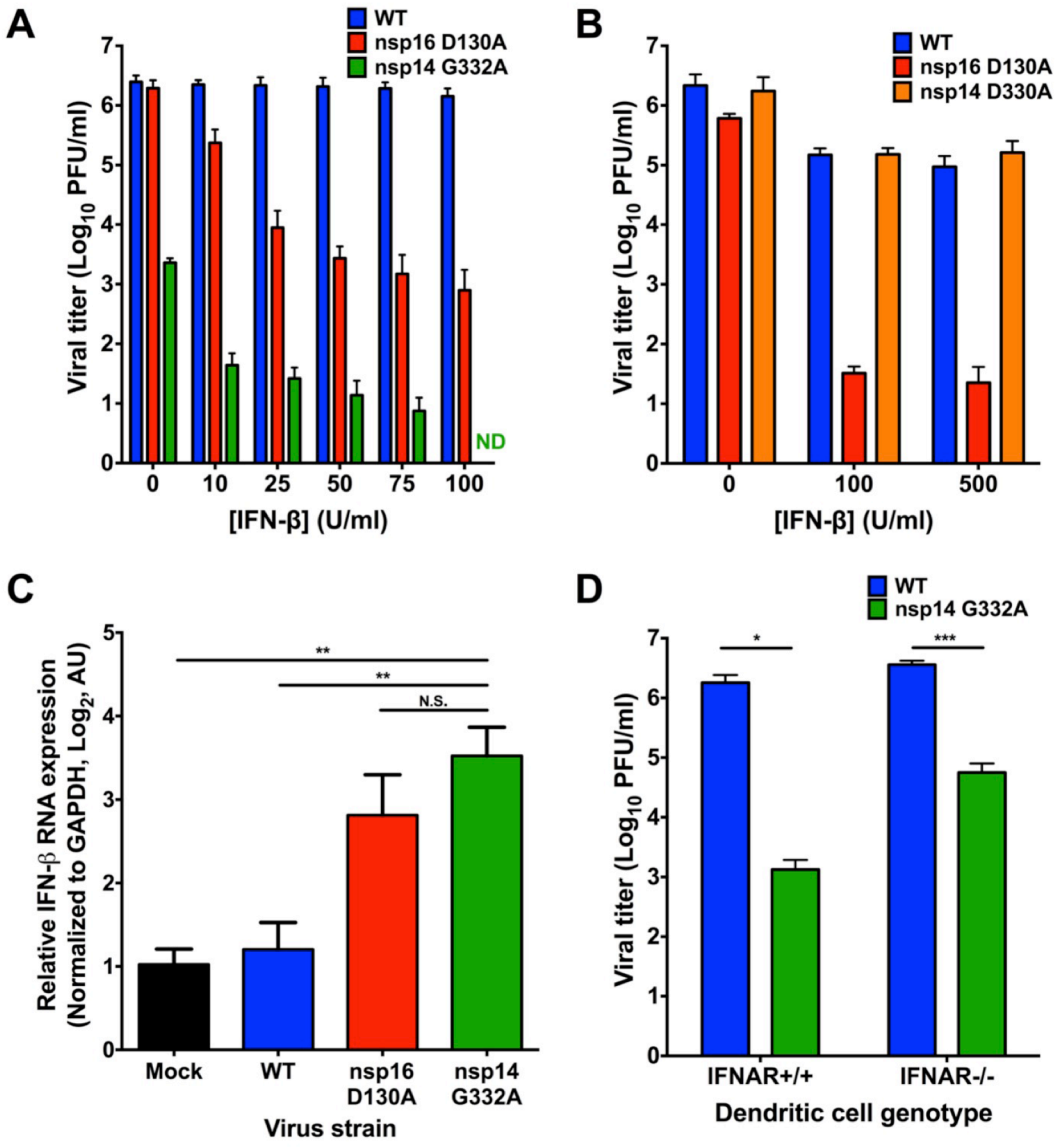

Figure 11. Nsp14 G332A virus exhibits increased induction of and sensitivity to IFN-β.

DBT cells were treated for 18 h with the indicated concentrations of mouse IFN-β. Cells were infected with WT, nsp16 D130A, or nsp14 G332A virus and incubated for 24 h (A) or infected with WT, nsp16 D130A, and nsp14 D330A virus and incubated for 12 h (B). Cell culture supernatants were collected, and viral titers were determined by plaque assay. For each panel, error bars represent SEM (n = 4). ND = not detectable. C) DBT cells were treated for 18 h with 10 U/ml mouse IFN-β. Cells were mock infected or infected with WT, nsp16 D130A, or nsp14 G332A virus at an MOI of 0.1 PFU/cell. At 12 h post-infection, cell lysates were harvested, total RNA extracted, cDNA generated, and IFN-β expression relative to GAPDH determined by qPCR. Error bars indicate SEM (n=9). N.S. = not significant, **, P <0.01 by Student's t-test. (D) BMDCs were infected with either WT or nsp14 G332A virus at an MOI of 0.01 PFU/cell. At 24 h post-infection, cell culture supernatants were collected, and viral titers were determined by plaque assay. Error bars indicate SEM (n = 6). *, P < 0.05, ***, P < 0.001 by Student's t-test.

In addition to an increased sensitivity to the effects of type I interferon pretreatment, coronaviruses lacking 2'O-MTase activity induce higher levels of IFN-β than WT (Habjan et al., 2013; Menachery et al., 2014; Züst et al., 2011). Therefore, to determine whether nsp14 G332A is also recognized by innate sensors and subsequently induces type I interferon expression, I pretreated DBT cells with 10 U/mL murine IFN-β for 18 h prior to infection with WT MHV, nsp16 D130A, nsp14 G332A viruses at an MOI of 0.1 PFU/cell. At 12 h post-infection, cell lysates were collected and the relative expression of IFN-β determined by qPCR (Figure 11C). As previously reported, infection with WT MHV marginally induced the expression of IFN-β (Roth-Cross et al., 2007) and infection with nsp16 D130A led to an up-regulation of IFN-β relative to mock infected cells (Habjan et al., 2013; Menachery et al., 2014; Züst et al., 2011). Furthermore, infection with nsp14 G332A led to a significant increase in the expression of IFN-β relative to mock and WT MHV infected cells. These data further suggest that nsp14 N7-MTase activity precedes nsp16 2'O-MTase activity and the absence of either activity results in innate detection of the virus leading to the induction of type I interferon gene expression.

To determine the effect that increased sensitivity to IFN-β has on nsp14 G332A replication, I tested whether nsp14 G332A virus replication could be rescued in BMDCs lacking the IFN alpha/beta receptor ($IFNAR^{-/-}$). $IFNAR^{-/-}$ cells lack the capacity to respond to type I IFNs and, thus, are incapable of mounting an effective IFN-dependent antiviral response (Katze et al., 2002). WT or $IFNAR^{-/-}$ BMDCs were infected with WT MHV or nsp14 G332A virus at an MOI of 0.01 PFU/cell, cell culture supernatants were collected 24 h post-infection, and viral titers were determined by plaque assay. Similar to experiments using DBT cells, nsp14 G332A virus replicated poorly in WT BMDCs relative to WT MHV (Figure 11D). Titers of nsp14 G332A

virus were increased by approximately 40-fold in IFNAR$^{-/-}$ BMDCs (5.6 x 10^4 PFU/ml) compared with the titers of this virus in WT BMDCs (1.3 x 10^3 PFU/ml). However, despite the increase in viral titers of nsp14 G332A in IFNAR$^{-/-}$ BMDCs, titers were not restored to the level of WT MHV in IFNAR$^{-/-}$ BMDCs (3.6 x 10^6 PFU/ml). These data suggest that the impaired replication capacity of nsp14 G332A virus is only in part attributable to IFN sensitivity and, instead, this virus may manifest a more general replication defect.

Nsp14 G332A genome translation is delayed during infection

Since the absence of the IFNAR was insufficient to restore nsp14 G332A replication, other mechanisms, such as decreased genome RNA stability or decreased viral genome translation, may contribute to the replication defect of this virus. 5' capping of cellular mRNAs serves several important functions, one of which is to increase RNA stability (Darnell, 1979; Decroly et al., 2011a). To test the stability of the nsp14 G332A genome upon entry into the cell, I infected DBT cells with WT MHV or nsp14 G332A virus at an MOI of 0.01 PFU/cell in the presence of vehicle (DMSO) or 100 μg/ml cycloheximide (CHX). CHX inhibits the translation of input viral genomes and prevents expression of the viral RNA dependent RNA polymerase, thereby allowing us to quantify the amount of coronavirus RNA present at later time-points relative to input. At the indicated times post-infection, cell lysates were collected, spiked with a known amount of *in vitro* transcribed *Renilla* luciferase, and the amount of viral RNA present relative to *Renilla* luciferase determined by qPCR (Figure 12). At each time-point post-infection for CHX treated samples, the level of nsp14 G332A RNA was similar to WT MHV, indicating that nsp14 G332A replication is not impaired due to decreased genome RNA stability.

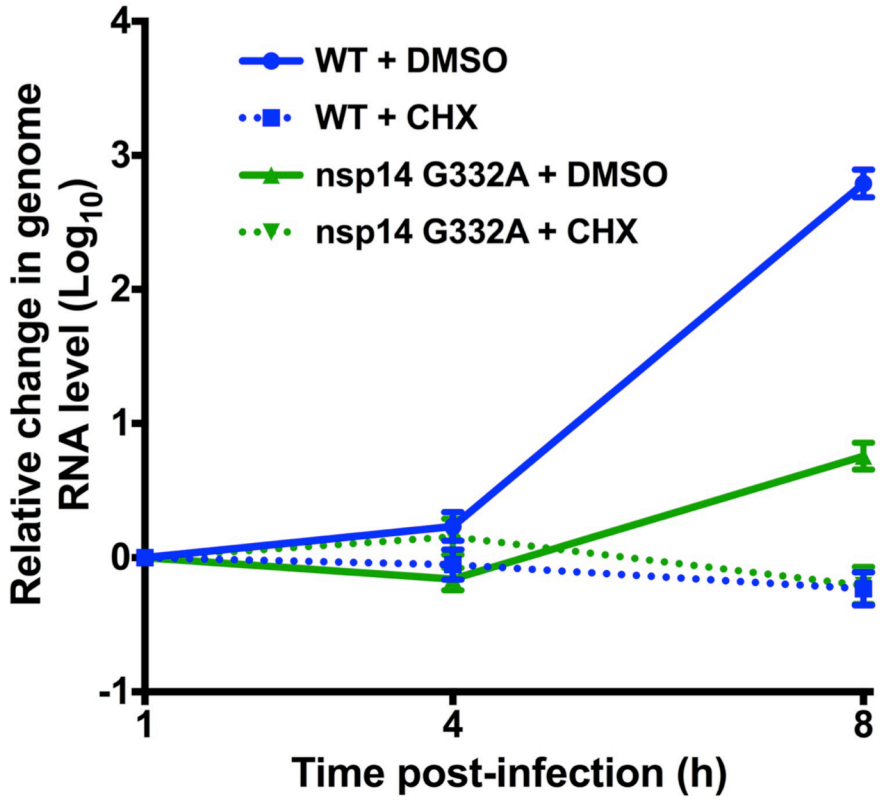

Figure 12. Nsp14 G332A genomic RNAs are stable.

DBT cells were infected with WT or nsp14 G332A virus at an MOI of 0.01 PFU/cell in the presence of vehicle (DMSO) or 100 µg/ml CHX. Cell lysates were harvested at indicated times post-infection, spiked with a known amount of *in vitro* transcribed *Renilla* luciferase RNA, and total RNA obtained by phenol/ chloroform extraction. cDNA was generated by RT-PCR and viral genome copies present relative to *Renilla* luciferase was determined by SYBR Green qPCR using MHV nsp10 and *Renilla* luciferase specific primers. Error bars indicate SEM (n=6).

In addition to serving as a precursor for 2'O-methylation, N7-methylated guanosine 5' caps are recognized by eIF4E and required for efficient translation of eukaryotic RNA (Decroly et al., 2011a; Gebauer et al., 2004). To determine whether the nsp14 G332A mutation impairs viral translation efficiency, I first engineered virus encoding FFL as an in-frame N-terminal fusion with MHV nsp2 (Freeman et al., 2014) in the ORF1a polyprotein coding sequence of the isogenic nsp14 G332A cloned genome. In this setting, FFL-nsp2 is the second protein translated from the input viral genome and becomes a reporter for viral protein translation. I infected DBT cells with either WT-FFL or nsp14 G332A-FFL virus at an MOI of 0.1 PFU/cell, and lysates were prepared at various intervals post-infection to quantify luciferase activity and viral genome RNA copy number. Luciferase activity accumulated more slowly following infection by nsp14 G332A-FFL virus relative to WT-FFL virus (Figure 13A). WT-FFL signal began to decline after 16 h due to destruction of the cell monolayer. In addition, levels of nsp14 G332A-FFL genomic RNA increased more slowly than those of WT-FFL (Figure 13B). By quantifying both luciferase activity and viral genome copies, I was able to calculate the kinetics of translation. To determine the rate of translation at each time-point post-infection, the ratio of luciferase activity to genome copies was determined using data from Figure 13A and 13B. The ratio of luciferase activity to genome copies for WT-FFL was highest at early times post-infection (Figure 13C). In contrast, the ratio of luciferase activity to genome copies was substantially less for the nsp14 G332A-FFL virus at early time-points post-infection compared to WT-FFL and failed to reach peak WT-FFL levels. These data demonstrate that nsp14 G332A-FFL virus requires more genomic RNA to achieve WT levels of FFL activity, consistent with decreased translation efficiency of the mutant virus genome. Therefore, I next determined whether nsp14 G332A-FFL and WT-FFL virions are equivalently infectious by measuring the specific infectivity of each virus from infected DBT

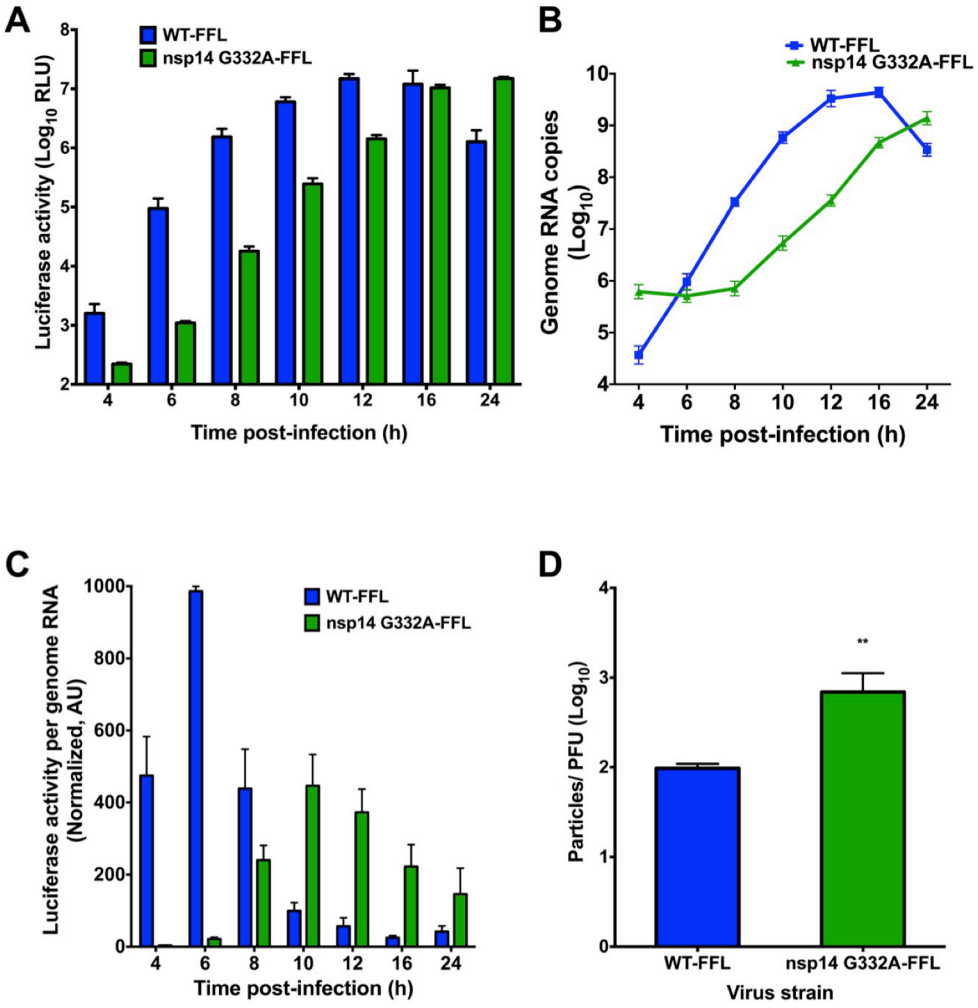

Figure 13. Nsp14 G332A genomic RNAs are translated with delayed kinetics during infection.

DBT cells were infected with either WT-FFL or nsp14 G332A-FFL virus at an MOI of 0.1 PFU/cell. At the times shown post-infection, cell culture supernatants were collected, and lysates were harvested and divided equally into two samples. For the first lysate sample, luciferase activity was quantified (A). For the remaining lysate sample, RNA was extracted, and genome RNA copies were quantified using real-time qRT-PCR with a standard curve and CoV nsp2-specific primers (B). (C) Translation of WT-FFL or nsp14 G332A-FFL genomes at the times shown post-infection as determined by luciferase activity per genome RNA copy number. Values were normalized to WT-FFL at 6 h post-infection. Error bars indicate SEM (n = 4). (D) Viral titers in cell culture supernatants from DBT cells infected with either WT-FFL or nsp14 G332A-FFL were determined by plaque assay and the number of genome RNA copies present in the input supernatant was determined by one-step real-time qRT-PCR. The particle to PFU ratio was calculated by dividing the number of genome RNA copies by viral titers. Error bars represent SEM (n = 4). **, $P < 0.01$ by Student's *t*-test.

cell culture supernatants. The ratio of nsp14 G332A-FFL particles per PFU was approximately 7-fold more than WT-FFL (Figure 13D). Thus, packaged nsp14 G332A-FFL genomes were less efficient at establishing infection than WT.

Nsp14 G332A-FFL genomes are translated less efficiently than WT-FFL genomes *in vitro*

To directly assess the translation capacity of nsp14 G332A-FFL virus genomes, I isolated genome RNA from purified virions. Increasing concentrations of genome RNAs were incubated with rabbit reticulocyte lysates at 30°C for 1.5 h, and luciferase activity was quantified (Figure 14A). Compared to WT-FFL genomes, FFL activity in the reticulocyte lysates was significantly reduced following incubation with nsp14 G332A-FFL genomes. In addition, I quantified the relative translation efficiency of equal amounts of WT-FFL and G332A-FFL genomic RNA over time. At all time points tested after 15 min, FFL activity was significantly reduced following incubation of reticulocyte lysates with nsp14 G332A-FFL genomes relative to WT-FFL genomes (Figure 14B). Taken together, my data indicate that the decreased replication capacity of the nsp14 G332A virus is attributable to IFN sensitivity and reduced translation efficiency.

Discussion

In this study, I engineered recombinant CoVs encoding alanine substitutions in the nsp14 N7-MTase at the SAM-binding site residues, D330 and G332. I found that the N7-MTase SAM-binding site mutants are viable and yield drastically different phenotypes during replication. Specifically, MHV nsp14 D330A virus replicates indistinguishably from WT MHV in all assays conducted, despite the requirement of this residue for SAM binding *in vitro* (Chen et al., 2013).

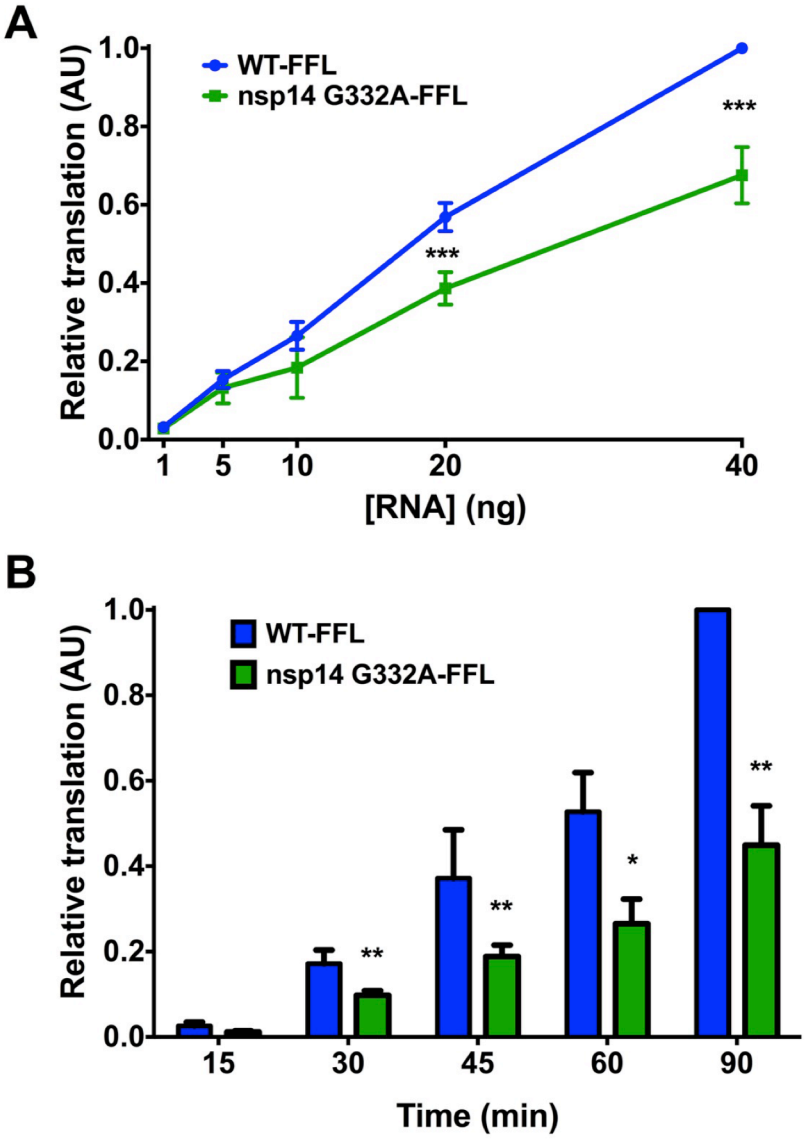

Figure 14. Purified nsp14 G332A genomic RNA is translated at lower efficiency *in vitro*.

BHK-R cells were infected at an MOI of 0.001 PFU/cell with either WT-FFL or nsp14 G332A-FFL virus. Supernatants were harvested and clarified, and virions were collected by ultracentrifugation. Virion pellets were resuspended, TRIzol was added, and virion RNAs were purified using phenol/chloroform phase separation. Genome RNA copies were quantified using one-step real-time qRT-PCR with a standard curve and CoV nsp2-specific primers. (A) The concentrations of WT-FFL or G332A-FFL genomic RNAs shown were translated *in vitro* at 30°C for 1.5 h, and luciferase activity was quantified. Translation values are relative to WT-FFL genomic RNA at 40 ng. Error bars represent SEM (n = 4). ***, $P < 0.001$ by Student's *t*-test. (B) Equivalent numbers of either WT-FFL or nsp14 G332A-FFL genomic RNAs were translated *in vitro* for the times shown, and luciferase activity was quantified. Error bars represent SEM (n = 6). *, $P < 0.05$, **, $P < 0.01$ by Student's *t*-test.

There is precedent for such a contradiction. A previous study using vesicular stomatitis virus identified a SAM-binding residue within the L protein (G1674) that, when altered, does not affect viral replication or N7-MTase activity (Li et al., 2005). The structure of the SARS-CoV nsp10-nsp14 complex reveals that D331 (D330 in MHV) is in close proximity to the SAM-binding site, but only G333 (G332 in MHV) directly contacts SAM (Ma et al., 2015). Since *in vitro* N7-MTase activity was assessed only for a SARS-CoV nsp14 D331A/G333A double mutant, it is not clear whether nsp14 D331 was required for N7-MTase activity in this study (Ma et al., 2015). However, a previous study using both *in vitro* functional assays and yeast complementation reported that SARS-CoV nsp14 D331 is essential for N7-MTase activity (Chen et al., 2013). My study examined nsp14 N7-MTase in the context of viral replication. A potential difference between my work and previous studies of the CoV nsp14 N7-MTase is the use of MHV versus SARS-CoV proteins, respectively. Purified MHV nsp14 N7-MTase is not available in my lab for biochemical studies. However, my results will guide future experiments when such a system is established. During my study, I attempted to recover SARS-CoV nsp14 D331A, I332A, and G333A N7-MTase mutant viruses. However, viable viruses were not recovered after at least three attempts for each mutant. Nonetheless, the high conservation of the SAM-binding residues makes it unlikely that the differences observed between my work and previous biochemical studies are due to profoundly different N7-MTase catalytic mechanisms.

In contrast to nsp14 D330A virus, nsp14 G332A virus replicated with delayed kinetics and reached peak titers that were 1000-fold less than those of WT MHV. CoV nsp14 has two domains: an N-terminal ExoN domain and a C-terminal N7-MTase domain. Mutations at D331 in SARS-CoV nsp14 do not affect ExoN activity *in vitro* (Chen et al., 2009; 2013). However, the

effect of altering residue G333 (G332 in MHV) on ExoN activity has not been reported using any system. It is unlikely that the G332A mutation in MHV nsp14 influences ExoN activity, as nsp14 G332A demonstrated WT-like sensitivity to the RNA mutagen, 5-FU. Even a subtle alteration in ExoN activity should result in a detectable change in 5-FU sensitivity, particularly since I performed the assay using low-MOI conditions, which would increase mutagen incorporation during multi-step replication (Smith et al., 2013; 2015). The lack of enhanced 5-FU sensitivity for the nsp14 D330A and nsp14 G332A viruses indicates that mutations at these SAM-binding residues do not significantly dampen ExoN activity during virus replication. Additionally, since nsp14 G332A is resistant to 5-FU treatment, it is unlikely that the G332A phenotype is due to nsp14 instability or degradation.

My data indicate that impaired replication of nsp14 G332A virus is likely due to a combination of factors, including increased detection by innate immune sensors and decreased translation efficiency of viral RNA. Binding of type I IFNs to the IFN receptor leads to expression of many IFN-stimulated genes and ultimately the establishment of an antiviral state (Schneider et al., 2014). Coronavirus RNAs lacking 2'O-methylation are sensed by IFIT1, which is one of the most highly up-regulated IFN-stimulated genes following IFN induction (Diamond and Farzan, 2012). While nsp14 D330A displayed WT-like sensitivity to pretreatment with IFN-β, nsp14 G332A virus did not replicate following IFN-β pretreatment with doses greater than 75 U/ml. However, initial titers were lower for nsp14 G332A. Thus, the concentration-dependent change in viral titer following IFN-β pretreatment was similar to the nsp16 D130A virus. The IFN-β sensitivity of nsp14 G332A likely results from a reduction in 2'O-methylation of viral RNA due to impaired N7-MTase activity. This hypothesis is supported by my data showing that infection

with either nsp16 D130A or nsp14 G332A virus results in the induction of IFN-β gene expression. In addition, decreased N7-MTase activity due to the G332A mutation results in the delayed translation and decreased translation efficiency observed during viral replication and *in vitro* assays. Due to the highly impaired replication capacity of the nsp14 G332A virus, it has not been possible to directly determine the cap methylation status of nsp14 G332A virus genomes. Nevertheless, my results are consistent with functions of the N7-methylated 5'cap in promoting both viral and cellular translation (Filipowicz et al., 1976; Marcotrigiano et al., 1997; Schibler and Perry, 1977). Decreased translation efficiency also could explain the lower specific infectivity observed for nsp14 G332A virus. Furthermore, it is possible that the delayed translation kinetics of nsp14 G332A genomic RNA increases innate sensing of the virus by delaying the early expression of multiple CoV IFN antagonists upon entry, resulting in decreased replication capacity.

My data provide additional support for a sequential model of CoV RNA capping wherein N7-methylation precedes 2'O-methylation. In addition, my studies suggest that small-molecule inhibitors of the CoV nsp14 N7-MTase would impair virus replication and provide a pathogen-associated molecular pattern that would be quickly recognized by the innate immune response. Given the conservation of these enzymes, such inhibitors may have activity against diverse groups of coronaviruses.

CHAPTER III

MURINE HEPATITIS VIRUS NSP14 EXORIBONUCLEASE ACTIVITY IS REQUIRED FOR RESISTANCE TO INNATE IMMUNITY

Introduction

Coronaviruses (CoVs) encode numerous innate immune antagonists that counteract the host innate immune response to facilitate efficient viral replication. CoV nsp14 3'-to-5' exoribonuclease (ExoN) activity performs a proofreading function and is required for high-fidelity replication (Bouvet et al., 2012; Eckerle et al., 2007; Minskaia et al., 2006; Smith et al., 2013). Further, nsp14 ExoN activity has a preference for dsRNA (Minskaia et al., 2006). The CoV nsp14 ExoN is a member of the DE-D-Dh superfamily of DNA and RNA exonucleases, so named for the three motifs of four active site residues (Minskaia et al., 2006). *Betacoronaviruses* SARS-CoV and MHV expressing engineered, ExoN-inactivating substitutions at active site residues in Motif I (DE→AA) [ExoN(-)] demonstrate increased mutation frequencies and are profoundly sensitive to inhibition by RNA mutagens (Eckerle et al., 2007; Smith et al., 2013). Additionally, SARS-CoV ExoN(-) virus is attenuated *in vivo* (Graham et al., 2012). Outside of the order *Nidovirales*, the only other known RNA virus-encoded 3'-to-5' exoribonucleases are found in the *Arenaviridae* family of viruses. Lassa fever virus nucleoprotein ExoN is not thought to participate in fidelity regulation, but rather it participates in immune evasion by degrading dsRNA and thereby prevents antigen-presenting cell-mediated NK cell activation (Hastie et al., 2011; Qi et al., 2010; Russier et al., 2014).

Prior to this dissertation research, CoV nsp14 had not been investigated as an innate immune antagonist. In Chapter II, I demonstrated CoV nsp14 N7-MTase activity is essential for efficient translation of the viral genome and preventing innate detection (Case et al., 2016). In this chapter, I demonstrate the CoV ExoN activity is required for resistance to the innate immune response. Recently, in the *Alphacoronavirus* transmissible gastroenteritis virus (TGEV), a mutation in the nsp14 ExoN zinc finger was shown to generate lower levels of dsRNA compared to wild-type (WT) TGEV. However, in that study viruses with mutations in ExoN active site motifs were non-viable and therefore, could not be directly tested for effects on innate immunity (Becares et al., 2016). Therefore, I tested the hypothesis that CoV ExoN may also function to antagonize the innate immune response. I demonstrate that viruses lacking ExoN activity are more sensitive to the effects of IFN pretreatment than WT-MHV. In addition, for viruses lacking ExoN activity, replication is restricted in wild-type bone marrow derived macrophages (B6, BMMs) but is restored in interferon alpha/beta receptor deficient (IFNAR-/-) BMMs. Despite an increased sensitivity to the effects of IFN treatment, MHV ExoN mutants fail to induce detectable IFN-β gene expression or RNase L-mediated ribosomal RNA (rRNA) degradation and only a limited decrease in viral RNA accumulation is observed. Finally, I demonstrate that ExoN(-) virus replicated in the presence of an IFN-β-mediated antiviral state has both a decreased specific infectivity and decreased relative fitness compared to untreated ExoN(-) virus. Thus, nsp14 ExoN appears to block or correct the restriction of MHV infection by an IFN-mediated mechanism that may involve damaging nascent viral RNA and affecting subsequent infectivity.

I performed all experiments and final analyses for the data presented in this chapter with exceptions as noted below. The coauthors provided the following contributions: Xiaotao Lu and I generated the ExoN(-) P250 virus, Nicole Sexton and Kevin Graepel generated the ExoN(-) silent virus stocks used for the co-infection assay, and Clint Smith developed the Taqman probes used in viral specific infectivity and co-infection assays. For some replicates, Ruth Elliott generated the BMMs and performed viral replication curves. For other replicates involving BMMs, Henry Li assisted me in generating the BMMs, and I performed the replication curves.

Viruses lacking ExoN activity are more sensitive to the effects of IFN-β than WT-MHV

Binding of type I interferon to the IFNAR receptor on the cell surface leads to a Jak/STAT signaling cascade that ultimately results in the up-regulation and expression of hundreds of antiviral ISGs (Schneider et al., 2014). In addition, WT-MHV replication has been shown to be relatively resistant to the effects of IFN (Rose et al., 2010; Rose and Weiss, 2009; Roth-Cross et al., 2007). To determine whether the ExoN activity of MHV nsp14 was required for resistance to IFN, I pretreated murine delayed brain tumor (DBT) cells with increasing concentrations of mouse IFN-β for 18 h prior to infecting with WT-MHV or ExoN(-) virus at a multiplicity of infection (MOI) of 1 plaque-forming unit (PFU) per cell (Figure 15A). In response to IFN-β pretreatment, WT-MHV viral titer decreased by approximately 1 $\log_{10}$ as previously reported (Roth-Cross et al., 2007). In contrast, ExoN(-) viral titer demonstrated a dose-dependent decrease and resulted in an approximately 3 $\log_{10}$ decrease in viral titer relative to untreated ExoN(-) viral titers. The ExoN activity of nsp14 is conferred by active site residues present in 3 different motifs within the ExoN domain (Ma et al., 2015). Therefore, to determine whether the observed

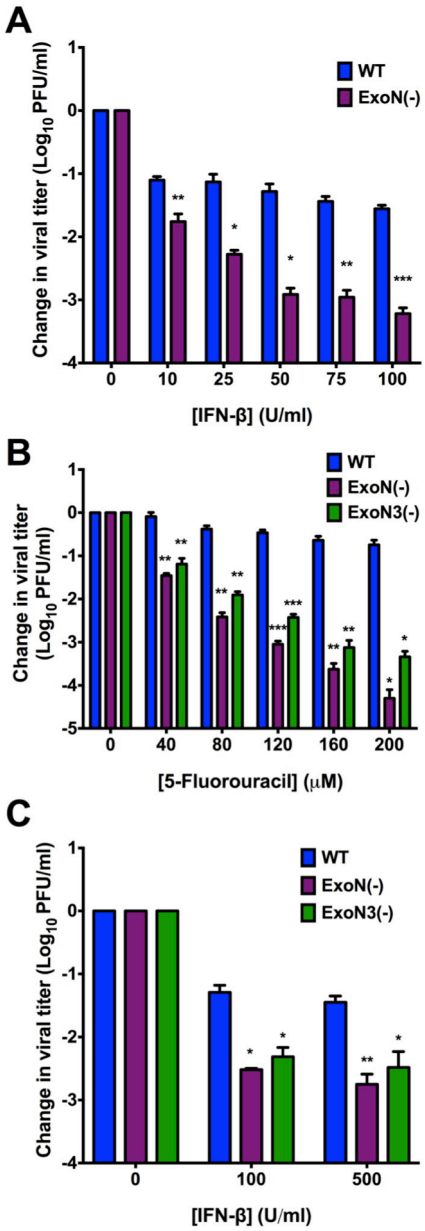

Figure 15. Viruses lacking ExoN activity are sensitive to IFN-β pretreatment.

(A) DBT cells were pretreated with the indicated concentrations of mouse IFN-β for 18 h and then infected with WT-MHV or ExoN(-) virus (A) or WT, ExoN(-), or ExoN3(-) virus (C) at an MOI of 1 PFU/cell. At 12 h post-infection, cell culture supernatants were collected and the viral titers present determined by plaque assay. (B) DBT cells were pretreated with the indicated concentrations of 5-FU for 30 min. Following pretreatment, cells were infected with WT, ExoN(-), or ExoN3(-) virus at an MOI of 1 PFU/cell for 45 min., inocula were removed, and fresh medium containing vehicle or the appropriate concentration of 5-FU were added. Cell culture supernatants were harvested 12 h post-infection and viral titers were determined by plaque assay. For each panel, the change in viral titer was calculated by dividing viral titers following the indicated treatment by the untreated controls and error bars indicate SEM (n = 4). Statistical significance compared to WT-MHV is denoted and was determined by Student's *t* –test. *, $P < 0.05$, **$P < 0.01$, *** $P < 0.001$.

increase in sensitivity to IFN-β pretreatment for ExoN(-) virus in Figure 15A was due specifically to the absence of ExoN activity in nsp14, I engineered and recovered a virus encoding only an aspartic acid to alanine substitution in Motif III [ExoN3(-)]. Previously, we have demonstrated that viruses lacking ExoN activity have decreased replication fidelity and are sensitive to the RNA mutagen 5-fluorouracil (5-FU) (Smith et al., 2013). Hence, 5-FU sensitivity is an *in vitro* indicator of ExoN activity. Therefore, first, I tested whether ExoN3(-) and ExoN(-) demonstrated similar sensitivity to 5-FU to ensure that the ExoN activity of ExoN3(-) virus had been ablated. Similar to ExoN(-), ExoN3(-) viral replication in cells treated with increasing concentrations of 5-FU demonstrated a dose-dependent decrease in viral titer relative to vehicle treated cells (Figure 15B). Further, ExoN(-) and ExoN3(-) displayed similar sensitivities to pretreatment with 100 or 500 U/mL IFN-β following infection at an MOI of 1 PFU/cell (Figure 15C). Thus, these data suggest nsp14 ExoN activity is required for resistance to the effects of IFN-β pretreatment.

Increased replication capacity does not confer resistance to the effects of IFN-β pretreatment for viruses lacking ExoN activity

ExoN(-) virus demonstrates an approximately 2 h delay in exponential replication and a 1 $\log_{10}$ decrease in peak titer relative to WT-MHV (Eckerle et al., 2007). Therefore, I tested whether the IFN sensitivity phenotype observed for ExoN(-) and ExoN3(-) viruses is due to the decreased replication capacity of these viruses. To do so, I utilized an ExoN(-) virus developed by our lab that has been blindly passaged in DBT cells for 250 passages [ExoN(-) P250]. Over the course of passage, the ExoN(-) P250 virus did not revert the engineered ExoN(-) (DE→AA) mutations. In addition, ExoN(-) P250 accumulated 171 total mutations (74 non-synonymous mutations) across

the genome (Graepel et al., 2017). The replication capacity of the resulting ExoN(-) P250 virus exceeds that of WT-MHV (Figure 16A). However, despite increased replication capacity, ExoN(-) P250 demonstrated similar sensitivity to IFN-β pretreatment as ExoN(-) virus (Figure 16A and B). Hence, the IFN-β sensitivity phenotype of viruses lacking ExoN activity is not dependent on viral replication capacity but instead, is directly associated with a specific function of nsp14 ExoN that is required for efficient replication in the presence of an IFN-β-mediated antiviral state.

Nsp14 ExoN activity is required for replication in wild-type B6 BMMs

I next wanted to test whether ExoN activity was required for replication in primary innate immune cells, such as BMMs. Replication of WT-MHV in primary BMMs is well described, and data suggest that wild-type B6 BMMs (B6) express many PRRs and ISGs at a higher basal level than many mouse cell lines (Rose and Weiss, 2009; Zhao et al., 2013; 2011). In contrast, BMMs lacking the IFNAR receptor (IFNAR-/-) have lower basal and expressed levels of ISGs; thus, making B6 and IFNAR-/- BMMs excellent cell types for interrogating the role of ExoN activity on viral replication and antagonism of the innate immune response (Zhao et al., 2011). BMMs from B6 or IFNAR-/- mice were generated and infected with WT-MHV or ExoN(-) virus at an MOI of 1 PFU/cell. Samples were harvested at the indicated time-points, and viral titers were determined by plaque assay (Figure 17A). WT-MHV replication increased gradually in both B6 and IFNAR-/- BMMs at each time-point post-infection. In contrast, ExoN(-) virus replication in B6 BMMs was only detectable at 6 and 9 h post-infection. However, when IFNAR-/- BMMs were infected with ExoN(-) virus, viral titers were partially restored and increased at each time-point post-infection. To further test the replication of viruses lacking ExoN activity and the effect

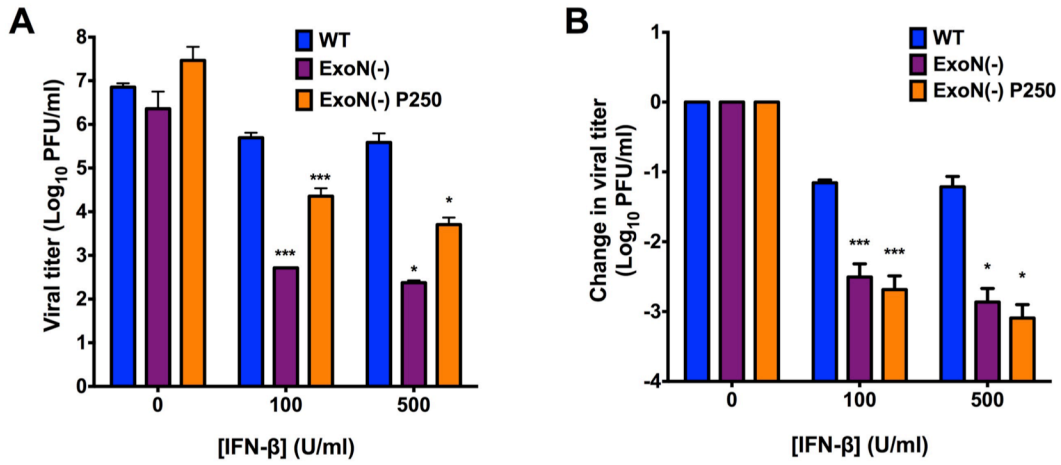

Figure 16. Increased replication capacity does not restore virus resistance to IFN-β.

DBT cells were pretreated with the indicated concentrations of mouse IFN-β for 18 h and then infected with WT, ExoN(-), or ExoN(-) P250 virus at an MOI of 1 PFU/cell. At 12 h post-infection, cell culture supernatants were collected and the viral titers present determined by plaque assay. Raw viral titers (A) or the change in viral titers relative to untreated controls (B) are reported. Error bars indicate SEM (n = 4). Statistical significance compared to WT-MHV is denoted and was determined by Student's *t* – test. *, $P < 0.05$, **$P < 0.01$, *** $P < 0.001$.

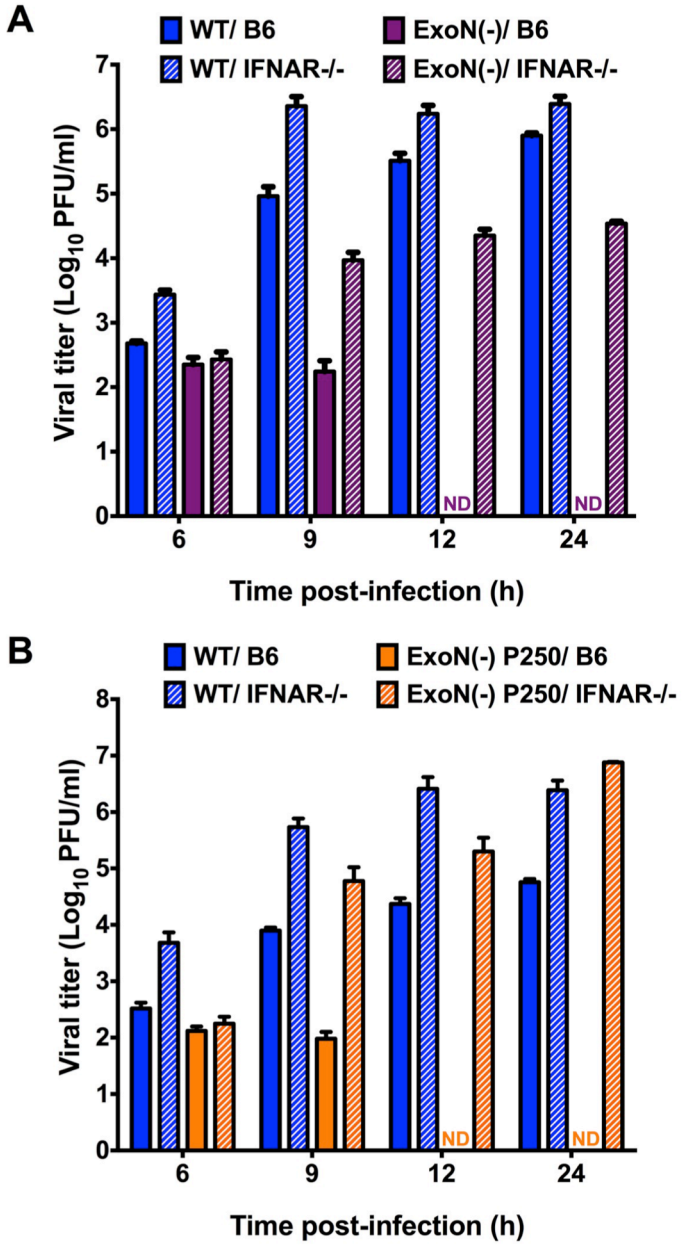

Figure 17. Replication of viruses lacking ExoN activity is restricted in wild-type B6 BMMs.

B6 BMMs or IFNAR-/- BMMs were infected with WT-MHV or ExoN(-) virus (A) or WT-MHV or ExoN(-) P250 virus (B) at an MOI of 1 PFU/cell. At the indicated times post-infection, cell culture supernatant aliquots were collected and the viral titers present were determined by plaque assay. For each panel, error bars represent SEM (n = 6 to 7). ND = not detectable.

of an increased replication capacity in BMMs, B6 and IFNAR-/- BMMs were infected with WT-MHV or ExoN(-) P250 viruses at an MOI of 1 PFU/cell. Similar to the results shown in Figure 17A, WT-MHV viral titers steadily increased in B6 and IFNAR-/- BMMs at each time-point post-infection (Figure 17B). However, similar to ExoN(-) virus, ExoN(-) P250 virus replication in B6 BMMs was restricted and not detected beyond 9 h post-infection. In addition, ExoN(-) P250 virus replication in IFNAR-/- BMMs was restored to similar levels as WT-MHV. These data show that ExoN activity is required for replication in B6 BMMs. Further, they suggest that restriction of ExoN(-) or ExoN(-) P250 is mediated by a gene or genes down-stream of IFNAR.

Loss of ExoN activity does not result in the induction of IFN and replication is not rescued by RNase L/PKR deficiency

Upon detection of a pathogen-associated molecular pattern (PAMP) by innate sensors, signaling pathways lead to transcription factor activation and nuclear translocation resulting in expression of IFN-β mRNA (Schneider et al., 2014). WT-MHV is well known to prevent or delay the induction of IFN expression (Rose et al., 2010; Rose and Weiss, 2009). However, ExoN activity may help prevent the detection of a PAMP, namely dsRNA, which has been shown to be increased in an nsp15 EndoU mutant (Kindler et al., 2017). Therefore, to determine whether the loss of ExoN activity resulted in the generation and subsequent detection of a PAMP, I determined the level of IFN-β gene expression in DBT cells infected with mock, WT-MHV, ExoN(-), or ExoN(-) P250 virus at an MOI of 0.1 PFU/ cell (Figure 18A). In addition, I infected DBT cells with Sendai virus (SenV), a positive control and a potent inducer of IFN, at an MOI of 200 hemagglutination units/ml. SenV infection resulted in IFN expression by 3 h post-infection and peaked between 9 and 12 h post-infection prior to returning nearly to mock infected levels

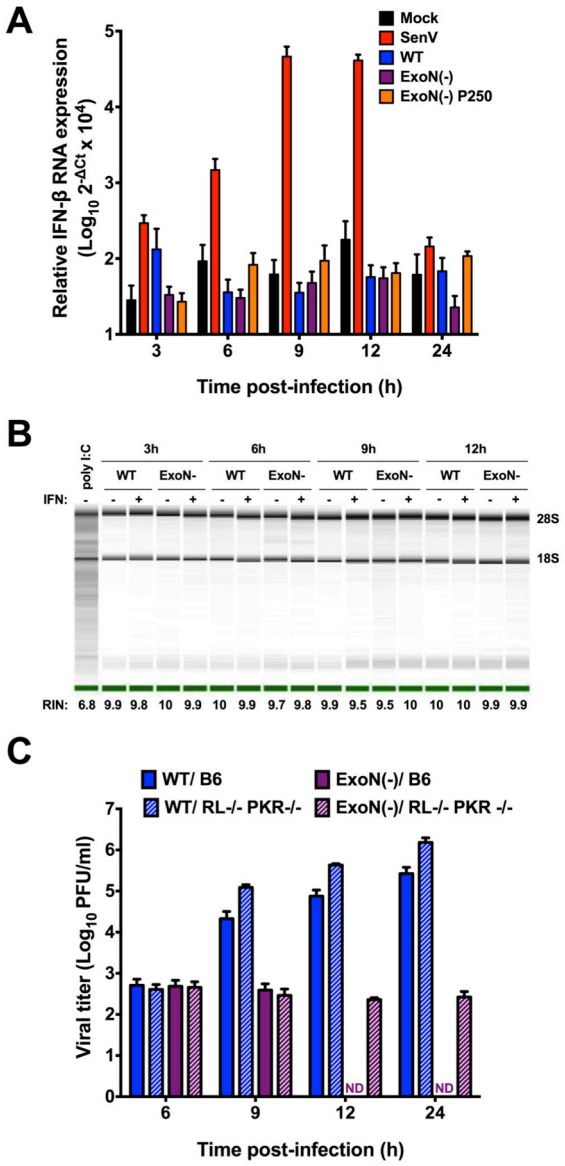

Figure 18. Loss of ExoN activity does not result in the generation of a detectable PAMP.

(A) DBT cells were infected with mock, WT, ExoN(-) or ExoN(-) P250 virus at an MOI of 0.1 PFU/cell or infected with Sendai virus at an MOI of 200 HA units/ml. At the indicated times post-infection, cell culture supernatants were removed, cell lysates were harvested, total RNA was extracted, cDNA was generated, and IFN-β expression relative to GAPDH was determined by qPCR. Error bars indicate SEM (n=4). (B) DBT cells were pretreated for 18 h with 0 or 50U/ml mouse IFN-β and subsequently infected with WT-MHV or ExoN(-) virus or transfected with 25μg/ml poly I:C. At the indicated times post-infection, cell culture supernatants were removed, cell lysates harvested, and total RNA extracted. rRNA integrity was assessed using an Agilent Bioanlyzer. One representative image is shown for each sample from 2 independent experiments. Images spliced for labeling purposes. The averaged RNA integrity values for each condition are reported. (C) B6 BMMs or RL -/- / PKR -/- BMMs were infected with WT-MHV or ExoN(-) virus at an MOI of 1 PFU/cell. At the indicated times post-infection, cell culture supernatant aliquots were collected and the viral titers present were determined by plaque assay. Error bars represent SEM (n = 5). ND = not detectable.

by 24 h post-infection, demonstrating that DBT cells are capable of expressing IFN-β. In contrast, no CoV infection, regardless of whether intact ExoN activity was present, resulted in IFN-β gene expression over mock-infected cells with the exception of WT-MHV at 3 h post-infection. Further, upon detection of dsRNA by OAS and subsequent activation of RNase L, viral and cellular RNAs are degraded as an antiviral mechanism (Schneider et al., 2014). To determine whether infection with ExoN(-) virus results in increased dsRNA levels that activate the OAS/RNase L pathway, DBT cells were pretreated with 0 or 50 U/ml mouse IFN-β and infected with WT-MHV or ExoN(-) virus at an MOI of 1 PFU/cell. As a positive control, DBT cells were transfected with 25μg/ml poly I:C, a dsRNA surrogate. At the indicated times post-infection, cell lysates were harvested, total RNA extracted, and the integrity of cellular rRNA determined using a bioanalyzer (Figure 18B). Transfection of DBT cells with poly I:C resulted in rRNA degradation, whereas, infection of DBT cells with WT-MHV or ExoN(-) virus did not result in rRNA degradation under any tested conditions. Lastly, when B6 or RNase L -/- / PKR -/- BMMs (RL -/- / PKR -/-) were infected with ExoN(-)virus, replication was restricted (Figure 18C). In contrast to infection of B6 BMMs, ExoN(-) viral titer from RL -/- / PKR -/- BMMs was detectable at 12 and 24 h post-infection. However, viral yield was minimal. These data suggest that loss of nsp14 ExoN activity does not lead to the transcriptional activation of IFN-β or a notable dsRNA sensor such as OAS/RNase L during infection of DBT cells. In addition, BMMs deficient in the antiviral effectors RNase L and PKR were not sufficient to restore ExoN(-) viral replication.

IFN treatment does not substantially alter ExoN(-) viral RNA accumulation or particle release

Since ExoN activity is required for resistance to IFN but had no effect on IFN induction, I sought to discern the stage of viral replication that was restricted by IFN-β treatment. To determine the effect of IFN-β pretreatment on viral RNA accumulation, DBT cells were pretreated with 0 or 100 U/ml mouse IFN-β for 18 h and subsequently infected with WT-MHV or ExoN(-) virus at an MOI of 1 PFU/cell. At the indicated times post-infection, the number of genomic RNA copies present were determined by one-step RT-qPCR. IFN-β pretreatment had minimal effect on the accumulation of WT-MHV genomic RNA (Figure 19A). Whereas ExoN(-) genomic RNA accumulation is delayed relative to WT-MHV (Eckerle et al., 2007), pretreatment with IFN-β did not substantially decrease ExoN(-) genomic RNA levels (Figure 19A). In addition, I determined the effects of IFN-β pretreatment on the levels of subgenomic viral RNA. For both WT-MHV and ExoN(-) viruses, IFN-β pretreatment did not substantially reduce subgenomic RNA levels at any time-point (Figure 19B). These data indicate that IFN pretreatment did not result in the gross degradation or inhibition of ExoN(-) viral RNA accumulation. While slight reductions in viral RNA could explain a small portion of the IFN phenotype, these data suggest that decreased replication or transcription is not the primary driver of ExoN(-) IFN sensitivity.

Since pretreatment of DBT cells with IFN-β does not grossly alter ExoN(-) viral RNA accumulation but does reduce ExoN(-) viral titers, I sought to determine whether IFN pretreatment prior to infection resulted in a measurable difference in the number of viral particles released from WT-MHV or ExoN(-) infected cells. DBT cells were pretreated with 0 or 100 U/ml mouse IFN-β for 18 h and subsequently infected with WT-MHV or ExoN(-) virus at an MOI of 1 PFU/cell. At 12 h post-infection, cell culture supernatants were harvested and an

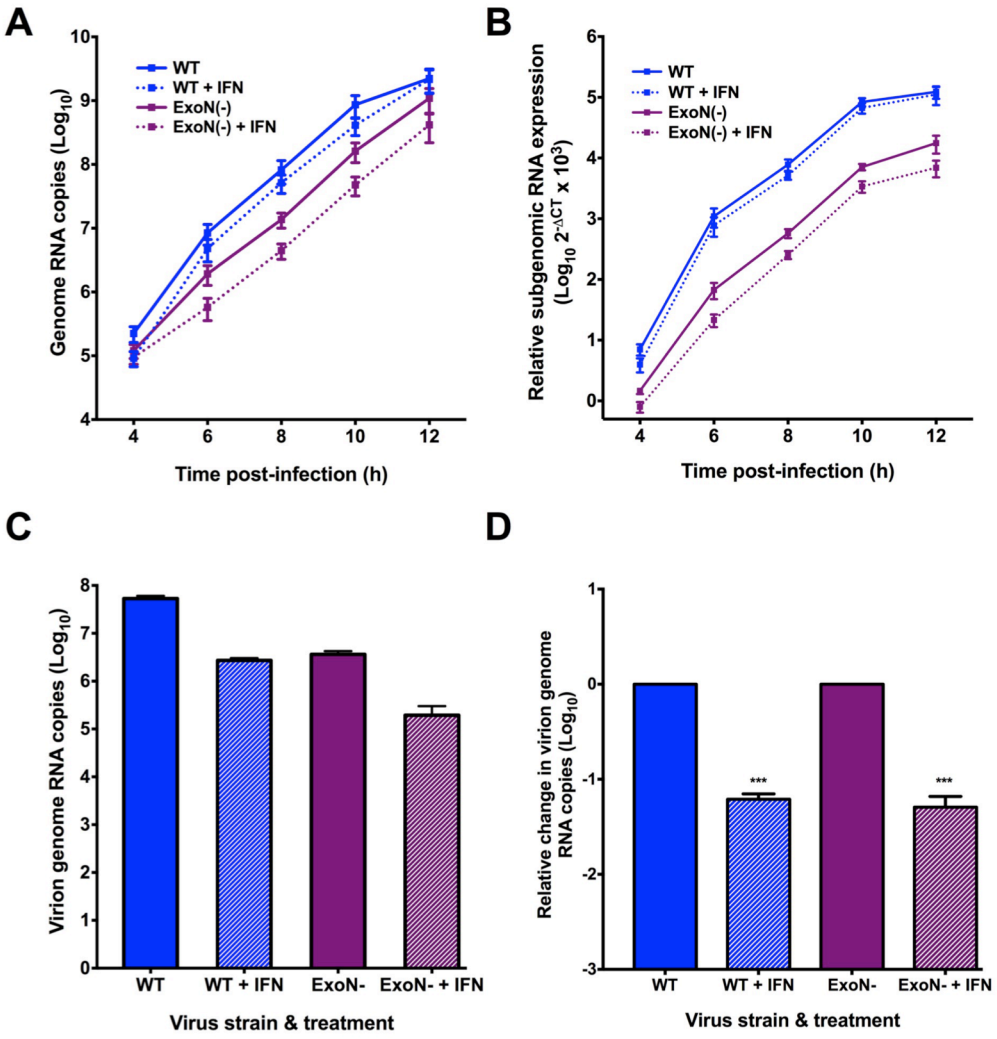

Figure 19. ExoN(-) viral RNA accumulation and particle release is marginally affected by IFN-β pretreatment.

DBT cells were pretreated with 0 or 100U/ml mouse IFN-β for 18 h and subsequently infected with WT-MHV or ExoN(-) virus at an MOI of 1 PFU/cell. At the indicated times post-infection, total cell lysates were harvested and RNA was extracted. The viral genomic RNA copies present relative to an RNA standard were determined by one-step RT-qPCR (A) or cDNA was generated and the subgenomic RNA copies relative to GAPDH were determined by qPCR (B). For each panel (A and B), error bars represent SEM (n= 6 to 9). DBT cells were pretreated with 0 or 100U/ml mouse IFN-β for 18 h and subsequently infected with WT-MHV or ExoN(-) virus at an MOI of 1 PFU/cell. At 12 h post-infection, cell culture supernatants were collected. Equivalent volumes of cell culture supernatant for each sample were divided into two samples. For the first cell culture supernatant sample, total RNA was extracted and the number of virion genome RNA copies present (particles) was determined by one-step RT-qPCR (C) or reported as the change in virion genome RNA copies (D). Error bars represent SEM (n = 13 to 15). Statistical significance compared to untreated WT-MHV or ExoN(-) infection, respectively, is denoted and was determined by Student's *t* –test. *** $P < 0.001$.

aliquot of two equal volumes were removed. From the first volume of each sample, RNA was extracted and used to perform one-step RT-qPCR to determine the number of genome RNAs present, and hence, the number of genome RNA containing particles present in the given volume of supernatant (Figure 19C). The second volume was saved for a plaque assay as described below. Pretreatment of cells with IFN-β resulted in approximately a 1 $\log_{10}$ decrease in the number of supernatant viral particles for both WT-MHV and ExoN(-) viruses compared to the number of supernatant viral particles from untreated cells, demonstrating that IFN pretreatment affects the release of WT-MHV and ExoN(-) virus particles equally (Figure 19D). Thus, these data suggest that IFN pretreatment does not restrict the primary replication of viruses lacking ExoN activity, but rather, renders them potentially inadequate for subsequent infection.

ExoN(-) virus progeny generated in the presence of an IFN-induced antiviral state have decreased specific infectivity and fitness upon subsequent infection

While many ISGs antagonize viral replication, some could alter the infectivity of progeny particles (Neil and Bieniasz, 2009; Tomaselli et al., 2015). To test whether IFN pretreatment affected the infectivity of ExoN(-) viral particles, the remaining cell culture supernatant volume described above was used to perform a plaque assay to determine the number of PFUs present (data not shown). Using the number of particles determined in Figure 19C and the number of PFUs present in an equivalent volume; I calculated the specific infectivity, or particle-to-PFU ratio, of each virus generated under each condition (Figure 20A). Regardless of IFN-β pretreatment during the initial infection, the specific infectivity of WT-MHV was approximately 10 particles per 1 PFU upon subsequent infection. Infection of untreated DBT cells with ExoN(-) virus resulted in a similar particle to PFU ratio as WT-MHV during subsequent infection. In

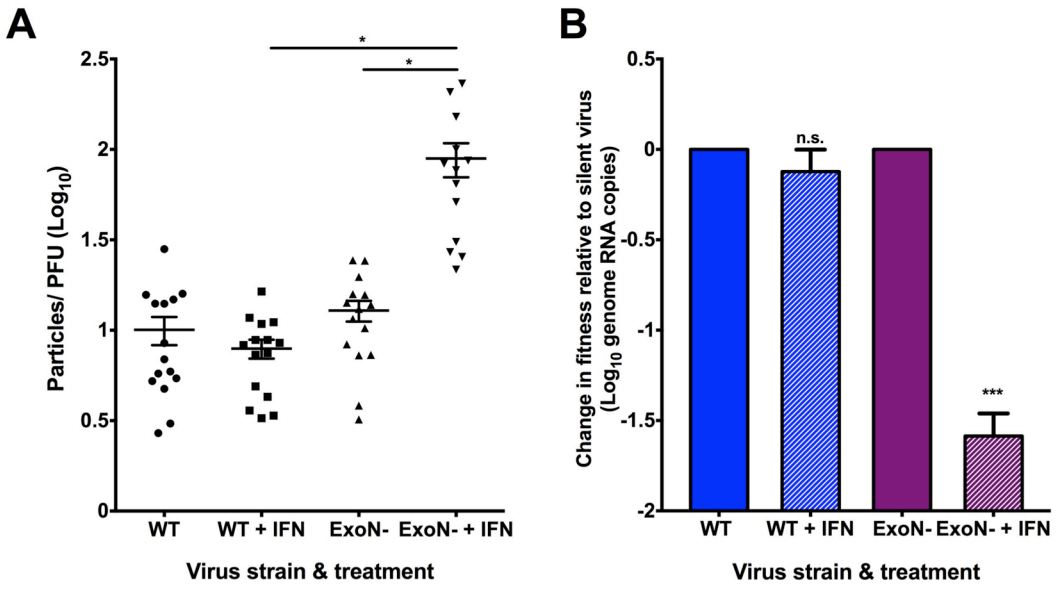

Figure 20. ExoN(-) viruses generated in the presence of an antiviral state have decreased specific infectivity and are less fit relative to untreated.

(A) DBT cells were pretreated with 0 or 100U/ml mouse IFN-β for 18 h and subsequently infected with WT-MHV or ExoN(-) virus at an MOI of 1 PFU/cell. At 12 h post-infection, cell culture supernatants were collected. Equivalent volumes of cell culture supernatant for each sample were divided into two samples. For the first cell culture supernatant sample, total RNA was extracted and the number of virion genome RNA copies present (particles) was determined by one-step RT-qPCR [Fig. 5C]. For the second cell culture supernatant sample, the viral titer present was determined by plaque assay (PFUs) (data not shown). The particle to PFU ratio for each virus and treatment was calculated by dividing the number of particles by the number of PFUs. Error bars represent SEM (n = 13 to 15). (B) DBT cells were pretreated with 0 or 100 U/ml mouse IFN-β for 18 h and subsequently infected with WT-MHV or ExoN(-) virus at an MOI of 1 PFU/cell. At 12 h post-infection, cell culture supernatants were harvested for each virus and treatment group and the number of virion genome RNA copies present (particles) in the supernatant was determined by one-step RT-qPCR. Using the determined number of particles, an equivalent number of virus particles from each virus and treatment group were mixed with an equal number of WT silent or ExoN(-) silent virus particles. This mixture was then used to infect a fresh monolayer of untreated DBT cells. At 24 h post-infection, cell culture supernatants were collected, RNA was extracted, and the number of virion genome RNA copies for each original virus and treatment group relative to their respective silent standard viruses was determined by one-step RT-qPCR and is reported as the change in fitness relative to the silent virus standard. Error bars represent SEM (n=6). For each panel, statistical significance compared to untreated WT-MHV or ExoN(-) infection, respectively, is denoted and was determined by Student's *t* –test. *, $P < 0.05$, *** $P < 0.001$, n.s.= not significant.

contrast, when DBT cells were pretreated with IFN-β prior to initial infection with ExoN(-) virus, the resulting specific infectivity of ExoN(-) virus was 100 particles per 1 PFU, a significant decrease in specific infectivity. Therefore, ExoN(-) virus generated in the presence of an IFN-β-mediated antiviral state requires 10-fold more genome RNA containing particles to generate 1 PFU than WT-MHV generated in cells pretreated with or without IFN or ExoN(-) virus generated in untreated cells. These data suggest that the IFN-mediated restriction of ExoN(-) virus in DBT cells occurs at the level of subsequent infection by reducing particle infectivity.

Next, I tested whether the effects of IFN on ExoN(-) viruses were intrinsic to the viruses produced. To do so, I performed a co-infection assay, which utilized WT-MHV and ExoN(-) viruses harboring 10 silent mutations in the nsp2-coding region (WT silent and ExoN(-) silent, respectively) along with WT-MHV and ExoN(-) viruses. The genome RNAs of the silent viruses are recognized exclusively by a separate probe than the one used to detect the "WT" nsp2 probe-binding region of WT-MHV or ExoN(-) viruses (Graepel et al., 2017). Thus, allowing WT silent and ExoN(-) silent to act as internal controls for a co-infection assay under identical conditions. DBT cells were pretreated with 0 or 100 U/ml mouse IFN-β for 18 h and subsequently infected with WT-MHV or ExoN(-) virus at an MOI of 1 PFU/cell. At 12 h post-infection, total cell culture supernatants were collected. The number of viral particles present in a representative aliquot was determined from purified virion genome RNA by one-step RT-qPCR. In addition, I determined the number of genome RNA containing particles in an equivalent volume of WT silent or ExoN(-) silent viral p1 stock tubes. Using the calculated number of genome RNA-containing viral particles, I added an equal number of WT-MHV viral particles generated in the absence of IFN pretreatment to WT silent viral particles and an equal number of WT-MHV viral

particles generated in the presence of IFN pretreatment to WT silent viral particles. This same set-up was repeated for ExoN(-) viral particles generated in the presence or absence of IFN pretreatment with ExoN(-) silent viral particles. Finally, each combination was used to infect a fresh monolayer of untreated DBT cells. At 24 h post-co-infection, total cell culture supernatants were collected and virion genome RNA was extracted to determine the number of supernatant viral particles present from each combination of input viruses by one-step RT-qPCR and is reported as the change in fitness relative to the respective silent virus standard (Figure 20B). The number of WT-MHV particles generated in the presence of IFN pretreatment was similar to the number of WT-MHV particles generated in the absence of IFN pretreatment over the course of co-infection, relative to their respective silent standards. However, the number of viral particles present from ExoN(-) virus generated in the presence of IFN pretreatment during the course of co-infection decreased by approximately 1.5 $\log_{10}$ in comparison with ExoN(-) viral particles generated in the absence of IFN pretreatment relative to their respective silent standards. These data indicate that a loss in nsp14 ExoN activity sensitizes viruses to IFN pretreatment and reduces the infectivity and fitness of progeny during subsequent rounds of infection in the absence of an antiviral state.

Discussion

CoVs encode multiple IFN antagonists that prevent the induction of or mediate resistance to the innate immune response; thus, allowing efficient viral replication early during infection (Rose and Weiss, 2009). Moreover, an insufficient innate immune response has been proposed to be a major contributor of SARS-CoV pathogenesis (Gu and Korteweg, 2007). In this study, I sought to determine the contributions of nsp14 ExoN activity in the induction of and resistance to the

innate immune response. I demonstrate that ExoN(-) virus is more sensitive to cellular pretreatment with IFN-β than WT-MHV. Further, because ExoN3(-) and ExoN(-) P250 viruses were also more sensitive to the effects of IFN, I conclude that IFN sensitivity is specifically due to a loss of ExoN activity.

Because the ExoN activity of the Lassa fever virus nucleoprotein degrades dsRNA intermediates (Hastie et al., 2011; Qi et al., 2010), I hypothesized that CoV nsp14 ExoN could function in a similar manner. In fact, since my current study began, CoV nsp14 ExoN activity has also been proposed by others to function as an innate immune antagonist (Becares et al., 2016; Kindler and Thiel, 2014). If nsp14 ExoN is degrading viral dsRNA, ExoN inactivation should increase intracellular dsRNA accumulation, resulting in a concomitant increase in IFN-β expression or activation of RNase L during infection. I neither observed IFN-β up-regulation nor RNase L activation over the course of ExoN(-) virus infection (Figure 18A and B), and rRNA was intact at all time-points tested (Figure 18B). Therefore, at least two possible explanations exist: 1.) MHV ExoN does not function to degrade dsRNA or 2.) MHV ExoN does degrade dsRNA, but the detection of this PAMP is unchanged during ExoN(-) virus infection due to sufficient antagonism by other CoV proteins. Basal OAS expression levels correlate with RNase L activation (Birdwell et al., 2016). Thus, I pretreated DBTs with IFN-β to up-regulate OAS and RNase L expression. However, rRNA degradation was only observed in cells transfected with poly I:C (Figure 18B). Further, nsp15 EndoU and NS2 phosphodiesterase activities were intact during all of my experiments. Thus, it is possible that in the absence of nsp14 ExoN activity, other CoV innate antagonists were sufficient to prevent innate detection by the cell or prevent the induction of a detectable signal in the experiments I performed. However, one would expect the

endonucleolytic products of nsp15 to be smaller dsRNAs that could still activate RIG-I or MDA5, similar to RNase L products, unless another RNA degradation mechanism were in place (Malathi et al., 2007; Schneider et al., 2014). In addition, despite an intact NS2 phosphodiesterase, nsp15 mutants still activate RNase L-mediated rRNA degradation (Kindler et al., 2017). Lastly, when RNaseL -/- / PKR -/- BMMs were infected with ExoN(-) virus, viral replication was not rescued, suggesting that RNase L and PKR are not required for ExoN(-) virus restriction (Figure 18C). Moreover, these data suggest dsRNA is not detected and the antiviral effectors RNaseL and PKR are not activated during ExoN(-) virus infection.

During my study, Becares et al. reported that a TGEV nsp14 zinc-finger mutant modulated the innate immune response of swine testis cells by reducing the levels of dsRNA and induction of IFN (Becares et al., 2016). Unlike TGEV, *Betacoronaviruses* such as SARS-CoV and MHV, do not induce IFN expression in most cell types (Frieman et al., 2008; Rose and Weiss, 2009; Roth-Cross et al., 2007) (Figure 18A). Interestingly, TGEV ExoN active site mutants were non-viable; although, this is not the first report of non-viable ExoN active site residue mutants in *Alphacoronaviruses* (Becares et al., 2016). In the initial report of CoV nsp14 ExoN activity, human CoV 229E ExoN active site mutants were also non-viable, suggesting a common essential function for nsp14 ExoN in *Alphacoronavirus* replication and/or innate antagonism (Minskaia et al., 2006). Altogether, the possibility of a common innate immune antagonism function for nsp14 across *Alpha*- and *Beta*-CoVs is apparent but clearly differing requirements exist that may be dependent on the CoV genus and cell types used.

My results clearly demonstrate that viruses lacking ExoN activity are more sensitive to IFN-β

pretreatment than WT-MHV in a dose-dependent manner (Figure 15A,C and Figure 16). Further, replication of viruses lacking ExoN activity was dependent on the capacity of BMMs to express genes downstream of IFNAR signaling (Figure 17). This is due to the fact that B6 and IFNAR-/- cells have different levels of basal ISG expression and thus, two very different intracellular environments for viral replication to occur (Rose and Weiss, 2009; Zhao et al., 2013; 2011). In IFNAR-/- BMMs, ExoN(-) and ExoN(-) P250 virus replication capacity was restored to levels approaching or exceeding WT-MHV levels (Figure 17). Further, my specific infectivity (Figure 20A) and co-infection (Figure 20B) data show that ExoN(-) virus generated in the presence of an antiviral state is less viable upon subsequent infection. Altogether, my results suggest that an ISG or ISGs is (are) acting on ExoN(-) virus, specifically resulting in progeny that are less viable upon subsequent infection. Thus, it will be interesting to determine the specific ISG (or ISGs) responsible for mediating the observed restriction. In addition, it will be important to determine whether a greater proportion of the incoming ExoN(-) viral particles are strictly non-viable or whether cells are now sensing the progeny ExoN(-) viruses and inhibiting replication. My specific infectivity data support the possibility that the effects of IFN treatment results in non-infectious ExoN(-) virus particles, which could potentially compete with infectious ExoN(-) virus particles for viral receptors during subsequent entry. Due to the pleiotropic nature of IFN-β, more than one mechanism may be acting.

To date, the majority of our understanding of nsp14 ExoN activity is in the context of proofreading during CoV replication (Bouvet et al., 2012; Eckerle et al., 2007; Minskaia et al., 2006; Smith et al., 2013). CoVs lacking ExoN activity demonstrate an increase in mutation frequency relative to WT (Eckerle et al., 2007; Smith et al., 2013). Thus, it is possible that

ExoN(-) virus replication in IFN pretreated cells results in further alteration of ExoN(-) virus mutation frequency. Certainly, an increase or decrease in mutation frequency could impair viral replication during a subsequent infection. Moreover, a recent study demonstrated that optimal viral replication fidelity is required for poliovirus to overcome tissue-specific innate immune responses (Xiao et al., 2017). In addition, IFN pretreatment may up-regulate an ISG that acts to hypermutate the large CoV genome in the absence of ExoN activity, rendering viral progeny less viable. ISGs that increase viral mutation frequency have been described such as adenosine deaminase acting on RNA 1 (ADAR1) and apolipoprotein B mRNA editing enzyme, catalytic polypeptide-like 3G (APOBEC3G) (Neil and Bieniasz, 2009; Tomaselli et al., 2015). Further, another ISG, SAMHD1, may inhibit HIV replication by limiting nucleotide pools, a known contributor to increased viral mutation frequency (Hrecka et al., 2011; Lahouassa et al., 2012; Sanjuán and Domingo-Calap, 2016). Moreover, other possible mechanisms outside of altered mutation frequency exist. For instance, in the absence of ExoN activity, terminal RNA modifications, recombination, and/or replicase protein interactions mediated by nsp14 ExoN may be disrupted to a greater extent in the presence of an IFN-β-mediated antiviral state.

Since CoVs encode the largest genome known for RNA viruses, they have the luxury of encoding multiple IFN antagonists that limit the capacity of a cell to detect and respond to infection. Collectively, my data suggest that MHV nsp14 ExoN activity is a contributor to CoV innate immune antagonism. I clearly demonstrate that viruses lacking ExoN activity are more sensitive to the effects of an IFN-β-mediated antiviral state. Further, my data reveal a critical role for nsp14 ExoN activity in CoV replication and provide additional rationale for targeting nsp14 ExoN activity as a means of viral attenuation. Our future studies will probe the specific

mechanism of restriction for viruses lacking ExoN activity and assess how the requirement of ExoN activity for resistance to innate immunity can be utilized for treatment during human coronavirus infections.

CHAPTER IV

DETERMINATION OF THE INTERFERON-STIMULATED GENE(S) RESPONSIBLE FOR RESTRICTING EXON(-) VIRUS REPLICATION

Introduction

Prior to this dissertation research, coronavirus (CoV) nonstructural protein 14 (nsp14) 3'-to-5' exoribonuclease (ExoN) activity had been investigated solely in the context of proofreading and maintaining viral replication fidelity (Bouvet et al., 2012; Eckerle et al., 2010; Minskaia et al., 2006; Smith et al., 2013). However, the discovery that arenaviruses also encode an ExoN, which functions as an innate immune antagonist, led me to hypothesize that CoV ExoN may act in a similar manner (Hastie et al., 2011; Qi et al., 2010). Further, a recent study using transmissible gastroenteritis virus, an *Alphacoronavirus*, nsp14 supports this hypothesis. However, viruses lacking ExoN activity were non-viable in that report; thus, preventing the direct study of the role of ExoN activity in innate immune antagonism (Becares et al., 2016). In Chapter III of this dissertation, I presented the first evidence suggesting that for murine hepatitis virus (MHV), a *Betacoronavirus*, nsp14 ExoN activity is required to confer resistance to the interferon beta (IFN-β)-mediated innate immune response. IFN-β pretreatment of cells did not restrict ExoN(-) viral RNA replication or particle release compared to wild-type (WT) MHV. Rather, my data suggest that viruses lacking ExoN activity that were generated in the presence of an antiviral state are specifically incapable of establishing a subsequent infection. Despite my efforts, the specific antiviral interferon stimulated gene (ISG) that restricts ExoN(-) virus has yet to be determined.

Until recently, there were thought to only be 30-40 ISGs. However, today we know the expression levels of hundreds of genes are altered in response to interferon (IFN). (Katze et al., 2002). The number of genes induced and the relative level of expression is dependent on the specific cell-type and stimulus, but the general mechanism for their induction is the same. Upon secretion from a cell, type I IFNs bind to interferon alpha/ beta receptors (IFNARs) in an autocrine and paracrine manner. Binding triggers an intracellular signaling cascade that culminates in the formation of a complex known as interferon stimulated gene factor 3 (ISGF3), which is comprised of phosphorylated signal transducer and activator of transcription proteins 1 and 2 and interferon regulatory factor 9 (IRF9). Next, ISGF3 translocates to the nucleus of the cell and binds to interferon-stimulated response elements, facilitating the expression of ISGs. ISGs are the workhorses of the antiviral innate immune response (Katze et al., 2002). ISGs may act as direct antiviral effectors by targeting a specific stage of viral replication or as positive regulators to reinforce the antiviral response. In addition, ISGs can be negative regulators of the IFN-mediated innate immune response to limit the duration of the response and prevent excessive damage to cells or tissues (Schneider et al., 2014). The specific role of many ISGs in controlling viral replication has been described (Katze et al., 2002; Schneider et al., 2014). However, the identification of novel ISGs or new roles for previously identified ISGs in response to different viral infections is currently a rapidly evolving area in virus research. Accordingly, innovative approaches to identify ISGs are needed.

In this chapter, I present preliminary data investigating the contributions of specific antiviral ISGs toward restricting ExoN(-) virus infection. In addition, I present the results of an RNA sequencing experiment to determine the ISGs up-regulated in DBT cells upon addition of

exogenous IFN-β. Lastly, I present the development of a high-throughput screening approach to determine the interferon stimulated gene or genes, responsible for restricting ExoN(-) virus replication. Data presented in this chapter are from experiments performed and analyzed by me with the exceptions mentioned below. In all cases, I designed the experiments and performed all final analyses. Ruth Elliot in the Weiss lab performed the WT and ExoN(-) virus replication curve in MDA5-/- bone marrow derived macrophages (BMMs). Henry Li generated ADAR1-/- A549 cells expressing the MHV CEACAM receptor, the Vanderbilt VANTAGE core performed the RNA sequencing, and Xiaotao Lu cloned the ExoN(-) P250 spike into the MHV A-59 G fragment used to generate WT and ExoN(-) RFP- ExoN(-) P250S viruses.

ExoN(-) virus demonstrates an increased sensitivity to a fully activated OAS/ RNase L antiviral response in DBT cells

The oligoadenylate synthetase/ latent ribonuclease (OAS/ RNase L) pathway is a major dsRNA sensor. Upon detection of viral dsRNA, OAS generates 2'-5' oligadenylates, which act as secondary signaling molecules to activate RNase L. Once RNase L becomes activated, it functions to degrade all RNAs, both of cellular and viral origin, inside a cell. The degradation of viral RNAs directly limits viral replication, and RNase L RNA products also act to stimulate sensors such as MDA5, creating a positive feedback loop (Drappier and Michiels, 2015; Malathi et al., 2007; Silverman, 2007). Arenaviruses encode the only ExoN known for RNA viruses outside of the order *Nidovirales*. Studies have demonstrated that the arenavirus ExoN functions to antagonize the innate immune response by degrading viral dsRNA intermediates (Hastie et al., 2011; Qi et al., 2010; Russier et al., 2014). In addition, coronaviruses are known to demonstrate a relatively high level of resistance to the innate immune response (Rose and Weiss, 2009).

Therefore, I sought to determine whether ExoN functions to degrade dsRNA viral replication intermediates and thus, whether viruses lacking ExoN exhibit an increased sensitivity to the OAS/ RNase L antiviral response. Previous studies have demonstrated that in order for the OAS/ RNase L antiviral response to become fully activated, OAS must be expressed basally or up-regulated by IFN to a sufficient level and dsRNA must be present (Birdwell et al., 2016; Li et al., 2016; Marcus and Sekellick, 2001; Zhao et al., 2013). In addition, in this context, viruses that were previously refractory to pretreatment with exogenous IFN became sensitive (Marcus and Sekellick, 2001). Therefore, I pretreated cells with mock treatment, 100U/ml IFN-β, or 100U/ml IFN-β + 25μg poly I:C (a dsRNA surrogate). After pretreatment, I infected cells treated with each condition with WT or ExoN(-) virus at a multiplicity of infection (MOI) of 1 plaque forming unit (PFU)/ml (Figure 21). In the presence of IFN-β alone, ExoN(-) viral titers were decreased by approximately 2.5 $\log_{10}$ compared to untreated. However, in the presence of IFN-β + poly I:C, ExoN(-) viral titers were not detectable. In addition, WT MHV titers in the presence of IFN-β + poly I:C were similar to ExoN(-) viral titers in the presence of IFN-β alone. If ExoN activity were functioning to also degrade dsRNA, I would expect ExoN(-) virus to be no more sensitive to IFN-β + poly I:C than IFN-β alone. Therefore, while it remains possible that ExoN functions to degrade dsRNA, it is hard to draw a conclusion from these results alone.

ExoN(-) virus replication is not rescued in MDA5-/- BMMs

In Figure 17 of Chapter III, I demonstrated that ExoN(-) virus replication is restricted in wild-type (B6) BMMs. Further, ExoN(-) viral replication was not restored in BMMs deficient in the dsRNA effectors RNase L and PKR. These data suggest that in the context of ExoN(-) virus replication, dsRNA does not activate RNase L or PKR resulting in decreased viral replication.

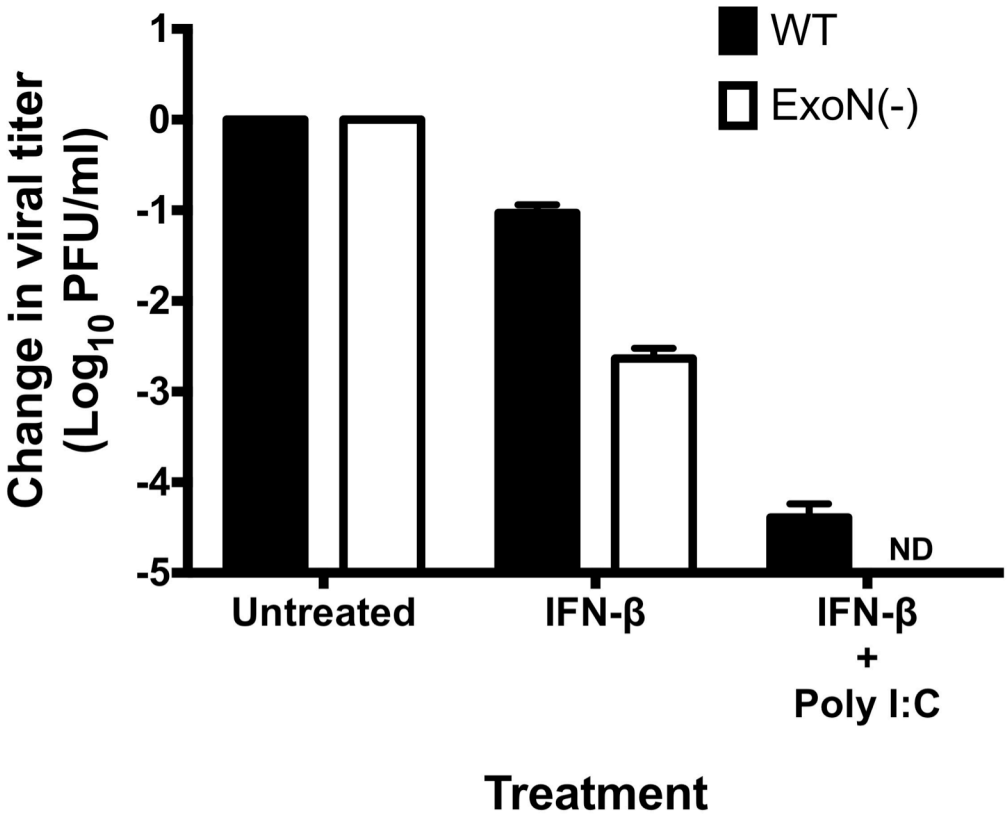

Figure 21. ExoN(-) virus is more sensitive to a fully activated OAS/ RNase L antiviral response.

DBT cells were pretreated for 18 h with 100 U/ml mouse IFN-β or mock treated. For IFN-β + poly I:C treatment, cells were transfected with 25 μg poly I:C and incubated for the final hour of IFN treatment. After pretreatment, cells were infected with WT or ExoN(-) viruses at an MOI of 1 PFU/cell. At 12 h post-infection, cell culture supernatants were collected and viral titers were determined by plaque assay. Values are reported as the change in viral titer relative to untreated viral titers for each respective virus. Error bars represent SEM. n=6.

Another pattern recognition receptor (PRR) that functions to detect dsRNA during viral infection is melanoma differentiation-associated gene 5 (MDA5). MDA5 is a member of the RIG-I-like family of PRRs that localizes in the cell cytoplasm and functions to detect long, double-stranded RNA as well as cap-0 RNAs (Decroly et al., 2011a; Schneider et al., 2014). MDA5 is positively reinforced by IFN expression and upon detection of viral RNA, signals downstream into the IFN-mediated antiviral response. To determine if MDA5 is necessary for ExoN(-) virus restriction in BMMs, we infected B6 or MDA5-/- BMMs with WT or ExoN(-) MHV at an MOI of 1 PFU/cell (Figure 22). Cell culture supernatants were harvested at the indicated times post-infection and viral titers were determined by plaque assay. My data indicate that ExoN(-) virus replication is not affected by MDA5 deficiency. These data are in agreement with my previous experiments using RNase L/PKR-/- BMMs and the conclusion presented in Chapter III that dsRNA is not detected in viruses lacking ExoN activity. Further, these data corroborate the data shown in Figure 18A in Chapter III that suggest ExoN(-) virus replication does not induce IFN-β expression. Therefore, all data to date suggest that MHV nsp14 ExoN activity does not function to degrade dsRNA during infection.

ADAR1 is not responsible for mediating ExoN(-) virus restriction

In chapter III of this dissertation, I presented data demonstrating that after ExoN(-) virus replicated in the presence of an antiviral state, the viruses produced were less viable and capable of establishing a subsequent infection. This observation was highlighted by a decreased specific infectivity and decreased replicative fitness exclusively for ExoN(-) virus in IFN-β pretreated cells. Therefore, I concluded that CoV ExoN activity is required for resistance to the IFN-β-mediated innate immune response. In addition, considering the fact that nsp14 ExoN functions as

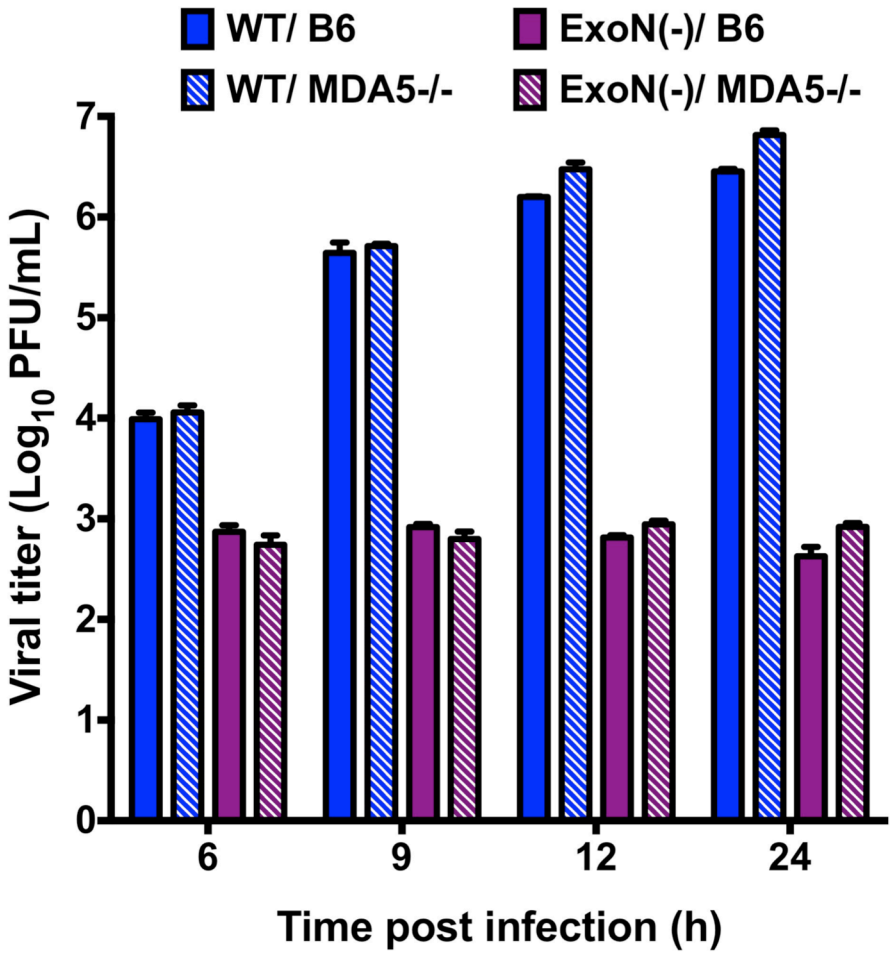

Figure 22. ExoN(-) virus replication is not rescued in MDA5 -/- BMMs.

B6 BMMs or MDA5-/- BMMs were infected with WT-MHV or ExoN(-) virus at an MOI of 1 PFU/cell. At the indicated times post-infection, cell culture supernatant aliquots were collected and the viral titers present were determined by plaque assay. For each panel, error bars represent SEM (n = 3).

a proofreading enzyme, I reasoned that an ISG may act to increase or decrease the mutation frequency of ExoN(-) virus genomes. One ISG that has been demonstrated to hypermutate viral genomes is adenosine deaminase acting on RNA 1 (ADAR1) (Mannion et al., 2014; Piontkivska et al., 2017; Schoggins et al., 2011; Tomaselli et al., 2015). ADAR1 is an IFN-inducible protein, and previous studies have demonstrated that the hypermutation activity of ADAR1 on viral RNA genomes can be pro-viral (in the case of HIV infection) or antiviral (in the case of influenza virus). ADAR1 binds dsRNA and deaminates adenosine sequences to inosine (Samuel, 2011; Tomaselli et al., 2015). Inosine prefers to base pair with cytosine, resulting in an adenosine to guanosine transition (Mannion et al., 2014). Henry Li in the Weiss Lab generously engineered A549 cells that were deficient for ADAR1 and express the MHV CEACAM receptor using CRISPR/ Cas technology. To determine whether ADAR1 was responsible for mediating ExoN(-) virus sensitivity to IFN-β, I performed a replication curve using these cells. I infected WT or ADAR1-/- A549 cells with WT or ExoN(-) virus at an MOI of 1 PFU/cell and collected cell culture supernatants at the indicated times post-infection (Figure 23). I observed similar viral titers for ExoN(-) virus in WT A549 cells and ADAR1-/- A549 cells at each time-point post-infection. Therefore, I conclude that ADAR1 does not restrict ExoN(-) virus replication in A549 cells.

Determining the ISGs up-regulated in DBT cells upon treatment with IFN-β

In Chapter III of this dissertation, I demonstrated that pretreatment of DBT cells with exogenous IFN-β restricted ExoN(-) virus replication upon subsequent infection. Treatment with IFN is known to alter the expression of hundreds of genes (Katze et al., 2002). However, the specific genes and the degree in which they up-regulated is cell-type specific. Therefore, to further

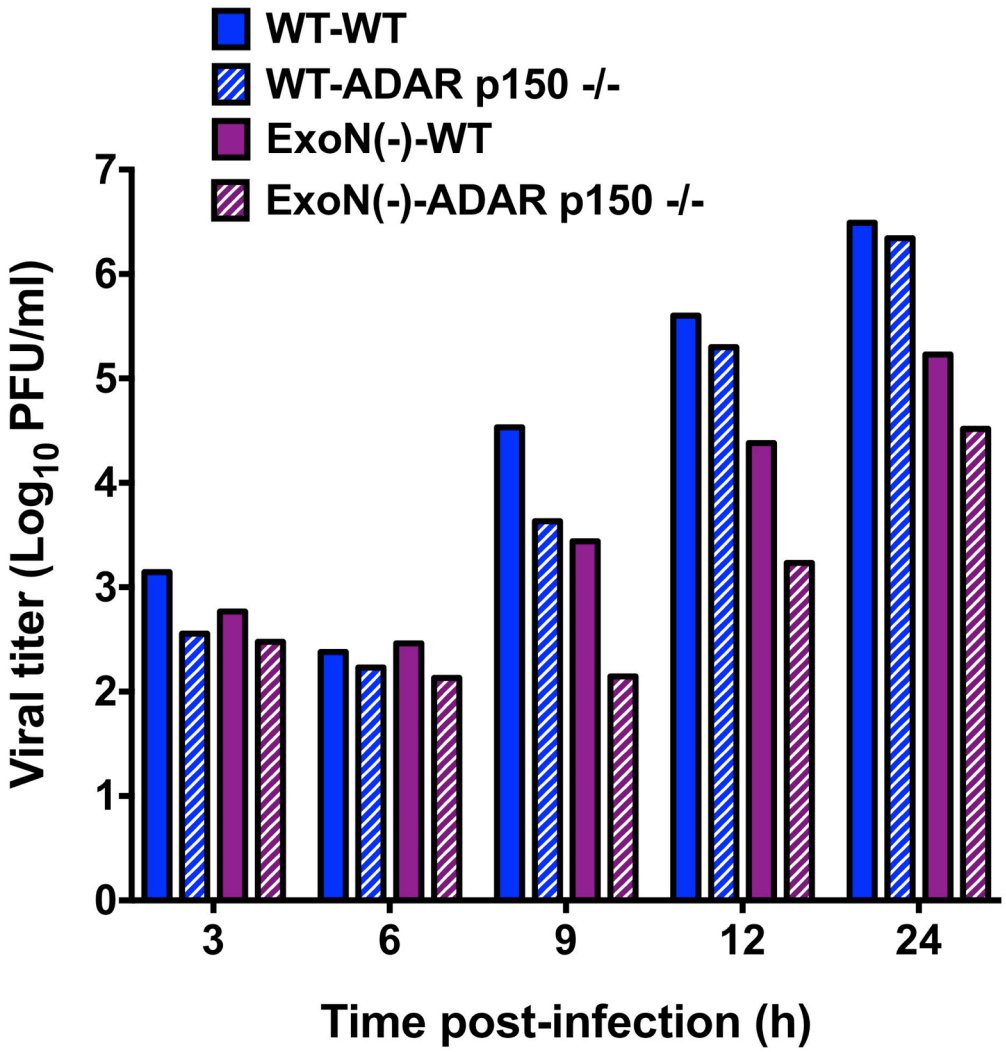

Figure 23. ExoN(-) virus replication in ADAR1 p150 -/- A549 cells

WT or ADAR1 p150-/- A549 cells stably expressing the MHV receptor, CEACAM, were infected at an MOI of 1 PFU/cell and aliquots of cell culture supernatants were collected at the indicated times post-infection. Viral titers present were determined by plaque assay. n=6.

understand the environment in which ExoN(-) virus is replicating after pretreatment of DBT cells with IFN-β, I performed RNA sequencing on cell lysates from cells pretreated with or without mouse IFN-β and analyzed the differential gene expression profile (Figure 24 and Appendix C). Uninfected DBT cells were treated with or without mouse IFN-β for 26 h and cell lysates were harvested. Upon extraction of total RNA, samples were submitted to the Vanderbilt VANTAGE core for mRNA enrichment, cDNA library preparation, and sequencing. After the VANGUARD core deconvoluted the sequencing reads, I analyzed the data set to determine genes that were statistically up or down-regulated. Over 23,160 annotated murine gene reads were observed. Moreover, 3,536 genes were significantly up or down-regulated in IFN treated DBT cells versus mock treated DBT cells. Of the 3,500+ differentially expressed genes, 1,607 were up-regulated by IFN-β treatment. In addition, antiviral genes such as Irf7, Oas1a, Ifitm3, Bst2 (also known as tetherin), Mx2, Ddx58, and Ifit1 were among the most highly up-regulated genes (Figure 24). The full list of statistically significant, differentially expressed genes is presented in Appendix C. These data demonstrate, and reveal for the first time, the exact cellular environment in which ExoN(-) virus is replicating after IFN treatment. Although many genes are differentially expressed upon IFN-β pretreatment, these data will allow us to preferentially select genes that are now known to be up-regulated in DBT cells during future experiments to elucidate the mechanism of ExoN(-) restriction by IFN.

Development of a high-throughput ISG screen to determine the ISG(s) mediating ExoN(-) virus restriction in DBT cells

To this point in this chapter, I have described experiments aimed at determining the specific

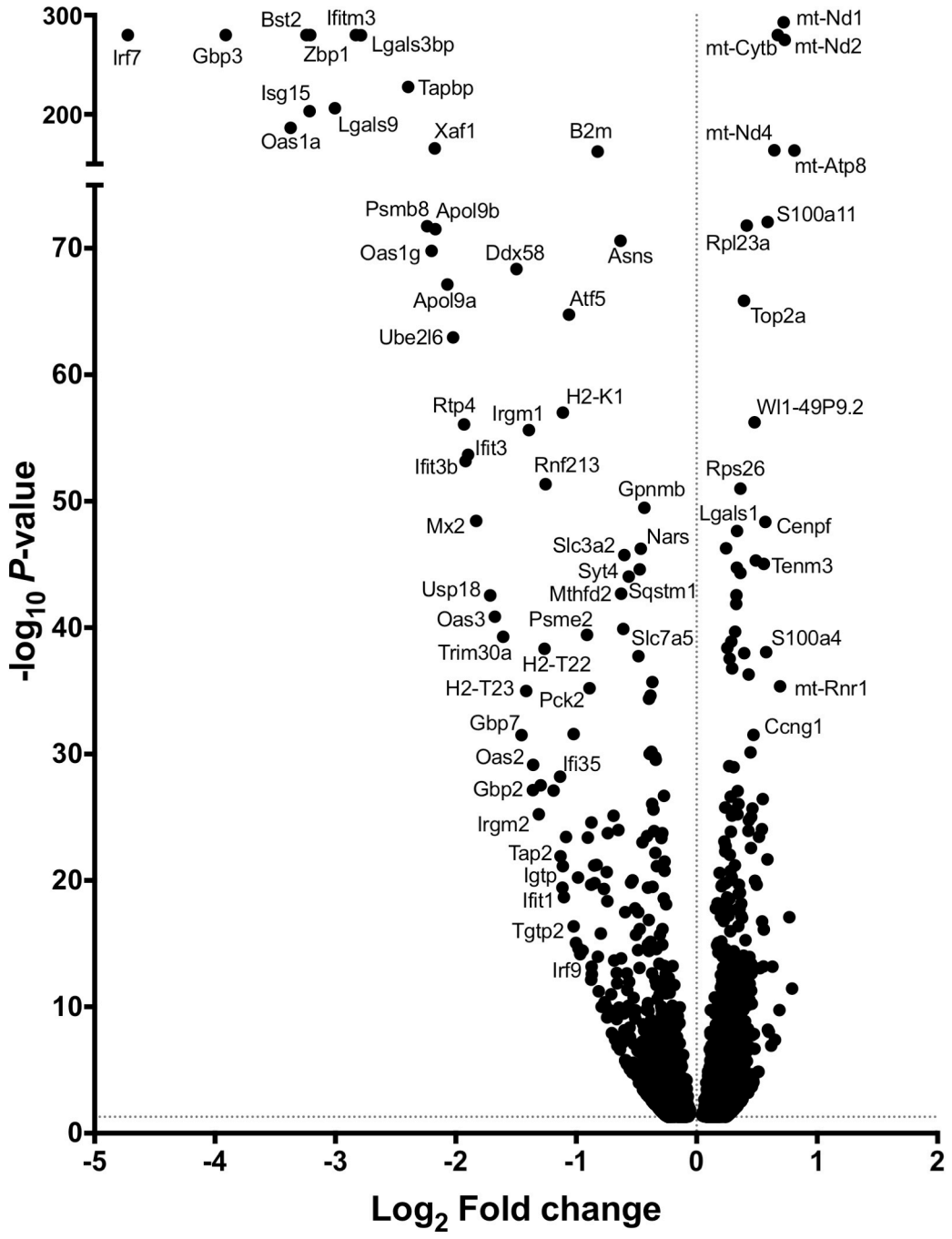

Figure 24. Statistically up and down-regulated genes in DBT cells upon IFN-β treatment.

DBT cells were pretreated with 0 or 100 U/ml mouse IFN-β for 26 h. After pretreatment, cell culture supernatants were removed and total cell lysates were harvested using TRIzol reagent. Total RNA was extracted and RNA sequencing performed to identify gene expression profiles. The DeSeq algorithm was used to identify statistically differentially expressed genes. Genes that were statistically up or down-regulated in IFN-β treated cells relative to untreated cells are plotted with notable genes labeled.

mechanism of ExoN(-) virus restriction when replicated in the presence of IFN-β. While taking a targeted approach allows for a quick result, the conclusions that can be made and the limitations of isolating a single gene or pathway may not reveal all mechanisms of action. Further, the experiments I have performed are based off existing knowledge of ISGs and antiviral pathways and may not reveal novel interactions. Most importantly, the ISG or ISGs responsible for restricting ExoN(-) virus replication have not been identified by previous methods. Therefore, I have developed an unbiased high-throughput screening approach.

Several different high-throughput ISG screening approaches have been developed using ISG overexpression constructs, siRNA-mediated knockdown of ISGs, shRNA-mediated knockdown of ISGs, or CRISPR-Cas9 directed genome editing (Li et al., 2013; Schneider et al., 2014; Schoggins et al., 2011; 2014; Zhao et al., 2012a). Each screening approach has its own caveats and limitations. However, the amount of information that can be gathered in a short amount of time and subsequently validated make them attractive approaches. The screen I have worked to develop is outlined in (Figure 25). The benefits of using this screening approach include but are not limited to: 1.) this screen can define the relative contribution of any given ISG in the context of an intact IFN response for a desired cell type, 2.) this screen will allow one to identify ISGs that are part of a multicomponent complex, and 3.) this screen will allow the differential antiviral activities of ISGs against WT and ExoN(-) viruses to be simultaneously determined (Li et al., 2013). The general concept of the ISG is screen is as follows: 1.) within cells, the expression of a single ISG is targeted and knocked down by lentiviral transduction of a green fluorescent protein (GFP) and shRNA expressing plasmid, 2.) cells are treated with IFN-β

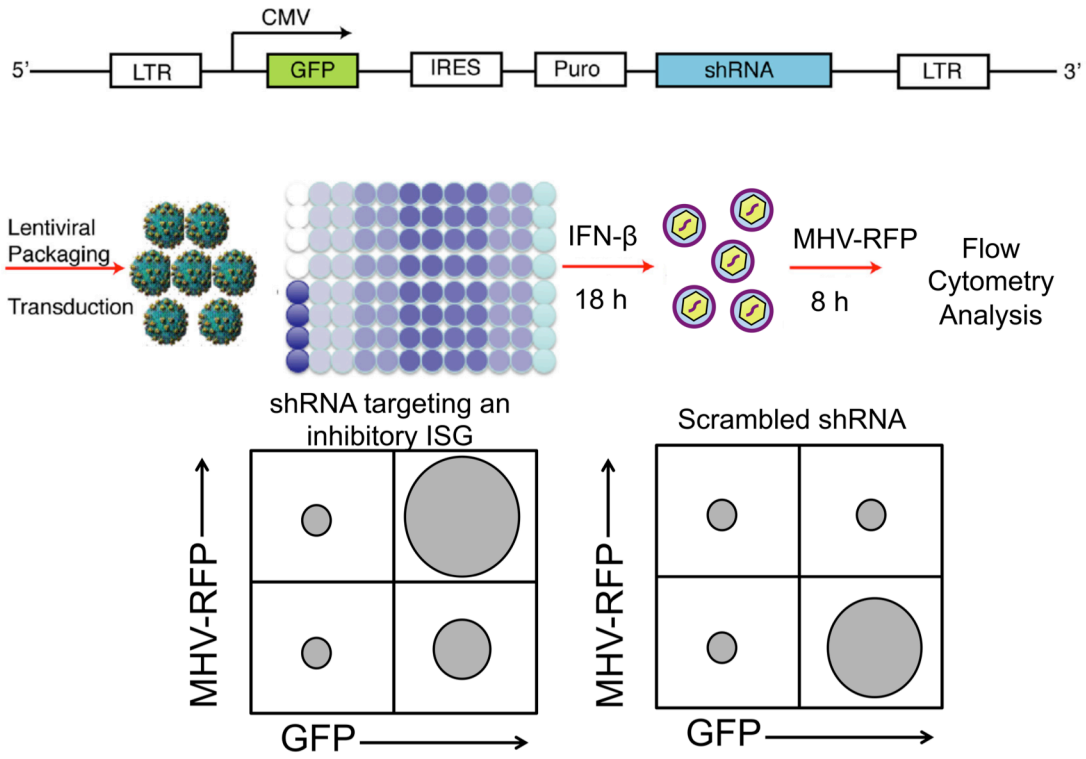

Figure 25. High-throughput ISG screen outline

The workflow of the high-throughput screen I developed is outlined. An shRNA targeting an ISG is expressed downstream of a CMV promoter and GFP. 293T cells are co-transfected with shRNA and lentiviral packaging plasmids to generated lentiviral pseudoparticles. DBT cells are transduced with the lentiviral particles targeting a specific ISG. DBT cells are pretreated with mouse IFN-β for 18 h to up-regulate all other ISGs in the cell. DBT cells are infected with an RFP expressing virus of interest and viral infection in transduced, GFP+ cells is quantified by flow cytometry.

to up-regulate all ISGs (except the expression of the single ISG that has been knocked-down), 3.) a red fluorescent protein (RFP) expressing virus of interest is used to infect the transduced cells, 4.) flow cytometry is used to quickly detect and determine the percentage of successfully transduced cells (GFP+) and successfully infected cells (RFP+) for a given well, 5.) the contribution of each ISG in the library on viral infection is discernable based on the increase or decrease in RFP+ cells relative to controls, which is indicative of viral infection level in a particular well. The mouse ISG targeting shRNA plasmid library was kindly shared with me by Dr. Michael Diamond and contains shRNAs targeting over 250 known ISGs. The ISGs targeted by this library were selected based on published microarray analyses of genes that were induced by at least 2-fold upon treatment with IFN-α or IFN-β (Boonyaratanakornkit et al., 2009; Fernald et al., 2007; Hayashi et al., 2005; Indraccolo et al., 2007; Li et al., 2013; Pfeffer et al., 2004). In this library, each well of a 96-well plate contains a purified pGIPZ lentiviral plasmid that encodes GFP and an ISG-targeting shRNA downstream of the human cytomegalovirus promoter. Each shRNA plasmid is co-transfected along with pSPAX and pMD2G lentiviral plasmids into a packaging cell line, 293T cells. In the 293T cells, each plasmid is expressed, generating pseudoviruses that contain the pGIPZ ISG-targeting shRNA as the payload. 293T cell culture supernatants containing the pseudoviruses are harvested and placed on the cell type of choice for transduction. Cells that are sufficiently transduced by the pseudoviruses will now stably express GFP and the downstream ISG-targeting shRNA. The ISG targeted in each well is known due to the well location and each well contains only a single shRNA. However, different shRNA sequences targeting the same ISG are located in different wells, allowing additional coverage and repeated testing of a single ISG. In addition, shRNA plasmids can be combined during subsequent experiments to identify multi-component ISG interactions. The ExoN(-) IFN

sensitive phenotype was initially observed in DBT cells. Therefore, I decided to use these cells for the ISG screen. To up-regulate all ISGs that are not knocked-down by the shRNA in a particular well, IFN-β is added to the DBT cells and incubated for 18h. Next, WT or ExoN(-) viruses that have been engineered to express RFP as fusion protein with nsp2 and the ExoN(-) P250 virus spike protein (Ex- P250S) are used to infect the transduced, IFN-β treated DBT cells (Figure 26A and B). Viruses utilizing the spike protein from the ExoN(-) P250 virus were engineered to limit syncytia formation. The ExoN(-) P250S confers a decrease in syncytia formation and thus, allows an infected monolayer of cells to become a suspension of single-cells during flow cytometry analysis. When 293T cells were transfected for packaging, they were routinely 80% GFP+ or greater (data not shown). To validate successful transductions, DBT cells were mock transduced or transduced for 3 days using pseudoviruses that contained a non-silencing control (NSC), or one of five different sequences targeting signal transducer and activator of transcription 1 (STAT1) and monitored for GFP fluorescence by flow cytometry (Figure 27). For the NSC and each STAT1-targeting shRNA sample, approximately 84-94% of cells were successfully transduced. Importantly, the mock transduced cells were 100% GFP-. In addition, DBT cells were pretreated with 0 or 250 U/ml mouse IFN-β for 18h and subsequently infected with WT or ExoN(-) –RFPnsp2-Ex(-)P250S viruses at an MOI of 0.1 PFU/cell. Cells were harvested at 6h and 8h post-infection and analyzed by flow cytometry (Figure 28). IFN-β treatment reduced the number of WT-RFP+ cells by 2 and 3-fold at 8h and 6h post-infection, respectively. In contrast, IFN-β treatment reduced the number of ExoN(-)-RFP+ cells by 6 and 6.5-fold at 6h and 8h post-infection, respectively. These data indicate that DBT cells can be readily transduced with ISG-targeting shRNAs. In addition, these data demonstrate that WT and ExoN(-) –RFPnsp2-Ex(-)P250S virus infected cells are detectable by flow cytometry.

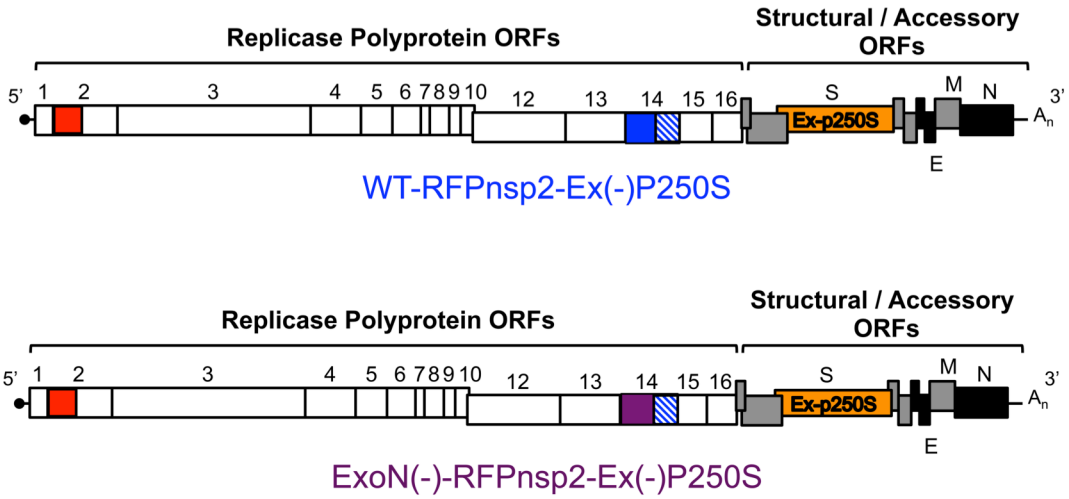

Figure 26. Diagram of reporter viruses developed for high-throughput screen

WT or ExoN(-) viruses harboring an RFP fusion protein with nsp2 and expressing the MHV ExoN(-) P250 spike (S) protein were developed to detect viral infection levels during high-throughput screening experiments.

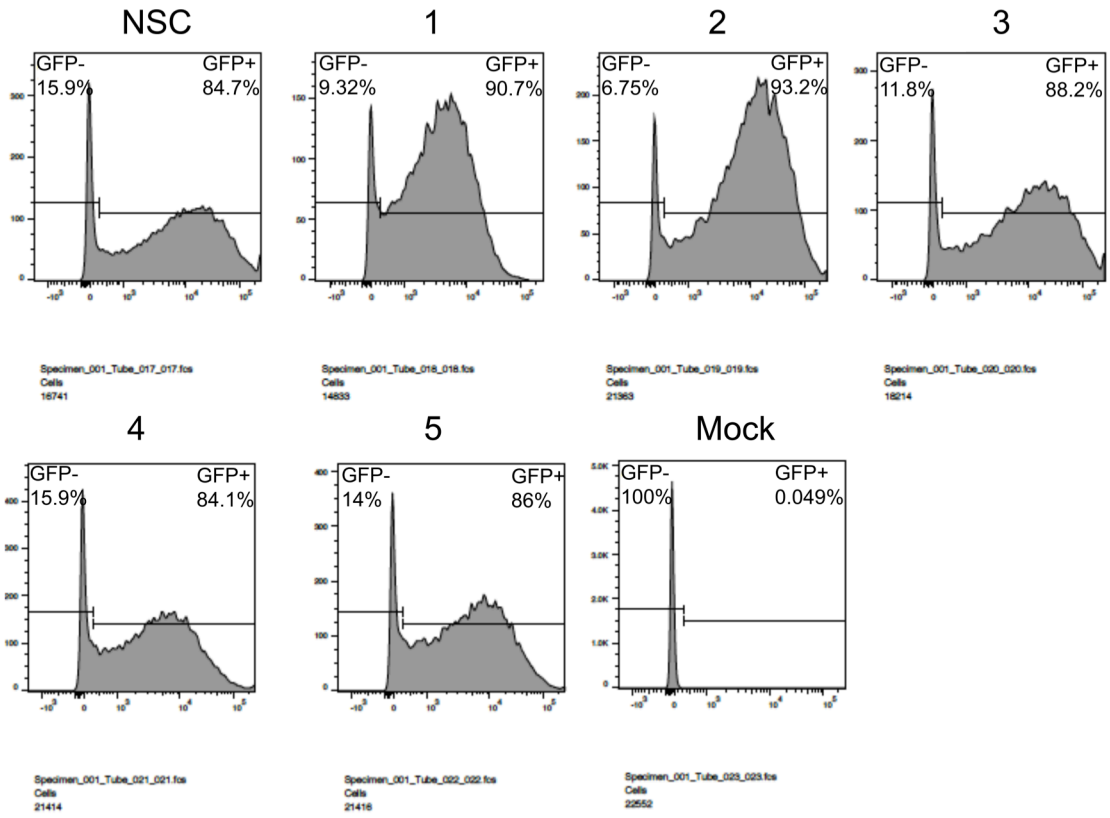

Figure 27. DBT cell transduction efficiency

DBT cells were transduced with lentiviral pseudoparticles encoding a non-silencing control (NSC), five different shRNA sequences directed against STAT1 (1-5, respectively), or mock transduced. At 3 d post-transduction, cells harvested and the percentage of GFP+ cells was determined by flow cytometry.

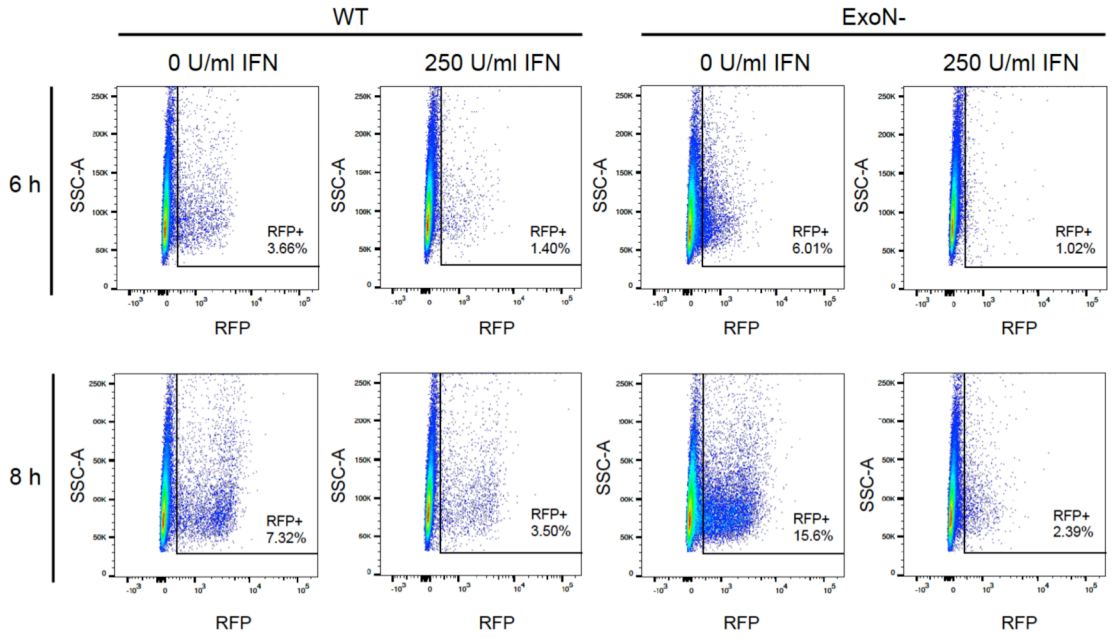

Figure 28. Infection of DBT cells with RFP reporter viruses

DBT cells were pretreated with 0 or 250 U/ml mouse IFN-β for 18 h and subsequently infected at an MOI of 0.1 PFU/cell with WT-RFPnsp2-Ex(-)P250S or ExoN(-)-RFPnsp2-Ex(-)P250S virus. At the indicated times post-infection, cells were harvested and the percentage of RFP+ cells determined by flow cytometry.

Discussion

In Chapter III of this dissertation, I demonstrated that CoV nsp14 ExoN activity is required for resistance to the innate immune response. My data show that viruses lacking ExoN activity are sensitive to pretreatment of cells with IFN-β. Interestingly, the ExoN(-) sensitivity was not observed during primary replication in IFN treated cells. Rather, the ExoN(-) viral progeny generated in the presence of IFN exhibited decreased viability and fitness during subsequent infection. These data suggest that ExoN activity directly or indirectly counteracts one or more ISGs during infection.

In this chapter, I sought to determine the specific ISG responsible for mediating restriction of ExoN(-) virus. My initial studies tested the hypothesis that ExoN(-) functions to degrade dsRNA, which is an obligatory replication intermediate and potent inducer of type I IFN expression. Outside of the order *Nidovirales*, arenaviruses encode the only other known ExoN for RNA viruses, which functions to degrade dsRNA (Hastie et al., 2011; Qi et al., 2010). In addition, infection with a TGEV zinc finger mutant virus elicited a decreased innate immune response by generating lower levels of dsRNA than WT TGEV (Becares et al., 2016). Thus, suggesting a novel role for coronavirus nsp14 in innate immune antagonism. However, the experiments performed in this chapter are in agreement with the conclusions presented in Chapter III; MHV nsp14 ExoN activity does not function to degrade dsRNA. ExoN(-) virus replication was not rescued in BMMs deficient in MDA5, a dsRNA sensor. Further, since the effects of IFN-β are not observed during primary infection of ExoN(-) virus but rather, during subsequent infection, I hypothesized that an ISG could alter ExoN(-) virus mutation frequency. ADAR1 is an RNA editing enzyme that is up-regulated by IFN signaling (Katze et al., 2002; Piontkivska et al., 2017;

Samuel, 2011; Tomaselli et al., 2015). However, ExoN(-) virus replication in A549 cells deficient in ADAR1 was similar to ExoN(-) virus replication in WT A549 cells. Thus, it is unlikely ADAR1 is hypermutating MHV genomes in the absence of ExoN activity. It is noteworthy that in my A549 replication curves, WT and ADAR1-/- A549 cells were not treated with human IFN-β prior to infection. Therefore, assessing the contributions of ADAR1 on ExoN(-) replication are limited to basal expression of ADAR1 in WT A549 cells. In separate experiments that were not shown, I pretreated WT and ADAR1-/- A549 cells with human IFN-β for 24 h prior to infection with WT or ExoN(-) virus. Unfortunately, the results of this experiment were not interpretable due to the fact that IFN signaling in ADAR1-/- cells results in a cell lethal phenotype that has only recently been described (Li et al., 2017). Therefore, it is possible that basal ADAR1 expression in WT A549 cells is not sufficient to inhibit ExoN(-) virus replication. To identify ISGs that are differentially expressed in DBT cells upon IFN-β pretreatment, we performed RNA sequencing on uninfected cells treated with or without IFN-β. Our results revealed that DBT cells generate a robust response to IFN signaling. In future experiments, these results with allow us to focus on specific ISGs that are differentially expressed by DBT cells.

Due to my previous lack of success using targeted methods, I sought to develop a high-throughput ISG screen to determine the gene or genes involved in mediating ExoN(-) virus restriction. While the screen has yet to be carried out, I have developed the necessary reagents and optimized conditions for generating transduced DBT cells expressing an ISG-targeting shRNA. In addition, I have generated RFP-tagged viruses that form a limited number of syncytia during infection compared to WT MHV. Interestingly, during the studies outlined in Chapter III

of this dissertation, IFN-β did not result in a significant decrease in viral RNA levels or an overall decrease in the change in particle output for ExoN(-) virus relative to WT MHV (Figure 19). However, in my preliminary RFP-tagged virus flow cytometry experiments, ExoN(-) – RFPnsp2-Ex-P250S virus demonstrated a 2-3 fold decrease in RFP+ cells in response to IFN-β compared to WT-RFPnsp2-Ex-P250S virus. Although, it is important to note, DBT cells were pretreated with 250 U/ml mouse IFN-β for my preliminary flow experiments rather than the 100 U//ml IFN-β used in the aforementioned experiments presented in Chapter III. For my flow cytometry experiments, I started with 250 U/ml IFN-β in an attempt to get the highest fold change in viral infection between untreated and treated cells, which would allow for a larger dynamic range between ISGs that minimally versus highly affect ExoN(-) virus replication. Moreover, experiments in Chapter III detected viral RNAs present, whereas RFP-tagged virus flow experiments detected the presence of RFP+ cells; meaning, the cell had been infected and the RFP encoded by the viral genome RNA was translated. Thus, when performing the screen, it will be important to distinguish not only between RFP+/RFP- cells, but also the difference in mean fluorescence intensities among a given population of RFP+ cells. Further, since ExoN(-) virus demonstrated reduced replication capacity and fitness upon subsequent infection, the screen may need to be altered to measure viral replication upon a subsequent infection of untreated cells. Overall, my data suggest CoV nsp14 ExoN activity functions to antagonize the innate immune response by a potentially novel mechanism. Thus, it will be exciting to determine the specific ISG nsp14 ExoN activity counteracts.

CHAPTER V

MATERIALS AND METHODS

Virus and cell culture

Murine delayed brain tumor (DBT) cells (Chen and Baric, 1996), baby hamster kidney 21 cells expressing the MHV receptor (BHK-R) (Yount et al., 2002), and 293T cells were maintained at 37°C in Dulbecco's modified Eagle medium (DMEM; Gibco) supplemented to contain 10% fetal bovine serum (FBS;Invitrogen), 100 U/ml penicillin and streptomycin (Gibco), and 0.25 μg/ml amphotericin B (Corning). BHK-R cells were further supplemented to contain 0.8 mg/ml of G418 (Mediatech). Bone-marrow-derived dendritic cells (BMDCs) were maintained in R10 medium (RPMI 1640 [Gibco] supplemented to contain 10% FBS, 2 mM L-glutamine, 100 μg/ml gentamicin [MP Biomedicals], 0.25 μg/ml amphotericin B, 50 μM beta-mercaptoethanol, 20 ng/ml GM-CSF, and 10 ng/ml IL-4). WT and ADAR1 p150-/- A549 cells were maintained at 37°C in RPMI 1640 [Gibco] supplemented to contain 10% FBS and 100U/ml penicillin and streptomycin (Gibco). Recombinant MHV strain A59 (GenBank accession number AY910861) was propagated as described (Yount et al., 2002).

Cloning, recovery, and verification of mutant viruses

Site-directed mutagenesis was used to engineer point mutations in individual MHV genome cDNA fragment plasmids using the MHV infectious clone reverse genetics system (Yount et al., 2002). ExoN(-) (nsp14 D89A and E91A) has been previously described (Eckerle et al., 2007). To generate ExoN(-) P250 virus, sub-confluent monolayers of DBT cells in 25cm^2 flasks were infected using the ExoN(-) parental stock and blindly passaged for a total of 250 passages

(Graepel et al., 2017). For ExoN3(-) virus (nsp14 D272A), nsp14 D330A virus, nsp14 G332A virus, and nsp16 D130A virus, site-directed mutagenesis was used to engineer point mutations in the MHV genome cDNA F fragment plasmid using the MHV infectious clone reverse genetics system (Yount et al., 2002). Viruses encoding firefly luciferase (FFL) fused to nsp2 were recovered using MHV A frag-FFL2 (Freeman et al., 2014). RFP expressing WT and ExoN(-) viruses were generated using MHV A frag-RFPnsp2, MHV WT or ExoN(-) F frag, and MHV ExoN(-) P250S G frag (Eckerle et al., 2007; Graepel et al., 2017). Mutant viruses were recovered using BHK-R cells following electroporation of *in vitro*-transcribed genomic RNA and in some instances, overlaid onto DBT cells. All mutagenized plasmids and recovered mutant viruses were sequenced (GenHunter Corporation, Nashville, TN) to verify the engineered mutations were present and to ensure that no additional mutations were introduced.

Viral replication kinetics

Sub-confluent DBT or A549 cell monolayers were infected at a multiplicity of infection (MOI) of 1 plaque-forming unit (PFU) per cell at 37°C for 45 min. Inocula were removed, cells were washed with 1X PBS, and fresh medium was added. Aliquots were harvested at various times post-infection. Viral titer at various intervals was determined by plaque assay (Eckerle et al., 2007).

5-FU sensitivity assays

5-fluorouracil (5-FU, Sigma) was prepared as a 200 mM stock solution in DMSO. Sub-confluent DBT cells were treated with DMEM supplemented to contain various concentrations of 5-FU or DMSO alone at 37°C for 30 min (Smith et al., 2013). After incubation, drug was removed, and

cells were infected with virus at an MOI of 0.01 PFU/cell at 37°C for 1 h or at an MOI of 1 PFU/cell at 37°C for 1 h. Inocula were removed, and cells were incubated in medium containing 5-FU or DMSO. Cell culture supernatants were collected at 24 h or 12 h post-infection corresponding to the respective MOI, and viral titers were determined by plaque assay.

Interferon-β sensitivity assays

Sub-confluent DBT cells were treated for 18 h with the indicated concentrations of mouse IFN-β (PBL Assay Science) prior to infection with virus at a multiplicity of infection (MOI) of 1 plaque-forming unit (PFU) per cell at 37°C for 45 min. After incubation, inocula were removed, cells were washed with PBS, and fresh medium was added. Cell culture supernatants were collected at indicated times post-infection, and viral titers were determined by plaque assay (Eckerle et al., 2007).

Interferon-β induction assays

Sub-confluent DBT cells were treated with 10 U/ml mouse IFN-β for 18 h prior to infection with mock, WT, nsp14 G332A, or nsp16 D130A virus at an MOI of 0.1 PFU/cell at 37°C for 45 min. Alternatively, sub-confluent DBT cells were infected with mock, WT, ExoN(-), or ExoN(-) P250 virus at an MOI of 0.1 PFU/cell or with Sendai virus (SenV) at an MOI of 200 HA (hemagglutination units)/ml at 37°C for 45 min. Inocula were removed, cells were washed with PBS, and fresh medium was added. At the indicated times post-infection, cell culture supernatants were aspirated and cell lysates were harvested by adding TRIzol reagent. Total RNA present in lysates was purified using the phenol/chloroform method. cDNA was generated by RT-PCR using 1μg of total RNA as described (Smith et al., 2013). Mouse IFN-β expression

levels relative to GAPDH were determined by qPCR using the Applied Biosciences 7500 Real-Time PCR System with Power SYBR Green PCR Master Mix and IFN-β primers: FWD: 5'-TCCGCCCTGTAGGTGAGGTTGAT-3' and REV: 5'-GTTCCTGCTGTGCTTCTCCACCA-3' and GAPDH primers previously reported (Smith et al., 2013).

Generation and infection of BMDCs

Primary BMDCs were isolated from the hind limbs of WT and IFN-α/β receptor-deficient (IFNAR-/-) C57BL/6J mice. Mice were euthanized by isoflurane overdose, and hind limbs were resected. Bone marrow cells were collected by flushing the femurs and tibiae with medium. Cells were strained through a 70-μm cell strainer, and red blood cells were lysed. Cells were cultured at 37°C in R10 medium supplemented to contain 20 ng/ml GM-CSF and 10 ng/ml IL-4. At 3 d post-plating, cell culture supernatants were removed and replaced with fresh R10 medium. Six days post-plating, cells were lifted using Cellstripper (Corning) and replated with fresh R10 medium in 24-well plates at a density of 10^5 cells/well and incubated at 37°C overnight. WT and $IFNAR^{-/-}$ BMDCs were infected with virus at an MOI of 0.01 PFU/cell at 37°C for 45 min. Inocula were removed, and fresh medium was added. Cell culture supernatants were collected 24 h post-infection, and viral titers were determined by plaque assay. All experiments with animals were performed in accordance with Vanderbilt University School of Medicine Institutional Animal Care and Use Committee guidelines.

Generation and infection of BMMs

Bone-marrow derived macrophages (BMMs) were generated from the hind limbs of WT, IFNAR-/-, RNaseL-/-/PKR-/-, or MDA5-/- C57/B6 mice as previously described (Zhao et al.,

2012b). BMMs were infected with virus at an MOI of 1 PFU/cell at 37°C for 1 h. After incubation, inocula were removed, cells were washed with 3 times with PBS, and fresh medium was added. At the indicated times post-infection, cell culture supernatant aliquots were collected and viral titers determined by plaque assay.

Purification of virions and extraction of RNA

Virion RNA was purified from sub-confluent T150 flasks of BHK-R cells infected with WT-FFL or nsp14 G332A-FFL viruses at an MOI of 0.001 PFU/cell. When CPE was apparent throughout the monolayer, cell culture supernatants were collected and pooled into 50 ml conical tubes (Corning), clarified by centrifugation at 1,000 x *g* for 10 min, and stored at -80°C. Upon thawing, virus particles in the clarified supernatants were collected by ultra-centrifugation at 106,750 x *g* overnight through a 5 ml, 20% (w/w) sucrose cushion in an SW32Ti rotor. The pelleted particles were resuspended in 200 µl MSE buffer (10 mM MOPS [pH 6.8], 150 mM NaCl, 1 mM EDTA) and incubated at 4°C overnight prior to resuspension by gently pipetting several times. Viral RNA was isolated from purified viral particles using TRIzol reagent (Invitrogen) and phenol/chloroform extraction.

In vitro translation reactions

Viral genomic RNAs containing an in-frame firefly luciferase encoding sequence were translated at 30°C for various intervals in 10 µl of rabbit reticulocyte lysate (Promega) in the presence of both 10 µM amino acid mixture minus leucine and 10 µM amino acid mixture minus methionine.

Firefly luciferase assays

Sub-confluent DBT cells were infected with virus at an MOI of 0.1 PFU/cell. At various intervals, cell culture supernatants were removed, cells were washed with PBS, and 100 µl of reporter cell lysis buffer (Promega) was added to each well. Cells lysates were frozen at -80°C to promote lysis and thawed at room temperature prior to quantifying firefly luciferase activity. Luciferase activity from cell lysates or *in vitro* translation reactions was quantified using a Veritas luminometer (Turner Biosystems) and the firefly luciferase assay system (Promega).

Determination of viral specific infectivity

Sub-confluent monolayers of DBT cells were infected with virus at the indicated MOI at 37°C for 45 min. After incubation, inocula were removed, cells were washed with PBS, and fresh medium was added. At the indicated times post-infection, cell culture supernatants were collected, and viral titers were determined by plaque assay. Supernatants also were used for RNA genome isolation by adding 100 µl supernatant to 900 µl TRIzol reagent, chloroform extraction by phase separation, and final purification using the PureLink Mini RNA kit (Ambion). Genome RNA was quantified using one-step qRT-PCR, and the particle to PFU ratio was calculated.

Determination of rRNA integrity

Sub-confluent monolayers of DBT cells were treated with 0 or 50 U/ml mouse IFN-β for 18 h prior to being infected with virus at an MOI of 1 PFU/cell at 37°C for 45 min. After incubation, inocula were removed, cells were washed with PBS, and fresh medium was added. At the indicated times post-infection, cell culture supernatants were removed and total RNA was harvested by adding 1ml TRIzol reagent. For a positive control, cells were transfected with 25ug/ml polyI:C (Sigma) using Lipofectamine 2000 (Thermo Fisher Scientific). Total RNA from

all samples was purified using the Purelink RNA Mini Purification System (Life Technologies) by following the manufacturers instructions. Upon purification, total RNA was analyzed on an Agilent Bioanalyzer by the Vanderbilt VANTAGE core facility and the rRNA integrity reported.

Genome RNA stability assay

Sub–confluent monolayers of DBT-9 cells were infected with virus at an MOI of 0.01 PFU/cell at 37°C for 45 min in the presence of DMSO or 100 μg/ml cycloheximide (CHX) (Sigma). Inocula were removed, media containing DMSO or 100 μg/ml CHX was added, and cell lysates were harvested at indicated times post-infection by removing the cell culture supernatant and adding TRIzol reagent. Lysates were spiked with a known amount of *in vitro* transcribed *Renilla* luciferase RNA and total RNA was obtained by phenol/ chloroform extraction. cDNA was generated by RT-PCR and viral genome copies present relative to *Renilla* luciferase was determined by SYBR Green qPCR using nsp10 (Smith et al., 2013) and *Renilla* luciferase specific primers (Habjan et al., 2013)**.**

Quantification of subgenomic RNA by qPCR

Sub-confluent DBT cells were treated with 0 or 100 U/mL mouse IFN-β for 18 h prior to being infected with virus at an MOI of 1 PFU/cell at 37°C for 45 min. After incubation, inocula were removed, cells were washed with PBS, and fresh medium was added. At the indicated times post-infection, cell culture supernatants were removed and total RNA was harvested by adding 1ml TRIzol reagent. Total RNA was extracted using the Purelink RNA mini purification system by following the manufacturers instructions. cDNA was generated by RT-PCR using 1ug of total RNA as previously described (Smith et al., 2013). Primers used to detect subgenomic

nucleocapsid and GAPDH gene expression have been reported (Donaldson et al., 2007; Smith et al., 2013). Subgenomic (N) expression levels relative to GAPDH were determined using the Applied Biosciences 7500 Real-Time PCR System with Power SYBR Green PCR Master Mix.

Quantification of viral genomic RNA by qRT-PCR

An RNA standard was prepared using the MHV A fragment (Yount et al., 2002) to generate a 931 nucleotide RNA. First, cDNA was generated by PCR amplification using the primers: forward 5'-TAATACGACTCACTATAGGGGGCTATGTGGATTGTTGTGG-3', which initiates with a T7 promoter, and reverse 5'-AATTCTTGACAAGCTCAGGC-3'. RNA for the standard curve was prepared using an mMessage mMachine T7 kit (Ambion) and purified using an RNeasy Mini kit (Qiagen). A standard curve was generated using 10-fold dilutions from 10^3 to 10^8 copies. A 5' 6-carboxyfluorescein (FAM)-labeled probe (5'-TTCTGACAACGGCTACACCCAACG-3' [Biosearch Technologies]) was used with forward (5'-AGAAGGTTACTGGCAACTG-3') and reverse (5'-TGTCCACGGCTAAATCAAAC-3') primers. Reactions were incubated on ice with enzyme added last. Final volume for reactions was 20 µl with 150 nM probe, 900 nM each primer, 2 µl sample RNA, and 10 µl 2X ToughMix, one-step, low ROX enzyme mix (Quantas) per reaction. Samples were quantified in duplicate using an Applied Biosciences 7500 Real-Time PCR System with the conditions 55°C for 10 min, 95°C for 5 min, 95°C for 30 s, and 60°C for 1 min, with the last two steps repeated 40 times. The standard curve was plotted using GraphPad Prism 6 software, and genomes/µl were calculated.

Co-infection assays

Sub-confluent monolayers of DBT cells were treated with 0 or 100 U/ml mouse IFN-β for 18 h

prior to being infected with virus at an MOI of 1 PFU/cell at 37°C for 45 min. After incubation, inocula were removed, cells were washed with PBS, and fresh medium was added. At 12 h post-infection, cell culture supernatants were removed and 100 µl of supernatant was added to 900 µl TRIzol reagent. Viral genome RNA was purified and the number of viral genome RNA copies present relative to an RNA standard curve were determined as described above. Based on the number of viral genome RNA copies determined by one-step RT-qPCR, an equal number of virus particles from each virus and each condition were combined with an equal number of WT silent or ExoN(-) silent virus particles, respectively. WT silent and ExoN(-) silent viruses were engineered to harbor 10 silent mutations in the probe-binding region of nsp2, allowing separate detection from WT-MHV or ExoN(-) virus genomes, respectively, using a separate probe upon co-infection (Graepel et al., 2017). Next, a fresh, sub-confluent monolayer of DBT cells were co-infected with each combination of viruses at 37°C for 45 min. After incubation, inocula were removed, cells were washed with PBS, and fresh medium was added. At 24 h post-infection, cell culture supernatants were removed and 100 µl of supernatant was added to 900 µl TRIzol reagent. Viral genome RNA was purified. The number of viral genome RNA copies of both reference and silent viruses were determined relative to the appropriate standard curve. The number of viral genome RNA copies relative to the number of silent virus genome RNA copies was determined for each virus and condition. Values are reported as the change in fitness relative to the silent virus.

RNA sequencing

RNA sequencing experiments were performed using DBT cells pretreated with 0 or 100U/ml mouse IFN-β for 26h. After pretreatment, cell culture supernatants were removed and total cell

lysates harvested using TRIzol reagent. Total RNA was extracted using the phenol/chloroform method and submitted to the Vanderbilt VANTAGE core for mRNA enrichment and cDNA library preparation utilizing stranded mRNA (poly-A-selected) sample preparation kit. Sequencing was performed at paired-end 75bp on an Illumina HiSeq 3000. Demultiplexed FASTQ files were analyzed by the Vanderbilt VANGUARD core using DESeq2, edgeR, and BaySeq algorithms to generate a multi-rank seq, fold change, and p-Value file.

DBT cell RNase L activation assays

DBT cells were untreated or pretreated with IFN-β for 18h. For IFN-β and polyI:C pretreated samples, cells were pretreated with IFN-β for 17h and then transfected with 25μg poly I:C in the presence of IFN-β for the final hour prior to infection with WT or ExoN(-) virus at an MOI of 1 PFU/cell. At 12h post-infection, cell culture supernatants were collected and viral titers were determined by plaque assay.

Detection of viral infection by flow cytometry

In order to determine the percentage of DBT cells infected with WT-RFPnsp2-Ex(-)-P250S or ExoN(-)-nsp2-Ex(-)P250S virus by flow cytometry, DBT cells were pretreated with 0 or 250 U/ml mouse IFN-β for 18h. Next, cells were infected with WT-RFPnsp2-Ex(-)-P250S or ExoN(-)-nsp2-Ex(-)P250S virus at an MOI of 0.1 PFU/cell. At 6 and 8h post-infection, cell culture supernatants were removed and cells were dislodged using Cellstripper (Corning). Cells were diluted in MACS wash (PBS, 5% FBS, and 2% EDTA) and RFP expression was analyzed using a Fortessa 4-laser flow cytometer (BD Biosciences). Flow cytometry data were analyzed using FlowJo software (Treestar).

Generation of lentiviral pseudoparticles

In order to generate lentiviral pseudoparticles, 293T cells were reverse transfected with 100ng pSpax, 50ng pMD2G, and 150ng shRNA encoding plasmid using 1.2 µl FuGENE 6 reagent in a T.V. of 10 µl serum-free media per well. After plating the DNA/ FuGENE mix, 293T cells were added at a density of $2x10^4$ cells in a T.V. of 100 µl per well. At 48 h post-transfection, 293T cells were checked for GFP expression and cell culture supernatants were collected and respectively pooled.

Transduction of DBT cells

DBT cells were plated in 96-well flat bottom plates at a density of $0.25x10^4$ cells per well and incubated at 37°C. At 24 h post-plating, cell culture supernatants were removed from DBT cells and 20 µl of cell culture media supplemented to contain 50 µg/ml polybrene (Millipore) was added. Next, 80 µl of lentiviral supernatant was added to respective wells and gently mixed. Cells were spinoculated for 30 min. at room temperature at 800x *g* and incubated overnight at 37°C. After incubation, cell culture supernatants were carefully removed and replaced with fresh cell culture media. Cells were allowed to grow for an additional 2 days and then checked for GFP expression. For flow cytometry, cell culture supernatants were removed and cells were fixed using 1% paraformaldehyde. GFP expression was analyzed using a Fortessa 4-laser flow cytometer (BD Biosciences). Flow cytometry data were analyzed using FlowJo software (TreeStar).

Statistical analysis

Statistical tests were conduced as described in the respective figure legends using GraphPad Prism 6 software (La Jolla, CA). Error bars and the number of replicates for each experiment are also listed in respective figure legends.

Primers generated for this dissertation research

Table 2: Primers generated for this dissertation research (IDT)

Primer Name	Sequence 5′-3′
Quick-change primers for mutant viruses	
Nsp14 D272A Fwd	GCTCATGTTGCATCATCT**GCG**GCTATCATGACCCGGTGT
Nsp14 D272A Rev	ACACCGGGTCATGATAGC**CGC**AGATGATGCAACATGAGC
Nsp14 D330A Fwd	GGTATGATGTGTGTTAT**GCA**ATTGGCAACCCTAAAGG
Nsp14 D330A Rev	CCTTTAGGGTTGCCAAT**TGC**ATAACACACATCATACC
Nsp14 G332A Fwd	GGTATGATGTGTGTTATGACATT**GCT**AACCCTAAAGGTCTTGCC
Nsp14 G332A Rev	GGCAAGACCTTTAGGGTT**AGC**AATGTCATAACACACATCATACC
Nsp16 D130A Fwd	GGGATCTGATAATTTCT**GCG**ATGTACGACCCTCTTAC
Nsp16 D130A Rev	GTAAGAGGGTCGTACAT**CGC**AGAAATTATCAGATCCC
qPCR primers	
Mouse IFN-β Fwd	TCCGCCCTGTAGGTGAGGTTGAT
Mouse IFN-β Rev	GTTCCTGCTGTGCTTCTCCACCA
Renilla Luc Fwd	CGAAAGTTTATGATCCAGAAC
Renilla Luc Rev	AATCATAATAATTAATAAATG

Chapter VI

SUMMARY AND FUTURE DIRECTIONS

Introduction

Coronaviruses have demonstrated a capacity to infect numerous mammalian and avian species. Potentially one of the most important observations made over the past decade and a half of coronavirus (CoV) research is that CoVs have and, undoubtedly, will continue to spill over into human populations (Perlman and Netland, 2009). When a future cross-species transmission event occurs, the disease may be mild, as seen in human coronavirus 229E and OC43 infections, or disease may be severe, as seen in SARS-CoV and MERS-CoV patients. Regardless of disease severity, specific antiviral therapies are currently not available to treat human CoV infections. Thus, it is essential to understand the contributions of conserved CoV proteins in viral replication and pathogenesis. One probable reason CoVs are successful pathogens is they encode multiple innate immune antagonists within their uniquely large RNA genomes (de Wit et al., 2016; Frieman et al., 2008; Perlman and Netland, 2009). Studies have suggested that SARS-CoV pathogenesis is due, at least in part, to an insufficient innate immune response (Cheung et al., 2005; Gu and Korteweg, 2007). In addition, excessive induction of pro-inflammatory cytokines and chemokines in SARS-CoV patients, and potentially MERS-CoV patients, suggest that dysregulation of the innate immune response is also a major contributor of the observed immunopathogenesis associated with these infections (de Wit et al., 2016; Gu and Korteweg, 2007). Therefore, disarming a conserved CoV antagonist may provide a window of opportunity for prospective antiviral therapies or our own immune systems to attenuate viral replication and disease.

At the beginning of this dissertation research, CoV non-structural protein (nsp) 14 had not been investigated as an innate immune antagonist. Rather, it was known that nsp14 3'-to-5' exoribonuclease (ExoN) activity potentially performed a proofreading function during viral RNA replication and that nsp14 also encoded N7-methyltransferase (N7-MTase) activity (Bouvet et al., 2012; Chen et al., 2009; Minskaia et al., 2006; Smith et al., 2014). The overall goal of this dissertation research was to determine whether nsp14 ExoN or N7-MTase activities played a role in counteracting the innate immune response. In this chapter, I summarize the main findings of my dissertation research and highlight important future directions generated as a result of my work.

Coronavirus nsp14 N7-MTase activity is required for efficient viral RNA translation

In the nucleus, nascent cellular mRNAs are capped at the 5' end of the RNA molecule (Shatkin, 1976). The 5' cap has several important biological roles such as providing RNA stability, directing pre-mRNA splicing, and mRNA export from the nucleus (Darnell, 1979; Decroly et al., 2011b). Moreover, the 5' cap is critical for recognition by eukaryotic translation initiation factor 4 E (eIF4E) and thus, efficient translation (Decroly et al., 2011b; Filipowicz et al., 1976; Schibler and Perry, 1977). To ensure efficient viral protein translation, viruses have also evolved mechanisms in which to cap their RNAs. When I started this dissertation research, it was known that CoVs encoded multiple capping enzymes. Further, it had been demonstrated that CoV nsp14 encoded N7-MTase activity *in vitro* and that nsp14-mediated N7-methylation of an RNA template necessarily preceded CoV nsp10-16 2'O-methylation (Bouvet et al., 2010; Chen et al., 2009). In addition, it had been demonstrated that CoV nsp14 N7-MTase activity and S-adenosyl-

L-methionine (SAM) binding was conferred by a conserved DxG motif in the N7-MTase domain (Bouvet et al., 2010; Chen et al., 2009; 2013). My dissertation research was the first study to investigate the requirements of nsp14 N7-MTase activity during coronavirus replication. My data show that alanine substitution of nsp14 residue G332 results in attenuated viral replication and decreased viral RNA translation both during viral replication and during *in vitro* translation of purified viral RNA. In direct contrast to existing biochemical data, my data also demonstrate that murine hepatitis virus (MHV) nsp14 residue D330 is dispensable for virus replication. In addition to the DxG motif, other residues were identified as important for N7-MTase activity in recombinant *in vitro* assays. Mutation of SARS-CoV nsp14 at position R310 or D352 resulted in a decrease or total loss of SAM binding and N7-MTase activity (Chen et al., 2013). Future studies should address the contributions of these residues in CoV nsp14 N7-MTase activity. In fact, the nsp10/nsp14 co-crystal structure suggests SARS-CoV nsp14 R310 contributes positive potential for binding the triphosphate portion of the RNA molecule and residue D352 forms hydrogen bonds with the O3' and O2' atoms of the ribose of SAM (Ma et al., 2015). These studies will be important for determining the precise residues of nsp14 that are responsible for coordinating the N7-methylation reaction in order to inform cap analog and small molecule inhibitor studies.

Coronavirus nsp14 N7-MTase activity is required for evasion of and resistance to the innate immune response

In addition to N7-methylation, the mRNAs of higher eukaryotes are methylated at the 2'O position of the ribose sugar of the penultimate nucleotide (Wei et al., 1975). 2'O-methylation provides a molecule signature for the cell to discriminate between 'self' and 'non-self' mRNAs

(Daffis et al., 2010; Züst et al., 2011). Not surprisingly, many viruses have evolved to encode 2'O-methyltransferases (2'O-MTases) in order to subvert this mechanism and thus, mask viral RNAs from host innate immune sensors (Daffis et al., 2010; Züst et al., 2011). Innate sensors such as MDA5 and IFIT1 have been demonstrated to detect viral RNAs lacking fully capped structures and to subsequently function to restrict viral replication (Daffis et al., 2010; Decroly et al., 2011b; Habjan et al., 2013; Menachery et al., 2014; Züst et al., 2011). Prior to my dissertation research, data suggested that CoVs used the canonical capping pathway to cap viral RNAs (Bouvet et al., 2010; Chen et al., 2013). I tested the hypothesis that by ablating CoV N7-MTase activity, not only should viral RNA translation be delayed/ reduced, but also, that downstream 2'O-methylation should be inhibited. In Chapter II, my data demonstrate that CoV nsp14 G332A mutant viruses are sensed by the cell, leading to induction of type I interferon (IFN). Since G332A virus demonstrated reduced translation in addition to induction of and sensitivity to IFN, my data further support the hypothesis and agree with all data to date that suggest CoVs use the canonical capping pathway to cap viral RNAs. In previous studies, 2'O-MTase deficient CoVs and avian metapneuomoviruses were protective against lethal challenge (Menachery et al., 2014; Sun et al., 2014). Thus, methyltransferase-defective viruses are excellent candidates for live-attenuated vaccines. Future experiments from my work should investigate the replication capacity and attenuation of MHV nsp14 D330A and MHV nsp14 G332A viruses in animal models of disease. While nsp14 D330A mutant virus demonstrated WT-like phenotypes in all assays performed *in vitro*, this virus may be attenuated *in vivo*. To further attenuate virus replication, my data suggest that combining CoV N7-MTase and 2'O-MTase ablating mutations should provide at least two mechanisms of attenuating viral replication. To perform these future studies, I have engineered and recovered MHV nsp14

D330A-nsp16 D130A and MHV nsp14 G332A-nsp16D130A mutant viruses but phenotype characterization has not begun at this time.

Coronavirus nsp14 ExoN activity is required for counteracting the innate immune response

In Chapter III of this dissertation, I reported my discovery that CoV nsp14 ExoN activity is required for resistance to the innate immune response. This study yields exciting new questions that will need to be answered to further understand CoV nsp14 ExoN activity and its role in innate immunity. Recently, it was demonstrated that loss of CoV nsp15 endonuclease (EndoU) activity resulted in increased viral dsRNA levels during replication, suggesting that nsp15 endonucleolytically cleaves viral dsRNAs to prevent detection by the host (Kindler et al., 2017). In addition, a transmissible gastroenteritis virus nsp14 ExoN domain, gain-of-function mutant demonstrated decreased dsRNA accumulation during viral replication (Becares et al., 2016). As a result, it has been proposed that CoV nsp14 ExoN activity may function to further degrade the viral dsRNA products of nsp15 (Becares et al., 2016; Kindler et al., 2017). While my data did not reveal a role for MHV nsp14 in degrading dsRNA, this potential function should be further evaluated in bone marrow-derived macrophages (BMMs). Viruses lacking ExoN activity did not replicate beyond 9 h post-infection in WT BMMs. However, replication of viruses lacking ExoN activity was partially or fully restored to WT-MHV levels in IFN alpha/beta receptor deficient (IFNAR-/-) BMMs. Therefore, the mechanism of attenuation in WT BMMs should be elucidated by assessing viral RNA levels for WT and ExoN(-) viruses during replication in BMMs. In murine delayed brain tumor (DBT) cells, ExoN(-) viral RNA was not substantially reduced. However, if ExoN(-) virus RNA levels are decreased in WT BMMs, this result would suggest

potentially two different mechanisms of attenuation between DBT cells and BMMs. In addition, ExoN(-) virus replication in BMMs should be assessed for the induction of IFN and the secretion of pro-inflammatory cytokines. Again, if IFN were induced, this would suggest a potentially different mechanism of attenuation for ExoN(-) virus in BMMs in comparison with DBT cells within which ExoN(-) virus replication did not induce IFN-β expression.

In DBT cells, my data suggest that ExoN(-) virus is restricted upon subsequent infection of cells specifically when the ExoN(-) progeny are generated in the presence of an IFN-β-induced antiviral state. Future experiments should be performed to determine if the restricted ExoN(-) progeny are purely non-viable or if the incoming ExoN(-) viruses are sensed and restricted by the innate immune response of newly infected cells. To facilitate these discoveries, I have developed and generated 293T cells stably expressing the MHV viral receptor (MHV-R), murine carcinoembryonic antigen-related cell adhesion molecule 1a. Using 293T-MHV-R cells will render any potential mouse IFN-β carryover from a primary experiment nonfunctional in downstream experiments and will also allow additional approaches for determining whether IFN-β generated ExoN(-) progeny are inducing an immune response in recipient cells (for instance using an IFN-β-luciferase reporter plasmid). If IFN-β generated ExoN(-) progeny are not inducing an innate immune response during subsequent infection, this would suggest that the viral genome or an RNA modification is altered during antiviral conditions. Therefore, IFN-β-generated ExoN(-) virus progeny genomes should be assessed by deep sequencing methods to determine if an ISG is further increasing or decreasing ExoN(-) virus mutation frequency. In addition, the high-throughput screen developed and described in Chapter IV of this dissertation could be used to identify the specific gene or genes responsible. Alternative and complimentary

approaches should include but are not limited to crosslinking viral RNA and RNA binding proteins in the presence and absence of IFN-β treatment and ExoN activity to identify proteins that may be preferentially acting on the ExoN(-) viral genome.

Previously, it was shown that ExoN(-) mouse adapted SARS-CoV (MA-SARS-CoV) is attenuated *in vivo*, and protects mice from lethal challenge (Graham et al., 2012). However, the mechanism of attenuation *in vivo* was presumed to be due to decreased viral replication fidelity and was not investigated further. Future experiments with WT and ExoN(-) MA-SARS-CoV should be performed in immunocompenent and immunocompromised mice to determine the extent of viral dissemination, viral loads in peripheral organs, and to determine IFN-β and pro-inflammatory cytokine gene expression. Recently, an increased replication fidelity, decreased genome recombination strain of poliovirus was demonstrated to be restricted *in vivo* due to an incapacity to overcome tissue specific innate immune responses (Xiao et al., 2017). Therefore, analyses of these experiments should focus on the effects of altered fidelity in ExoN(-) viruses as well as the contributions of ExoN activity to either directly or indirectly antagonize the innate immune response. Together, these studies will further elucidate the requirement of CoV ExoN activity in counteracting an immune response and will provide rationale for the development of ExoN(-) viruses as live-attenuated vaccines.

Concluding Remarks: nsp14 is the Achilles' heel of coronaviruses

Nsp14 encoded ExoN and N7-MTase activities are conserved across coronaviruses (Gorbalenya et al., 2006; Lauber et al., 2013). My dissertation research alone suggests that the absence of a functional nsp14 can be linked to at least four different mechanisms of viral attenuation: 1) viral

protein translation (N7-MTase activity), preventing induction of IFN (N7-MTase activity), required for resistance to IFN (N7-MTase and ExoN activities), and required for efficient viral replication (ExoN and N7-MTase activities). The research described in this dissertation is my small contribution to the overall human understanding of coronaviruses. It is my hope that this dissertation research provides the basis and rationale for the development of antiviral therapies directed against coronavirus nsp14 to treat or prevent coronavirus infections. Due to the conservation of nsp14 activities, such therapies should be broadly applicable to existing or emerging coronaviruses of the future.

APPENDIX A:

MUTAGENESIS OF S-ADENOSYL-L-METHIONINE-BINDING RESIDUES IN CORONAVIRUS NSP14 N7-METHYLTRANSFERASE DEMONSTRATES DIFFERING REQUIREMENTS FOR GENOME TRANSLATION AND RESISTANCE TO INNATE IMMUNITY

AMERICAN SOCIETY FOR MICROBIOLOGY | Journal of Virology

Mutagenesis of *S*-Adenosyl-L-Methionine-Binding Residues in Coronavirus nsp14 N7-Methyltransferase Demonstrates Differing Requirements for Genome Translation and Resistance to Innate Immunity

James Brett Case,[a,b] Alison W. Ashbrook,[b,c] Terence S. Dermody,[a,b,c] Mark R. Denison[a,b,c]

Departments of Pathology, Microbiology, and Immunology[a] and Pediatrics,[c] and Elizabeth B. Lamb Center for Pediatric Research,[b] Vanderbilt University Medical Center, Nashville, Tennessee, USA

ABSTRACT

Eukaryotic mRNAs possess a methylated 5′-guanosine cap that is required for RNA stability, efficient translation, and protection from cell-intrinsic defenses. Many viruses use 5′ caps or other mechanisms to mimic a cap structure to limit detection of viral RNAs by intracellular innate sensors and to direct efficient translation of viral proteins. The coronavirus (CoV) nonstructural protein 14 (nsp14) is a multifunctional protein with N7-methyltransferase (N7-MTase) activity. The highly conserved *S*-adenosyl-L-methionine (SAM)-binding residues of the DxG motif are required for nsp14 N7-MTase activity *in vitro*. However, the requirement for CoV N7-MTase activity and the importance of the SAM-binding residues during viral replication have not been determined. Here, we engineered mutations in murine hepatitis virus (MHV) nsp14 N7-MTase at residues D330 and G332 and determined the effects of these mutations on viral replication, sensitivity to mutagen, inhibition by type I interferon (IFN), and translation efficiency. Virus encoding a G332A substitution in nsp14 displayed delayed replication kinetics and decreased peak titers relative to wild-type (WT) MHV. In addition, replication of nsp14 G332A virus was diminished following treatment of cells with IFN-β, and nsp14 G332A genomes were translated less efficiently both *in vitro* and during viral infection. In contrast, substitution of alanine at MHV nsp14 D330 did not affect viral replication, sensitivity to mutagen, or inhibition by IFN-β compared to WT MHV. Our results demonstrate that the conserved MHV N7-MTase SAM-binding-site residues are not required for MHV viability and suggest that the determinants of CoV N7-MTase activity differ *in vitro* and during virus infection.

IMPORTANCE

Human coronaviruses, most notably severe acute respiratory syndrome (SARS)-CoV and Middle East respiratory syndrome (MERS)-CoV, cause severe and lethal human disease. Since specific antiviral therapies are not available for the treatment of human coronavirus infections, it is essential to understand the functions of conserved CoV proteins in viral replication. Here, we show that substitution of alanine at G332 in the N7-MTase domain of nsp14 impairs viral replication, enhances sensitivity to the innate immune response, and reduces viral RNA translation efficiency. Our data support the idea that coronavirus RNA capping could be targeted for development of antiviral therapeutics.

Eukaryotic mRNAs possess a methylated 5′ guanosine cap linked to the penultimate nucleotide by a 5′-5′ triphosphate bridge (1). The 5′ capping of cellular mRNAs functions in RNA stability, pre-mRNA splicing, mRNA export from the nucleus, translation, and protection against cellular antiviral defenses (2). The canonical cellular capping process involves three enzymes: (i) an RNA triphosphatase (RTPase), which is responsible for cleaving the γ-phosphate of the nascent transcript, (ii) a guanylyltransferase (GTase), which transfers a GMP moiety to the 5′ diphosphate RNA, and (iii) an N7-methyltransferase (N7-MTase), which is responsible for transferring a methyl group from the methyl donor, *S*-adenosyl-L-methionine (SAM), to the N7 position of the guanosine base (3). These sequential reactions lead to formation of a cap-0 (7-methyl-Gppp) structure, which is thought to be the minimal cap determinant required for eIF4E recognition and efficient translation (4–6). Higher eukaryotes express 2′O-methyltransferases (2′O-MTase), which add a methyl group to the ribose 2′O position of the penultimate nucleotide of the cap-0 RNA. This reaction results in the formation of a cap-1 structure that allows cells to differentiate self from nonself RNAs in the cytoplasm (7, 8).

Eukaryotic viruses use host translation machinery, and many of these viruses encode capping enzymes. The diversity of enzymes and mechanisms used by viruses to synthesize capped RNA products suggests that there is selective pressure on viruses to cap their RNAs (9). Coronaviruses (CoVs) encode several enzymes within their large, positive-sense RNA genomes (27 to 34 kb) that are implicated in viral RNA capping. The coronavirus genome possesses a 5′ terminal cap and a 3′ poly(A) tail (10–12). All data to

Received 22 March 2016 Accepted 24 May 2016

Accepted manuscript posted online 1 June 2016

Citation Case JB, Ashbrook AW, Dermody TS, Denison MR. 2016. Mutagenesis of *S*-adenosyl-L-methionine-binding residues in coronavirus nsp14 N7-methyltransferase demonstrates differing requirements for genome translation and resistance to innate immunity. J Virol 90:7248–7256. doi:10.1128/JVI.00542-16.

Editor: S. Perlman, University of Iowa

Address correspondence to Mark R. Denison, mark.denison@vanderbilt.edu.

date support the hypothesis that CoV genomes are capped using the canonical mRNA capping pathway (13). Severe acute respiratory syndrome coronavirus (SARS-CoV) nsp13 displays RTPase activity *in vitro* (14). The CoV guanylyltransferase has not been identified but, according to the current model, would function to add a GMP to the diphosphate RNA product of nsp13. The RNA-dependent RNA polymerase (RdRp) of equine arteritis virus and SARS-CoV displays nucleotidylation activity (15). While further study is required to define the function of this activity in viral replication, it is possible that the RdRp participates in CoV RNA capping. nsp16 of feline coronavirus functions independently as a 2′O-MTase (16–18), but SARS-CoV nsp16 requires nsp10 as a cofactor for 2′O-MTase activity. SARS-CoVs lacking 2′O-MTase activity are recognized and sequestered by IFIT1 (13, 19–23) due to the lack of a cap-1 structure.

CoV nsp14 is a multifunctional protein with 3′-5′ exoribonuclease activity and N7-MTase activity (24, 25). nsp14-mediated N7-methylation of Gppp-RNA to form a cap-0 structure is a prerequisite for nsp10/16-mediated 2′O-methylation *in vitro* (13). A conserved DxG motif within the MTase domain is required for SAM binding *in vitro*, and alteration of these residues abolishes MTase activity *in vitro* (13, 26). However, the requirements of the CoV nsp14 N7-MTase during viral replication are not known. Therefore, we assessed the effect of mutations in the DxG motif of the MHV nsp14 N7-MTase on viral replication. We show that substitution of alanine at nsp14 D330 does not alter viral replication kinetics or increase sensitivity to beta interferon (IFN-β) treatment relative to wild-type (WT) MHV. However, substitution of alanine at nsp14 G332 impaired virus replication, resulting in delayed replication kinetics and decreased peak titer relative to WT MHV. In addition, nsp14 G332A virus displayed increased sensitivity to treatment of cells with IFN-β, and nsp14 G332A genomes were translated less efficiently *in vitro* and during infection. These data suggest that residue G332, but not residue D330, is required for MHV nsp14 N7-MTase activity and, collectively, that the regulation of CoV capping is likely more complex in the context of replicating virus than during *in vitro* biochemical studies with isolated proteins.

MATERIALS AND METHODS

Cells and viruses. Murine delayed brain tumor (DBT) cells (27) and baby hamster kidney 21 cells expressing the MHV receptor (BHK-R) (28) were maintained at 37°C in Dulbecco's modified Eagle medium (DMEM; Gibco) supplemented to contain 10% fetal bovine serum (FBS; Invitrogen), 100 U/ml penicillin and streptomycin (Gibco), and 0.25 μg/ml amphotericin B (Corning). BHK-R cells were further supplemented to contain 0.8 mg/ml of G418 (Mediatech). Bone marrow-derived dendritic cells (BMDCs) were maintained in R10 medium (RPMI 1640 [Gibco] supplemented to contain 10% FBS, 2 mM L-glutamine, 100 μg/ml gentamicin [MP Biomedicals], 0.25 μg/ml amphotericin B, 50 μM beta-mercaptoethanol, 20 ng/ml granulocyte-macrophage colony-stimulating factor [GM-CSF], and 10 ng/ml interleukin-4 [IL-4]). Recombinant MHV strain A59 (GenBank accession number AY910861) was propagated as described previously (28).

Cloning, recovery, and verification of mutant viruses. Site-directed mutagenesis was used to engineer point mutations in individual MHV genome cDNA fragment plasmids using the MHV infectious clone reverse genetics system (28). Viruses encoding firefly luciferase (FFL) fused to nsp2 were recovered using MHV A frag-FFL2 (29). Mutant viruses were recovered using BHK-R cells following electroporation of *in vitro*-transcribed genomic RNA. All mutagenized plasmids were sequenced (GenHunter Corporation, Nashville, TN) to ensure that no additional mutations were introduced. Recovered viruses also were sequenced to verify the engineered mutations.

Virus replication kinetics. Subconfluent DBT cell monolayers were infected at a multiplicity of infection (MOI) of 1 PFU per cell at 37°C for 45 min. Inocula were removed, cells were washed with 1× phosphate-buffered saline (PBS), and fresh medium was added. Aliquots were harvested at various times postinfection. Viral titer at various intervals was determined by plaque assay (30).

5-FU sensitivity assays. 5-Fluorouracil (5-FU; Sigma) was prepared as a 200 mM stock solution in dimethyl sulfoxide (DMSO). Subconfluent DBT cells were treated with DMEM supplemented to contain various concentrations of 5-FU or DMSO alone at 37°C for 30 min (31). Drug was removed, and cells were infected with virus at an MOI of 0.01 PFU/cell at 37°C for 1 h. Inocula were removed, and cells were incubated in medium containing 5-FU or DMSO. Cell culture supernatants were collected at 24 h postinfection, and viral titers were determined by plaque assay.

IFN-β sensitivity assays. Subconfluent DBT cells were treated with various concentrations of mouse IFN-β (PBL Assay Science) for 18 h prior to infection with virus at an MOI of 1 PFU/cell at 37°C for 45 min. Inocula were removed, cells were washed with PBS, and fresh medium was added. Cell culture supernatants were collected at the indicated times postinfection, and viral titers were determined by plaque assay.

IFN-β induction assays. Subconfluent DBT cells were treated with 10 U/ml mouse IFN-β for 18 h prior to infection with virus at an MOI of 0.1 PFU/cell at 37°C for 45 min. Inocula were removed, cells were washed with PBS, and fresh medium was added. At 12 h postinfection, cell culture supernatants were aspirated and cell lysates were harvested by adding TRIzol reagent. Total RNA present in lysates was purified using the phenol-chloroform method. cDNA was generated by reverse transcription (RT)-PCR using 1 μg of total RNA as described previously (31). Mouse IFN-β expression levels relative to GAPDH (glyceraldehyde-3-phosphate dehydrogenase) were determined by quantitative real-time PCR (qPCR) using the Applied Biosciences 7500 real-time PCR system with the Power SYBR green PCR master mix and the IFN-β primers FWD, 5′-TCCGCC CTGTAGGTGAGGTTGAT-3′, and REV, 5′-GTTCCTGCTGTGCTTCT CCACCA-3′ and the GAPDH primers previously reported (31).

Generation and infection of BMDCs. Primary BMDCs were isolated from the hind limbs of WT and IFN-α/β receptor-deficient ($IFNAR^{-/-}$) C57BL/6J mice. Mice were euthanized by isoflurane overdose, and hind limbs were resected. Bone marrow cells were collected by flushing the femurs and tibiae with medium. Cells were strained through a 70-μm cell strainer, and red blood cells were lysed. Cells were cultured at 37°C in R10 medium supplemented to contain 20 ng/ml GM-CSF and 10 ng/ml IL-4. At 3 days postplating, cell culture supernatants were removed and replaced with fresh R10 medium. Six days postplating, cells were lifted using Cellstripper (Corning) and replated with fresh R10 medium in 24-well plates at a density of 10^5 cells/well and incubated at 37°C overnight. WT and $IFNAR^{-/-}$ BMDCs were infected with virus at an MOI of 0.01 PFU/cell at 37°C for 45 min. Inocula were removed, and fresh medium was added. Cell culture supernatants were collected 24 h postinfection, and viral titers were determined by plaque assay. All experiments with animals were performed in accordance with Vanderbilt University School of Medicine Institutional Animal Care and Use Committee guidelines.

Purification of virions and extraction of RNA. Virion RNA was purified from subconfluent T150 flasks of BHK-R cells infected with WT-FFL or nsp14 G332A-FFL viruses at an MOI of 0.001 PFU/cell. When cytopathic effect was apparent throughout the monolayer, cell culture supernatants were collected and pooled into 50-ml conical tubes (Corning), clarified by centrifugation at 1,000 × *g* for 10 min, and stored at −80°C. Upon thawing, virus particles in the clarified supernatants were collected by ultracentrifugation at 106,750 × *g* overnight through a 5-ml, 20% (wt/wt) sucrose cushion in an SW32Ti rotor. The pelleted particles were resuspended in 200 μl MSE buffer (10 mM MOPS [morpholinepropanesulfonic acid] [pH 6.8], 150 mM NaCl, 1 mM EDTA) and incubated

at 4°C overnight prior to resuspension by gently pipetting several times. Viral RNA was isolated from purified viral particles using TRIzol reagent (Invitrogen) and phenol-chloroform extraction.

***In vitro* translation reactions.** Viral genomic RNAs containing an in-frame firefly luciferase-encoding sequence were translated at 30°C for various intervals in 10 μl of rabbit reticulocyte lysate (Promega) in the presence of both 10 μM amino acid mixture without leucine and 10 μM amino acid mixture without methionine.

Firefly luciferase assays. Subconfluent DBT cells were infected with virus at an MOI of 0.1 PFU/cell. At various intervals, cell culture supernatants were removed, cells were washed with PBS, and 100 μl of reporter cell lysis buffer (Promega) was added to each well. Cells lysates were frozen at −80°C to promote lysis and thawed at room temperature prior to quantifying firefly luciferase activity. Luciferase activity from cell lysates or *in vitro* translation reactions was quantified using a Veritas luminometer (Turner Biosystems) and the firefly luciferase assay system (Promega).

Determination of specific infectivity. Subconfluent monolayers of DBT-9 cells were infected with virus at an MOI of 0.1 PFU/cell at 37°C for 45 min. Inocula were removed, fresh medium was added, and cells were incubated at 37°C for 24 h. Cell culture supernatants were collected, and viral titers were determined by plaque assay. Supernatants also were used for RNA genome isolation by addition of 100 μl supernatant to 900 μl TRIzol reagent, chloroform extraction by phase separation, and final purification using the PureLink Mini RNA kit (Ambion). Genome RNA was quantified using one-step qRT-PCR, and the particle-to-PFU ratio was calculated.

Genome RNA stability assay. Subconfluent monolayers of DBT-9 cells were infected with virus at an MOI of 0.01 PFU/cell at 37°C for 45 min in the presence of DMSO or 100 μg/ml cycloheximide (CHX; Sigma). Inocula were removed, medium containing DMSO or 100 μg/ml CHX was added, and cell lysates were harvested at the indicated times postinfection by removing the cell culture supernatant and adding TRIzol reagent. Lysates were spiked with a known amount of *in vitro*-transcribed *Renilla* luciferase RNA, and total RNA was obtained by phenol-chloroform extraction. cDNA was generated by RT-PCR, and the number of viral genome copies present relative to *Renilla* luciferase was determined by SYBR green qPCR using nsp10 (31) and *Renilla* luciferase-specific primers (22).

Quantification of viral genomic RNA by qRT-PCR. An RNA standard was prepared using the MHV A fragment (28) to generate a 931-nucleotide RNA. First, cDNA was generated by PCR amplification using the following primers: forward, 5′-TAATACGACTCACTATAGGGGGC TATGTGGATTGTTGTGG-3′, which initiates with a T7 promoter, and reverse, 5′-AATTCTTGACAAGCTCAGGC-3′. RNA for the standard curve was prepared using an mMessage mMachine T7 kit (Ambion) and purified using an RNeasy minikit (Qiagen). A standard curve was generated using 10-fold dilutions from 10^3 to 10^8 copies. A 5′ 6-carboxyfluorescein (FAM)-labeled probe (5′-TTCTGACAACGGCTACACCCAAC G-3′ [Biosearch Technologies]) was used with forward (5′-AGAAGGTT ACTGGCAACTG-3′) and reverse (5′-TGTCCACGGCTAAATCAAAC-3′) primers. Reaction mixtures were incubated on ice with enzyme added last. The final volume for reaction mixtures was 20 μl, with 150 nM probe, 900 nM each primer, 2 μl sample RNA, and 10 μl 2× ToughMix, one-step, low ROX enzyme mix (Quantas) per reaction mixture. Samples were quantified in duplicate using an Applied Biosciences 7500 real-time PCR system under the following conditions: 55°C for 10 min, 95°C for 5 min, 95°C for 30 s, and 60°C for 1 min, with the last two steps repeated 40 times. The standard curve was plotted using GraphPad Prism 6 software, and the number of genomes per microliter was calculated.

Statistical analysis. Statistical tests were conducted using GraphPad Prism 6 software (La Jolla, CA) as indicated in the respective figure legends.

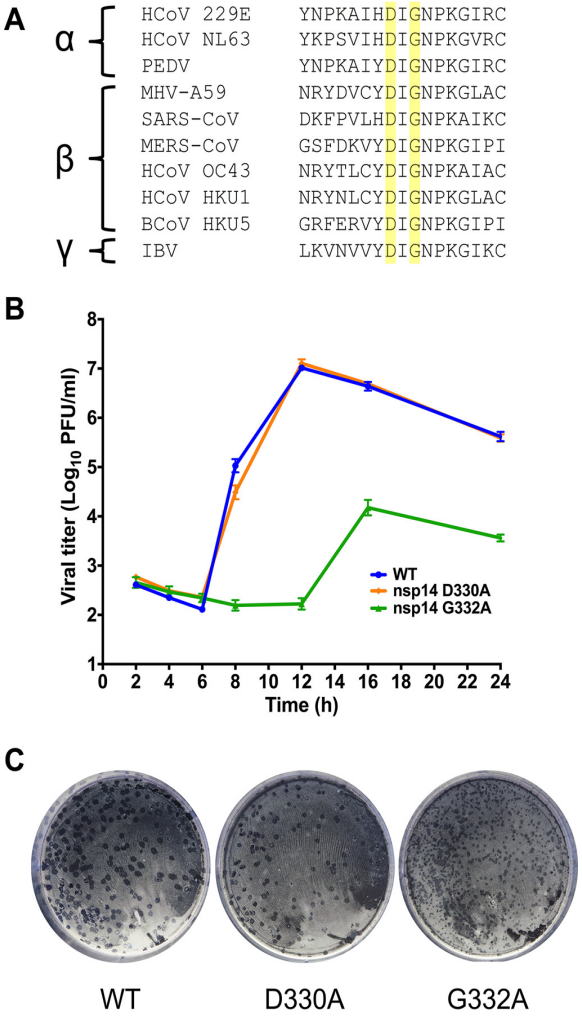

FIG 1 Replication kinetics of viruses with altered N7-MTase SAM-binding residues. (A) Alignment of GenBank ORF1b sequences of the α-, β-, and γ-CoVs shown demonstrates that SAM-binding residues (highlighted in yellow) are highly conserved. (B) DBT cells were infected with the viruses shown at an MOI of 1 PFU/cell. Cell culture supernatants were collected at the indicated times postinfection, and viral titers were determined by plaque assay. Error bars indicate standard errors of the means (SEM) ($n = 6$). (C) Plaque morphology of the viruses following agarose overlay plaque assay and fixation with 3.7% paraformaldehyde 24 h postinfection.

RESULTS

Recovery and replication kinetics of MHV nsp14 N7-MTase mutants. The DxG SAM-binding motif is conserved among the nsp14 N7-MTase domains of alpha-, beta-, and gammacoronaviruses (Fig. 1A). Mutations in this motif of SARS-CoV nsp14 ablate N7-MTase activity of purified proteins *in vitro* (13, 25, 26). To determine whether this motif is required for viral replication, we engineered alanine substitutions at the DxG SAM-binding motif in the MHV nsp14 N7-MTase domain. Virus containing either a D330A or G332A substitution in nsp14 was recovered, and the nucleotide sequence of each virus was confirmed across the nsp14-coding region. Following infection of DBT cells at an MOI of 1 PFU/cell, nsp14 D330A virus replicated with kinetics compa-

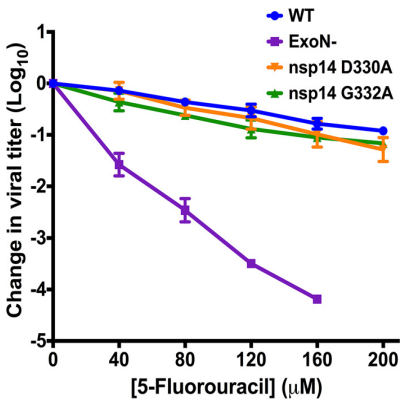

FIG 2 N7-MTase mutants display WT-like sensitivity to the RNA mutagen 5-FU. DBT cells were treated with the indicated concentrations of 5-FU for 30 min prior to infection with the viruses shown at an MOI of 0.01 PFU/cell. Medium containing 5-FU or vehicle was added 30 min postinfection. After 24 h, cell culture supernatants were collected, and viral titers were determined by plaque assay. For each virus, titers were normalized to those following infection of DMSO-treated controls. Changes in viral titers for nsp14 D330A and nsp14 G332A viruses were not statistically significant relative to WT MHV by one-way ANOVA. Error bars indicate SEM ($n = 4$).

rable to that of WT MHV (Fig. 1B). nsp14 D330A plaque morphology also was similar to that of WT MHV (Fig. 1C). In contrast, the nsp14 G332A virus began exponential replication 4 to 6 h later than WT MHV and reached a lower peak titer (1.5×10^4 PFU/ml) than that of WT MHV (10^7 PFU/ml) (Fig. 1B). The nsp14 G332A virus plaque size was also decreased relative to that of WT MHV (Fig. 1C). Thus, despite the requirement of D330 for nsp14 N7-MTase activity *in vitro* (13, 25, 26, 32), our data indicate that the D330A mutation has no detectable effect on MHV replication kinetics in cell culture.

nsp14 D330A or G332A mutations do not significantly influence nsp14 ExoN activity. Coronavirus nsp14 is a multifunctional protein with two known enzymatic activities, a proofreading 3′-5′ exoribonuclease activity (ExoN) and N7-MTase activity (24, 25). Based on *in vitro* studies, the ExoN and N7-MTase domains of CoV nsp14 are interdependent (26). This conclusion is supported by the crystal structure of nsp14, demonstrating that the ExoN and N7-MTase domains interact through a large hydrophobic interface (32). In addition, disruption of ExoN (ExoN−) via mutations at two active-site residues decreases the replication fidelity of MHV and SARS-CoV and renders the viruses sensitive to the RNA mutagen 5-fluorouracil (5-FU) (30, 31, 33). Thus, 5-FU sensitivity has been shown to be an *in vitro* indicator of ExoN activity. Therefore, we tested whether the D330A or G332A mutations affect ExoN activity by treating cells with increasing concentrations of 5-FU or vehicle (DMSO) prior to infection with either nsp14 D330A or nsp14 G332A virus at an MOI of 0.01 PFU/cell (Fig. 2). The nsp14 D330A and nsp14 G332A viruses were not significantly altered in 5-FU sensitivity compared with WT MHV (no significant difference by one-way analysis of variance [ANOVA]). In contrast, the ExoN− virus displayed a concentration-dependent increase in 5-FU sensitivity. These results indicate that neither D330A nor G332A significantly alter ExoN activity during virus replication.

MHV nsp14 G332A is detected by and sensitive to the type I interferon-mediated innate immune response. Coronavirus RNA capping likely follows the conventional capping pathway, with nsp14 N7-methylation being a prerequisite for 2′O-methylation *in vitro* (13). Therefore, decreased nsp14 N7-MTase activity should reduce overall 2′O-methylation, thereby increasing virus sensitivity to exogenous type I IFN due to recognition by IFIT1 and MDA5 (22, 23). To test this hypothesis, we pretreated DBT cells with murine IFN-β prior to infection with WT MHV, nsp16 D130A, which is an IFN-sensitive positive-control mutant virus due to ablated 2′O-MTase activity (19, 22, 23, 34), or nsp14 D330A or nsp14 G332A N7-MTase mutant viruses at an MOI of 1 PFU/cell. Cell culture supernatants were collected at either 12 or 24 h postinfection, and viral titers were determined by plaque assay. As expected, the nsp16 D130A virus was sensitive to IFN-β pretreatment (Fig. 3A). The nsp14 G332A virus demonstrated a dose-dependent increase in IFN-β sensitivity, which became undetectable by plaque assay at IFN-β concentrations greater than 75 U/ml (Fig. 3A). In contrast, nsp14 D330A virus displayed sensitivity to IFN-β comparable to WT MHV (Fig. 3B). Because nsp14 D330A displayed replication kinetics and resistance to IFN-β pretreatment indistinguishable from those of WT MHV, it is likely that the D330A substitution does not significantly affect N7-MTase activity. Therefore, we focused solely on the nsp14 G332A mutant for the remainder of the experiments in this study.

In addition to an increased sensitivity to the effects of type I interferon pretreatment, coronaviruses lacking 2′O-MTase activity induce higher levels of IFN-β than do the WT viruses (8, 22, 23). Therefore, to determine whether nsp14 G332A is also recognized by innate sensors and subsequently induces type I interferon expression, we pretreated DBT cells with 10 U/ml murine IFN-β for 18 h prior to infection with WT MHV, nsp16 D130A, or nsp14 G332A viruses at an MOI of 0.1 PFU/cell. At 12 h postinfection, cell lysates were collected and the relative expression of IFN-β was determined by qPCR (Fig. 3C). As previously reported, infection with WT MHV marginally induced the expression of IFN-β (35) and infection with nsp16 D130A led to an upregulation of IFN-β relative to mock-infected cells (8, 22, 23). Furthermore, infection with nsp14 G332A led to a significant increase in the expression of IFN-β relative to mock and WT MHV-infected cells. These data further suggest that nsp14 N7-MTase activity precedes nsp16 2′O-MTase activity and the absence of either activity results in innate detection of the virus leading to the induction of type I interferon gene expression.

To determine the effect that increased sensitivity to IFN-β has on nsp14 G332A replication, we tested whether nsp14 G332A virus replication could be rescued in BMDCs lacking the IFN-α/β receptor ($IFNAR^{-/-}$). $IFNAR^{-/-}$ cells lack the capacity to respond to type I IFNs and are thus incapable of mounting an effective IFN-dependent antiviral response (36). WT or $IFNAR^{-/-}$ BMDCs were infected with WT MHV or nsp14 G332A virus at an MOI of 0.01 PFU/cell, cell culture supernatants were collected 24 h postinfection, and viral titers were determined by plaque assay. Similar to experiments using DBT cells, nsp14 G332A virus replicated poorly in WT BMDCs relative to WT MHV (Fig. 3D). Titers of nsp14 G332A virus were increased approximately 40-fold in $IFNAR^{-/-}$ BMDCs (5.6×10^4 PFU/ml) compared with the titers of this virus in WT BMDCs (1.3×10^3 PFU/ml). However, despite the increase in viral titers of nsp14 G332A in $IFNAR^{-/-}$ BMDCs, titers were not restored to the level of WT MHV in $IFNAR^{-/-}$ BMDCs (3.6×10^6 PFU/ml). These data suggest that the impaired

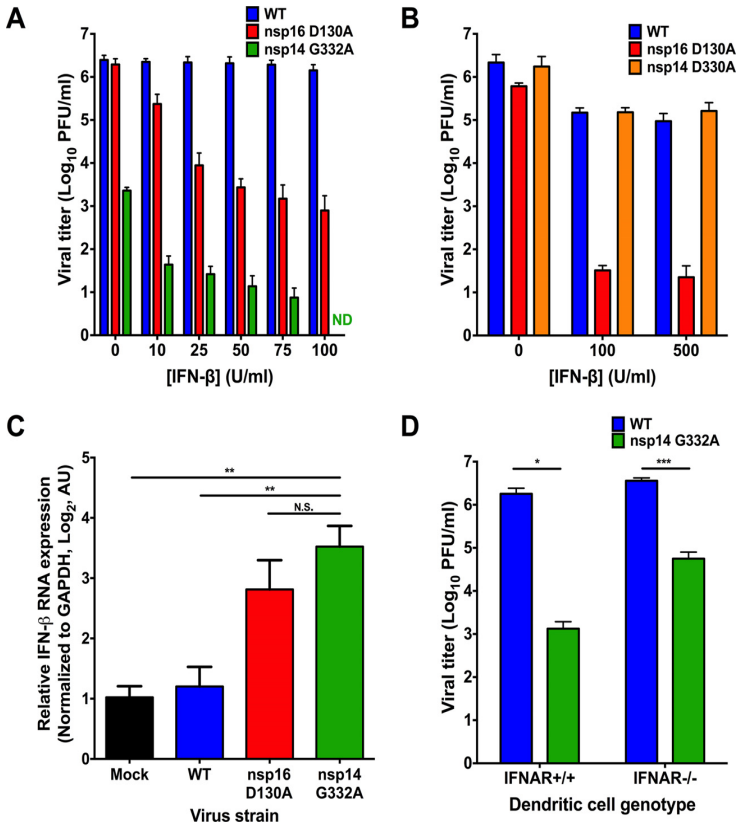

FIG 3 nsp14 G332A virus exhibits increased induction of and sensitivity to IFN-β. DBT cells were treated for 18 h with the indicated concentrations of mouse IFN-β. Cells were infected with WT, nsp16 D130A, or nsp14 G332A virus and incubated for 24 h (A) or infected with WT, nsp16 D130A, and nsp14 D330A virus and incubated for 12 h (B). Cell culture supernatants were collected, and viral titers were determined by plaque assay. For each panel, error bars represent SEM ($n = 4$). ND, not detectable. (C) DBT cells were treated for 18 h with 10 U/ml mouse IFN-β. Cells were mock infected or infected with WT, nsp16 D130A, or nsp14 G332A virus at an MOI of 0.1 PFU/cell. At 12 h postinfection, cell lysates were harvested, total RNA was extracted, cDNA was generated, and IFN-β expression relative to GAPDH was determined by qPCR. Error bars indicate SEM ($n = 9$). N.S., not significant; **, $P < 0.01$ by Student's t test. (D) BMDCs were infected with either WT or nsp14 G332A virus at an MOI of 0.01 PFU/cell. At 24 h postinfection, cell culture supernatants were collected, and viral titers were determined by plaque assay. Error bars indicate SEM ($n = 6$). *, $P < 0.05$; ***, $P < 0.001$ by Student's t test.

replication capacity of nsp14 G332A virus is only in part attributable to IFN sensitivity and, instead, this virus may manifest a more general replication defect.

nsp14 G332A genome translation is delayed during infection. Since the absence of the IFNAR was insufficient to restore nsp14 G332A replication, other mechanisms, such as decreased genome RNA stability or decreased viral genome translation, may contribute to the replication defect of this virus. The 5′ capping of cellular mRNAs serves several important functions, one of which is to increase RNA stability (2, 9). To test the stability of the nsp14 G332A genome upon entry into the cell, we infected DBT cells with WT MHV or nsp14 G332A virus at an MOI of 0.01 PFU/cell in the presence of vehicle (DMSO) or 100 μg/ml cycloheximide (CHX). CHX inhibits the translation of input viral genomes and prevents expression of the viral RNA-dependent RNA polymerase, thereby allowing us to quantify the amount of coronavirus RNA present at later time points relative to input. At the indicated times postinfection, cell lysates were collected and spiked with a known amount of *in vitro*-transcribed *Renilla* luciferase, and the amount of viral RNA present relative to *Renilla* luciferase was determined by qPCR (Fig. 4). At each time point postinfection for

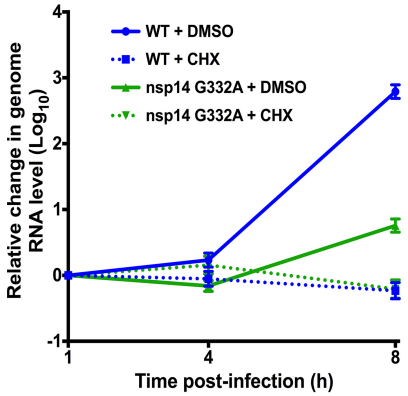

FIG 4 nsp14 G332A genomic RNAs are stable. DBT cells were infected with WT or nsp14 G332A virus at an MOI of 0.01 PFU/cell in the presence of vehicle (DMSO) or 100 μg/ml CHX. Cell lysates were harvested at the indicated times postinfection and spiked with a known amount of *in vitro*-transcribed *Renilla* luciferase RNA, and total RNA was obtained by phenol-chloroform extraction. cDNA was generated by RT-PCR, and the number of viral genome copies present relative to *Renilla* luciferase was determined by SYBR green qPCR using MHV nsp10 and *Renilla* luciferase-specific primers. Error bars indicate SEM ($n = 6$).

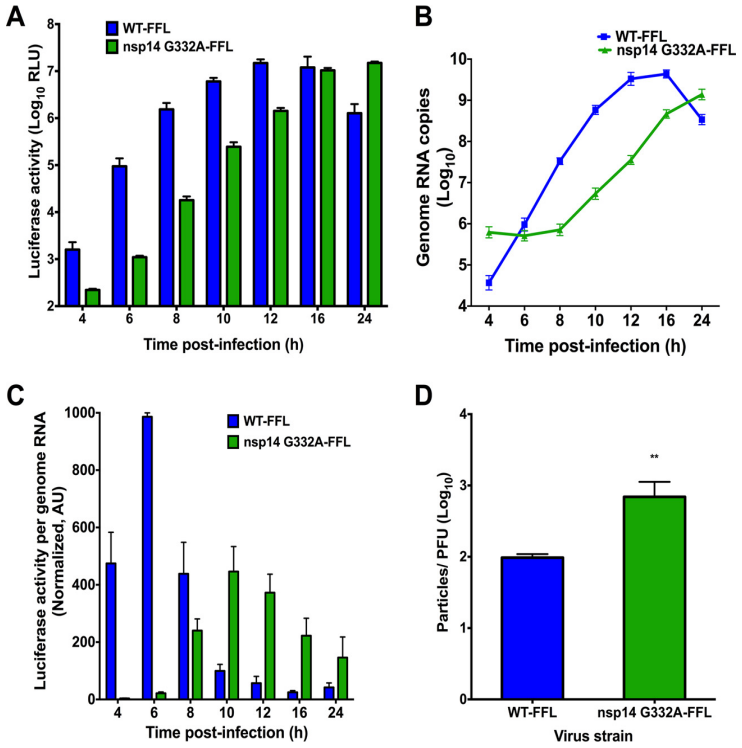

FIG 5 nsp14 G332A genomic RNAs are translated with delayed kinetics during infection. DBT cells were infected with either WT-FFL or nsp14 G332A-FFL virus at an MOI of 0.1 PFU/cell. At the times shown postinfection, cell culture supernatants were collected, and lysates were harvested and divided equally into two samples. For the first lysate sample, luciferase activity was quantified (A). For the remaining lysate sample, RNA was extracted, and genome RNA copies were quantified using real-time qRT-PCR with a standard curve and CoV nsp2-specific primers (B). (C) Translation of WT-FFL or nsp14 G332A-FFL genomes at the times shown postinfection as determined by luciferase activity per genome RNA copy number. Values were normalized to WT-FFL at 6 h postinfection. Error bars indicate SEM ($n = 4$). (D) Viral titers in cell culture supernatants from DBT cells infected with either WT-FFL or nsp14 G332A-FFL were determined by plaque assay, and the number of genome RNA copies present in the input supernatant was determined by one-step real-time qRT-PCR. The particle-to-PFU ratio was calculated by dividing the number of genome RNA copies by the viral titers. Error bars represent SEM ($n = 4$). **, $P < 0.01$ by Student's t test.

CHX-treated samples, the level of nsp14 G332A RNA was similar to that of WT MHV, indicating that nsp14 G332A replication is not impaired due to decreased genome RNA stability.

In addition to serving as a precursor for 2′O-methylation, N7-methylated guanosine 5′ caps are recognized by eIF4E and required for efficient translation of eukaryotic RNA (9, 37). To determine whether the nsp14 G332A mutation impairs viral translation efficiency, we first engineered virus encoding FFL as an in-frame N-terminal fusion with MHV nsp2 (29) in the open reading frame 1a (ORF1a) polyprotein coding sequence of the isogenic nsp14 G332A cloned genome. In this setting, FFL-nsp2 is the second protein translated from the input viral genome and becomes a reporter for viral protein translation. We infected DBT cells with either WT-FFL or nsp14 G332A-FFL virus at an MOI of 0.1 PFU/cell, and lysates were prepared at various intervals postinfection to quantify luciferase activity and viral genome RNA copy number. Luciferase activity accumulated more slowly following infection by nsp14 G332A-FFL virus relative to WT-FFL virus (Fig. 5A). The WT-FFL signal began to decline after 16 h due to destruction of the cell monolayer. In addition, levels of nsp14 G332A-FFL genomic RNA increased more slowly than those of WT-FFL (Fig. 5B). By quantifying both luciferase activity and viral genome copies, we were able to calculate the kinetics of translation. To determine the rate of translation at each time point postinfection, the ratio of luciferase activity to genome copies was determined using data shown in Fig. 5A and B. The ratio of luciferase activity to genome copies for WT-FFL was highest at early times postinfection (Fig. 5C). In contrast, the ratio of luciferase activity to genome copies was substantially less for the nsp14 G332A-FFL virus at early time points postinfection than for WT-FFL and failed to reach peak WT-FFL levels. These data demonstrate that nsp14 G332A-FFL virus requires more genomic RNA to achieve the WT levels of FFL activity, consistent with decreased translation efficiency of the mutant virus genome. Therefore, we next determined whether nsp14 G332A-FFL and WT-FFL virions are equivalently infectious by measuring the specific infectivity of each virus from infected DBT cell culture supernatants. The ratio of nsp14 G332A-FFL particles per PFU was approximately 7-fold more than WT-FFL (Fig. 5D). Thus, packaged nsp14 G332A-FFL genomes were less efficient at establishing infection than the WT.

nsp14 G332A-FFL genomes are translated less efficiently than WT-FFL genomes *in vitro*. To directly assess the translation capacity of nsp14 G332A-FFL virus genomes, we isolated genome RNA from purified virions. Increasing concentrations of genome RNAs were incubated with rabbit reticulocyte lysates at 30°C for 1.5 h, and luciferase activity was quantified (Fig. 6A). Compared to WT-FFL genomes, FFL activity in the reticulocyte lysates was significantly reduced following incubation with nsp14 G332A-

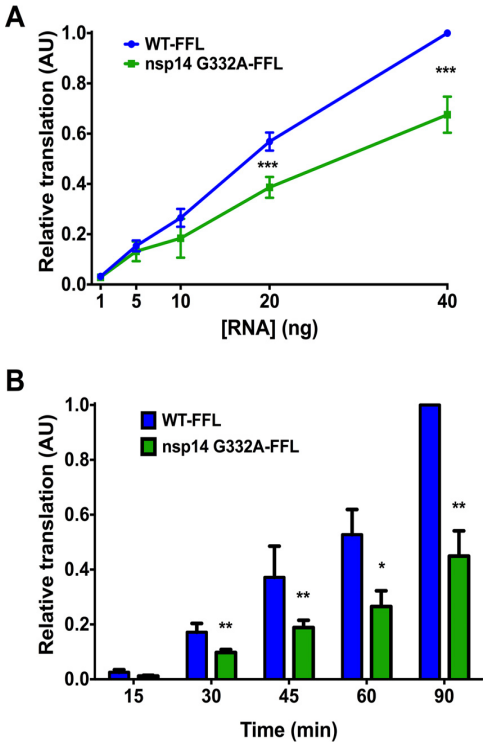

FIG 6 Purified nsp14 G332A genomic RNA is translated at lower efficiency *in vitro*. BHK-R cells were infected at an MOI of 0.001 PFU/cell with either WT-FFL or nsp14 G332A-FFL virus. Supernatants were harvested and clarified, and virions were collected by ultracentrifugation. Virion pellets were resuspended, TRIzol was added, and virion RNAs were purified using phenol-chloroform phase separation. Genome RNA copies were quantified using one-step real-time qRT-PCR with a standard curve and CoV nsp2-specific primers. (A) The concentrations of WT-FFL or nsp14 G332A-FFL genomic RNAs shown were translated *in vitro* at 30°C for 1.5 h, and luciferase activity was quantified. Translation values are relative to WT-FFL genomic RNA at 40 ng. Error bars represent SEM ($n = 4$). ***, $P < 0.001$ by Student's t test. (B) Equivalent numbers of either WT-FFL or nsp14 G332A-FFL genomic RNAs were translated *in vitro* for the times shown, and luciferase activity was quantified. Error bars represent SEM ($n = 6$). *, $P < 0.05$; **, $P < 0.01$ by Student's t test.

FFL genomes. In addition, we quantified the relative translation efficiency of equal amounts of WT-FFL and nsp14 G332A-FFL genomic RNA over time. At all time points tested after 15 min, FFL activity was significantly reduced following incubation of reticulocyte lysates with nsp14 G332A-FFL genomes relative to WT-FFL genomes (Fig. 6B). Taken together, our data indicate that the decreased replication capacity of the nsp14 G332A virus is attributable to IFN sensitivity and reduced translation efficiency.

DISCUSSION

In this study, we engineered recombinant CoVs encoding alanine substitutions in the nsp14 N7-MTase at the SAM-binding-site residues, D330 and G332. We found that the N7-MTase SAM-binding-site mutants are viable and yield drastically different phenotypes during replication. Specifically, MHV nsp14 D330A virus replicates indistinguishably from WT MHV in all assays conducted, despite the requirement of this residue for SAM binding *in vitro* (26). There is precedent for such a contradiction. A previous study using vesicular stomatitis virus identified a SAM-binding residue within the L protein (G1674) that, when altered, does not affect viral replication or N7-MTase activity (38). The structure of the SARS-CoV nsp10-nsp14 complex reveals that D331 (D330 in MHV) is in close proximity to the SAM-binding site, but only G333 (G332 in MHV) directly contacts SAM (32). Since *in vitro* N7-MTase activity was assessed only for a SARS-CoV nsp14 D331A/G333A double mutant, it is not clear whether nsp14 D331 was required for N7-MTase activity in this study (32). However, a previous study using both *in vitro* functional assays and yeast complementation reported that SARS-CoV nsp14 D331 is essential for N7-MTase activity (26). Our study examined nsp14 N7-MTase in the context of viral replication. A potential difference between our work and previous studies of the CoV nsp14 N7-MTase is the use of MHV versus SARS-CoV proteins, respectively. Purified MHV nsp14 N7-MTase is not available in our lab for biochemical studies. However, our results will guide future experiments when such a system is established. During our study, we attempted to recover SARS-CoV nsp14 D331A, I332A, and G333A N7-MTase mutant viruses. However, viable viruses were not recovered after at least three attempts for each mutant. Nonetheless, the high conservation of the SAM-binding residues makes it unlikely that the differences observed between our work and previous biochemical studies are due to profoundly different N7-MTase catalytic mechanisms.

In contrast to nsp14 D330A virus, nsp14 G332A virus replicated with delayed kinetics and reached peak titers that were 1,000-fold less than those of WT MHV. CoV nsp14 has two domains: an N-terminal ExoN domain and a C-terminal N7-MTase domain. Mutations at D331 in SARS-CoV nsp14 do not affect ExoN activity *in vitro* (25, 26). However, the effect of altering residue G333 (G332 in MHV) on ExoN activity has not been reported using any system. It is unlikely that the G332A mutation in MHV nsp14 influences ExoN activity, as nsp14 G332A demonstrated WT-like sensitivity to the RNA mutagen 5-FU. Even a subtle alteration in ExoN activity should result in a detectable change in 5-FU sensitivity, particularly since we performed the assay using low-MOI conditions, which would increase mutagen incorporation during multistep replication (31, 34). The lack of enhanced 5-FU sensitivity for the nsp14 D330A and nsp14 G332A viruses indicates that mutations at these SAM-binding residues do not significantly dampen ExoN activity during virus replication. Additionally, since nsp14 G332A is resistant to 5-FU treatment, it is unlikely that the G332A phenotype is due to nsp14 instability or degradation.

Our data indicate that impaired replication of nsp14 G332A virus is likely due to a combination of factors, including increased detection by innate immune sensors and decreased translation efficiency of viral RNA. Binding of type I IFNs to the IFN receptor leads to expression of many IFN-stimulated genes and ultimately the establishment of an antiviral state (39). Coronavirus RNAs lacking 2′O-methylation are sensed by IFIT1, which is one of the most highly upregulated IFN-stimulated genes following IFN induction (40). While nsp14 D330A displayed WT-like sensitivity to pretreatment with IFN-β, nsp14 G332A virus did not replicate following IFN-β pretreatment with doses of >75 U/ml. However, initial titers were lower for nsp14 G332A. Thus, the concentration-dependent change in viral titer following IFN-β pretreatment was similar to that for the nsp16 D130A virus. The IFN-β sensitivity of nsp14 G332A likely results from a reduction in 2′O-methylation of viral RNA due to impaired N7-MTase activity.

This hypothesis is supported by our data showing that infection with either nsp16 D130A or nsp14 G332A virus results in the induction of IFN-β gene expression. In addition, decreased N7-MTase activity due to the G332A mutation results in the delayed translation and decreased translation efficiency observed during viral replication and *in vitro* assays. Due to the highly impaired replication capacity of the nsp14 G332A virus, it has not been possible to directly determine the cap methylation status of nsp14 G332A virus genomes. Nevertheless, our results are consistent with functions of the N7-methylated 5′cap in promoting both viral and cellular translation (4–6). Decreased translation efficiency also could explain the lower specific infectivity observed for nsp14 G332A virus. Furthermore, it is possible that the delayed translation kinetics of nsp14 G332A genomic RNA increases innate sensing of the virus by delaying the early expression of multiple CoV IFN antagonists upon entry, resulting in decreased replication capacity.

Our data provide additional support for a sequential model of CoV RNA capping wherein N7-methylation precedes 2′O-methylation. In addition, our studies suggest that small-molecule inhibitors of the CoV nsp14 N7-MTase would impair virus replication and provide a pathogen-associated molecular pattern that would be quickly recognized by the innate immune response. Given the conservation of these enzymes, such inhibitors may have activity against diverse groups of coronaviruses.

ACKNOWLEDGMENTS

We thank Clint Smith for critical review of the manuscript and members of the Denison and Dermody laboratories for useful discussions.

FUNDING INFORMATION

This work, including the efforts of Terence S. Dermody, was funded by HHS | NIH | National Institute of Allergy and Infectious Diseases (NIAID) (R01 AI038296). This work, including the efforts of Mark R Denison, was funded by HHS | NIH | National Institute of Allergy and Infectious Diseases (NIAID) (R01 AI108197). This work, including the efforts of James Brett Case and Alison Whitney Ashbrook, was funded by HHS | NIH | National Heart, Lung, and Blood Institute (NHLBI) (T32HL07751).

REFERENCES

1. **Shatkin AJ.** 1976. Capping of eucaryotic mRNAs. Cell **9:**645–653. http://dx.doi.org/10.1016/0092-8674(76)90128-8.
2. **Darnell JE.** 1979. Transcription units for mRNA production in eukaryotic cells and their DNA viruses. Prog Nucleic Acid Res Mol Biol **22:**327–353. http://dx.doi.org/10.1016/S0079-6603(08)60803-X.
3. **Furuichi Y, Shatkin AJ.** 2000. Viral and cellular mRNA capping: past and prospects. Adv Virus Res **55:**135–184. http://dx.doi.org/10.1016/S0065-3527(00)55003-9.
4. **Marcotrigiano J, Gingras A-C, Sonenberg N, Burley SK.** 1997. Cocrystal structure of the messenger RNA 5′ cap-binding protein (eIF4E) bound to 7-methyl-GDP. Cell **89:**951–961. http://dx.doi.org/10.1016/S0092-8674(00)80280-9.
5. **Filipowicz W, Furuichi Y, Sierra JM, Muthukrishnan S, Shatkin AJ, Ochoa S.** 1976. A protein binding the methylated 5′-terminal sequence, m7GpppN, of eukaryotic messenger RNA. Proc Natl Acad Sci U S A **73:**1559–1563. http://dx.doi.org/10.1073/pnas.73.5.1559.
6. **Schibler U, Perry RP.** 1977. The 5′-termini of heterogeneous nuclear RNA: a comparison among molecules of different sizes and ages. Nucleic Acids Res **4:**4133–4150. http://dx.doi.org/10.1093/nar/4.12.4133.
7. **Wei CM, Gershowitz A, Moss B.** 1975. Methylated nucleotides block 5′ terminus of HeLa cell messenger RNA. Cell **4:**379–386. http://dx.doi.org/10.1016/0092-8674(75)90158-0.
8. **Züst R, Cervantes-Barragan L, Habjan M, Maier R, Neuman BW, Ziebuhr J, Szretter KJ, Baker SC, Barchet W, Diamond MS, Siddell SG, Ludewig B, Thiel V.** 2011. Ribose 2′-O-methylation provides a molecular signature for the distinction of self and non-self mRNA dependent on the RNA sensor Mda5. Nat Immunol **12:**137–143. http://dx.doi.org/10.1038/ni.1979.
9. **Decroly E, Ferron F, Lescar J, Canard B.** 2012. Conventional and unconventional mechanisms for capping viral mRNA. Nat Rev Microbiol **10:**51–65. http://dx.doi.org/10.1038/nrmicro2675.
10. **Lai MM, Stohlman SA.** 1981. Comparative analysis of RNA genomes of mouse hepatitis viruses. J Virol **38:**661–670.
11. **Lai MM, Patton CD, Stohlman SA.** 1982. Further characterization of mRNAs of mouse hepatitis virus: presence of common 5-′end nucleotides. J Virol **41:**557–565.
12. **Masters PS.** 2006. The molecular biology of coronaviruses. Adv Virus Res **66:**193–292. http://dx.doi.org/10.1016/S0065-3527(06)66005-3.
13. **Bouvet M, Debarnot C, Imbert I, Selisko B, Snijder EJ, Canard B, Decroly E.** 2010. In vitro reconstitution of SARS-coronavirus mRNA cap methylation. PLoS Pathog **6:**e1000863. http://dx.doi.org/10.1371/journal.ppat.1000863.
14. **Ivanov KA, Thiel V, Dobbe JC, van der Meer Y, Snijder EJ, Ziebuhr J.** 2004. Multiple enzymatic activities associated with severe acute respiratory syndrome coronavirus helicase. J Virol **78:**5619–5632. http://dx.doi.org/10.1128/JVI.78.11.5619-5632.2004.
15. **Lehmann KC, Gulyaeva A, Zevenhoven-Dobbe JC, Janssen GMC, Ruben M, Overkleeft HS, van Veelen PA, Samborskiy DV, Kravchenko AA, Leontovich AM, Sidorov IA, Snijder EJ, Posthuma CC, Gorbalenya AE.** 2015. Discovery of an essential nucleotidylating activity associated with a newly delineated conserved domain in the RNA polymerase-containing protein of all nidoviruses. Nucleic Acids Res **43:**8416–8434. http://dx.doi.org/10.1093/nar/gkv838.
16. **Snijder EJ, Bredenbeek PJ, Dobbe JC, Thiel V, Ziebuhr J, Poon LLM, Guan Y, Rozanov M, Spaan WJM, Gorbalenya AE.** 2003. Unique and conserved features of genome and proteome of SARS-coronavirus, an early split-off from the coronavirus group 2 lineage. J Mol Biol **331:**991–1004. http://dx.doi.org/10.1016/S0022-2836(03)00865-9.
17. **von Grotthuss M, Wyrwicz LS, Rychlewski L.** 2003. mRNA cap-1 methyltransferase in the SARS genome. Cell **113:**701–702. http://dx.doi.org/10.1016/S0092-8674(03)00424-0.
18. **Decroly E, Imbert I, Coutard B, Bouvet M, Selisko B, Alvarez K, Gorbalenya AE, Snijder EJ, Canard B.** 2008. Coronavirus nonstructural protein 16 is a cap-0 binding enzyme possessing (nucleoside-2′O)-methyltransferase activity. J Virol **82:**8071–8084. http://dx.doi.org/10.1128/JVI.00407-08.
19. **Daffis S, Szretter KJ, Schriewer J, Li J, Youn S, Errett J, Lin T-Y, Schneller S, Züst R, Dong H, Thiel V, Sen GC, Fensterl V, Klimstra WB, Pierson TC, Buller RM, Gale M, Shi P-Y, Diamond MS.** 2010. 2′-O methylation of the viral mRNA cap evades host restriction by IFIT family members. Nature **468:**452–456. http://dx.doi.org/10.1038/nature09489.
20. **Chen Y, Su C, Ke M, Jin X, Xu L, Zhang Z, Wu A, Sun Y, Yang Z, Tien P, Ahola T, Liang Y, Liu X, Guo D.** 2011. Biochemical and structural insights into the mechanisms of SARS coronavirus RNA ribose 2′-O-methylation by nsp16/nsp10 protein complex. PLoS Pathog **7:**e1002294. http://dx.doi.org/10.1371/journal.ppat.1002294.
21. **Decroly E, Debarnot C, Ferron F, Bouvet M, Coutard B, Imbert I, Gluais L, Papageorgiou N, Sharff A, Bricogne G, Ortiz-Lombardia M, Lescar J, Canard B.** 2011. Crystal structure and functional analysis of the SARS-coronavirus RNA cap 2′-O-methyltransferase nsp10/nsp16 complex. PLoS Pathog **7:**e1002059. http://dx.doi.org/10.1371/journal.ppat.1002059.
22. **Habjan M, Hubel P, Lacerda L, Benda C, Holze C, Eberl CH, Mann A, Kindler E, Gil-Cruz C, Ziebuhr J, Thiel V, Pichlmair A.** 2013. Sequestration by IFIT1 impairs translation of 2′O-unmethylated capped RNA. PLoS Pathog **9:**e1003663. http://dx.doi.org/10.1371/journal.ppat.1003663.
23. **Menachery VD, Yount BL, Jr, Josset L, Gralinski LE, Scobey T, Agnihothram S, Katze MG, Baric RS.** 2014. Attenuation and restoration of severe acute respiratory syndrome coronavirus mutant lacking 2′-O-methyltransferase activity. J Virol **88:**4251–4264. http://dx.doi.org/10.1128/JVI.03571-13.
24. **Minskaia E, Hertzig T, Gorbalenya AE, Campanacci V, Cambillau C, Canard B, Ziebuhr J.** 2006. Discovery of an RNA virus 3′->5′ exoribonuclease that is critically involved in coronavirus RNA synthesis. Proc Natl Acad Sci U S A **103:**5108–5113. http://dx.doi.org/10.1073/pnas.0508200103.
25. **Chen Y, Cai H, Pan J, Xiang N, Tien P, Ahola T, Guo D.** 2009. Functional screen reveals SARS coronavirus nonstructural protein nsp14

as a novel cap N7 methyltransferase. Proc Natl Acad Sci U S A **106:**3484–3489. http://dx.doi.org/10.1073/pnas.0808790106.

26. **Chen Y, Tao J, Sun Y, Wu A, Su C, Gao G, Cai H, Qiu S, Wu Y, Ahola T, Guo D.** 2013. Structure-function analysis of severe acute respiratory syndrome coronavirus RNA cap guanine-N7-methyltransferase. J Virol **87:**6296–6305. http://dx.doi.org/10.1128/JVI.00061-13.
27. **Chen W, Baric RS.** 1996. Molecular anatomy of mouse hepatitis virus persistence: coevolution of increased host cell resistance and virus virulence. J Virol **70:**3947–3960.
28. **Yount B, Denison MR, Weiss SR, Baric RS.** 2002. Systematic assembly of a full-length infectious cDNA of mouse hepatitis virus strain A59. J Virol **76:**11065–11078. http://dx.doi.org/10.1128/JVI.76.21.11065-11078.2002.
29. **Freeman MC, Graham RL, Lu X, Peek CT, Denison MR.** 2014. Coronavirus replicase-reporter fusions provide quantitative analysis of replication and replication complex formation. J Virol **88:**5319–5327. http://dx.doi.org/10.1128/JVI.00021-14.
30. **Eckerle LD, Lu X, Sperry SM, Choi L, Denison MR.** 2007. High fidelity of murine hepatitis virus replication is decreased in nsp14 exoribonuclease mutants. J Virol **81:**12135–12144. http://dx.doi.org/10.1128/JVI.01296-07.
31. **Smith EC, Blanc H, Vignuzzi M, Denison MR.** 2013. Coronaviruses lacking exoribonuclease activity are susceptible to lethal mutagenesis: evidence for proofreading and potential therapeutics. PLoS Pathog **9:**e1003565. http://dx.doi.org/10.1371/journal.ppat.1003565.
32. **Ma Y, Wu L, Shaw N, Gao Y, Wang J, Sun Y, Lou Z, Yan L, Zhang R, Rao Z.** 2015. Structural basis and functional analysis of the SARS coronavirus nsp14-nsp10 complex. Proc Natl Acad Sci U S A **112:**9436–9441. http://dx.doi.org/10.1073/pnas.1508686112.
33. **Eckerle LD, Becker MM, Halpin RA, Li K, Venter E, Lu X, Scherbakova S, Graham RL, Baric RS, Stockwell TB, Spiro DJ, Denison MR.** 2010. Infidelity of SARS-CoV nsp14-exonuclease mutant virus replication is revealed by complete genome sequencing. PLoS Pathog **6:**e1000896. http://dx.doi.org/10.1371/journal.ppat.1000896.
34. **Smith EC, Case JB, Blanc H, Isakov O, Shomron N, Vignuzzi M, Denison MR.** 2015. Mutations in coronavirus nonstructural protein 10 decrease virus replication fidelity. J Virol **89:**6418–6426. http://dx.doi.org/10.1128/JVI.00110-15.
35. **Roth-Cross JK, Martínez-Sobrido L, Scott EP, García-Sastre A, Weiss SR.** 2007. Inhibition of the alpha/beta interferon response by mouse hepatitis virus at multiple levels. J Virol **81:**7189–7199. http://dx.doi.org/10.1128/JVI.00013-07.
36. **Katze MG, He Y, Gale M.** 2002. Viruses and interferon: a fight for supremacy. Nat Rev Immunol **2:**675–687. http://dx.doi.org/10.1038/nri888.
37. **Gebauer FAT, Hentze MW.** 2004. Molecular mechanisms of translational control. Nat Rev Mol Cell Biol **5:**827–835.
38. **Li J, Fontaine-Rodriguez EC, Whelan SPJ.** 2005. Amino acid residues within conserved domain VI of the vesicular stomatitis virus large polymerase protein essential for mRNA cap methyltransferase activity. J Virol **79:**13373–13384. http://dx.doi.org/10.1128/JVI.79.21.13373-13384.2005.
39. **Schneider WM, Chevillotte MD, Rice CM.** 2014. Interferon-stimulated genes: a complex web of host defenses. Annu Rev Immunol **32:**513–545. http://dx.doi.org/10.1146/annurev-immunol-032713-120231.
40. **Diamond MS, Farzan M.** 2013. The broad-spectrum antiviral functions of IFIT and IFITM proteins. Nat Rev Immunol **13:**46–57. http://dx.doi.org/10.1038/nri3344.

APPENDIX B:

MURINE HEPATITIS VIRUS NSP14 EXORIBONUCLEASE ACTIVITY IS REQUIRED FOR RESISTANCE TO INNATE IMMUNITY

AMERICAN SOCIETY FOR MICROBIOLOGY | Journal of Virology®

CELLULAR RESPONSE TO INFECTION

Murine Hepatitis Virus nsp14 Exoribonuclease Activity Is Required for Resistance to Innate Immunity

James Brett Case,[a,c] Yize Li,[d] Ruth Elliott,[d] Xiaotao Lu,[b,c] Kevin W. Graepel,[a,c] Nicole R. Sexton,[a,b,c] Everett Clinton Smith,[e] Susan R. Weiss,[d] Mark R. Denison[a,b,c]

[a]Department of Pathology, Microbiology, and Immunology, Vanderbilt University Medical Center, Nashville, Tennessee, USA

[b]Department of Pediatrics, Vanderbilt University Medical Center, Nashville, Tennessee, USA

[c]Elizabeth B. Lamb Center for Pediatric Research, Vanderbilt University Medical Center, Nashville, Tennessee, USA

[d]Department of Microbiology, Perelman School of Medicine, University of Pennsylvania, Philadelphia, Pennsylvania, USA

[e]Department of Biology, The University of the South, Sewanee, Tennessee, USA

ABSTRACT Coronaviruses (CoVs) are positive-sense RNA viruses that infect numerous mammalian and avian species and are capable of causing severe and lethal disease in humans. CoVs encode several innate immune antagonists that counteract the host innate immune response to facilitate efficient viral replication. CoV nonstructural protein 14 (nsp14) encodes 3′-to-5′ exoribonuclease activity (ExoN), which performs a proofreading function and is required for high-fidelity replication. Outside of the order *Nidovirales*, arenaviruses are the only RNA viruses that encode an ExoN, which functions to degrade double-stranded RNA (dsRNA) replication intermediates. In this study, we tested the hypothesis that CoV ExoN also functions to antagonize the innate immune response. We demonstrate that viruses lacking ExoN activity [ExoN(−)] are sensitive to cellular pretreatment with interferon beta (IFN-β) in a dose-dependent manner. In addition, ExoN(−) virus replication was attenuated in wild-type bone marrow-derived macrophages (BMMs) and partially restored in interferon alpha/beta receptor-deficient (IFNAR$^{-/-}$) BMMs. ExoN(−) virus replication did not result in IFN-β gene expression, and in the presence of an IFN-β-mediated antiviral state, ExoN(−) viral RNA levels were not substantially reduced relative to those of untreated samples. However, ExoN(−) virus generated from IFN-β-pretreated cells had reduced specific infectivity and decreased relative fitness, suggesting that ExoN(−) virus generated during an antiviral state is less viable to establish a subsequent infection. Overall, our data suggest murine hepatitis virus (MHV) ExoN activity is required for resistance to the innate immune response, and antiviral mechanisms affecting the viral RNA sequence and/or an RNA modification act on viruses lacking ExoN activity.

IMPORTANCE CoVs encode multiple antagonists that prevent or disrupt an efficient innate immune response. Additionally, no specific antiviral therapies or vaccines currently exist for human CoV infections. Therefore, the study of CoV innate immune antagonists is essential for understanding how CoVs overcome host defenses and to maximize potential therapeutic interventions. Here, we sought to determine the contributions of nsp14 ExoN activity in the induction of and resistance to the innate immune response. We show that viruses lacking nsp14 ExoN activity are more sensitive than wild-type MHV to restriction by exogenous IFN-β and that viruses produced in the presence of an antiviral state are less capable of establishing a subsequent viral infection. Our results support the hypothesis that murine hepatitis virus ExoN activity is required for resistance to the innate immune response.

KEYWORDS coronavirus, MHV, exoribonuclease, ExoN, innate immunity, interferon

Received 30 August 2017 **Accepted** 12 October 2017

Accepted manuscript posted online 18 October 2017

Citation Case JB, Li Y, Elliott R, Lu X, Graepel KW, Sexton NR, Smith EC, Weiss SR, Denison MR. 2018. Murine hepatitis virus nsp14 exoribonuclease activity is required for resistance to innate immunity. J Virol 92:e01531-17. https://doi.org/10.1128/JVI.01531-17.

Editor Tom Gallagher, Loyola University Medical Center

Address correspondence to Mark R. Denison, mark.denison@vanderbilt.edu.

The innate immune response within a mammalian cell is the first line of defense against an invading pathogen. However, as obligate intracellular parasites, viruses have evolved numerous mechanisms to prevent and antagonize innate detection by host cells. Coronaviruses (CoVs), which are the largest known positive-sense, single-stranded RNA viruses, encode several type I interferon (IFN) antagonists. Many of these antagonists prevent the induction of IFN, while others mediate resistance to the effects of IFN (1–3). Upon secretion from a cell, IFNs bind to cell surface-expressed IFN-α/β receptors (IFNARs) in an autocrine and paracrine manner. Subsequently, an IFN signaling cascade utilizing the Janus kinase and signal transducer and activator of the transcription pathway leads to the induction and expression of hundreds of interferon-stimulated genes (ISGs) that act to limit or prevent viral replication and spread (4). However, during CoV infection, nonstructural protein 1 (nsp1) antagonizes the innate immune response by degrading host mRNAs and suppressing IFN-β expression (5, 6). The nsp3 of severe acute respiratory syndrome coronavirus (SARS-CoV) prevents IRF3 phosphorylation and NF-κB signaling (7). In addition, SARS-CoV nsp3 encodes deubiquitinating and deISGylating activities (3, 8). CoV RNA evades innate detection by pattern recognition receptors (PRRs), such as MDA5, and antiviral effectors, such as IFIT1, through formation of a 5′ cap-1 structure by encoding N7-methyltransferase and 2′O-methyltransferase activities within nsp14 and nsp16, respectively (9, 10). Murine hepatitis virus (MHV) and Middle East respiratory syndrome coronavirus (MERS-CoV) encode 2′-5′ phosphodiesterases that degrade 2′-5′ oligoadenylates, which are key signaling molecules generated by oligoadenylate synthetase (OAS) in response to innate detection of double-stranded RNA (dsRNA) that subsequently activate RNase L (11). Most recently, a CoV nsp15 endonuclease activity (EndoU) mutant virus was shown to have increased dsRNA levels, suggesting that nsp15 EndoU reduces dsRNA levels during infection (12).

CoV nsp14 encodes 3′-to-5′ exoribonuclease (ExoN) and N7-methyltransferase (N7-MTase) activities (9, 13). CoV nsp14 N7-MTase activity is essential for efficient translation of the viral genome and preventing innate detection (14). In addition, initial biochemical studies of nsp14 ExoN activity demonstrated that ExoN has a preference for dsRNA and the capacity to excise 3′-end misincorporated nucleotides (13). Moreover, nsp14 ExoN activity is required for high-fidelity replication. The CoV nsp14 ExoN is a member of the DE-D-Dh superfamily of DNA and RNA exonucleases, so named for the three motifs of four active-site residues (13). Betacoronaviruses SARS-CoV and MHV expressing engineered, ExoN-inactivating substitutions at active-site residues in motif I (DE→AA) [ExoN(−)] demonstrate increased mutation frequencies and are profoundly sensitive to inhibition by RNA mutagens (15, 16). Additionally, SARS-CoV ExoN(−) virus is attenuated *in vivo* (17). Interestingly, outside the order *Nidovirales*, the only other known RNA virus-encoded 3′-to-5′ exoribonucleases are found in the *Arenaviridae* family of viruses. Lassa fever virus nucleoprotein ExoN is not thought to participate in fidelity regulation; rather, it participates in immune evasion by degrading dsRNA and thereby prevents antigen-presenting cell-mediated NK cell activation (18–20). Recently, in the *Alphacoronavirus* transmissible gastroenteritis virus (TGEV), a mutation in the nsp14 ExoN zinc finger was shown to generate lower levels of dsRNA than wild-type (WT) TGEV. However, in that study viruses with mutations in ExoN active-site motifs were nonviable and therefore could not be directly tested for effects on innate immunity (21).

Here, we demonstrate that viruses lacking ExoN activity were more sensitive to the effects of IFN pretreatment than WT MHV. In addition, for viruses lacking ExoN activity, replication was restricted in wild-type bone marrow-derived macrophages (B6 BMMs) but restored in IFNAR-deficient (IFNAR$^{-/-}$) BMMs. Despite an increased sensitivity to the effects of IFN treatment, MHV ExoN mutants failed to induce detectable IFN-β gene expression or RNase L-mediated rRNA degradation, and only a limited decrease in viral RNA accumulation was observed. Finally, ExoN(−) virus replicated in the presence of an IFN-β-mediated antiviral state had both a decreased specific infectivity and decreased

relative fitness compared to that of untreated ExoN(−) virus. Thus, nsp14 ExoN appears to block or correct the restriction of MHV infection by an IFN-mediated mechanism that may involve damaging nascent viral RNA and affecting subsequent infectivity.

(This article was submitted to an online preprint archive [42].)

RESULTS

Viruses lacking ExoN activity are more sensitive to the effects of IFN-β than WT MHV. Binding of type I interferon to the IFNAR receptor on the cell surface leads to a Jak/STAT signaling cascade that ultimately results in the upregulation and expression of hundreds of antiviral ISGs (4). In addition, WT MHV replication has been shown to be relatively resistant to the effects of IFN (1, 3, 22). To determine whether the ExoN activity of MHV nsp14 was required for resistance to IFN, we pretreated murine delayed brain tumor (DBT) cells with increasing concentrations of mouse IFN-β for 18 h prior to infection with WT MHV or ExoN(−) virus at a multiplicity of infection (MOI) of 1 PFU per cell (Fig. 1A). In response to IFN-β pretreatment, WT MHV viral titer decreased by approximately 1 $\log_{10}$, as previously reported (1). In contrast, ExoN(−) viral titer demonstrated a dose-dependent decrease and resulted in an approximately 3-$\log_{10}$ decrease in viral titer relative to untreated ExoN(−) viral titers. The ExoN activity of nsp14 is conferred by active-site residues present in 3 different motifs within the ExoN domain (23). Therefore, to determine whether the observed increase in sensitivity to IFN-β pretreatment for ExoN(−) virus shown in Fig. 1A was due specifically to the absence of ExoN activity in nsp14, we engineered and recovered a virus encoding only an aspartic acid-to-alanine substitution in motif III [ExoN3(−)]. Previously, we demonstrated that viruses lacking ExoN activity have decreased replication fidelity and are sensitive to the RNA mutagen 5-fluorouracil (5-FU) (16). Hence, 5-FU sensitivity is an *in vitro* indicator of ExoN activity. Therefore, first, we tested whether ExoN3(−) and ExoN(−) demonstrated similar sensitivity to 5-FU to ensure that the ExoN activity of ExoN3(−) virus had been ablated. Similar to that of ExoN(−), ExoN3(−) viral replication in cells treated with increasing concentrations of 5-FU demonstrated a dose-dependent decrease in viral titer relative to vehicle-treated cells (Fig. 1B). Further, ExoN(−) and ExoN3(−) displayed similar sensitivities to pretreatment with 100 or 500 U/ml IFN-β following infection at an MOI of 1 PFU/cell (Fig. 1C). Thus, these data suggest nsp14 ExoN activity is required for resistance to the effects of IFN-β pretreatment.

Increased replication capacity does not confer resistance to the effects of IFN-β pretreatment for viruses lacking ExoN activity. ExoN(−) virus demonstrates an approximately 2-h delay in exponential replication and a 1-$\log_{10}$ decrease in peak titer relative to WT MHV (15). Therefore, we tested whether the IFN sensitivity phenotypes observed for ExoN(−) and ExoN3(−) viruses are due to the decreased replication capacity of these viruses. To do so, we utilized an ExoN(−) virus developed by our laboratory that has been blindly passaged in DBT cells for 250 passages [ExoN(−) P250]. Over the course of passage, the ExoN(−) P250 virus did not revert the engineered ExoN(−) (DE→AA) mutations. In addition, ExoN(−) P250 accumulated 171 total mutations (74 nonsynonymous mutations) across the genome (24). The replication capacity of the resulting ExoN(−) P250 virus exceeds that of WT MHV (Fig. 2A). However, despite increased replication capacity, ExoN(−) P250 demonstrated sensitivity to IFN-β pretreatment similar to that of ExoN(−) virus (Fig. 2A and B). Hence, the IFN-β sensitivity phenotype of viruses lacking ExoN activity is not dependent on viral replication capacity but instead is directly associated with a specific function of nsp14 ExoN that is required for efficient replication in the presence of an IFN-β-mediated antiviral state.

nsp14 ExoN activity is required for replication in wild-type B6 BMMs. We next wanted to test whether ExoN activity was required for replication in primary innate immune cells, such as BMMs. Replication of WT MHV in primary BMMs is well described, and data suggest that wild-type B6 BMMs express many PRRs and ISGs at a higher basal level than many mouse cell lines (3, 25, 26). In contrast, BMMs lacking the IFNAR receptor (IFNAR$^{-/-}$) have lower basal and expressed levels of ISGs, making B6 and IFNAR$^{-/-}$ BMMs excellent cell types for interrogating the role of ExoN activity on viral

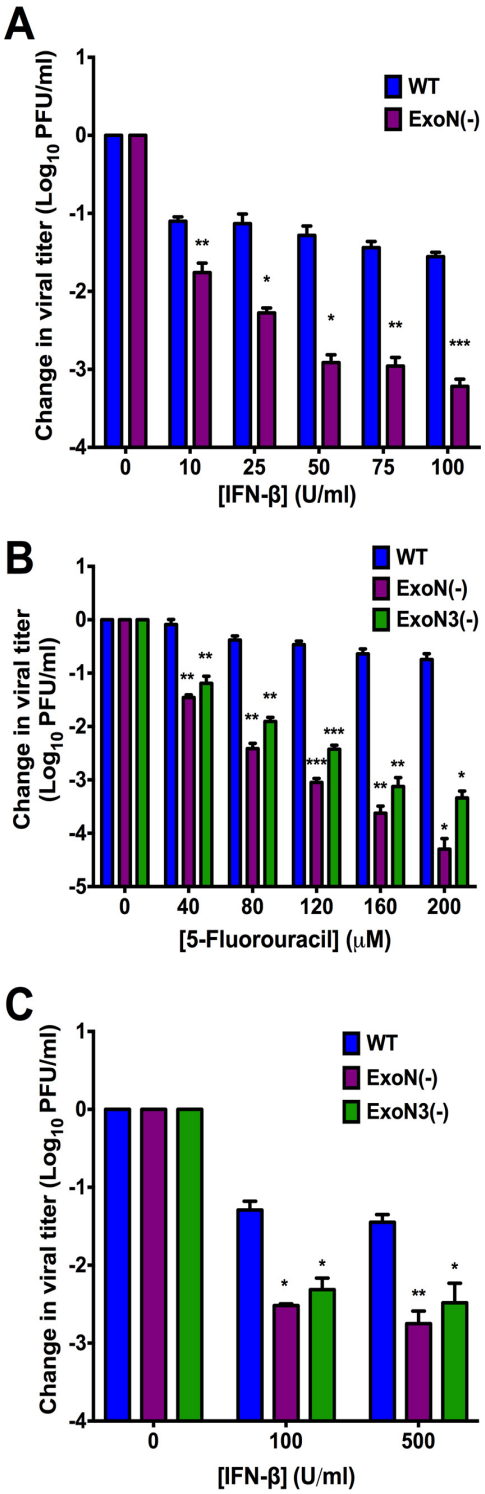

FIG 1 Viruses lacking ExoN activity are sensitive to IFN-β pretreatment. (A) DBT cells were pretreated with the indicated concentrations of mouse IFN-β for 18 h and then infected with WT MHV or ExoN(−) virus (A) or WT, ExoN(−), or ExoN3(−) virus (C) at an MOI of 1 PFU/cell. At 12 h postinfection, cell culture supernatants were collected and the viral titers determined by plaque assay. (B) DBT cells were pretreated with the indicated concentrations of 5-FU for 30 min. Following pretreatment, cells were infected with WT, ExoN(−), or ExoN3(−) virus at an MOI of 1 PFU/cell for 45 min, inocula were removed, and fresh medium containing vehicle or the appropriate concentration of 5-FU was added. Cell culture

(Continued on next page)

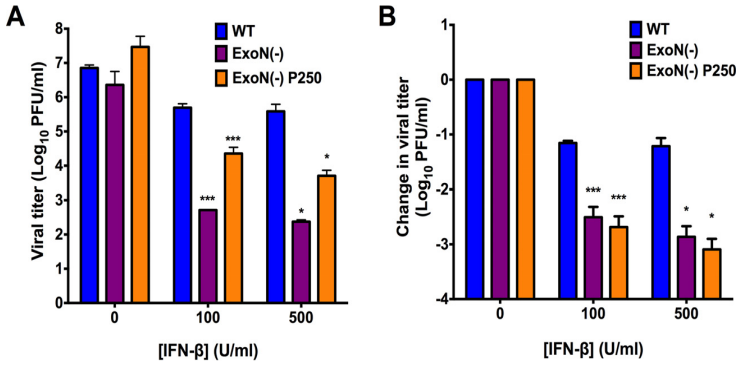

FIG 2 Increased replication capacity does not restore virus resistance to IFN-β. DBT cells were pretreated with the indicated concentrations of mouse IFN-β for 18 h and then infected with WT, ExoN(−), or ExoN(−) P250 virus at an MOI of 1 PFU/cell. At 12 h postinfection, cell culture supernatants were collected and the viral titers determined by plaque assay. Raw viral titers (A) or the change in viral titers relative to untreated controls (B) are reported. Error bars indicate SEM ($n = 4$). Statistical significance compared to WT MHV is denoted and was determined by Student's t test. *, $P < 0.05$; **, $P < 0.01$; ***, $P < 0.001$.

replication and antagonism of the innate immune response (25). BMMs from B6 or IFNAR$^{-/-}$ mice were generated and infected with WT MHV or ExoN(−) virus at an MOI of 1 PFU/cell. Samples were harvested at the indicated time points, and viral titers were determined by plaque assay (Fig. 3A). WT MHV replication increased gradually in both B6 and IFNAR$^{-/-}$ BMMs at each time point postinfection. In contrast, ExoN(−) virus replication in B6 BMMs was detectable only at 6 and 9 h postinfection. However, when IFNAR$^{-/-}$ BMMs were infected with ExoN(−) virus, viral titers were partially restored and increased at each time point postinfection. To further test the replication of viruses lacking ExoN activity and the effect of an increased replication capacity in BMMs, B6 and IFNAR$^{-/-}$ BMMs were infected with WT MHV or ExoN(−) P250 viruses at an MOI of 1 PFU/cell. Similar to the results shown in Fig. 3A, WT MHV viral titers steadily increased in B6 and IFNAR$^{-/-}$ BMMs at each time point postinfection (Fig. 3B). However, similar to that of ExoN(−) virus, ExoN(−) P250 virus replication in B6 BMMs was restricted and not detected beyond 9 h postinfection. In addition, ExoN(−) P250 virus replication in IFNAR$^{-/-}$ BMMs was restored to levels similar to those of WT MHV. These data show that ExoN activity is required for replication in B6 BMMs. Further, they suggest that restriction of ExoN(−) or ExoN(−) P250 is mediated by a gene or genes downstream of IFNAR.

Loss of ExoN activity does not result in the induction of IFN and replication is not rescued by RNase L/PKR deficiency. Upon detection of a pathogen-associated molecular pattern (PAMP) by innate sensors, signaling pathways lead to transcription factor activation and nuclear translocation, resulting in expression of IFN-β mRNA (4). WT MHV is well known to prevent or delay the induction of IFN expression (3, 22). However, ExoN activity may help prevent the detection of a PAMP, namely, dsRNA, which has been shown to be increased in an nsp15 EndoU mutant (12). Therefore, to determine whether the loss of ExoN activity resulted in the generation and subsequent detection of a PAMP, we determined the level of IFN-β gene expression in DBT cells either mock infected or infected with WT MHV, ExoN(−), or ExoN(−) P250 virus at an MOI of 0.1 PFU/cell (Fig. 4A). In addition, we infected DBT cells with Sendai virus (SenV), a positive control and a potent inducer of IFN, at an MOI of 200 hemagglutinin (HA)

FIG 1 Legend (Continued)
supernatants were harvested 12 h postinfection, and viral titers were determined by plaque assay. For each panel, the change in viral titer was calculated by dividing viral titers following the indicated treatment by the untreated controls, and error bars indicate standard errors of the means (SEM) ($n = 4$). Statistical significance compared to WT MHV is denoted and was determined by Student's t test. *, $P < 0.05$; **, $P < 0.01$; ***, $P < 0.001$.

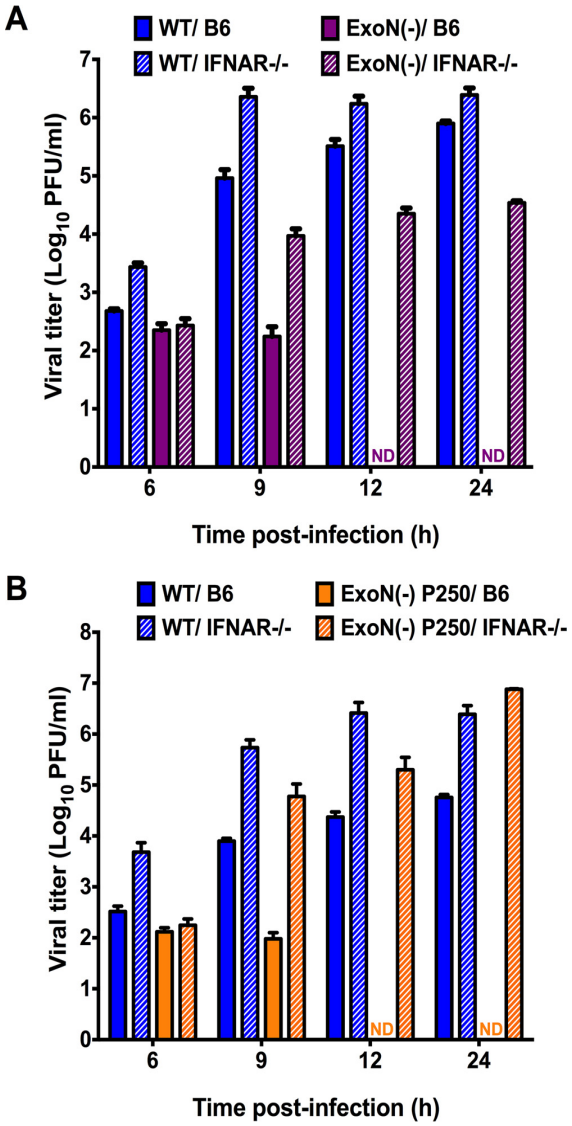

FIG 3 Replication of viruses lacking ExoN activity is restricted in wild-type B6 BMMs. B6 BMMs or IFNAR$^{-/-}$ BMMs were infected with WT MHV or ExoN(−) virus (A) or WT MHV or ExoN(−) P250 virus (B) at an MOI of 1 PFU/cell. At the indicated times postinfection, cell culture supernatant aliquots were collected and the viral titers present were determined by plaque assay. For each panel, error bars represent SEM (n = 6 to 7). ND, not detectable.

units/ml. SenV infection resulted in IFN expression by 3 h postinfection and peaked between 9 and 12 h postinfection before returning nearly to mock-infected levels by 24 h postinfection, demonstrating that DBT cells are capable of expressing IFN-β. In contrast, no CoV infection, regardless of whether or not intact ExoN activity was present, resulted in IFN-β gene expression over that of mock-infected cells, with the exception of WT MHV at 3 h postinfection. Further, upon detection of dsRNA by OAS and subsequent activation of RNase L, viral and cellular RNAs are degraded as an antiviral mechanism (4). To determine whether infection with ExoN(−) virus results in increased dsRNA levels that activate the OAS/RNase L pathway, DBT cells were pretreated with 0 or 50 U/ml mouse IFN-β and infected with WT MHV or ExoN(−) virus at an MOI of 1 PFU/cell. As a positive control, DBT cells were transfected with 25 μg/ml poly(I·C), a dsRNA surrogate. At the indicated times postinfection, cell lysates were

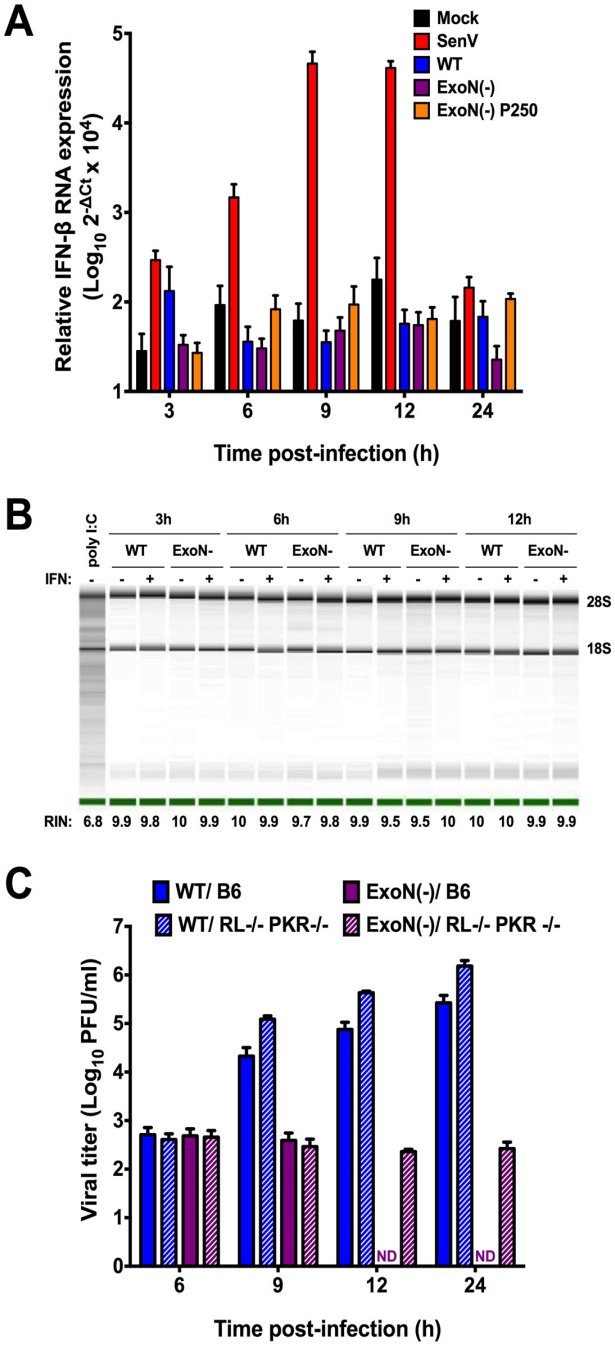

FIG 4 Loss of ExoN activity does not result in the generation of a detectable PAMP. (A) DBT cells were mock infected or infected with WT, ExoN(−), or ExoN(−) P250 virus at an MOI of 0.1 PFU/cell or infected with Sendai virus at an MOI of 200 HA units/ml. At the indicated times postinfection, cell culture supernatants were removed, cell lysates were harvested, total RNA was extracted, cDNA was generated, and IFN-β expression relative to that of GAPDH was determined by qPCR. Error bars indicate SEM ($n = 4$). (B) DBT cells were pretreated for 18 h with 0 or 50 U/ml mouse IFN-β and subsequently infected with WT MHV or ExoN(−) virus or transfected with 25 μg/ml poly(I-C). At the indicated times postinfection, cell culture supernatants were removed, cell lysates harvested, and total RNA extracted. rRNA integrity was assessed using an Agilent Bioanalyzer. One representative image is shown for each sample from 2 independent experiments. Images were spliced for labeling purposes. The averaged RNA integrity (RIN) values for each condition are reported. (C) B6 BMMs or RL $^{-/-}$/PKR $^{-/-}$ BMMs were infected with WT MHV or ExoN(−) virus at an MOI of 1 PFU/cell. At the indicated times postinfection, cell culture supernatant aliquots were collected and the viral titers present were determined by plaque assay. Error bars represent SEM ($n = 5$). ND, not detectable.

harvested, total RNA extracted, and the integrity of cellular rRNA determined using a bioanalyzer (Fig. 4B). Transfection of DBT cells with poly(I·C) resulted in rRNA degradation, whereas infection of DBT cells with WT MHV or ExoN(−) virus did not result in rRNA degradation under any tested conditions. Lastly, when B6 or RNase $L^{-/-}$/$PKR^{-/-}$ ($RL^{-/-}$/$PKR^{-/-}$) BMMs were infected with ExoN(−) virus, replication was restricted (Fig. 4C). In contrast to infection of B6 BMMs, ExoN(−) viral titer from $RL^{-/-}$/$PKR^{-/-}$ BMMs was detectable at 12 and 24 h postinfection. However, viral yield was minimal. These data suggest that loss of nsp14 ExoN activity does not lead to the transcriptional activation of IFN-β or a notable dsRNA sensor such as OAS/RNase L during infection of DBT cells. In addition, BMMs deficient in the antiviral effectors RNase L and PKR were not sufficient to restore ExoN(−) viral replication.

IFN treatment does not substantially alter ExoN(−) viral RNA accumulation or particle release. Since ExoN activity is required for resistance to IFN but had no effect on IFN induction, we sought to discern the stage of viral replication that was restricted by IFN-β treatment. To determine the effect of IFN-β pretreatment on viral RNA accumulation, DBT cells were pretreated with 0 or 100 U/ml mouse IFN-β for 18 h and subsequently infected with WT MHV or ExoN(−) virus at an MOI of 1 PFU/cell. At the indicated times postinfection, the number of genomic RNA copies present was determined by one-step reverse transcription-quantitative PCR (RT-qPCR). IFN-β pretreatment had minimal effect on the accumulation of WT MHV genomic RNA (Fig. 5A). Whereas ExoN(−) genomic RNA accumulation is delayed relative to that of WT MHV (15), pretreatment with IFN-β did not substantially decrease ExoN(−) genomic RNA levels (Fig. 5A). In addition, we determined the effects of IFN-β pretreatment on the levels of subgenomic viral RNA. For both WT MHV and ExoN(−) viruses, IFN-β pretreatment did not substantially reduce subgenomic RNA levels at any time point (Fig. 5B). These data indicate that IFN pretreatment did not result in the gross degradation or inhibition of ExoN(−) viral RNA accumulation. While slight reductions in viral RNA could explain a small portion of the IFN phenotype, these data suggest that decreased replication or transcription is not the primary driver of ExoN(−) IFN sensitivity.

Since pretreatment of DBT cells with IFN-β does not grossly alter ExoN(−) viral RNA accumulation but does reduce ExoN(−) viral titers, we sought to determine whether IFN pretreatment prior to infection resulted in a measurable difference in the number of viral particles released from WT MHV- or ExoN(−)-infected cells. DBT cells were pretreated with 0 or 100 U/ml mouse IFN-β for 18 h and subsequently infected with WT MHV or ExoN(−) virus at an MOI of 1 PFU/cell. At 12 h postinfection, cell culture supernatants were harvested and aliquots of two equal volumes were removed. From the first volume of each sample, RNA was extracted and used to perform one-step RT-qPCR to determine the number of genome RNAs present and, hence, the number of genome RNA-containing particles present in the given volume of supernatant (Fig. 5C). The second volume was saved for a plaque assay as described below. Pretreatment of cells with IFN-β resulted in an approximately 1-$\log_{10}$ decrease in the number of supernatant viral particles for both WT MHV and ExoN(−) viruses compared to the number of supernatant viral particles from untreated cells, demonstrating that IFN pretreatment affects the release of WT MHV and ExoN(−) virus particles equally (Fig. 5D). Thus, these data suggest that IFN pretreatment does not restrict the primary replication of viruses lacking ExoN activity but rather renders them inadequate for subsequent infection.

ExoN(−) virus progeny generated in the presence of an IFN-induced antiviral state have decreased specific infectivity and fitness upon subsequent infection. While many ISGs antagonize viral replication, some could alter the infectivity of progeny particles (27, 28). To test whether IFN pretreatment affected the infectivity of ExoN(−) viral particles, the remaining cell culture supernatant volume described above was used to perform a plaque assay to determine the number of PFU present (data not shown). Using the number of particles determined in Fig. 5C and the number of PFU present in an equivalent volume, we calculated the specific infectivity, or particle-to-PFU ratio, of each virus generated under each condition (Fig. 6A). Regardless of IFN-β

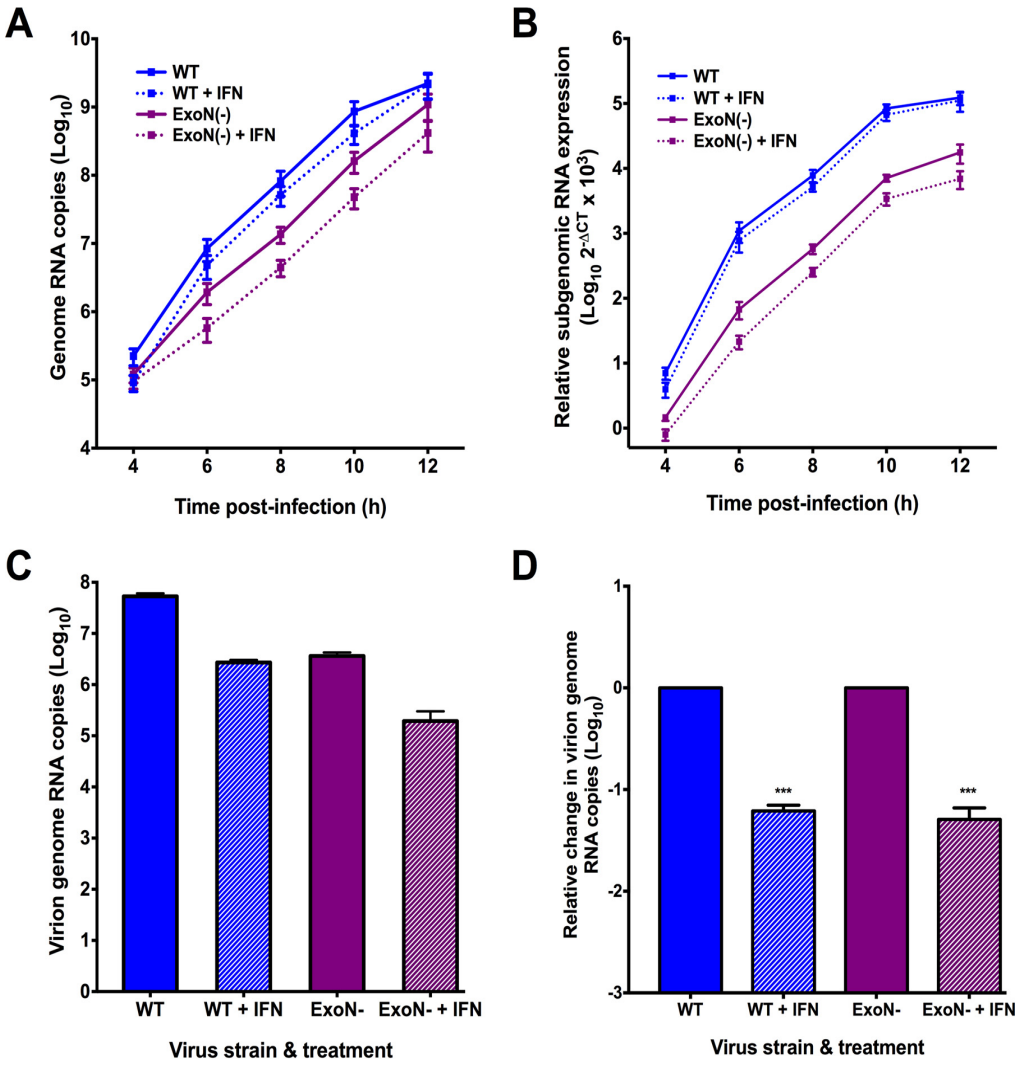

FIG 5 ExoN(−) viral RNA accumulation and particle release is marginally affected by IFN-β pretreatment. DBT cells were pretreated with 0 or 100 U/ml mouse IFN-β for 18 h and subsequently infected with WT MHV or ExoN(−) virus at an MOI of 1 PFU/cell. At the indicated times postinfection, total cell lysates were harvested and RNA was extracted. The viral genomic RNA copies present relative to an RNA standard were determined by one-step RT-qPCR (A), or cDNA was generated and the subgenomic RNA copies relative to those of GAPDH were determined by qPCR (B). For each of panels A and B, error bars represent SEM ($n = 6$ to 9). DBT cells were pretreated with 0 or 100 U/ml mouse IFN-β for 18 h and subsequently infected with WT MHV or ExoN(−) virus at an MOI of 1 PFU/cell. At 12 h postinfection, cell culture supernatants were collected. Equivalent volumes of cell culture supernatant for each sample were divided into two samples. For the first cell culture supernatant sample, total RNA was extracted and the number of virion genome RNA copies present (particles) was determined by one-step RT-qPCR (C) or reported as the change in virion genome RNA copies (D). Error bars represent SEM ($n = 13$ to 15). Statistical significance compared to untreated WT MHV or ExoN(−) infection, respectively, is denoted and was determined by Student's *t* test. ***, $P < 0.001$.

pretreatment during the initial infection, the specific infectivity of WT MHV was approximately 10 particles per 1 PFU upon subsequent infection. Infection of untreated DBT cells with ExoN(−) virus resulted in a particle-to-PFU ratio similar to that for WT MHV during subsequent infection. In contrast, when DBT cells were pretreated with IFN-β prior to initial infection with ExoN(−) virus, the resulting specific infectivity of ExoN(−) virus was 100 particles per 1 PFU, a significant decrease in specific infectivity. Therefore, ExoN(−) virus generated in the presence of an IFN-β-mediated antiviral state requires 10-fold more genome RNA-containing particles to generate 1 PFU than WT MHV generated in cells pretreated with or without IFN or ExoN(−) virus generated in

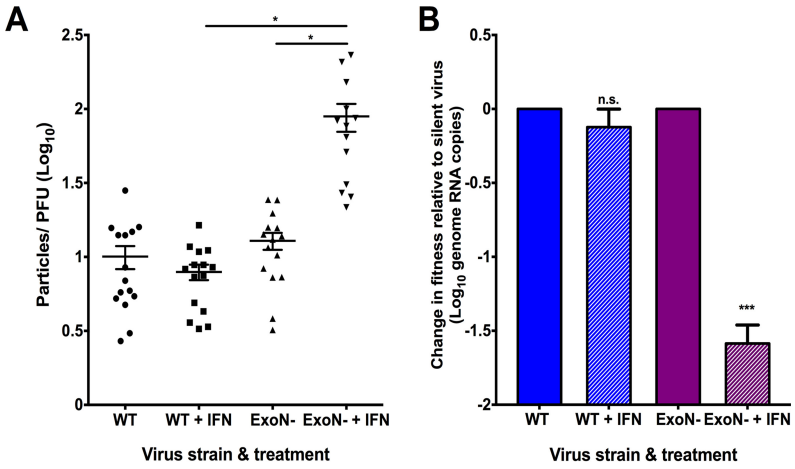

FIG 6 ExoN(−) viruses generated in the presence of an antiviral state have decreased specific infectivity and are less fit relative to untreated virus. (A) DBT cells were pretreated with 0 or 100 U/ml mouse IFN-β for 18 h and subsequently infected with WT MHV or ExoN(−) virus at an MOI of 1 PFU/cell. At 12 h postinfection, cell culture supernatants were collected. Equivalent volumes of cell culture supernatant for each sample were divided into two samples. For the first cell culture supernatant sample, total RNA was extracted and the number of virion genome RNA copies present (particles) was determined by one-step RT-qPCR (Fig. 5C). For the second cell culture supernatant sample, the viral titer present was determined by plaque assay (PFU) (data not shown). The particle-to-PFU ratio for each virus and treatment was calculated by dividing the number of particles by the number of PFU. Error bars represent SEM ($n = 13$ to 15). (B) DBT cells were pretreated with 0 or 100 U/ml mouse IFN-β for 18 h and subsequently infected with WT MHV or ExoN(−) virus at an MOI of 1 PFU/cell. At 12 h postinfection, cell culture supernatants were harvested for each virus and treatment group, and the number of virion genome RNA copies present (particles) in the supernatant was determined by one-step RT-qPCR. Using the determined number of particles, an equivalent number of virus particles from each virus and treatment group were mixed with an equal number of WT silent or ExoN(−) silent virus particles. This mixture then was used to infect a fresh monolayer of untreated DBT cells. At 24 h postinfection, cell culture supernatants were collected, RNA was extracted, and the number of virion genome RNA copies for each original virus and treatment group relative to their respective silent standard viruses was determined by one-step RT-qPCR and is reported as the change in fitness relative to the silent virus standard. Error bars represent SEM ($n = 6$). For each panel, statistical significance compared to untreated WT MHV or ExoN(−) infection is denoted and was determined by Student's *t* test. *, $P < 0.05$; ***, $P < 0.001$; n.s., not significant.

untreated cells. These data suggest that the IFN-mediated restriction of ExoN(−) virus in DBT cells occurs at the level of subsequent infection by reducing particle infectivity.

We next tested whether the effects of IFN on ExoN(−) viruses were intrinsic to the viruses produced. To do so, we performed a coinfection assay that utilized WT MHV and ExoN(−) viruses harboring 10 silent mutations in the nsp2 coding region (WT silent and ExoN(−) silent, respectively) along with WT MHV and ExoN(−) viruses. The genome RNAs of the silent viruses are recognized exclusively by a probe separate from the one used to detect the nsp2 probe-binding region of WT MHV or ExoN(−) virus (24), allowing WT silent and ExoN(−) silent viruses to act as internal controls for a coinfection assay under identical conditions. DBT cells were pretreated with 0 or 100 U/ml mouse IFN-β for 18 h and subsequently infected with WT MHV or ExoN(−) virus at an MOI of 1 PFU/cell. At 12 h postinfection, total cell culture supernatants were collected. The number of viral particles present in a representative aliquot was determined from purified virion genome RNA by one-step RT-qPCR. In addition, we determined the number of genome RNA-containing particles in an equivalent volume of WT silent or ExoN(−) silent viral p1 stock tubes. Using the calculated number of genome RNA-containing viral particles, we added an equal number of WT MHV viral particles generated in the absence of IFN pretreatment to WT silent viral particles and an equal number of WT MHV viral particles generated in the presence of IFN pretreatment to WT silent viral particles. This same setup was used for ExoN(−) viral particles generated in the presence or absence of IFN pretreatment with ExoN(−) silent viral particles. Finally, each combination was used to infect a fresh monolayer of untreated DBT cells. At 24 h

postcoinfection total cell culture supernatants were collected and virion genome RNA was extracted to determine the number of supernatant viral particles present from each combination of input viruses by one-step RT-qPCR and is reported as the change in fitness relative to the respective silent virus standard (Fig. 6B). The number of WT MHV particles generated in the presence of IFN pretreatment was similar to the number of WT MHV particles generated in the absence of IFN pretreatment over the course of coinfection, relative to their respective silent standards. However, the number of viral particles present from ExoN(−) virus generated in the presence of IFN pretreatment during the course of coinfection decreased by approximately 1.5 $\log_{10}$ compared with ExoN(−) viral particles generated in the absence of IFN pretreatment relative to their respective silent standards. These data indicate that a loss in nsp14 ExoN activity sensitizes viruses to IFN pretreatment and reduces the infectivity and fitness of progeny during subsequent rounds of infection in the absence of an antiviral state.

DISCUSSION

CoVs encode multiple IFN antagonists that prevent the induction of or mediate resistance to the innate immune response, allowing efficient viral replication early during infection (3). Moreover, an insufficient innate immune response has been proposed to be a major contributor to SARS-CoV pathogenesis (29). In this study, we sought to determine the contributions of nsp14 ExoN activity to the induction of and resistance to the innate immune response. We demonstrate that ExoN(−) virus is more sensitive to cellular pretreatment with IFN-β than WT MHV. Further, because ExoN3(−) and ExoN(−) P250 viruses also were more sensitive to the effects of IFN, we conclude that IFN sensitivity is specifically due to a loss of ExoN activity.

Because the ExoN activity of the Lassa fever virus nucleoprotein degrades dsRNA intermediates (18, 19), we hypothesized that CoV nsp14 ExoN could function in a similar manner. In fact, since our current study began, CoV nsp14 ExoN activity also has been proposed by others to function as an innate immune antagonist (21, 30). If nsp14 ExoN is degrading viral dsRNA, ExoN inactivation should increase intracellular dsRNA accumulation, resulting in a concomitant increase in IFN-β expression or activation of RNase L during infection. We observed neither IFN-β upregulation nor RNase L activation over the course of ExoN(−) virus infection (Fig. 4A and B), and rRNA was intact at all time points tested (Fig. 4B). Therefore, at least two possible explanations exist: (i) MHV ExoN does not function to degrade dsRNA or (ii) MHV ExoN does degrade dsRNA, but the detection of this PAMP is unchanged during ExoN(−) virus infection due to sufficient antagonism by other CoV proteins. Basal OAS expression levels correlate with RNase L activation (31). Thus, we pretreated DBTs with IFN-β to upregulate OAS and RNase L expression. However, rRNA degradation was observed only in cells transfected with poly(I·C) (Fig. 4B). Further, nsp15 EndoU and NS2 phosphodiesterase activities were intact during all of our experiments. Thus, it is possible that in the absence of nsp14 ExoN activity, other CoV innate antagonists were sufficient to prevent innate detection by the cell or prevent the induction of a detectable signal in the experiments we performed. However, one would expect the endonucleolytic products of nsp15 to be smaller dsRNAs that could still activate RIG-I or MDA5, similar to RNase L products, unless another RNA degradation mechanism were in place (4, 32). In addition, despite an intact NS2 phosphodiesterase, nsp15 mutants still activate RNase L-mediated rRNA degradation (12). Lastly, when $RL^{-/-}$/$PKR^{-/-}$ BMMs were infected with ExoN(−) virus, viral replication was not rescued, suggesting that RNase L and PKR are not required for ExoN(−) virus restriction (Fig. 4C). Moreover, these data suggest dsRNA is not detected and the antiviral effectors RNase L and PKR are not activated during ExoN(−) virus infection.

During our study, Becares et al. reported that a TGEV nsp14 zinc finger mutant modulated the innate immune response of swine testis cells by reducing the levels of dsRNA and induction of IFN (21). Unlike TGEV, betacoronaviruses such as SARS-CoV and MHV do not induce IFN expression in most cell types (1–3) (Fig. 4A). Interestingly, TGEV ExoN active-site mutants were nonviable, although this is not the first report of

nonviable ExoN active-site residue mutants in alphacoronaviruses (21). In the initial report of CoV nsp14 ExoN activity, human CoV 229E ExoN active-site mutants were also nonviable, suggesting a common essential function for nsp14 ExoN in *Alphacoronavirus* replication and/or innate antagonism (13). Altogether, the possibility of a common innate immune antagonism function for nsp14 across alpha- and beta-CoVs is apparent, but clearly differing requirements exist that may be dependent on the CoV genus and cell types used.

Our results clearly demonstrate that viruses lacking ExoN activity are more sensitive to IFN-β pretreatment than WT MHV in a dose-dependent manner (Fig. 1A and C and 2). Further, replication of viruses lacking ExoN activity was dependent on the capacity of BMMs to express genes downstream of IFNAR signaling (Fig. 3). This is due to the fact that B6 and IFNAR$^{-/-}$ cells have different levels of basal ISG expression and, thus, two very different intracellular environments for viral replication to occur (3, 25, 26). In IFNAR$^{-/-}$ BMMs, ExoN(−) and ExoN(−) P250 virus replication capacity was restored to levels approaching or exceeding WT MHV levels (Fig. 3). Further, our specific infectivity (Fig. 6A) and coinfection (Fig. 6B) data show that ExoN(−) virus generated in the presence of an antiviral state is less viable upon subsequent infection. Altogether, our results suggest that an ISG(s) is acting on ExoN(−) virus, specifically resulting in progeny that are less viable upon subsequent infection. Thus, it will be interesting to determine the specific ISG or ISGs responsible for mediating the observed restriction. In addition, it will be important to determine whether a greater proportion of the incoming ExoN(−) viral particles are strictly nonviable or whether cells are now sensing the progeny ExoN(−) viruses and inhibiting replication. Our specific infectivity data support the possibility that the effects of IFN treatment results in noninfectious ExoN(−) virus particles, which could compete with infectious ExoN(−) virus particles for viral receptors during subsequent entry. Due to the pleiotropic nature of IFN-β, more than one mechanism may be acting.

To date, the majority of our understanding of nsp14 ExoN activity is in the context of proofreading during CoV replication (13, 15, 16, 33). CoVs lacking ExoN activity demonstrate an increase in mutation frequency relative to that of the WT (15, 16). Thus, it is possible that ExoN(−) virus replication in IFN-pretreated cells results in further alteration of ExoN(−) virus mutation frequency. Certainly, an increase or decrease in mutation frequency could impair viral replication during a subsequent infection. Moreover, a recent study demonstrated that optimal viral replication fidelity is required for poliovirus to overcome tissue-specific innate immune responses (34). In addition, IFN pretreatment may upregulate an ISG that acts to hypermutate the large CoV genome in the absence of ExoN activity, rendering viral progeny less viable. ISGs that increase viral mutation frequency have been described, such as adenosine deaminase acting on RNA 1 (ADAR1) and apolipoprotein B mRNA editing enzyme, catalytic polypeptide-like 3G (APOBEC3G) (27, 28). Further, another ISG, SAMHD1, may inhibit HIV replication by limiting nucleotide pools, a known contributor to increased viral mutation frequency (35–37). Moreover, other possible mechanisms outside of altered mutation frequency exist. For instance, in the absence of ExoN activity, terminal RNA modifications, recombination, and/or replicase protein interactions mediated by nsp14 ExoN may be disrupted to a greater extent in the presence of an IFN-β-mediated antiviral state.

Since CoVs encode the largest genome known for RNA viruses, they have the luxury of encoding multiple IFN antagonists that limit the capacity of a cell to detect and respond to infection. Collectively, our data suggest that MHV nsp14 ExoN activity is a contributor to CoV innate immune antagonism. We clearly demonstrate that viruses lacking ExoN activity are more sensitive to the effects of an IFN-β-mediated antiviral state. Further, our data reveal a critical role for nsp14 ExoN activity in CoV replication and provide additional rationale for targeting nsp14 ExoN activity as a means of viral attenuation. Our future studies will probe the specific mechanism of restriction for viruses lacking ExoN activity and assess how the requirement of ExoN activity for resistance to innate immunity can be utilized for treatment during human coronavirus infections.

MATERIALS AND METHODS

Cell culture. Murine delayed brain tumor (DBT) cells (38) and baby hamster kidney 21 cells expressing the MHV receptor (BHK-R) (39) were maintained at 37°C in Dulbecco's modified Eagle medium (DMEM; Gibco) supplemented with 10% fetal bovine serum (FBS; Invitrogen), 100 U/ml penicillin and streptomycin (Gibco), and 0.25 μg/ml amphotericin B (Corning). BHK-R cells were further supplemented with 0.8 mg/ml of G418 (Mediatech).

Cloning, recovery, and verification of mutant viruses. Recombinant MHV strain A59 (GenBank accession number AY910861) has been previously described (39). ExoN(−) (nsp14 D89A and E91A) has been previously described (15). To generate ExoN(−) P250 virus, subconfluent monolayers of DBT cells in 25-cm^2 flasks were infected using the ExoN(−) parental stock and blindly passaged for a total of 250 passages (24). For ExoN3(−) virus (nsp14 D272A), site-directed mutagenesis was used to engineer point mutations in the MHV genome cDNA F fragment plasmid using the MHV infectious clone reverse genetics system (39). ExoN3(−) mutant virus was recovered using BHK-R cells following electroporation of *in vitro*-transcribed genomic RNA. Recovered ExoN3(−) virus was sequenced (GenHunter Corporation, Nashville, TN) to verify the engineered mutations were present and to ensure that no additional mutations were introduced.

IFN-β sensitivity assays. Subconfluent DBT cells were treated for 18 h with the indicated concentrations of mouse IFN-β (PBL Assay Science) prior to infection with virus at a multiplicity of infection (MOI) of 1 PFU per cell at 37°C for 45 min. After incubation, inocula were removed, cells were washed with phosphate-buffered saline (PBS), and fresh medium was added. Cell culture supernatants were collected at 12 h postinfection, and viral titers were determined by plaque assay (15).

5-FU sensitivity assays. Subconfluent DBT cells were treated with DMEM supplemented to contain the indicated concentrations of 5-fluorouracil (5-FU; Sigma) or dimethyl sulfoxide (DMSO) alone at 37°C for 30 min. After incubation, drug was removed and cells were infected with virus at an MOI of 1 PFU/cell at 37°C for 1 h. Inocula were removed, and cells were incubated in medium containing 5-FU or DMSO. Cell culture supernatants were collected at 12 h postinfection, and viral titers were determined by plaque assay.

Virus replication kinetics. Bone marrow-derived macrophages (BMMs) were generated from the hind limbs of WT, IFNAR$^{-/-}$, or RL$^{-/-}$/PKR$^{-/-}$ C57/B6 mice as previously described (11). BMMs were infected with virus at an MOI of 1 PFU/cell at 37°C for 1 h. After incubation, inocula were removed, cells were washed 3 times with PBS, and fresh medium was added. At the indicated times postinfection, cell culture supernatant aliquots were collected and viral titers determined by plaque assay.

IFN-β induction assays. Subconfluent DBT cells were mock infected or infected with WT, ExoN(−), or ExoN(−) P250 virus at an MOI of 0.1 PFU/cell or with Sendai virus (SenV) at an MOI of 200 HA units/ml at 37°C for 45 min. Inocula were removed, cells were washed with PBS, and fresh medium was added. At the indicated times postinfection, cell culture supernatants were removed and cell lysates were harvested by adding 1 ml TRIzol reagent. Total RNA present in the lysates was purified using the phenol-chloroform method. cDNA was generated by reverse transcriptase PCR (RT-PCR) using 1 μg of total RNA as previously described (16). Mouse IFN-β expression levels were determined relative to that for glyceraldehyde-3-phosphate dehydrogenase (GAPDH) by qPCR using the Applied Biosciences 7500 real-time PCR system with Power SYBR green PCR master mix and IFN-β primers (FWD, 5′-TCCGCCCTG TAGGTGAGGTTGAT-3′; REV, 5′-GTTCCTGCTGTGCTTCTCCACCA-3′) and GAPDH primers previously reported (16).

Determination of rRNA integrity. Subconfluent monolayers of DBT cells were treated with 0 or 50 U/ml mouse IFN-β for 18 h prior to being infected with virus at an MOI of 1 PFU/cell at 37°C for 45 min. After incubation, inocula were removed, cells were washed with PBS, and fresh medium was added. At the indicated times postinfection, cell culture supernatants were removed and total RNA was harvested by adding 1 ml TRIzol reagent. For a positive control, cells were transfected with 25 μg/ml poly(I:C) (Sigma) using Lipofectamine 2000 (Thermo Fisher Scientific). Total RNA from all samples was purified using the PureLink RNA mini purification system (Life Technologies) by following the manufacturer's instructions. Upon purification, total RNA was analyzed on an Agilent Bioanalyzer by the Vanderbilt VANTAGE core facility and the rRNA integrity reported.

Quantification of viral genomic RNA by one-step RT-qPCR. The quantification of viral genomic RNA has been previously described (14). Briefly, an RNA standard was prepared using the MHV A fragment (39), and a standard curve was generated using 10-fold dilutions from 10^3 to 10^8 copies. A 5′ 6-carboxyfluorescein (FAM)-labeled probe (5′-TTCTGACAACGGCTACACCCAACG-3′ [Biosearch Technologies]) was used with forward (5′-AGAAGGTTACTGGCAACTG-3′) and reverse (5′-TGTCCACGGCTAAATCA AAC-3′) nsp2 specific primers. The final volume for each reaction mixture was 20 μl with 150 nM probe, 900 nM each primer, 2 μl sample RNA, and 10 μl 2× ToughMix, one-step, low-ROX enzyme mix (Quanta Bio) per reaction. Samples were quantified using an Applied Biosciences 7500 real-time PCR system with conditions of 55°C for 10 min, 95°C for 5 min, 95°C for 30 s, and 60°C for 1 min, with the last two steps repeated 40 times. The standard curve was plotted using GraphPad Prism 6 software, and genomes per microliter were calculated.

Quantification of subgenomic RNA by qPCR. Subconfluent DBT cells were treated with 0 or 100 U/ml mouse IFN-β for 18 h prior to being infected with virus at an MOI of 1 PFU/cell at 37°C for 45 min. After incubation, inocula were removed, cells were washed with PBS, and fresh medium was added. At the indicated times postinfection, cell culture supernatants were removed and total RNA was harvested by adding 1 ml TRIzol reagent. Total RNA was extracted using the PureLink RNA mini purification system by following the manufacturer's instructions. cDNA was generated by RT-PCR using 1 μg of total RNA as previously described (16). Primers used to detect subgenomic nucleocapsid and GAPDH gene expression

have been reported (16, 40). Subgenomic expression levels relative to GAPDH were determined using the Applied Biosciences 7500 real-time PCR system with Power SYBR green PCR master mix.

Determination of specific infectivity. The quantification of virus-specific infectivity has been previously described (14, 24, 41). Briefly, subconfluent monolayers of DBT cells were infected with virus at an MOI of 1 PFU/cell at 37°C for 45 min. After incubation, inocula were removed, cells were washed with PBS, and fresh medium was added. At 12 h postinfection, cell culture supernatants were collected, and viral titers were determined by plaque assay. Supernatants also were used for RNA genome isolation by adding 100 μl supernatant to 900 μl TRIzol reagent, chloroform extraction by phase separation, and final purification using the PureLink RNA mini purification system. Genome RNA was quantified using one-step RT-qPCR as described above, and the particle-to-PFU ratio was calculated.

Coinfection assay. Subconfluent monolayers of DBT cells were treated with 0 or 100 U/ml mouse IFN-β for 18 h prior to being infected with virus at an MOI of 1 PFU/cell at 37°C for 45 min. After incubation, inocula were removed, cells were washed with PBS, and fresh medium was added. At 12 h postinfection, cell culture supernatants were removed and 100 μl of supernatant was added to 900 μl TRIzol reagent. Viral genome RNA was purified, and the number of viral genome RNA copies present relative to an RNA standard curve was determined as described above. Based on the number of viral genome RNA copies determined by one-step RT-qPCR, equal numbers of virus particles from each virus and each condition were combined with an equal number of WT silent or ExoN(−) silent virus particles, respectively. WT silent and ExoN(−) silent viruses were engineered to harbor 10 silent mutations in the probe-binding region of nsp2, allowing separate detection from WT MHV or ExoN(−) virus genomes, respectively, using a separate probe upon coinfection (24). A fresh, subconfluent monolayer of DBT cells next was coinfected with each combination of viruses at 37°C for 45 min. After incubation, inocula were removed, cells were washed with PBS, and fresh medium was added. At 24 h postinfection, cell culture supernatants were removed and 100 μl of supernatant was added to 900 μl TRIzol reagent. Viral genome RNA was purified. The number of viral genome RNA copies of both reference and silent viruses were determined relative to the appropriate standard curve. The number of viral genome RNA copies relative to the number of silent virus genome RNA copies was determined for each virus and condition. Values are reported as the change in fitness relative to the silent virus.

Statistical analysis. Statistical tests were applied as noted in the respective figure legends and were determined using GraphPad Prism 6 software (La Jolla, CA).

ACKNOWLEDGMENTS

We thank members of the Vanderbilt Technologies for Advanced Genomics (VANTAGE) core for rRNA integrity determination services. We thank fellow members of the Denison and Weiss laboratories, specifically Maria Agostini, for helpful discussions.

This work was supported by Public Health Service award T32 HL07751 (J.B.C.) from the National Heart, Lung, and Blood Institute and R01 AI108197 (M.R.D.) and R01 AI104887 (S.R.W.) from the National Institute of Allergy and Infectious Diseases. Additional support was provided by the Elizabeth B. Lamb Center for Pediatric Research.

REFERENCES

1. Roth-Cross JK, Martinez-Sobrido L, Scott EP, Garcia-Sastre A, Weiss SR. 2007. Inhibition of the alpha/beta interferon response by mouse hepatitis virus at multiple levels. J Virol 81:7189–7199. https://doi.org/10.1128/JVI.00013-07.
2. Frieman M, Heise M, Baric R. 2008. SARS coronavirus and innate immunity. Virus Res 133:101–112. https://doi.org/10.1016/j.virusres.2007.03.015.
3. Rose KM, Weiss SR. 2009. Murine coronavirus cell type dependent interaction with the type I interferon response. Viruses 1:689–712. https://doi.org/10.3390/v1030689.
4. Schneider WM, Chevillotte MD, Rice CM. 2014. Interferon-stimulated genes: a complex web of host defenses. Annu Rev Immunol 32:513–545. https://doi.org/10.1146/annurev-immunol-032713-120231.
5. Kamitani W, Narayanan K, Huang C, Lokugamage K, Ikegami T, Ito N, Kubo H, Makino S. 2006. Severe acute respiratory syndrome coronavirus nsp1 protein suppresses host gene expression by promoting host mRNA degradation. Proc Natl Acad Sci U S A 103:12885–12890. https://doi.org/10.1073/pnas.0603144103.
6. Zhang R, Li Y, Cowley TJ, Steinbrenner AD, Phillips JM, Yount BL, Baric RS, Weiss SR. 2015. The nsp1, nsp13, and M proteins contribute to the hepatotropism of murine coronavirus JHM.WU. J Virol 89:3598–3609. https://doi.org/10.1128/JVI.03535-14.
7. Devaraj SG, Wang N, Chen Z, Chen Z, Tseng M, Barretto N, Lin R, Peters CJ, Tseng C-TK, Baker SC, Li K. 2007. Regulation of IRF-3-dependent innate immunity by the papain-like protease domain of the severe acute respiratory syndrome coronavirus. J Biol Chem 282:32208–32221. https://doi.org/10.1074/jbc.M704870200.
8. Barretto N, Jukneliene D, Ratia K, Chen Z, Mesecar AD, Baker SC. 2005. The papain-like protease of severe acute respiratory syndrome coronavirus has deubiquitinating activity. J Virol 79:15189–15198. https://doi.org/10.1128/JVI.79.24.15189-15198.2005.
9. Chen Y, Cai H, Pan J, Xiang N, Tien P, Ahola T, Guo D. 2009. Functional screen reveals SARS coronavirus nonstructural protein nsp14 as a novel cap N7 methyltransferase. Proc Natl Acad Sci U S A 106:3484–3489. https://doi.org/10.1073/pnas.0808790106.
10. Decroly E, Imbert I, Coutard B, Bouvet M, Selisko B, Alvarez K, Gorbalenya AE, Snijder EJ, Canard B. 2008. Coronavirus nonstructural protein 16 is a cap-0 binding enzyme possessing (nucleoside-2′O)-methyltransferase activity. J Virol 82:8071–8084. https://doi.org/10.1128/JVI.00407-08.
11. Zhao L, Jha BK, Wu A, Elliott R, Ziebuhr J, Gorbalenya AE, Silverman RH, Weiss SR. 2012. Antagonism of the interferon-induced OAS-RNase L pathway by murine coronavirus ns2 protein is required for virus replication and liver pathology. Cell Host Microbe 11:607–616. https://doi.org/10.1016/j.chom.2012.04.011.
12. Kindler E, Gil-Cruz C, Spanier J, Li Y, Wilhelm J, Rabouw HH, Züst R, Hwang M, V'kovski P, Stalder H, Marti S, Habjan M, Cervantes-Barragan L, Elliot R, Karl N, Gaughan C, van Kuppeveld FJM, Silverman RH, Keller M, Ludewig B, Bergmann CC, Ziebuhr J, Weiss SR, Kalinke U, Thiel V. 2017. Early endonuclease-mediated evasion of RNA sensing ensures

efficient coronavirus replication. PLoS Pathog 13:e1006195. https://doi.org/10.1371/journal.ppat.1006195.
13. Minskaia E, Hertzig T, Gorbalenya AE, Campanacci V, Cambillau C, Canard B, Ziebuhr J. 2006. Discovery of an RNA virus 3′->5′ exoribonuclease that is critically involved in coronavirus RNA synthesis. Proc Natl Acad Sci U S A 103:5108–5113. https://doi.org/10.1073/pnas.0508200103.
14. Case JB, Ashbrook AW, Dermody TS, Denison MR. 2016. Mutagenesis of S-adenosyl-l-methionine-binding residues in coronavirus nsp14 N7-methyltransferase demonstrates differing requirements for genome translation and resistance to innate immunity. J Virol 90:7248–7256. https://doi.org/10.1128/JVI.00542-16.
15. Eckerle LD, Lu X, Sperry SM, Choi L, Denison MR. 2007. High fidelity of murine hepatitis virus replication is decreased in nsp14 exoribonuclease mutants. J Virol 81:12135–12144. https://doi.org/10.1128/JVI.01296-07.
16. Smith EC, Blanc H, Vignuzzi M, Denison MR. 2013. Coronaviruses lacking exoribonuclease activity are susceptible to lethal mutagenesis: evidence for proofreading and potential therapeutics. PLoS Pathog 9:e1003565. https://doi.org/10.1371/journal.ppat.1003565.
17. Graham RL, Becker MM, Eckerle LD, Bolles M, Denison MR, Baric RS. 2012. A live, impaired-fidelity coronavirus vaccine protects in an aged, immunocompromised mouse model of lethal disease. Nat Med 18:1820–1826. https://doi.org/10.1038/nm.2972.
18. Qi X, Lan S, Wang W, Schelde LM, Dong H, Wallat GD, Ly H, Liang Y, Dong C. 2010. Cap binding and immune evasion revealed by Lassa nucleoprotein structure. Nature 468:779–783. https://doi.org/10.1038/nature09605.
19. Hastie KM, Kimberlin CR, Zandonatti MA, MacRae IJ, Saphire EO. 2011. Structure of the Lassa virus nucleoprotein reveals a dsRNA-specific 3′ to 5′ exonuclease activity essential for immune suppression. Proc Natl Acad Sci U S A 108:2396–2401. https://doi.org/10.1073/pnas.1016404108.
20. Russier M, Reynard S, Carnec X, Baize S. 2014. The exonuclease domain of Lassa virus nucleoprotein is involved in antigen-presenting-cell-mediated NK cell responses. J Virol 88:13811–13820. https://doi.org/10.1128/JVI.01908-14.
21. Becares M, Pascual-Iglesias A, Nogales A, Sola I, Enjuanes L, Zuñiga S. 2016. Mutagenesis of coronavirus nsp14 reveals its potential role in modulation of the innate immune response. J Virol 90:5399–5414. https://doi.org/10.1128/JVI.03259-15.
22. Rose KM, Elliott R, Martinez-Sobrido L, Garcia-Sastre A, Weiss SR. 2010. Murine coronavirus delays expression of a subset of interferon-stimulated genes. J Virol 84:5656–5669. https://doi.org/10.1128/JVI.00211-10.
23. Ma Y, Wu L, Shaw N, Gao Y, Wang J, Sun Y, Lou Z, Yan L, Zhang R, Rao Z. 2015. Structural basis and functional analysis of the SARS coronavirus nsp14–nsp10 complex. Proc Natl Acad Sci U S A 112:9436–9441. https://doi.org/10.1073/pnas.1508686112.
24. Graepel K, Lu X, Case JB, Sexton NR, Smith EC, Denison MR. 2017. Proofreading-deficient coronaviruses adapt for increased fitness over long-term passage without reversion of exoribonuclease-inactivating mutations. bioRxiv https://doi.org/10.1101/175562.
25. Zhao L, Rose KM, Elliott R, Van Rooijen N, Weiss SR. 2011. Cell-type-specific type I interferon antagonism influences organ tropism of murine coronavirus. J Virol 85:10058–10068. https://doi.org/10.1128/JVI.05075-11.
26. Zhao L, Birdwell LD, Wu A, Elliott R, Rose KM, Phillips JM, Li Y, Grinspan J, Silverman RH, Weiss SR. 2013. Cell-type-specific activation of the oligoadenylate synthetase-RNase L pathway by a murine coronavirus. J Virol 87:8408–8418. https://doi.org/10.1128/JVI.00769-13.
27. Tomaselli S, Galeano F, Locatelli F, Gallo A. 2015. ADARs and the balance game between virus infection and innate immune cell response. Curr Issues Mol Biol 17:37–51.
28. Neil S, Bieniasz P. 2009. Human immunodeficiency virus, restriction factors, and interferon. J Interferon Cytokine Res 29:569–580. https://doi.org/10.1089/jir.2009.0077.
29. Gu J, Korteweg C. 2007. Pathology and pathogenesis of severe acute respiratory syndrome. Am J Pathol 170:1136–1147. https://doi.org/10.2353/ajpath.2007.061088.
30. Kindler E, Thiel V. 2014. To sense or not to sense viral RNA–essentials of coronavirus innate immune evasion. Curr Opin Microbiol 20:69–75. https://doi.org/10.1016/j.mib.2014.05.005.
31. Birdwell LD, Zalinger ZB, Li Y, Wright PW, Elliott R, Rose KM, Silverman RH, Weiss SR. 2016. Activation of RNase L by murine coronavirus in myeloid cells is dependent on basal *Oas* gene expression and independent of virus-induced interferon. J Virol 90:3160–3172. https://doi.org/10.1128/JVI.03036-15.
32. Malathi K, Dong B, Gale M, Silverman RH. 2007. Small self-RNA generated by RNase L amplifies antiviral innate immunity. Nature 448:816–819. https://doi.org/10.1038/nature06042.
33. Bouvet M, Imbert I, Subissi L, Gluais L, Canard B, Decroly E. 2012. RNA 3′-end mismatch excision by the severe acute respiratory syndrome coronavirus nonstructural protein nsp10/nsp14 exoribonuclease complex. Proc Natl Acad Sci U S A 109:9372–9377. https://doi.org/10.1073/pnas.1201130109.
34. Xiao Y, Dolan PT, Goldstein EF, Li M, Farkov M, Brodsky L, Andino R. 2017. Poliovirus intrahost evolution is required to overcome tissue-specific innate immune responses. Nat Commun 8:375. https://doi.org/10.1038/s41467-017-00354-5.
35. Lahouassa H, Daddacha W, Hofmann H, Ayinde D, Logue EC, Dragin L, Bloch N, Maudet C, Bertrand M, Gramberg T, Pancino G, Priet S, Canard B, Laguette N, Benkirane M, Transy C, Landau NR, Kim B, Margottin-Goguet F. 2012. SAMHD1 restricts the replication of human immunodeficiency virus type 1 by depleting the intracellular pool of deoxynucleoside triphosphates. Nat Immunol 13:223–228. https://doi.org/10.1038/ni.2236.
36. Hrecka K, Hao C, Gierszewska M, Swanson SK, Kesik-Brodacka M, Srivastava S, Florens L, Washburn MP, Skowronski J. 2011. Vpx relieves inhibition of HIV-1 infection of macrophages mediated by the SAMHD1 protein. Nature 474:658–661. https://doi.org/10.1038/nature10195.
37. Sanjuán R, Domingo-Calap P. 2016. Mechanisms of viral mutation. Cell Mol Life Sci 73:4433–4448. https://doi.org/10.1007/s00018-016-2299-6.
38. Chen W, Baric RS. 1996. Molecular anatomy of mouse hepatitis virus persistence: coevolution of increased host cell resistance and virus virulence. J Virol 70:3947–3960.
39. Yount B, Denison MR, Weiss SR, Baric RS. 2002. Systematic assembly of a full-length infectious cDNA of mouse hepatitis virus strain A59. J Virol 76:11065–11078. https://doi.org/10.1128/JVI.76.21.11065-11078.2002.
40. Donaldson EF, Sims AC, Graham RL, Denison MR, Baric RS. 2007. Murine hepatitis virus replicase protein nsp10 is a critical regulator of viral RNA synthesis. J Virol 81:6356–6368. https://doi.org/10.1128/JVI.02805-06.
41. Sexton NR, Smith EC, Blanc H, Vignuzzi M, Peersen OB, Denison MR. 2016. Homology-based identification of a mutation in the coronavirus RNA-dependent RNA polymerase that confers resistance to multiple mutagens. J Virol 90:7415–7428. https://doi.org/10.1128/JVI.00080-16.
42. Case JB, Li Y, Elliott R, Lu X, Graepel KW, Sexton NR, Smith EC, Weiss SR, Denison MR. 2017. Mouse hepatitis virus nsp14 exoribonuclease activity is required for resistance to innate immunity. bioRxiv https://doi.org/10.1101/182196.

APPENDIX C:

DIFFERENTIALLY EXPRESSED ISGS IN DBT CELLS

Gene		Log_2 Fold Change	pValue	Gene		Log_2 Fold Change	pValue
ENSMUSG00000025498	Irf7	-4.724135798	0	ENSMUSG00000026222	Sp100	-0.705276261	1.22E-08
ENSMUSG00000028268	Gbp3	-3.909806849	0	ENSMUSG00000022216	Psme1	-0.691133394	7.73E-26
ENSMUSG00000052776	Oas1a	-3.372201251	3.38E-187	ENSMUSG00000038393	Txnip	-0.685904569	2.13E-14
ENSMUSG00000046718	Bst2	-3.241894357	0	ENSMUSG00000041642	Kif21b	-0.678424039	3.74E-08
ENSMUSG00000035692	Isg15	-3.214844637	4.94E-204	ENSMUSG00000037997	Parp11	-0.665638164	9.37E-10
ENSMUSG00000027514	Zbp1	-3.209775701	0	ENSMUSG00000021453	Gadd45g	-0.664847689	2.09E-13
ENSMUSG00000001123	Lgals9	-3.00395842	6.97E-207	ENSMUSG00000021281	Tnfaip2	-0.661824392	1.34E-12
ENSMUSG00000028037	Ifi44	-2.836579535	4.38E-118	ENSMUSG00000057143	Trim12c	-0.659266823	1.17E-07
ENSMUSG00000025492	Ifitm3	-2.830792551	0	ENSMUSG00000029446	Psph	-0.650094495	1.02E-24
ENSMUSG00000033880	Lgals3bp	-2.788878802	1.32E-280	ENSMUSG00000032596	Uba7	-0.647982126	1.38E-07
ENSMUSG00000024308	Tapbp	-2.396669443	2.11E-228	ENSMUSG00000026104	Stat1	-0.646126754	1.16E-10
ENSMUSG00000024338	Psmb8	-2.237581537	1.82E-72	ENSMUSG00000002983	Relb	-0.639256053	2.37E-08
ENSMUSG00000029561	Oasl2	-2.204782831	8.42E-80	ENSMUSG00000091373	Gm8810	-0.636135233	2.33E-07
ENSMUSG00000066861	Oas1g	-2.201822243	1.61E-70	ENSMUSG00000029752	Asns	-0.63304898	2.51E-71
ENSMUSG00000040483	Xaf1	-2.174360841	1.64E-166	ENSMUSG00000005667	Mthfd2	-0.627734176	2.10E-43
ENSMUSG00000068246	Apol9b	-2.169814146	3.08E-72	ENSMUSG00000060950	Trmt61a	-0.627404205	1.43E-14
ENSMUSG00000027313	Chac1	-2.105040676	3.67E-110	ENSMUSG00000027071	P2rx3	-0.611724629	6.30E-08
ENSMUSG00000057346	Apol9a	-2.069572242	7.12E-68	ENSMUSG00000040010	Slc7a5	-0.610944125	1.28E-40
ENSMUSG00000027078	Ube2l6	-2.022067931	1.13E-63	ENSMUSG00000085156	Gm11974	-0.604955404	3.38E-10
ENSMUSG00000033355	Rtp4	-1.93170957	8.50E-57	ENSMUSG00000010095	Slc3a2	-0.602497421	1.83E-46
ENSMUSG00000062488	Ifit3b	-1.918709202	6.85E-54	ENSMUSG00000024330	Col11a2	-0.602210223	7.23E-09
ENSMUSG00000074896	Ifit3	-1.897224158	2.12E-54	ENSMUSG00000020638	Cmpk2	-0.595525932	1.76E-06
ENSMUSG00000023341	Mx2	-1.830166471	3.56E-49	ENSMUSG00000086841	2410006H16Rik	-0.594815543	3.24E-18
ENSMUSG00000032715	Trib3	-1.735709686	2.59E-119	ENSMUSG00000037321	Tap1	-0.594485032	1.69E-06
ENSMUSG00000030107	Usp18	-1.715782616	2.90E-43	ENSMUSG00000026628	Atf3	-0.588443036	1.66E-06
ENSMUSG00000032661	Oas3	-1.677240108	1.33E-41	ENSMUSG00000090272	Mndal	-0.583872268	2.80E-06
ENSMUSG00000030921	Trim30a	-1.608580593	5.26E-40	ENSMUSG00000034394	Lif	-0.581453743	2.21E-13
ENSMUSG00000064215	Ifi27	-1.594532605	6.82E-83	ENSMUSG00000034855	Cxcl10	-0.579790866	3.28E-06
ENSMUSG00000040296	Ddx58	-1.497769143	4.36E-69	ENSMUSG00000039236	Isg20	-0.576563844	4.57E-12
ENSMUSG00000040253	Gbp7	-1.455014505	3.12E-32	ENSMUSG00000037580	Gch1	-0.568643872	3.57E-06
ENSMUSG00000067212	H2-T23	-1.41660395	1.03E-35	ENSMUSG00000049502	Dtx3l	-0.568495207	8.33E-11
ENSMUSG00000046879	Irgm1	-1.393861453	2.42E-56	ENSMUSG00000024261	Syt4	-0.565727767	9.30E-45
ENSMUSG00000028270	Gbp2	-1.359860823	7.41E-28	ENSMUSG00000028480	Glipr2	-0.562138562	1.05E-12
ENSMUSG00000032690	Oas2	-1.358630825	7.08E-30	ENSMUSG00000079492	Gm11127	-0.558931441	5.81E-06
ENSMUSG00000069874	Irgm2	-1.311312445	5.84E-26	ENSMUSG00000035773	Kiss1r	-0.558109772	4.41E-09
ENSMUSG00000028179	Cth	-1.294791171	3.00E-28	ENSMUSG00000050022	Amz1	-0.555297334	8.34E-06
ENSMUSG00000056116	H2-T22	-1.263191437	4.67E-39	ENSMUSG00000029605	Oas1b	-0.553693315	2.54E-08
ENSMUSG00000070327	Rnf213	-1.255026518	4.65E-52	ENSMUSG00000035828	Pim3	-0.544658293	1.48E-20
ENSMUSG00000038507	Parp12	-1.189084475	7.87E-28	ENSMUSG00000031026	Trim66	-0.53533792	1.56E-05
ENSMUSG00000010358	Ifi35	-1.133070153	6.17E-29	ENSMUSG00000001918	Slc1a5	-0.533027915	9.88E-21
ENSMUSG00000024339	Tap2	-1.130790166	1.22E-22	ENSMUSG00000053560	Ier2	-0.532651729	2.01E-10
ENSMUSG00000078853	Igtp	-1.114359946	3.78E-20	ENSMUSG00000030785	Cox6a2	-0.528097766	2.68E-06
ENSMUSG00000061232	H2-K1	-1.111859931	9.89E-58	ENSMUSG00000040569	Slc26a7	-0.526673336	2.50E-06
ENSMUSG00000068245	Phf11d	-1.110359135	7.28E-22	ENSMUSG00000032591	Mst1	-0.526051496	1.37E-05
ENSMUSG00000034459	Ifit1	-1.102356162	2.10E-19	ENSMUSG00000034765	Dusp5	-0.523621742	1.95E-11
ENSMUSG00000028838	Extl1	-1.084286501	3.58E-24	ENSMUSG00000030717	Nupr1	-0.523004681	8.60E-08
ENSMUSG00000038539	Atf5	-1.060307455	1.75E-65	ENSMUSG00000031202	Rab39b	-0.520345651	5.85E-06
ENSMUSG00000078921	Tgtp2	-1.02205456	4.36E-17	ENSMUSG00000020812	1810032O08Rik	-0.518137428	1.10E-05
ENSMUSG00000028893	Sesn2	-1.021164465	2.61E-32	ENSMUSG00000079442	St6galnac4	-0.518116226	4.08E-10
ENSMUSG00000026946	Nmi	-1.002540294	8.71E-16	ENSMUSG00000058402	Zfp420	-0.515839498	9.99E-06
ENSMUSG00000035929	H2-Q4	-0.985299947	5.78E-21	ENSMUSG00000000275	Trim25	-0.513042293	1.65E-18
ENSMUSG00000079017	Ifi27l2a	-0.980916864	2.37E-15	ENSMUSG00000039997	Ifi203	-0.50994698	8.32E-10
ENSMUSG00000021186	Fbln5	-0.966474479	6.60E-15	ENSMUSG00000039646	Vasn	-0.509256476	1.88E-10
ENSMUSG00000040328	Olfr56	-0.94778222	3.48E-15	ENSMUSG00000097971	Gm26917	-0.505393546	2.02E-16
ENSMUSG00000079197	Psme2	-0.910405618	3.75E-40	ENSMUSG00000023947	Nfkbie	-0.500582635	2.80E-05
ENSMUSG00000027737	Slc7a11	-0.90358632	4.03E-24	ENSMUSG00000106734	RP24-328P2.5	-0.494310756	1.36E-05
ENSMUSG00000040618	Pck2	-0.88890164	6.40E-36	ENSMUSG00000028982	Slc25a33	-0.492376703	2.79E-07
ENSMUSG00000028542	Slc6a9	-0.876158045	2.21E-20	ENSMUSG00000036390	Gadd45a	-0.492249446	2.96E-05
ENSMUSG00000091705	H2-Q2	-0.875159717	7.10E-13	ENSMUSG00000041736	Tspo	-0.488420416	3.26E-15
ENSMUSG00000038418	Egr1	-0.873642464	2.59E-25	ENSMUSG00000052837	Junb	-0.486222164	3.26E-18
ENSMUSG00000002325	Irf9	-0.872219199	6.38E-14	ENSMUSG00000041313	Slc7a1	-0.484255738	1.79E-38
ENSMUSG00000032315	Cyp1a1	-0.870902277	2.55E-13	ENSMUSG00000035385	Ccl2	-0.480624279	9.83E-05
ENSMUSG00000020142	Slc1a4	-0.85060697	6.52E-22	ENSMUSG00000023045	Soat2	-0.478286138	1.80E-05
ENSMUSG00000022906	Parp9	-0.847818949	1.63E-20	ENSMUSG00000042659	Arrdc4	-0.475350083	1.95E-07
ENSMUSG00000086290	Snhg12	-0.83175718	5.86E-22	ENSMUSG00000016995	Matn4	-0.475077075	8.09E-14
ENSMUSG00000060802	B2m	-0.82329657	4.06E-163	ENSMUSG00000040613	Apobec1	-0.473519152	3.96E-05
ENSMUSG00000025408	Ddit3	-0.820755284	1.05E-14	ENSMUSG00000037465	Klf10	-0.47348131	7.09E-17
ENSMUSG00000047735	Samd9l	-0.813601853	5.85E-12	ENSMUSG00000015837	Sqstm1	-0.473155973	2.55E-45
ENSMUSG00000063268	Parp10	-0.7968143	1.62E-16	ENSMUSG00000074063	Osgin1	-0.472305601	5.10E-05
ENSMUSG00000041827	Oasl1	-0.790413126	9.76E-11	ENSMUSG00000029298	Gbp9	-0.470761267	3.66E-07
ENSMUSG00000021583	Erap1	-0.770028937	4.64E-20	ENSMUSG00000024587	Nars	-0.464190485	5.81E-47
ENSMUSG00000025140	Pycr1	-0.765033822	4.42E-11	ENSMUSG00000031897	Psmb10	-0.455947243	3.34E-06
ENSMUSG00000026896	Ifih1	-0.75917511	6.63E-11	ENSMUSG00000041028	Ghitm	-0.451357192	9.46E-24
ENSMUSG00000026601	Axdnd1	-0.751693172	1.07E-10	ENSMUSG00000026456	Cyb5r1	-0.450884348	5.64E-08
ENSMUSG00000060519	Tor3a	-0.747553172	2.19E-21	ENSMUSG00000029377	Ereg	-0.448251906	2.75E-06
ENSMUSG00000040264	Gbp2b	-0.744142123	7.04E-10	ENSMUSG00000042165	Gm9774	-0.447684049	4.36E-05
ENSMUSG00000002227	Mov10	-0.742445398	4.34E-19	ENSMUSG00000032841	Prr5l	-0.446607587	0.0003377
ENSMUSG00000031700	Gpt2	-0.73816388	1.82E-24	ENSMUSG00000060183	Cxcl11	-0.445924471	3.96E-07
ENSMUSG00000078920	Ifi47	-0.733725432	3.12E-10	ENSMUSG00000054520	Sh3bp2	-0.445395699	2.41E-09
ENSMUSG00000024066	Xdh	-0.718714938	1.96E-10	ENSMUSG00000038046	Rnmtl1	-0.442034467	1.70E-06
ENSMUSG00000027580	Helz2	-0.710939534	1.01E-11	ENSMUSG00000054855	Rnd1	-0.441608928	0.0002466

Gene		Log_2 Fold Change	pValue	Gene		Log_2 Fold Change	pValue
ENSMUSG00000015312	Gadd45b	-0.440513883	1.40E-07	ENSMUSG00000095687	Rnaset2a	-0.363588439	0.0034009
ENSMUSG00000037428	Vgf	-0.440133256	8.74E-05	ENSMUSG00000074754	Gm561	-0.363495143	0.0010328
ENSMUSG00000073418	C4b	-0.43967142	0.0001181	ENSMUSG00000079008	Gm14124	-0.363196871	0.0001083
ENSMUSG00000029009	Mthfr	-0.439198878	4.39E-06	ENSMUSG00000060002	Chpt1	-0.362344927	4.51E-05
ENSMUSG00000034437	Gm9761	-0.437812742	0.0004387	ENSMUSG00000021481	Zfp346	-0.36224828	0.0001425
ENSMUSG00000044948	Cfap43	-0.437424819	7.29E-09	ENSMUSG00000044576	Gareml	-0.361467013	0.0017918
ENSMUSG00000031355	Arhgap6	-0.435219497	5.94E-06	ENSMUSG00000006930	Hap1	-0.360790056	0.0001558
ENSMUSG00000029816	Gpnmb	-0.434784079	3.30E-50	ENSMUSG00000020256	Aldh1l2	-0.359269187	2.49E-26
ENSMUSG00000063765	Chadl	-0.434352508	2.43E-07	ENSMUSG00000036181	Hist1h1c	-0.356692769	0.0041802
ENSMUSG00000044037	Als2cl	-0.429509449	3.71E-05	ENSMUSG00000023809	Rps6ka2	-0.354972163	0.0007458
ENSMUSG00000068794	Col28a1	-0.428422968	8.31E-05	ENSMUSG00000039782	Cpeb2	-0.354605197	0.0012313
ENSMUSG00000034271	Jdp2	-0.427641944	2.41E-06	ENSMUSG00000053398	Phgdh	-0.354377614	1.25E-24
ENSMUSG00000021203	Otub2	-0.423009617	0.0006545	ENSMUSG00000074151	Nlrc5	-0.354193804	0.0044529
ENSMUSG00000044033	Ccdc141	-0.420084211	0.0002746	ENSMUSG00000006445	Epha2	-0.354121587	9.54E-07
ENSMUSG00000038292	Ccdc155	-0.418530005	2.43E-05	ENSMUSG00000050714	Zbtb26	-0.35366363	0.0009848
ENSMUSG00000056216	Cebpg	-0.417111472	1.66E-10	ENSMUSG00000003032	Klf4	-0.352393758	0.000138
ENSMUSG00000030966	Trim21	-0.416865707	0.000805	ENSMUSG00000032724	Abtb2	-0.351124694	2.39E-05
ENSMUSG00000101431	Gm7901	-0.415139131	1.70E-07	ENSMUSG00000033909	Usp36	-0.350772456	8.72E-07
ENSMUSG00000042106	Fam212a	-0.413250807	4.38E-06	ENSMUSG00000030747	Dgat2	-0.349868101	0.0044189
ENSMUSG00000024493	Lars	-0.411795779	3.15E-24	ENSMUSG00000025375	Aatk	-0.349786604	1.87E-05
ENSMUSG00000083716	Gm13436	-0.410042434	0.0002788	ENSMUSG00000061330	Gm11361	-0.347986162	1.46E-05
ENSMUSG00000027951	Adar	-0.409456561	1.27E-10	ENSMUSG00000039221	Rpl22l1	-0.347631572	5.84E-09
ENSMUSG00000020707	Rnf135	-0.407724409	0.0006479	ENSMUSG00000037126	Psd	-0.347455925	0.0015788
ENSMUSG00000021306	Gpr137b	-0.407133259	3.78E-06	ENSMUSG00000055148	Klf2	-0.3472119	0.0050951
ENSMUSG00000095115	Itpripl2	-0.405846065	1.14E-15	ENSMUSG00000106714	RP23-76J15.4	-0.346242786	4.33E-05
ENSMUSG00000036528	Ppfibp2	-0.40569207	5.05E-11	ENSMUSG00000056758	Hmga2	-0.344993692	1.77E-30
ENSMUSG00000098234	Snhg6	-0.405625485	4.49E-05	ENSMUSG00000083022	Rps15a-ps6	-0.344656961	0.004938
ENSMUSG00000037820	Tgm2	-0.404868792	2.41E-05	ENSMUSG00000020334	Slc22a4	-0.34420456	0.0014302
ENSMUSG00000066000	2610305D13Rik	-0.404818389	0.0001405	ENSMUSG00000031960	Aars	-0.344150314	6.49E-23
ENSMUSG00000046798	Cldn12	-0.404328056	3.73E-20	ENSMUSG00000029826	Zc3hav1	-0.34346576	1.10E-07
ENSMUSG00000022346	Myc	-0.40311586	1.96E-07	ENSMUSG00000030281	Il17rc	-0.343426655	5.61E-05
ENSMUSG00000106968	RP23-276J7.2	-0.40259702	0.0004906	ENSMUSG00000020876	Snx11	-0.343082145	7.60E-05
ENSMUSG00000078435	AU041133	-0.402307323	0.0012051	ENSMUSG00000006273	Atp6v1b2	-0.342892418	7.49E-13
ENSMUSG00000007812	Zfp655	-0.401626373	4.11E-09	ENSMUSG00000073411	H2-D1	-0.34194583	0.0029143
ENSMUSG00000078922	Tgtp1	-0.400244724	8.12E-06	ENSMUSG00000027995	Tlr2	-0.341799712	0.0010277
ENSMUSG00000062054	Iah1	-0.400093608	0.0003674	ENSMUSG00000105134	RP23-328P19.4	-0.340865987	0.0004017
ENSMUSG00000074578	1500012F01Rik	-0.398991535	2.12E-10	ENSMUSG00000097810	G730046D07Rik	-0.340848599	0.0038857
ENSMUSG00000107092	RP23-57A17.2	-0.398909993	0.0007193	ENSMUSG00000039461	Tcta	-0.340586373	0.0041419
ENSMUSG00000034708	Grn	-0.398350976	1.38E-17	ENSMUSG00000027368	Dusp2	-0.340240983	0.0039799
ENSMUSG00000039158	Akna	-0.396479799	0.0007748	ENSMUSG00000027603	Ggt7	-0.340204296	0.0003716
ENSMUSG00000029777	Gars	-0.395808956	4.33E-35	ENSMUSG00000058922	Gm10052	-0.340115661	1.78E-05
ENSMUSG00000055301	Adh7	-0.395637636	3.84E-08	ENSMUSG00000057895	Zfp105	-0.340086279	0.001539
ENSMUSG00000025007	Aldh18a1	-0.395569181	3.70E-15	ENSMUSG00000015766	Eps8	-0.339993668	2.81E-30
ENSMUSG00000060487	Samd5	-0.392970009	4.32E-05	ENSMUSG00000038534	Osbpl7	-0.33892532	0.0001582
ENSMUSG00000025403	Shmt2	-0.390327485	9.57E-31	ENSMUSG00000021326	Trim27	-0.338840127	5.82E-08
ENSMUSG00000097772	5430416N02Rik	-0.389603919	0.0005787	ENSMUSG00000056749	Nfil3	-0.338302389	0.0018152
ENSMUSG00000031530	Dusp4	-0.389128015	3.70E-06	ENSMUSG00000063652	Slc22a21	-0.338255299	0.00611
ENSMUSG00000091549	Gm6548	-0.389000288	0.0007812	ENSMUSG00000005951	Shpk	-0.33804748	0.0042023
ENSMUSG00000037434	Slc30a1	-0.387825637	6.47E-05	ENSMUSG00000015652	Steap1	-0.337645691	2.09E-06
ENSMUSG00000034259	Exosc4	-0.384475903	2.51E-06	ENSMUSG00000082082	Gm13230	-0.336058089	5.38E-06
ENSMUSG00000041936	Agrn	-0.384417695	2.40E-35	ENSMUSG00000062421	Arf2	-0.335384855	1.92E-07
ENSMUSG00000025854	Fam20c	-0.383967042	1.15E-08	ENSMUSG00000097960	A330074K22Rik	-0.335236044	0.0043743
ENSMUSG00000010755	Cars	-0.383820509	7.23E-16	ENSMUSG00000040435	Ppp1r15a	-0.334816285	0.0002189
ENSMUSG00000027122	Arl14ep	-0.383095229	3.99E-09	ENSMUSG00000031431	Tsc22d3	-0.334651136	0.0004785
ENSMUSG00000001436	Slc19a1	-0.382082474	1.36E-06	ENSMUSG00000020099	Unc5b	-0.334469723	1.88E-12
ENSMUSG00000049124	Gm8186	-0.381747529	0.0018733	ENSMUSG00000035064	Eef2k	-0.334410838	1.44E-06
ENSMUSG00000028599	Tnfrsf1b	-0.381161045	0.0001794	ENSMUSG00000057561	Eif1a	-0.334328756	2.60E-15
ENSMUSG00000048065	Cyb5r2	-0.380693695	0.0004097	ENSMUSG00000024327	Slc39a7	-0.333097136	0.0002548
ENSMUSG00000053581	Zfand2a	-0.379325525	1.10E-09	ENSMUSG00000048007	Timm8a1	-0.332835868	4.11E-05
ENSMUSG00000087590	Epb4.1l4aos	-0.37888342	0.0005648	ENSMUSG00000002393	Nr2f6	-0.332343578	0.0002486
ENSMUSG00000058638	Zfp110	-0.377617995	3.62E-09	ENSMUSG00000107215	RP23-253G12.9	-0.332059231	0.0060316
ENSMUSG00000050796	B3galt6	-0.37672922	0.0002077	ENSMUSG00000000530	Acvrl1	-0.331300969	1.49E-07
ENSMUSG00000037411	Serpine1	-0.374734727	6.68E-31	ENSMUSG00000079225	Gm9531	-0.330842362	0.0004383
ENSMUSG00000032515	Csrnp1	-0.373073635	0.0001091	ENSMUSG00000068739	Sars	-0.330744843	7.28E-22
ENSMUSG00000085385	Snhg17	-0.373031127	5.97E-06	ENSMUSG00000097195	Snhg5	-0.330741103	5.21E-07
ENSMUSG00000042997	Nhlrc3	-0.372993921	0.00025	ENSMUSG00000046269	Usp27x	-0.328127718	0.003553
ENSMUSG00000026630	Batf3	-0.372830372	0.0027568	ENSMUSG00000084319	Tpt1-ps3	-0.327611687	4.61E-05
ENSMUSG00000026956	Uap1l1	-0.371664061	1.28E-07	ENSMUSG00000034957	Cebpa	-0.327596473	0.0023606
ENSMUSG00000030268	Bcat1	-0.370588692	2.20E-13	ENSMUSG00000010601	Apol7a	-0.327280232	0.00416
ENSMUSG00000078606	Gm4070	-0.370406252	0.0015231	ENSMUSG00000108218	Olfr1372-ps1	-0.327228415	0.0074648
ENSMUSG00000056501	Cebpb	-0.369792355	0.0003086	ENSMUSG00000029019	Nppb	-0.32712305	0.0043341
ENSMUSG00000032372	Plscr2	-0.369524743	8.75E-27	ENSMUSG00000012519	Mlkl	-0.326941627	0.0001295
ENSMUSG00000022548	Apod	-0.36847993	2.03E-36	ENSMUSG00000026942	Traf2	-0.326615887	0.0006387
ENSMUSG00000013415	Igf2bp1	-0.368418973	0.0030887	ENSMUSG00000000184	Ccnd2	-0.326560384	2.35E-11
ENSMUSG00000075609	Gm7935	-0.367206619	0.0020658	ENSMUSG00000046909	Tefm	-0.326398581	0.001763
ENSMUSG00000047603	Zfp235	-0.366743471	0.0015239	ENSMUSG00000050212	Eva1b	-0.326253654	0.0058359
ENSMUSG00000028059	Arhgef2	-0.366212383	3.25E-20	ENSMUSG00000053801	Grwd1	-0.325194064	1.67E-09
ENSMUSG00000053038	Gm6180	-0.365693371	0.0028947	ENSMUSG00000050621	Rps27rt	-0.324025896	0.0049963
ENSMUSG00000027722	Spata5	-0.365038023	3.68E-07	ENSMUSG00000061286	Exosc5	-0.323185258	3.80E-05
ENSMUSG00000052861	Dnah6	-0.36442046	0.0031376	ENSMUSG00000032281	Acsbg1	-0.322821862	1.40E-05
ENSMUSG00000024079	Eif2ak2	-0.364239019	7.75E-09	ENSMUSG00000078349	AW011738	-0.320762248	0.0062624

Gene		Log_2 Fold Change	pValue	Gene		Log_2 Fold Change	pValue
ENSMUSG00000000489	Pdgfb	-0.320327309	0.0001937	ENSMUSG00000027435	Cd93	-0.289058086	0.01711
ENSMUSG00000068240	Gm11808	-0.319763686	0.0024509	ENSMUSG00000072621	Slfn10-ps	-0.288728175	0.0177297
ENSMUSG00000022554	Hgh1	-0.317025261	1.30E-05	ENSMUSG00000038335	Tsr1	-0.288496614	1.82E-10
ENSMUSG00000034430	Zxdc	-0.316963463	9.40E-05	ENSMUSG00000087141	Plcxd2	-0.288430067	0.0087461
ENSMUSG00000078851	Hist3h2a	-0.316863476	0.0104914	ENSMUSG00000079491	H2-T10	-0.288302758	0.0168268
ENSMUSG00000046027	Stard5	-0.316830447	1.54E-05	ENSMUSG00000021266	Wars	-0.287899279	4.17E-12
ENSMUSG00000048755	Mcat	-0.315898769	0.0015934	ENSMUSG00000020121	Srgap1	-0.287737964	0.0089758
ENSMUSG00000098923	Tmem185b	-0.315631701	0.0048581	ENSMUSG00000106549	RP23-332O18.2	-0.286771174	0.0059661
ENSMUSG00000029314	Agpat9	-0.314959076	0.0107317	ENSMUSG00000033793	Atp6v1h	-0.286530452	9.92E-07
ENSMUSG00000022043	Trim35	-0.31482745	1.78E-06	ENSMUSG00000019558	Slc6a8	-0.286007531	1.18E-15
ENSMUSG00000038517	Tbkbp1	-0.313674102	0.0004956	ENSMUSG00000021226	Acot2	-0.285848776	0.0217776
ENSMUSG00000043289	Mei4	-0.313397692	0.0104476	ENSMUSG00000103009	Gm4430	-0.285717443	0.0099449
ENSMUSG00000097039	Pvt1	-0.313115152	0.0038354	ENSMUSG00000051675	Trim32	-0.285589083	0.0021006
ENSMUSG00000073002	Vamp5	-0.312947875	0.0002147	ENSMUSG00000032513	Gorasp1	-0.285441699	0.0033961
ENSMUSG00000020941	Map3k14	-0.312451806	0.0016859	ENSMUSG00000030057	Cnbp	-0.285252913	1.79E-24
ENSMUSG00000031916	Cog8	-0.312283213	0.0012736	ENSMUSG00000046516	Cox17	-0.284964024	0.0011725
ENSMUSG00000030905	Crym	-0.312001756	1.59E-06	ENSMUSG00000047767	Atg16l2	-0.284893132	0.0116728
ENSMUSG00000054203	Ifi205	-0.311983463	0.0026293	ENSMUSG00000022615	Tymp	-0.284780024	0.0223121
ENSMUSG00000038037	Socs1	-0.311468406	0.0020679	ENSMUSG00000016534	Lamp2	-0.284759944	3.12E-12
ENSMUSG00000038550	Ciart	-0.311431935	0.0089137	ENSMUSG00000022698	Naa50	-0.284740985	7.06E-17
ENSMUSG00000033538	Casp4	-0.311008564	0.0105016	ENSMUSG00000087396	4933407K13Rik	-0.284728207	0.0223438
ENSMUSG00000034667	Xpot	-0.309947682	3.77E-14	ENSMUSG00000031976	Urb2	-0.284380675	5.10E-06
ENSMUSG00000042419	Nfkbil1	-0.309500418	0.0025876	ENSMUSG00000026820	Ptges2	-0.283775424	0.0014704
ENSMUSG00000018405	Mrm1	-0.309064849	0.0059406	ENSMUSG00000001053	N4bp3	-0.283736084	0.0132789
ENSMUSG00000024883	Rin1	-0.308729667	1.05E-11	ENSMUSG00000014177	Tvp23b	-0.283229595	0.0003387
ENSMUSG00000020715	Ern1	-0.308342509	0.0003932	ENSMUSG00000030782	Tgfb1i1	-0.283107476	0.0046302
ENSMUSG00000028811	Yars	-0.308179603	4.72E-09	ENSMUSG00000045886	Gm9803	-0.282203029	0.0109237
ENSMUSG00000000791	Il12rb1	-0.308005821	0.0106966	ENSMUSG00000008435	Rdh13	-0.282042226	0.0004855
ENSMUSG00000030347	D6Wsu163e	-0.30791469	7.36E-05	ENSMUSG00000101188	Eif4a-ps4	-0.282021353	4.99E-09
ENSMUSG00000068335	Dok1	-0.307727861	2.15E-06	ENSMUSG00000042549	Map2k3os	-0.281726566	0.0085933
ENSMUSG00000006463	Zdhhc24	-0.307640475	0.0032814	ENSMUSG00000021458	2010111I01Rik	-0.2815697	0.0001268
ENSMUSG00000090440	Gm9732	-0.30762307	0.0116752	ENSMUSG00000020629	Adi1	-0.281083271	1.12E-05
ENSMUSG00000089682	Bcl2l2	-0.307430896	0.0011425	ENSMUSG00000021770	Samd8	-0.28104422	0.0001542
ENSMUSG00000029173	Sepsecs	-0.305545446	0.0004015	ENSMUSG00000000078	Klf6	-0.280710215	2.26E-08
ENSMUSG00000079009	Gm14139	-0.305302716	0.0017249	ENSMUSG00000037474	Dtl	-0.280600179	2.56E-08
ENSMUSG00000053338	Tarm1	-0.305274777	0.014301	ENSMUSG00000026857	Ntmt1	-0.280533604	0.0016339
ENSMUSG00000099875	Gm15453	-0.305199688	0.0094736	ENSMUSG00000057101	Zfp180	-0.280515928	1.52E-06
ENSMUSG00000030042	Pole4	-0.30489992	2.92E-08	ENSMUSG00000012640	Zfp715	-0.280485135	0.0041797
ENSMUSG00000037104	Socs5	-0.304682992	1.92E-16	ENSMUSG00000040883	Tmem205	-0.2801093	0.0225619
ENSMUSG00000022792	Yars2	-0.302456038	3.40E-06	ENSMUSG00000032834	Pwp2	-0.27964085	3.41E-08
ENSMUSG00000028850	Gpatch3	-0.302210825	0.0137679	ENSMUSG00000045917	6330416G13Rik	-0.27946082	0.0083708
ENSMUSG00000033467	Crlf2	-0.3018929	0.0126578	ENSMUSG00000058809	Hspd1-ps3	-0.278981195	0.0004527
ENSMUSG00000021759	Ppap2a	-0.301791777	0.0002006	ENSMUSG00000028744	Pqlc2	-0.278718701	0.0252818
ENSMUSG00000049969	Plekhf2	-0.301702661	0.0018478	ENSMUSG00000043822	Adamtsl5	-0.278544971	0.0131718
ENSMUSG00000074876	Spata5l1	-0.301020224	0.011588	ENSMUSG00000051444	Bbs12	-0.278537123	0.0037189
ENSMUSG00000082809	Gm14150	-0.300336421	0.0117161	ENSMUSG00000027955	Fam198b	-0.278346023	0.0111814
ENSMUSG00000033728	Lrrc14	-0.29891295	4.97E-05	ENSMUSG00000004446	Bid	-0.278257171	0.0010371
ENSMUSG00000032952	Ap4b1	-0.298879656	0.016456	ENSMUSG00000094614	Gm21769	-0.278239597	0.0216555
ENSMUSG00000040521	Tsfm	-0.298723554	8.59E-06	ENSMUSG00000031425	Plp1	-0.278210455	1.26E-09
ENSMUSG00000044716	Dok7	-0.298717062	0.0161546	ENSMUSG00000022299	Slc25a32	-0.278166203	0.0001519
ENSMUSG00000031691	Tnpo2	-0.29822189	2.05E-08	ENSMUSG00000041623	D11Wsu47e	-0.278092524	0.0025158
ENSMUSG00000082319	Gm8822	-0.297807922	0.0080606	ENSMUSG00000048807	Slc35e4	-0.277544745	4.29E-06
ENSMUSG00000052751	Repin1	-0.297685835	1.47E-05	ENSMUSG00000035969	Rusc2	-0.27743052	2.48E-05
ENSMUSG00000035517	Tdrd7	-0.297424014	7.33E-05	ENSMUSG00000050721	Plekho2	-0.277425638	0.0004236
ENSMUSG00000047098	Rnf31	-0.297402655	0.0020754	ENSMUSG00000045822	Zswim3	-0.277296321	0.0158056
ENSMUSG00000006301	Tmbim1	-0.29715196	1.14E-08	ENSMUSG00000023883	Phf10	-0.277019777	7.28E-07
ENSMUSG00000036368	Rmdn2	-0.296844727	0.0143052	ENSMUSG00000068206	Pick1	-0.276878838	0.0001262
ENSMUSG00000047143	Dmrta2	-0.296785586	0.0140792	ENSMUSG00000015776	Med22	-0.276248672	1.17E-05
ENSMUSG00000025225	Nfkb2	-0.296475662	5.78E-07	ENSMUSG00000089728	Clec2f	-0.275202987	0.02696
ENSMUSG00000078498	Gm13151	-0.29565548	0.0156778	ENSMUSG00000067203	H2-K2	-0.274481246	0.0073179
ENSMUSG00000036534	Slc38a7	-0.295071942	0.0064557	ENSMUSG00000002343	Armc6	-0.274232757	0.0021577
ENSMUSG00000037868	Egr2	-0.294453541	0.0178023	ENSMUSG00000002108	Nr1h3	-0.274055496	0.0045769
ENSMUSG00000021890	Eaf1	-0.294359642	9.27E-11	ENSMUSG00000091086	Gm5428	-0.274048428	0.0275417
ENSMUSG00000028345	Tex10	-0.293578979	8.39E-09	ENSMUSG00000027346	Gpcpd1	-0.273967053	0.0041368
ENSMUSG00000095588	Gm12350	-0.293162795	0.0071795	ENSMUSG00000028540	Dph2	-0.273955677	0.0005072
ENSMUSG00000091803	Cox16	-0.293054334	0.0080868	ENSMUSG00000069014	Gm5641	-0.273843259	0.0117905
ENSMUSG00000045455	Gm9797	-0.292490534	0.0187826	ENSMUSG00000017307	Acot8	-0.273206548	0.0270493
ENSMUSG00000045140	Pigw	-0.29234715	0.0062889	ENSMUSG00000022365	Derl1	-0.273178328	2.11E-08
ENSMUSG00000035530	Eif1	-0.292321493	4.36E-24	ENSMUSG00000054793	Cadm4	-0.273004586	2.65E-19
ENSMUSG00000081999	Gm13461	-0.291274932	0.0190237	ENSMUSG00000034854	Mfsd12	-0.272918771	0.0003098
ENSMUSG00000040354	Mars	-0.290561469	9.98E-13	ENSMUSG00000035397	Klf16	-0.272438734	0.0013993
ENSMUSG00000049957	Ccdc137	-0.290429174	3.32E-06	ENSMUSG00000003526	Prodh	-0.272426928	0.0195574
ENSMUSG00000021079	Timm9	-0.290326207	0.0001937	ENSMUSG00000094497	Gm8210	-0.272280521	0.0004507
ENSMUSG00000071722	Spin4	-0.290204017	0.0196123	ENSMUSG00000030029	Lrig1	-0.272247768	3.40E-12
ENSMUSG00000091811	Inafm1	-0.290179577	0.0164887	ENSMUSG00000050335	Lgals3	-0.272094359	2.08E-27
ENSMUSG00000058838	Rps27a-ps2	-0.289861674	0.0055684	ENSMUSG00000038888	Ctu1	-0.271765558	0.0124256
ENSMUSG00000003948	Mmd	-0.289769508	0.0024229	ENSMUSG00000045027	Prss22	-0.271512799	0.0288003
ENSMUSG00000027845	Dclre1b	-0.289639935	0.0025355	ENSMUSG00000057411	Fam173a	-0.2712561	0.0039446
ENSMUSG00000009292	Trpm2	-0.28962244	0.0198584	ENSMUSG00000066362	Rps13-ps1	-0.271152591	0.0211067
ENSMUSG00000018932	Map2k3	-0.289397796	4.51E-10	ENSMUSG00000079507	H2-Q1	-0.271090222	0.021646
ENSMUSG00000069972	Rps13-ps2	-0.289224894	0.01779	ENSMUSG00000021385	Ippk	-0.270744571	0.0048576

Gene		Log_2 Fold Change	pValue	Gene		Log_2 Fold Change	pValue
ENSMUSG00000042854	Trp53rkb	-0.270556772	0.0291882	ENSMUSG00000023000	Dhh	-0.25455891	0.0129126
ENSMUSG00000036067	Slc2a6	-0.270485156	0.0277036	ENSMUSG00000042178	Armc5	-0.254472512	0.0055606
ENSMUSG00000080848	Gm9385	-0.270354027	0.0140941	ENSMUSG00000001751	Naglu	-0.254282794	0.0094678
ENSMUSG00000022241	Tars	-0.270315893	5.50E-14	ENSMUSG00000024640	Psat1	-0.254102996	7.71E-19
ENSMUSG00000024593	Megf10	-0.27028186	8.46E-05	ENSMUSG00000079260	Tmppe	-0.254052551	0.004513
ENSMUSG00000028708	Mknk1	-0.270212604	0.0058709	ENSMUSG00000026640	Plxna2	-0.253906887	0.002278
ENSMUSG00000020790	Ankfy1	-0.269859012	3.15E-10	ENSMUSG00000024785	Rcl1	-0.253573841	4.57E-05
ENSMUSG00000036106	Prr5	-0.269801161	0.0081893	ENSMUSG00000065999	Gm13154	-0.253564449	0.0206044
ENSMUSG00000007872	Id3	-0.269732181	1.46E-07	ENSMUSG00000032788	Pdxk	-0.253481499	2.85E-07
ENSMUSG00000024276	Zfp397	-0.269617403	0.0003936	ENSMUSG00000083626	Gm4459	-0.253320415	0.0362535
ENSMUSG00000046731	Kctd11	-0.269410117	0.0132214	ENSMUSG00000029179	Zcchc4	-0.253018768	0.0013594
ENSMUSG00000002289	Angptl4	-0.269335761	8.14E-06	ENSMUSG00000024427	Spry4	-0.252881863	0.0241547
ENSMUSG00000055184	Fam72a	-0.269161688	0.0119919	ENSMUSG00000022507	1810013L24Rik	-0.252774778	5.95E-05
ENSMUSG00000041506	Rrp9	-0.269072606	1.96E-05	ENSMUSG00000066892	Fbxl12	-0.252429878	0.0356353
ENSMUSG00000027472	Pdrg1	-0.268891068	6.13E-06	ENSMUSG00000033918	Parl	-0.252330676	8.40E-06
ENSMUSG00000082361	Btc	-0.268851249	0.0304965	ENSMUSG00000078789	Dph1	-0.252330564	0.0046655
ENSMUSG00000001750	Tcirg1	-0.268670426	0.0002976	ENSMUSG00000043131	Mob1a	-0.252194107	8.60E-12
ENSMUSG00000034998	Foxn2	-0.268529066	0.0001657	ENSMUSG00000087259	2610035D17Rik	-0.251853573	0.0223943
ENSMUSG00000027395	Polr1b	-0.268428736	3.70E-06	ENSMUSG00000034379	Wdr5b	-0.251464323	0.0332211
ENSMUSG00000043801	Oaz1-ps	-0.268421015	0.0309856	ENSMUSG00000048222	Mfap1b	-0.251418418	0.0345869
ENSMUSG00000049323	Smcr8	-0.26829666	7.25E-07	ENSMUSG00000085101	Platr16	-0.251401924	0.0374632
ENSMUSG00000039774	Galnt12	-0.267608745	0.0306808	ENSMUSG00000024610	Cd74	-0.251049392	0.0032886
ENSMUSG00000001281	Itgb7	-0.267410877	0.0295784	ENSMUSG00000054716	Zfp771	-0.250923045	0.0100561
ENSMUSG00000062432	Cyp26c1	-0.267241706	0.0056608	ENSMUSG00000103965	Gm30173	-0.250601122	0.0322631
ENSMUSG00000027800	Tm4sf1	-0.267084281	3.21E-22	ENSMUSG00000066640	Fbxl18	-0.250579977	0.0005716
ENSMUSG00000032911	Cspg4	-0.267075342	4.31E-09	ENSMUSG00000041571	Sepw1	-0.250564085	6.62E-06
ENSMUSG00000026475	Rgs16	-0.26703365	1.74E-21	ENSMUSG00000027495	Fam210b	-0.250462657	0.0016942
ENSMUSG00000038299	Wdr36	-0.266859519	2.58E-09	ENSMUSG00000040658	Dnph1	-0.250179127	0.0007856
ENSMUSG00000033386	Frrs1	-0.265984559	3.34E-05	ENSMUSG00000001166	Oas1c	-0.250090117	0.0009107
ENSMUSG00000036867	Smad6	-0.264564673	0.0221858	ENSMUSG00000032044	Rpusd4	-0.249583425	0.0027707
ENSMUSG00000042410	Agps	-0.264523306	1.51E-07	ENSMUSG00000029028	Lrrc47	-0.249256125	7.38E-05
ENSMUSG00000050846	Zfp623	-0.264322123	0.0067085	ENSMUSG00000022772	Senp5	-0.249179344	2.73E-05
ENSMUSG00000081272	Gm13509	-0.264036796	0.0077135	ENSMUSG00000083899	Gm12346	-0.249047666	0.0112665
ENSMUSG00000062382	Gm10116	-0.263746647	0.0003239	ENSMUSG00000026303	Mlph	-0.248500722	0.0088153
ENSMUSG00000020397	Med7	-0.263179687	0.0085973	ENSMUSG00000044763	Trmt10c	-0.248244201	0.0027204
ENSMUSG00000045374	Wdr81	-0.263135364	0.0022382	ENSMUSG00000035505	Cox18	-0.247815687	0.0066534
ENSMUSG00000037509	Arhgef4	-0.262983601	0.0297249	ENSMUSG00000046441	Cmtr2	-0.247757764	0.0060809
ENSMUSG00000034898	Filip1	-0.262894173	0.0190598	ENSMUSG00000030621	Me3	-0.247488534	0.031174
ENSMUSG00000066724	Gm10175	-0.262866928	0.0222463	ENSMUSG00000021311	Mtr	-0.247478477	0.0036551
ENSMUSG00000085783	Gm9816	-0.262646996	0.0346081	ENSMUSG00000039384	Dusp10	-0.247458142	0.0125059
ENSMUSG00000043079	Synpo	-0.262519025	5.34E-07	ENSMUSG00000021532	Fastkd3	-0.247391214	0.0164837
ENSMUSG00000034842	Art3	-0.262470748	0.018757	ENSMUSG00000026283	Ing5	-0.247184118	0.0005587
ENSMUSG00000075227	Znhit2	-0.262384372	0.0027212	ENSMUSG00000032531	Amotl2	-0.247005546	1.14E-08
ENSMUSG00000000555	Itga5	-0.260537373	1.07E-08	ENSMUSG00000079144	A130010J15Rik	-0.24687357	0.0403859
ENSMUSG00000035735	Dagla	-0.260534864	5.62E-07	ENSMUSG00000036061	Smug1	-0.246436841	0.0144147
ENSMUSG00000031770	Herpud1	-0.260517787	0.0010562	ENSMUSG00000029500	Pgam5	-0.246096875	0.0017134
ENSMUSG00000005413	Hmox1	-0.260482621	0.0015706	ENSMUSG00000000278	Scpep1	-0.245960865	1.75E-06
ENSMUSG00000079056	Kcnip3	-0.260158837	0.0255784	ENSMUSG00000101940	Akp-ps1	-0.245342654	0.0387467
ENSMUSG00000014599	Csf1	-0.25977207	3.42E-09	ENSMUSG00000029596	Sdsl	-0.245253142	0.0331342
ENSMUSG00000005045	Chd5	-0.259646781	0.0342733	ENSMUSG00000020788	Atp2a3	-0.245198616	0.0011127
ENSMUSG00000070709	1700049G17Rik	-0.259447146	0.0354948	ENSMUSG00000042719	Naa25	-0.244815118	1.65E-08
ENSMUSG00000022178	Ajuba	-0.259248655	0.0004306	ENSMUSG00000021025	Nfkbia	-0.244361342	0.001632
ENSMUSG00000061979	Wbscr16	-0.258972911	0.0003483	ENSMUSG00000070493	Chchd2	-0.244306838	5.17E-09
ENSMUSG00000002274	Metrn	-0.258792021	0.0003852	ENSMUSG00000004221	Ikbkg	-0.24415744	0.0001842
ENSMUSG00000027613	Eif6	-0.258754724	5.68E-08	ENSMUSG00000059588	Calcrl	-0.244138657	0.0458232
ENSMUSG00000071256	Zfp213	-0.258567452	0.037979	ENSMUSG00000058173	Smco4	-0.244118603	0.0256946
ENSMUSG00000027534	Snx16	-0.258345934	0.0030649	ENSMUSG00000067787	Blcap	-0.243952357	0.0035552
ENSMUSG00000040165	Cd209c	-0.258120692	0.0142107	ENSMUSG00000032122	Slc37a2	-0.24393159	0.0261036
ENSMUSG00000075602	Ly6a	-0.25810421	0.0031383	ENSMUSG00000025602	Zfp202	-0.243519723	0.0234611
ENSMUSG00000032508	Myd88	-0.257673858	0.0055791	ENSMUSG00000050891	Tatdn1	-0.243179888	0.0315735
ENSMUSG00000021282	Eif5	-0.257653626	2.41E-13	ENSMUSG00000045316	Fahd1	-0.242968528	0.0305006
ENSMUSG00000103041	Gm37305	-0.257023146	0.0391803	ENSMUSG00000048351	Coa7	-0.242932912	0.0094909
ENSMUSG00000030657	Xylt1	-0.256904513	0.022578	ENSMUSG00000046994	Mars2	-0.242928781	0.0014649
ENSMUSG00000050312	Nsun3	-0.256880321	0.0138229	ENSMUSG00000060548	Tnfrsf19	-0.242868345	0.0292149
ENSMUSG00000019122	Ccl9	-0.256753622	0.0247949	ENSMUSG00000026181	Ppm1f	-0.242667018	2.07E-10
ENSMUSG00000020605	Hs1bp3	-0.256736904	0.0018013	ENSMUSG00000047368	Abhd17b	-0.242516982	0.0015218
ENSMUSG00000031785	Adgrg1	-0.256656799	5.73E-06	ENSMUSG00000039512	Uhrf1bp1	-0.242374248	1.67E-05
ENSMUSG00000074811	Hps6	-0.256654738	0.0040319	ENSMUSG00000031387	Renbp	-0.242168861	0.0016139
ENSMUSG00000056300	Gm13247	-0.256594768	0.03587	ENSMUSG00000030428	Ttyh1	-0.241873589	0.0149906
ENSMUSG00000021149	Gtpbp4	-0.256541539	1.94E-07	ENSMUSG00000039182	AW209491	-0.241359831	0.0111224
ENSMUSG00000022515	Anks3	-0.256398934	0.0092088	ENSMUSG00000105504	Gbp5	-0.24127343	0.0213179
ENSMUSG00000080776	Gm12174	-0.256214357	0.0313105	ENSMUSG00000036432	Siah2	-0.24125115	0.0108212
ENSMUSG00000026177	Slc11a1	-0.256180902	0.0032596	ENSMUSG00000067038	Rps12-ps3	-0.241068459	0.0052267
ENSMUSG00000048486	Fitm2	-0.256027146	0.0016038	ENSMUSG00000029560	Snx8	-0.240885804	7.87E-05
ENSMUSG00000024019	Cmtr1	-0.255879702	0.007598	ENSMUSG00000018143	Mafk	-0.24064242	0.0005283
ENSMUSG00000038213	Tapbpl	-0.25572967	0.0229592	ENSMUSG00000025138	Sirt7	-0.240608681	0.0201794
ENSMUSG00000020092	Pald1	-0.255369538	0.0012207	ENSMUSG00000098702	1500015A07Rik	-0.240599749	0.0493515
ENSMUSG00000029060	Mib2	-0.2552655	0.0234322	ENSMUSG00000039826	Trub2	-0.240017615	0.0006598
ENSMUSG00000045896	Paip2b	-0.255106286	1.72E-06	ENSMUSG00000046223	Plaur	-0.239744484	1.31E-09
ENSMUSG00000051671	Coa6	-0.255030914	0.0184157	ENSMUSG00000031490	Eif4ebp1	-0.239673763	2.03E-07
ENSMUSG00000028857	Tmem222	-0.254944813	0.0023716	ENSMUSG00000090700	Cyp4f40	-0.239369741	0.0004609

Gene		Log_2 Fold Change	pValue	Gene		Log_2 Fold Change	pValue
ENSMUSG00000107383	RP24-246N21.1	-0.239262887	1.59E-06	ENSMUSG00000039853	Trim14	-0.228050946	0.0465197
ENSMUSG00000040652	Oaz2	-0.239126088	0.000117	ENSMUSG00000070953	Rabepk	-0.227756078	0.0181981
ENSMUSG00000070034	Sp110	-0.239009303	0.0280131	ENSMUSG00000025971	9430016H08Rik	-0.227452263	0.0262403
ENSMUSG00000071456	1110002L01Rik	-0.238988976	0.0347539	ENSMUSG00000027628	Aar2	-0.227291006	0.0011563
ENSMUSG00000041645	Ddx24	-0.238835388	5.29E-08	ENSMUSG00000020691	Mettl2	-0.227188702	0.0047532
ENSMUSG00000003949	Hlf	-0.238528057	0.0468702	ENSMUSG00000054364	Rhob	-0.226654362	1.04E-06
ENSMUSG00000094441	Zfp955a	-0.238475355	0.0325182	ENSMUSG00000025384	Faap100	-0.226051518	0.0204459
ENSMUSG00000008136	Fhl2	-0.238341298	0.0383102	ENSMUSG00000034159	2310007B03Rik	-0.226036883	0.0278664
ENSMUSG00000066800	Rnasel	-0.238276518	0.0479737	ENSMUSG00000053080	2700081O15Rik	-0.22582906	0.0027975
ENSMUSG00000037190	Cyb561d2	-0.238210294	0.0189735	ENSMUSG00000031875	Cmtm3	-0.22549842	0.0020103
ENSMUSG00000021908	Gm6768	-0.237960449	0.0487437	ENSMUSG00000063953	Amd2	-0.225307077	0.0261483
ENSMUSG00000024013	Fgd2	-0.237856261	0.0456719	ENSMUSG00000052253	Zfp622	-0.225205165	0.0011942
ENSMUSG00000096910	Zfp955b	-0.237571477	0.0370897	ENSMUSG00000001588	Acap1	-0.22484507	8.31E-05
ENSMUSG00000022842	Ece2	-0.237235986	0.0006926	ENSMUSG00000074182	Znhit6	-0.224007041	0.004657
ENSMUSG00000026202	Tuba4a	-0.237077392	0.0074668	ENSMUSG00000062661	Ncs1	-0.224007013	0.0111657
ENSMUSG00000031751	Amfr	-0.236999091	2.16E-06	ENSMUSG00000072940	Gm10443	-0.223950472	0.0468054
ENSMUSG00000032714	Syde1	-0.236837504	0.000119	ENSMUSG00000042406	Atf4	-0.223886844	7.74E-12
ENSMUSG00000024164	C3	-0.236820505	0.0303929	ENSMUSG00000039463	Slc9a8	-0.223868457	0.0017707
ENSMUSG00000054072	Iigp1	-0.236487339	0.000643	ENSMUSG00000067825	Pex26	-0.223857766	0.0309749
ENSMUSG00000089824	Rbm12	-0.236478318	0.0101902	ENSMUSG00000028980	H6pd	-0.223842199	0.0105469
ENSMUSG00000039754	Alkbh4	-0.236335602	0.0293832	ENSMUSG00000069020	Urm1	-0.223629766	0.0139566
ENSMUSG00000084384	Gm12251	-0.236122346	0.0242563	ENSMUSG00000031711	Zfp330	-0.222888045	0.0032359
ENSMUSG00000021280	Exoc3l4	-0.236043466	0.0486043	ENSMUSG00000038174	Fam126b	-0.222515608	0.0326537
ENSMUSG00000015143	Actn1	-0.235890675	7.24E-07	ENSMUSG00000033983	Coil	-0.222237547	0.0075617
ENSMUSG00000026142	Rhbdd1	-0.235723111	0.0011625	ENSMUSG00000041438	Cirh1a	-0.222158115	9.51E-05
ENSMUSG00000039483	Asb6	-0.235165716	0.0022689	ENSMUSG00000032180	Tmed1	-0.222053969	0.0004281
ENSMUSG00000020544	Cox11	-0.234882931	0.0481576	ENSMUSG00000037594	BC022687	-0.221970317	0.0407613
ENSMUSG00000038172	Ttc39b	-0.234782463	0.0006551	ENSMUSG00000066235	Pomgnt2	-0.221792766	0.0153267
ENSMUSG00000013076	Amotl1	-0.234459936	1.29E-07	ENSMUSG00000027170	Eif3m	-0.221529294	1.28E-06
ENSMUSG00000033186	Mzt1	-0.234406313	0.0288488	ENSMUSG00000104960	Snhg8	-0.22147711	0.0042854
ENSMUSG00000020781	Tsen54	-0.234256146	0.0021919	ENSMUSG00000000561	Wdr77	-0.221338179	4.05E-05
ENSMUSG00000039474	Wfs1	-0.233914628	0.0070518	ENSMUSG00000030880	Polr3e	-0.221293879	0.0004635
ENSMUSG00000054342	Kcnn4	-0.233765207	3.48E-08	ENSMUSG00000036908	Unc93b1	-0.221213569	0.0414308
ENSMUSG00000062168	Ppef1	-0.233683124	0.0296354	ENSMUSG00000043629	1700019D03Rik	-0.220813617	0.0198629
ENSMUSG00000035378	Shq1	-0.233624188	0.0181253	ENSMUSG00000020692	Nle1	-0.220726663	0.001578
ENSMUSG00000025512	Chid1	-0.233603539	0.001275	ENSMUSG00000101892	9130401M01Rik	-0.220587589	0.0191005
ENSMUSG00000025465	Echs1	-0.233328035	0.0008328	ENSMUSG00000056209	Npm3	-0.220222382	5.03E-06
ENSMUSG00000018169	Mfng	-0.233260975	0.0431977	ENSMUSG00000043453	Magea10	-0.220083472	0.0090545
ENSMUSG00000023755	Rhebl1	-0.233098548	0.0497865	ENSMUSG00000026694	Mettl13	-0.219953198	0.0022893
ENSMUSG00000034429	Zfp707	-0.232995531	0.0370926	ENSMUSG00000028917	Plekhm2	-0.219829614	0.0077357
ENSMUSG00000066191	Anks6	-0.232788517	0.0494625	ENSMUSG00000021094	Dhrs7	-0.219682087	0.0493455
ENSMUSG00000046691	Chtf8	-0.232530536	2.49E-07	ENSMUSG00000031352	Hccs	-0.219540832	0.0010997
ENSMUSG00000027808	Serp1	-0.232523717	3.27E-07	ENSMUSG00000001569	Nom1	-0.219284125	0.0001843
ENSMUSG00000046229	Scand1	-0.232474512	0.0229052	ENSMUSG00000030287	Itpr2	-0.219136468	0.0486582
ENSMUSG00000050271	D8Ertd82e	-0.232437871	0.0111259	ENSMUSG00000029551	Psmg3	-0.219071251	0.0044852
ENSMUSG00000000058	Cav2	-0.232418092	0.0007175	ENSMUSG00000040464	Gtpbp10	-0.218977018	0.0024576
ENSMUSG00000107853	RP24-409C18.1	-0.232395717	0.0404559	ENSMUSG00000022108	Itm2b	-0.218938624	0.0011882
ENSMUSG00000033722	BC034090	-0.231945961	0.004569	ENSMUSG00000030942	Thumpd1	-0.218575421	5.38E-05
ENSMUSG00000059423	Zfp933	-0.231805053	0.0361883	ENSMUSG00000026171	Rnf25	-0.218561476	0.0104956
ENSMUSG00000029544	Cabp1	-0.231704697	0.0074997	ENSMUSG00000038150	Ormdl3	-0.218513668	0.0009365
ENSMUSG00000085795	Zfp703	-0.231679973	0.0101667	ENSMUSG00000049482	Ctu2	-0.218498062	0.0104436
ENSMUSG00000022849	Hspbap1	-0.231548158	0.0160394	ENSMUSG00000025647	Shisa5	-0.218217214	7.41E-05
ENSMUSG00000096983	2010015M23Rik	-0.23136072	0.0351601	ENSMUSG00000025722	Wdr73	-0.217661222	0.0118796
ENSMUSG00000024831	Ighmbp2	-0.231330743	0.0233858	ENSMUSG00000022150	Dab2	-0.217635712	0.0153527
ENSMUSG00000037242	Clic4	-0.231313883	2.01E-12	ENSMUSG00000042594	Sh2b3	-0.217484713	0.0001646
ENSMUSG00000020641	Rsad2	-0.231288762	0.0147547	ENSMUSG00000031832	Taf1c	-0.216814465	0.0477589
ENSMUSG00000038742	Angptl6	-0.231123568	0.0450526	ENSMUSG00000000386	Mx1	-0.216660472	0.0009239
ENSMUSG00000064326	Siva1	-0.231081625	0.0003503	ENSMUSG00000067161	Gm5560	-0.216546413	0.0430845
ENSMUSG00000042211	Fbxo38	-0.230904356	0.0002136	ENSMUSG00000025198	Erlin1	-0.216212639	6.11E-05
ENSMUSG00000039518	Cdsn	-0.23085365	0.0016741	ENSMUSG00000022718	Dgcr8	-0.216075817	0.000235
ENSMUSG00000030400	Ercc2	-0.230775331	0.0024763	ENSMUSG00000002808	Epdr1	-0.216012936	0.0188042
ENSMUSG00000000120	Ngfr	-0.230718766	5.01E-13	ENSMUSG00000024732	Ccdc86	-0.215835631	0.0023114
ENSMUSG00000025485	Ric8	-0.230586048	0.0010029	ENSMUSG00000016496	Cd274	-0.215800298	0.0290401
ENSMUSG00000044636	Csrnp2	-0.230246078	0.0096995	ENSMUSG00000058392	Rrp1b	-0.215587132	0.0002203
ENSMUSG00000026600	Soat1	-0.230133758	1.13E-08	ENSMUSG00000038806	Sde2	-0.215528372	0.0006914
ENSMUSG00000002763	Pex6	-0.230098526	0.0127121	ENSMUSG00000020528	Prpsap2	-0.215287701	0.0037316
ENSMUSG00000038214	Bend3	-0.230000363	0.0062708	ENSMUSG00000017677	Wsb1	-0.215204217	1.50E-05
ENSMUSG00000060708	Bloc1s4	-0.229920472	0.0302393	ENSMUSG00000049680	Urgcp	-0.215136897	0.0006631
ENSMUSG00000006585	Cdt1	-0.229912699	1.06E-05	ENSMUSG00000045045	Lrfn4	-0.215076702	0.0004818
ENSMUSG00000007613	Tgfbr1	-0.229900352	0.0002268	ENSMUSG00000020087	Tysnd1	-0.214982933	0.0106847
ENSMUSG00000028339	Col15a1	-0.229717306	0.0413336	ENSMUSG00000096916	Zfp850	-0.214970496	0.0171177
ENSMUSG00000032712	2810474O19Rik	-0.229443874	0.0055402	ENSMUSG00000022407	Adsl	-0.214949191	9.04E-07
ENSMUSG00000041966	Dcaf17	-0.229347006	0.0107619	ENSMUSG00000022560	Slc52a2	-0.214874296	0.0012735
ENSMUSG00000073755	5730409E04Rik	-0.228954224	0.0352796	ENSMUSG00000029397	Rchy1	-0.214268339	0.0173299
ENSMUSG00000029591	Ung	-0.228941347	0.0021678	ENSMUSG00000032409	Atr	-0.214229545	0.0004954
ENSMUSG00000026596	Abl2	-0.228931309	2.44E-08	ENSMUSG00000044768	D1Ertd622e	-0.214070829	0.0091117
ENSMUSG00000068196	Col8a1	-0.228774023	4.56E-07	ENSMUSG00000098178	Yam1	-0.213700729	0.0423566
ENSMUSG00000007610	Gtpbp3	-0.228683646	0.0042211	ENSMUSG00000023990	Tfeb	-0.213634128	0.0379693
ENSMUSG00000026000	Lancl1	-0.228677668	0.006009	ENSMUSG00000019261	Map1s	-0.213563465	0.0065057
ENSMUSG00000008318	Relt	-0.228555074	0.0034328	ENSMUSG00000020107	Anapc16	-0.213295576	0.0030277
ENSMUSG00000039005	Tlr4	-0.228410505	0.0447003	ENSMUSG00000032035	Ets1	-0.213203561	2.84E-10

Gene		Log_2 Fold Change	pValue	Gene		Log_2 Fold Change	pValue
ENSMUSG00000036281	Snapc4	-0.212859111	0.016237	ENSMUSG00000024843	Chka	-0.199689232	0.0343283
ENSMUSG00000043140	Tmem186	-0.212689356	0.0048629	ENSMUSG00000075419	Dolk	-0.19966477	0.0409065
ENSMUSG00000069682	Gm10275	-0.212559436	0.0005902	ENSMUSG00000032633	Flcn	-0.199526842	0.0125952
ENSMUSG00000062202	Btbd9	-0.211691082	0.0025637	ENSMUSG00000026806	Ddx31	-0.19951244	0.0302176
ENSMUSG00000062014	Gmfb	-0.211386055	2.14E-05	ENSMUSG00000051067	Lingo3	-0.199433292	0.0192647
ENSMUSG00000029186	Pi4k2b	-0.211298364	0.0004395	ENSMUSG00000030452	Nipa2	-0.19942066	0.0003093
ENSMUSG00000031482	Slc25a15	-0.211272789	0.0486991	ENSMUSG00000039623	Ap5z1	-0.19928478	0.0364221
ENSMUSG00000054099	Slc25a40	-0.211182656	0.0165571	ENSMUSG00000020534	Shmt1	-0.199217611	0.0003168
ENSMUSG00000036693	Nop14	-0.210934033	3.33E-05	ENSMUSG00000082016	Pgam1-ps2	-0.199072166	0.0090434
ENSMUSG00000030748	Il4ra	-0.210528218	4.86E-05	ENSMUSG00000026520	Pycr2	-0.199022141	0.0006661
ENSMUSG00000040007	Bahd1	-0.210526003	0.0047593	ENSMUSG00000032733	Snx33	-0.198986907	0.0221243
ENSMUSG00000023905	Tnfrsf12a	-0.210159882	1.35E-10	ENSMUSG00000049580	Tsku	-0.198879393	0.0072708
ENSMUSG00000017830	Dhx58	-0.209657185	0.0422512	ENSMUSG00000017664	Slc35c2	-0.198760114	0.0032538
ENSMUSG00000079509	Zfx	-0.209600164	0.000332	ENSMUSG00000024664	Fads3	-0.198672252	0.0002197
ENSMUSG00000007570	Fance	-0.209471489	0.0214735	ENSMUSG00000079562	Maea	-0.198371128	5.52E-06
ENSMUSG00000030161	Gabarapl1	-0.209410295	0.0061254	ENSMUSG00000018322	Tomm34	-0.198223093	0.005039
ENSMUSG00000032305	Fam219b	-0.209330113	0.0191096	ENSMUSG00000029513	Prkab1	-0.198213379	0.0195839
ENSMUSG00000028381	Ugcg	-0.209217277	0.0056104	ENSMUSG00000034203	Chchd4	-0.198089972	0.0024969
ENSMUSG00000030741	Spns1	-0.209139243	0.0075866	ENSMUSG00000028889	Yrdc	-0.19791265	0.0059753
ENSMUSG00000020561	Twistnb	-0.209130573	0.0040488	ENSMUSG00000020133	2310011J03Rik	-0.197685243	0.0076977
ENSMUSG00000016206	H2-M3	-0.208880982	0.0468191	ENSMUSG00000056708	Ier5	-0.197564358	0.0078473
ENSMUSG00000024317	Rnf138	-0.208723648	0.011129	ENSMUSG00000067724	Gbx1	-0.197423655	0.0358363
ENSMUSG00000038323	1700066M21Rik	-0.208580325	0.030205	ENSMUSG00000023009	Nckap5l	-0.197353957	0.0269325
ENSMUSG00000029708	Gcc1	-0.208115625	0.0210282	ENSMUSG00000028688	Toe1	-0.197353247	0.0189029
ENSMUSG00000032014	Oaf	-0.208054687	6.46E-06	ENSMUSG00000020289	Nprl3	-0.197057288	0.0182138
ENSMUSG00000035992	Fnip1	-0.208022084	0.0008661	ENSMUSG00000041747	Utp15	-0.197017199	0.0063913
ENSMUSG00000061878	Sphk1	-0.207835333	0.020359	ENSMUSG00000036992	Nxt1	-0.196966354	0.0075383
ENSMUSG00000040865	Ino80d	-0.207709475	0.0143033	ENSMUSG00000071748	Gm14698	-0.196802495	0.0370605
ENSMUSG00000042328	Hps4	-0.207653235	0.0406778	ENSMUSG00000037344	Slc12a9	-0.19666576	0.023926
ENSMUSG00000037531	Mrpl47	-0.207494911	0.0086214	ENSMUSG00000006599	Gtf2h1	-0.196664647	5.76E-05
ENSMUSG00000040022	Rab11fip2	-0.20725231	0.044918	ENSMUSG00000094411	Snord16a	-0.196662287	0.0499608
ENSMUSG00000060121	Gemin2	-0.207189118	0.0230235	ENSMUSG00000024486	Hbegf	-0.196514946	0.0018157
ENSMUSG00000032020	Ubash3b	-0.206995158	4.41E-05	ENSMUSG00000026289	Atg16l1	-0.195876727	0.0073669
ENSMUSG00000039130	Zc3hc1	-0.206708448	0.0027947	ENSMUSG00000002307	Daxx	-0.19587248	0.0154515
ENSMUSG00000026535	Ifi202b	-0.20660095	0.000724	ENSMUSG00000021147	Wdr37	-0.195870496	0.0426427
ENSMUSG00000025880	Smad7	-0.206493228	0.0028117	ENSMUSG00000026342	Slc35f5	-0.195746414	0.0295066
ENSMUSG00000025024	Smndc1	-0.206414836	0.0012791	ENSMUSG00000025511	Tspan4	-0.195621752	0.0001867
ENSMUSG00000026064	Ptp4a1	-0.206011618	1.98E-05	ENSMUSG00000018733	Pex12	-0.195530177	0.0354793
ENSMUSG00000044835	Ankrd45	-0.205839282	0.0045726	ENSMUSG00000034867	Ankrd27	-0.195436128	5.51E-05
ENSMUSG00000026315	Serpinb8	-0.205768219	0.0442108	ENSMUSG00000042793	Lgr6	-0.194961156	0.0068457
ENSMUSG00000029594	Rbm19	-0.205534306	4.35E-05	ENSMUSG00000079036	Alkbh1	-0.194906536	0.0216428
ENSMUSG00000061024	Rrs1	-0.205468799	7.57E-05	ENSMUSG00000079426	Arpc4	-0.194877788	0.0001628
ENSMUSG00000032902	Slc16a1	-0.205330837	2.18E-06	ENSMUSG00000001524	Gtf2h4	-0.194801913	0.010856
ENSMUSG00000019818	Cd164	-0.205088474	1.68E-08	ENSMUSG00000073771	Btbd19	-0.194661801	0.0401327
ENSMUSG00000090290	Gm17296	-0.205024184	0.0224426	ENSMUSG00000042729	Wdr74	-0.194509556	0.0013844
ENSMUSG00000027660	Skil	-0.205010555	0.0002916	ENSMUSG00000015133	Lrrk1	-0.19438641	0.0001598
ENSMUSG00000022500	Litaf	-0.205002926	2.11E-07	ENSMUSG00000053746	Ptrh1	-0.194069513	0.0204287
ENSMUSG00000071359	Tbpl1	-0.204669454	0.0063138	ENSMUSG00000063406	Tmed5	-0.193733133	0.0002776
ENSMUSG00000023977	Ubr2	-0.204488739	4.23E-05	ENSMUSG00000079478	Sssca1	-0.193629966	0.0045422
ENSMUSG00000092558	Med20	-0.204391836	0.0293451	ENSMUSG00000030469	Zfp719	-0.193559969	0.0422176
ENSMUSG00000084807	Gm13073	-0.204034897	0.0055011	ENSMUSG00000040663	Clcf1	-0.193508129	0.0040907
ENSMUSG00000048387	Osr1	-0.203900737	0.0176276	ENSMUSG00000004996	Mri1	-0.193482875	0.0426192
ENSMUSG00000038671	Arfrp1	-0.203758585	0.0122365	ENSMUSG00000024955	Esrra	-0.193454803	0.0069668
ENSMUSG00000058979	Cecr5	-0.203339245	0.0344928	ENSMUSG00000030208	Emp1	-0.193451768	7.42E-08
ENSMUSG00000063235	Ptpmt1	-0.203176776	0.0041022	ENSMUSG00000030353	Tead4	-0.193287216	0.0273801
ENSMUSG00000047221	Fam185a	-0.202739637	0.0248036	ENSMUSG00000019796	Lrp11	-0.193060746	0.0272131
ENSMUSG00000073490	AI607873	-0.202624833	0.0229949	ENSMUSG00000024132	Eci1	-0.192977064	0.0250998
ENSMUSG00000033213	AA467197	-0.202509699	0.0151751	ENSMUSG00000024188	Luc7l	-0.192944163	0.0006985
ENSMUSG00000015790	Surf1	-0.20235942	0.0418643	ENSMUSG00000027276	Jag1	-0.192918041	0.0003077
ENSMUSG00000041153	Osgin2	-0.202226339	0.0237326	ENSMUSG00000080242	Gm15487	-0.192840613	0.0311954
ENSMUSG00000075040	Zfp408	-0.20214522	0.0419109	ENSMUSG00000026766	Mmadhc	-0.19283731	0.0004154
ENSMUSG00000025612	Bach1	-0.202089498	0.0202415	ENSMUSG00000024780	Cdc37l1	-0.192811554	0.0067877
ENSMUSG00000027423	Snx5	-0.201820792	8.10E-11	ENSMUSG00000056952	Tatdn2	-0.192797992	0.0017605
ENSMUSG00000020000	Moxd1	-0.201796063	2.08E-09	ENSMUSG00000024841	Eif1ad	-0.19273107	0.0006384
ENSMUSG00000039242	B3galnt2	-0.201654823	0.0099366	ENSMUSG00000038181	Chpf2	-0.192540895	0.0172674
ENSMUSG00000043858	Nup62	-0.201640185	5.61E-06	ENSMUSG00000020255	D10Wsu102e	-0.192447289	0.001444
ENSMUSG00000000384	Tbrg4	-0.201509623	5.48E-05	ENSMUSG00000041390	Mdfic	-0.192308669	0.0111154
ENSMUSG00000068742	Cry2	-0.201443187	0.0397721	ENSMUSG00000032344	Mb21d1	-0.192299304	0.0230681
ENSMUSG00000029128	Rab28	-0.200867635	0.0017721	ENSMUSG00000028423	Nfx1	-0.192150053	3.15E-07
ENSMUSG00000028431	Ikbkap	-0.200829714	2.63E-05	ENSMUSG00000028948	Nol9	-0.192057691	0.0005397
ENSMUSG00000026615	Eprs	-0.200653413	9.14E-10	ENSMUSG00000062510	Nsl1	-0.191790628	0.012857
ENSMUSG00000015750	Aph1a	-0.200576552	0.0005592	ENSMUSG00000011179	Odc1	-0.191770674	3.93E-09
ENSMUSG00000081534	Slc48a1	-0.200546807	0.0056455	ENSMUSG00000069844	Sco1	-0.191525483	0.0148043
ENSMUSG00000055737	Ghr	-0.200435818	0.0045476	ENSMUSG00000022837	Iqcb1	-0.191313597	0.0220358
ENSMUSG00000045409	Trim39	-0.200430462	0.0283906	ENSMUSG00000025185	Loxl4	-0.191261007	0.0352345
ENSMUSG00000092203	1110038B12Rik	-0.200411825	5.65E-05	ENSMUSG00000038843	Gcnt1	-0.19111693	0.0107712
ENSMUSG00000036305	Rpl39-ps	-0.200300474	0.0095645	ENSMUSG00000074405	Zfp865	-0.190754732	0.0333195
ENSMUSG00000029569	Tmem168	-0.200209493	0.0061117	ENSMUSG00000020032	Nuak1	-0.190627055	0.0001706
ENSMUSG00000030738	Eif3c	-0.200156282	5.88E-14	ENSMUSG00000007836	Hnrnpa0	-0.190574054	1.03E-05
ENSMUSG00000039911	Spsb1	-0.199800345	0.0060137	ENSMUSG00000037885	Stk35	-0.190553977	0.003722
ENSMUSG00000027522	Stx16	-0.199789998	0.0028299	ENSMUSG00000078899	Gm4631	-0.19044717	0.0038285

Gene		Log_2 Fold Change	pValue	Gene		Log_2 Fold Change	pValue
ENSMUSG00000025648	Pfkfb4	-0.190346048	0.0006237	ENSMUSG00000028967	Errfi1	-0.179402095	0.0031443
ENSMUSG00000021906	Oxnad1	-0.190140985	0.0149745	ENSMUSG00000039929	Urb1	-0.179347743	0.0285372
ENSMUSG00000003346	Abhd17a	-0.18940306	0.0038292	ENSMUSG00000048429	1810026J23Rik	-0.179316012	0.0078431
ENSMUSG00000024360	Etf1	-0.189160842	6.71E-10	ENSMUSG00000005057	Sh2b2	-0.179078456	0.0402394
ENSMUSG00000020300	Cpeb4	-0.189081682	0.0221194	ENSMUSG00000039753	Fbxl5	-0.178894483	0.0160826
ENSMUSG00000029408	Abcb9	-0.189002501	0.0042216	ENSMUSG00000027599	Armc1	-0.178819676	0.0007443
ENSMUSG00000037003	Tns2	-0.188975149	0.015804	ENSMUSG00000086150	Bach2os	-0.178337237	0.0254754
ENSMUSG00000046675	Tmem251	-0.188843808	0.0222681	ENSMUSG00000028986	Klhl7	-0.178153893	0.015285
ENSMUSG00000024037	Wdr4	-0.188731619	0.0065818	ENSMUSG00000032112	Trappc4	-0.177948335	0.0014713
ENSMUSG00000002395	Use1	-0.188600765	0.0191132	ENSMUSG00000038462	Uqcrfs1	-0.177830764	0.0025672
ENSMUSG00000063019	Manbal	-0.188462393	0.0333662	ENSMUSG00000001143	Lman2l	-0.177703951	0.044553
ENSMUSG00000060038	Dhps	-0.188134623	0.0422151	ENSMUSG00000036282	Naa30	-0.177439568	0.0409641
ENSMUSG00000019823	Mical1	-0.188120739	0.0225688	ENSMUSG00000027076	Timm10	-0.177375447	0.0373705
ENSMUSG00000070420	Zscan25	-0.188020145	0.0457994	ENSMUSG00000040631	Dok4	-0.177359286	0.0098704
ENSMUSG00000078440	Dohh	-0.187884201	0.0023521	ENSMUSG00000022570	Tsta3	-0.177165264	0.003146
ENSMUSG00000079499	6530402F18Rik	-0.187820994	0.0453239	ENSMUSG00000037921	Ddx60	-0.176833797	0.0090614
ENSMUSG00000020280	Pus10	-0.187801137	0.0044492	ENSMUSG00000022601	Zbtb11	-0.176804322	0.042825
ENSMUSG00000057359	Gm17494	-0.187504325	0.0433132	ENSMUSG00000038975	Rabggtb	-0.17668422	6.62E-05
ENSMUSG00000055093	Gm8430	-0.187162486	0.0438816	ENSMUSG00000020310	Madcam1	-0.176648019	0.0033377
ENSMUSG00000024097	Srsf7	-0.186934845	1.35E-07	ENSMUSG00000022476	Polr3h	-0.176312309	0.0002555
ENSMUSG00000057134	Ado	-0.186923505	0.0039509	ENSMUSG00000021400	Wrnip1	-0.176237077	0.0107609
ENSMUSG00000035049	Rrp12	-0.186767125	0.0005835	ENSMUSG00000020937	Plcd3	-0.175871672	0.0488704
ENSMUSG00000059336	Slc14a1	-0.186140898	0.0068003	ENSMUSG00000021733	Slc4a7	-0.175830432	0.014457
ENSMUSG00000056220	Pla2g4a	-0.186054315	0.0230097	ENSMUSG00000034157	Cipc	-0.175794797	0.0022098
ENSMUSG00000036442	Thap11	-0.18584796	0.0180416	ENSMUSG00000032435	Dync1li1	-0.174829296	0.0006553
ENSMUSG00000000916	Nsun5	-0.185713925	0.0078291	ENSMUSG00000029507	Pus1	-0.174808694	0.0102435
ENSMUSG00000024359	Hspa9	-0.185619683	1.82E-12	ENSMUSG00000028403	Zdhhc21	-0.174784758	0.023572
ENSMUSG00000026889	Rbm18	-0.185410575	0.0234596	ENSMUSG00000024170	Telo2	-0.174778525	0.0186294
ENSMUSG00000051375	Pcdh1	-0.185384953	4.31E-06	ENSMUSG00000004393	Ddx56	-0.174635587	0.000593
ENSMUSG00000047843	Bri3	-0.185208855	0.0109638	ENSMUSG00000026413	Pkp1	-0.174579934	0.0149033
ENSMUSG00000033955	Tnks1bp1	-0.184984531	4.31E-05	ENSMUSG00000087153	Gm6483	-0.174293883	0.0472327
ENSMUSG00000002635	Pdcd2l	-0.184857428	0.037239	ENSMUSG00000002017	Fam98a	-0.174280193	0.0008066
ENSMUSG00000022369	Mtbp	-0.184608025	0.0013823	ENSMUSG00000027944	Hax1	-0.174202883	0.0045537
ENSMUSG00000029415	Sdad1	-0.184534616	0.002431	ENSMUSG00000070730	Rmdn3	-0.174158277	0.0196766
ENSMUSG00000050812	AI314180	-0.184472169	4.64E-05	ENSMUSG00000036160	Surf6	-0.174046605	0.0191459
ENSMUSG00000045932	Ifit2	-0.184332119	0.0138774	ENSMUSG00000016252	Atp5e	-0.17402035	0.0026707
ENSMUSG00000005779	Psmb4	-0.184224508	3.41E-05	ENSMUSG00000020530	Ggnbp2	-0.173937957	0.0007295
ENSMUSG00000037656	Slc20a2	-0.184210557	0.0001578	ENSMUSG00000021607	Mrpl36	-0.173714824	0.0333542
ENSMUSG00000039747	Orai2	-0.184035028	0.0087609	ENSMUSG00000051343	Rab11fip5	-0.173646427	0.0049254
ENSMUSG00000031750	Il34	-0.183787835	0.0277328	ENSMUSG00000084416	Rpl10a-ps1	-0.173390605	0.0102871
ENSMUSG00000037225	Fgf2	-0.183766156	0.0136038	ENSMUSG00000028140	Mrpl9	-0.173329525	0.0022977
ENSMUSG00000052419	2610001J05Rik	-0.183667056	0.028934	ENSMUSG00000038028	Tigar	-0.173242229	0.0302656
ENSMUSG00000020875	Hoxb9	-0.183592546	0.0256918	ENSMUSG00000022905	Kpna1	-0.173201719	7.99E-05
ENSMUSG00000092225	Gm2381	-0.183576501	0.0288994	ENSMUSG00000056536	Pign	-0.172885334	0.0013897
ENSMUSG00000031007	Atp6ap2	-0.183456668	0.0008257	ENSMUSG00000047648	Fbxo30	-0.17271933	0.0326064
ENSMUSG00000020857	Nme2	-0.183428706	0.000594	ENSMUSG00000039841	Zfp800	-0.172706819	0.0424022
ENSMUSG00000005846	Rsl1d1	-0.183373085	5.12E-09	ENSMUSG00000059482	2610301B20Rik	-0.17196754	0.0260116
ENSMUSG00000074221	Zfp568	-0.18329273	0.0226383	ENSMUSG00000041168	Lonp1	-0.171802459	6.62E-05
ENSMUSG00000025785	Exosc7	-0.183249512	0.0198441	ENSMUSG00000074892	B3galt5	-0.171769783	0.0362237
ENSMUSG00000060568	Fam78b	-0.183210406	0.0122959	ENSMUSG00000007739	Cct4	-0.171392552	6.17E-10
ENSMUSG00000037419	Endod1	-0.1829502	0.0337638	ENSMUSG00000022031	Elp3	-0.171251739	0.0179089
ENSMUSG00000022257	Laptm4b	-0.182796699	7.59E-05	ENSMUSG00000077737	Snord72	-0.171141757	0.0419035
ENSMUSG00000059713	Rcan3	-0.1827794	0.0113811	ENSMUSG00000051469	Zfp191	-0.171080241	0.0028207
ENSMUSG00000022770	Dlg1	-0.182760066	1.08E-05	ENSMUSG00000040236	Trappc5	-0.170926577	0.0462004
ENSMUSG00000049401	Ogfr	-0.182325684	0.0003343	ENSMUSG00000084349	Rpl3-ps1	-0.170738044	0.0245646
ENSMUSG00000019920	Lims1	-0.182055433	0.000214	ENSMUSG00000019297	Nop9	-0.170700328	0.0104714
ENSMUSG00000096727	Psmb9	-0.181842733	0.0076851	ENSMUSG00000041057	Wdr43	-0.170533285	8.06E-06
ENSMUSG00000028617	Lrrc42	-0.181822693	0.0137099	ENSMUSG00000024953	Prdx5	-0.170479847	0.001939
ENSMUSG00000038170	Pde4dip	-0.18171573	0.00614	ENSMUSG00000055707	Klhl26	-0.170314316	0.0281274
ENSMUSG00000060098	Prmt7	-0.181602033	0.0023557	ENSMUSG00000044030	Irf2bp1	-0.170313516	0.0105214
ENSMUSG00000012017	Scarf2	-0.181503885	0.0001655	ENSMUSG00000020453	Patz1	-0.17007431	0.020916
ENSMUSG00000035172	Plekhh3	-0.181499144	0.0124944	ENSMUSG00000106744	Riok2	-0.170040112	0.0150939
ENSMUSG00000028633	Ctps	-0.181208364	2.06E-05	ENSMUSG00000026796	Fam129b	-0.169518756	1.12E-06
ENSMUSG00000029344	Tpst2	-0.181131628	0.0034734	ENSMUSG00000049922	Slc35c1	-0.169501003	0.0442575
ENSMUSG00000042644	Itpr3	-0.181128958	0.0023803	ENSMUSG00000022884	Eif4a2	-0.169422139	4.05E-09
ENSMUSG00000083327	Vcp-rs	-0.181073694	0.0022132	ENSMUSG00000041712	Ubr7	-0.169379147	0.002012
ENSMUSG00000027710	Acad9	-0.180861388	0.0045811	ENSMUSG00000027397	Slc20a1	-0.168622174	0.0077046
ENSMUSG00000003923	Tfam	-0.180820657	0.0011716	ENSMUSG00000003438	Timm50	-0.168426141	0.002778
ENSMUSG00000023452	Pisd	-0.18060993	0.0154572	ENSMUSG00000044986	Tst	-0.168376161	0.0099781
ENSMUSG00000026960	Arl6ip6	-0.180592185	0.0075754	ENSMUSG00000017679	Ttpal	-0.16778159	0.0175925
ENSMUSG00000026245	Farsb	-0.180580284	9.43E-05	ENSMUSG00000034290	Nek9	-0.167527204	4.47E-05
ENSMUSG00000026885	Ttll11	-0.180342367	0.041422	ENSMUSG00000039699	Batf2	-0.167205124	0.016934
ENSMUSG00000063800	Prpf38a	-0.180159515	0.0123277	ENSMUSG00000038615	Nfe2l1	-0.167199117	2.24E-06
ENSMUSG00000036430	Tbcc	-0.180062314	0.0495775	ENSMUSG00000047044	D030056L22Rik	-0.166560603	0.00905
ENSMUSG00000032997	Chpf	-0.179890019	2.19E-05	ENSMUSG00000020694	Tlk2	-0.166471577	0.0033579
ENSMUSG00000033285	Wdr3	-0.17981743	5.65E-05	ENSMUSG00000027367	Stard7	-0.16637926	0.00011
ENSMUSG00000030872	Gga2	-0.179794342	0.0190775	ENSMUSG00000041548	Hspb8	-0.16630698	0.0018885
ENSMUSG00000053950	Adnp2	-0.179786717	0.0083062	ENSMUSG00000039630	Hnrnpu	-0.166134439	0.0008409
ENSMUSG00000045598	Zfp553	-0.179681723	0.0176172	ENSMUSG00000024150	Mcfd2	-0.165809027	0.0023788
ENSMUSG00000039840	Epg5	-0.179645891	0.0365146	ENSMUSG00000025199	Chuk	-0.165795559	0.0034272
ENSMUSG00000026248	Mrpl44	-0.179451017	0.0287934	ENSMUSG00000025544	Tm9sf2	-0.165647372	0.0025572

Gene		Log_2 Fold Change	pValue	Gene		Log_2 Fold Change	pValue
ENSMUSG00000022564	Grina	-0.165592899	0.0001904	ENSMUSG00000020817	Rabep1	-0.153231609	0.0028364
ENSMUSG00000023034	Nr4a1	-0.165562893	0.0025052	ENSMUSG00000000743	Chmp1a	-0.153141668	0.0147362
ENSMUSG00000026726	Cubn	-0.165405628	0.0118683	ENSMUSG00000020843	Timm22	-0.15302961	0.0210049
ENSMUSG00000028180	Zranb2	-0.164848607	0.000221	ENSMUSG00000045411	2410002F23Rik	-0.15302209	0.0032402
ENSMUSG00000056121	Fez2	-0.164621226	0.0235103	ENSMUSG00000014550	Rbsn	-0.152669376	0.0174578
ENSMUSG00000050229	Pigm	-0.164532113	0.0362274	ENSMUSG00000024622	Hmgxb3	-0.152611374	0.0091918
ENSMUSG00000024142	Mlst8	-0.164516317	0.0372318	ENSMUSG00000024242	Map4k3	-0.152540549	0.0076934
ENSMUSG00000015806	Qdpr	-0.164378538	0.0255773	ENSMUSG00000045629	Sh3tc2	-0.152356871	0.0488624
ENSMUSG00000074570	Cass4	-0.164343193	0.027116	ENSMUSG00000008035	Mid1ip1	-0.152325692	0.0198227
ENSMUSG00000020611	Gna13	-0.164077857	0.003561	ENSMUSG00000094870	Zfp131	-0.152292555	0.0477186
ENSMUSG00000017765	Slc12a4	-0.163922663	0.0110596	ENSMUSG00000020393	Kremen1	-0.151920675	0.0290615
ENSMUSG00000021952	Xpo4	-0.163755623	0.0357984	ENSMUSG00000025381	Cnpy2	-0.151795009	0.0059349
ENSMUSG00000075700	Selt	-0.163483699	7.25E-06	ENSMUSG00000026761	Orc4	-0.151740665	0.0253511
ENSMUSG00000027312	Atrn	-0.163475878	0.0010765	ENSMUSG00000025894	Aasdhppt	-0.151565783	0.0343363
ENSMUSG00000029468	P2rx7	-0.163475448	0.008615	ENSMUSG00000054027	Nt5dc3	-0.151381137	0.030585
ENSMUSG00000027340	Slc23a2	-0.163468657	0.0018993	ENSMUSG00000043733	Ptpn11	-0.151355376	6.50E-06
ENSMUSG00000062190	Lancl2	-0.163302893	0.0296894	ENSMUSG00000037894	H2afz	-0.151305955	6.35E-07
ENSMUSG00000042660	Wdr55	-0.163229604	0.010762	ENSMUSG00000033596	Rfwd3	-0.150940801	0.0044748
ENSMUSG00000025616	Usp16	-0.162862934	0.0108124	ENSMUSG00000009470	Tnpo1	-0.150799299	7.05E-05
ENSMUSG00000024764	Naa40	-0.162602391	0.0122305	ENSMUSG00000036718	Micall2	-0.150786125	0.0399063
ENSMUSG00000020422	Tns3	-0.16233556	2.43E-08	ENSMUSG00000022894	Adamts5	-0.15075673	0.0129087
ENSMUSG00000042046	Dstyk	-0.162028345	0.0286083	ENSMUSG00000022503	Nubp1	-0.150689223	0.0221895
ENSMUSG00000020483	Dynll2	-0.162006641	0.000627	ENSMUSG00000020464	Pnpt1	-0.150347848	0.0017765
ENSMUSG00000056153	Socs6	-0.16144088	0.0225395	ENSMUSG00000071172	Srsf3	-0.150333475	7.27E-07
ENSMUSG00000030499	Kctd15	-0.161296146	0.0146388	ENSMUSG00000033706	Smyd5	-0.1502701	0.0152731
ENSMUSG00000044934	Zfp367	-0.160924618	0.0150674	ENSMUSG00000038650	Rnh1	-0.150115091	0.0072308
ENSMUSG00000005882	Uqcc1	-0.160715703	0.0215193	ENSMUSG00000038780	Smurf1	-0.150059347	1.78E-05
ENSMUSG00000035673	Sbno2	-0.160378797	0.0081571	ENSMUSG00000021189	Atxn3	-0.149887011	0.0478958
ENSMUSG00000041025	Iffo2	-0.160297065	0.0110319	ENSMUSG00000037851	Iars	-0.149834918	3.31E-05
ENSMUSG00000026319	2310035C23Rik	-0.160007072	0.0138449	ENSMUSG00000022412	Mief1	-0.148990014	0.0184258
ENSMUSG00000027309	4930402H24Rik	-0.159949313	0.0098811	ENSMUSG00000048170	Mcmbp	-0.148670252	0.0011583
ENSMUSG00000024293	Esco1	-0.159863152	0.0444403	ENSMUSG00000071793	2610005L07Rik	-0.148561784	0.0428648
ENSMUSG00000015804	Med28	-0.159533109	0.008411	ENSMUSG00000046722	Cdc42se1	-0.148404569	1.27E-05
ENSMUSG00000046671	Mtfr1l	-0.159457456	0.0075272	ENSMUSG00000051232	Tmem199	-0.148111706	0.0479061
ENSMUSG00000024580	Grpel2	-0.159241759	0.0239495	ENSMUSG00000020015	Cdk17	-0.147926021	0.0138495
ENSMUSG00000107470	CAAA01093177.1	-0.159057366	0.0402237	ENSMUSG00000017802	Fam134c	-0.147847398	0.0236241
ENSMUSG00000028195	Cyr61	-0.159014528	0.0006625	ENSMUSG00000026112	Coa5	-0.14728639	0.0048489
ENSMUSG00000064080	Fbln2	-0.158660878	5.65E-10	ENSMUSG00000040390	Map3k10	-0.147218285	0.0270832
ENSMUSG00000017929	B4galt5	-0.158515123	0.000466	ENSMUSG00000000378	Ccm2	-0.14720108	0.0070215
ENSMUSG00000021701	Plk2	-0.158419676	0.0005916	ENSMUSG00000070462	Mesdc1	-0.147178814	0.0349566
ENSMUSG00000020413	Hus1	-0.15837201	0.0085827	ENSMUSG00000031904	Slc7a6	-0.147174374	0.0197278
ENSMUSG00000079297	Gm2223	-0.158297999	0.0472283	ENSMUSG00000078249	Hmga1-rs1	-0.146527505	0.040229
ENSMUSG00000026204	Ptprn	-0.158285827	0.0129426	ENSMUSG00000029246	Ppat	-0.14639193	0.0092131
ENSMUSG00000027822	Slc33a1	-0.158235473	0.0361948	ENSMUSG00000024589	Nedd4l	-0.146341863	0.0006808
ENSMUSG00000026389	Steap3	-0.158181694	0.0006729	ENSMUSG00000047213	Ythdf3	-0.14630411	0.0066174
ENSMUSG00000091089	A930018M24Rik	-0.158082041	0.018543	ENSMUSG00000053835	H2-T24	-0.14629517	0.0258821
ENSMUSG00000026135	Zfp142	-0.158054378	0.0207501	ENSMUSG00000024937	Ehbp1l1	-0.145808527	0.0076282
ENSMUSG00000040661	Rad54l2	-0.157993589	0.002127	ENSMUSG00000022528	Hes1	-0.145742596	0.0294124
ENSMUSG00000022514	Il1rap	-0.157644317	5.25E-08	ENSMUSG00000026123	Plekhb2	-0.145725573	0.0238794
ENSMUSG00000018736	Ndel1	-0.157581108	0.0070482	ENSMUSG00000096458	Moap1	-0.145529087	0.0403894
ENSMUSG00000076437	2700094K13Rik	-0.157385371	0.0048412	ENSMUSG00000010453	Kansl3	-0.145305076	0.0106253
ENSMUSG00000027787	Nmd3	-0.157158877	0.0048981	ENSMUSG00000047434	Xxylt1	-0.145288474	0.0153124
ENSMUSG00000022992	Kansl2	-0.157108745	0.0005283	ENSMUSG00000032386	Trip4	-0.145239787	0.0287273
ENSMUSG00000026663	Atf6	-0.157044482	0.0017969	ENSMUSG00000022426	Josd1	-0.1451623	0.0013552
ENSMUSG00000027488	Snta1	-0.156969333	0.0408207	ENSMUSG00000041801	Phlda3	-0.144994612	0.0021852
ENSMUSG00000040699	Limd2	-0.156901348	0.0419119	ENSMUSG00000022367	Has2	-0.144974414	0.0253111
ENSMUSG00000030403	Vasp	-0.156775895	0.0042075	ENSMUSG00000024457	Trim26	-0.14491961	0.0499218
ENSMUSG00000040463	Mybbp1a	-0.156523709	5.57E-10	ENSMUSG00000014030	Pax5	-0.14456865	0.0114498
ENSMUSG00000040688	Tbl3	-0.156436908	0.0012662	ENSMUSG00000022175	Lrp10	-0.143883144	0.0184196
ENSMUSG00000024404	Riok3	-0.156370583	0.0082716	ENSMUSG00000041135	Ripk2	-0.143834405	0.0495745
ENSMUSG00000002458	Rgs19	-0.156364887	0.0193521	ENSMUSG00000038305	Spats2l	-0.143390539	0.0071585
ENSMUSG00000024778	Fas	-0.156293245	0.0342803	ENSMUSG00000026674	Ddr2	-0.143257437	0.0046392
ENSMUSG00000052429	Prmt1	-0.156134741	6.53E-06	ENSMUSG00000021567	Nkd2	-0.143241699	0.0003371
ENSMUSG00000016477	E2f3	-0.156065136	0.0467025	ENSMUSG00000023087	Ccrn4l	-0.143107607	0.0050536
ENSMUSG00000062397	Zfp706	-0.155700113	2.51E-05	ENSMUSG00000020386	Sar1b	-0.143081036	0.0193811
ENSMUSG00000051256	Jagn1	-0.155629894	0.0231452	ENSMUSG00000015745	Plekho1	-0.143052704	0.0003889
ENSMUSG00000028514	Usp24	-0.155493393	0.0017243	ENSMUSG00000009585	Apobec3	-0.142936781	0.0475581
ENSMUSG00000016946	Kctd5	-0.15539754	0.0094904	ENSMUSG00000031365	Zfp275	-0.142837019	0.0134356
ENSMUSG00000033096	Apmap	-0.155191135	0.0237763	ENSMUSG00000038047	Haus6	-0.14282981	0.0360742
ENSMUSG00000032369	Plscr1	-0.154877494	0.002102	ENSMUSG00000106106	Rn18s-rs5	-0.142722407	0.0009233
ENSMUSG00000033964	Zbtb41	-0.154648421	0.0060552	ENSMUSG00000003848	Nob1	-0.142475829	0.0210962
ENSMUSG00000058569	Tmed9	-0.15456738	0.0025125	ENSMUSG00000026974	Zmynd19	-0.142406175	0.022314
ENSMUSG00000024571	Gm16286	-0.154476132	0.0012264	ENSMUSG00000034707	Gns	-0.142301436	0.0005738
ENSMUSG00000038855	Itpkb	-0.154465471	0.0252192	ENSMUSG00000073700	Klhl21	-0.142059088	0.0008581
ENSMUSG00000034595	Ppp1r18	-0.154362596	3.76E-05	ENSMUSG00000038279	Nop2	-0.141907445	0.0003732
ENSMUSG00000047036	Zfp445	-0.154203013	0.0221436	ENSMUSG00000006418	Rnf114	-0.14180357	0.0199641
ENSMUSG00000032381	Fam96a	-0.15397569	0.0119224	ENSMUSG00000026019	Wdr12	-0.141324398	0.0077531
ENSMUSG00000021018	Polr2h	-0.153826535	0.0231111	ENSMUSG00000037315	Jade3	-0.141227958	0.0489537
ENSMUSG00000028318	Polr1e	-0.153691701	0.0116745	ENSMUSG00000033161	Atp1a1	-0.141220346	1.86E-09
ENSMUSG00000037275	Gemin5	-0.153326804	4.50E-05	ENSMUSG00000034640	Tiparp	-0.140896162	0.0479895
ENSMUSG00000027424	Mgme1	-0.153292396	0.0399478	ENSMUSG00000048782	Insc	-0.140809525	0.0168353

Gene		Log_2 Fold Change	pValue	Gene		Log_2 Fold Change	pValue
ENSMUSG00000020152	Actr2	-0.140688241	7.65E-08	ENSMUSG00000022704	Qtrtd1	-0.128170517	0.0196755
ENSMUSG00000019082	Slc25a22	-0.140190099	0.0478304	ENSMUSG00000005397	Nid1	-0.128050007	0.002194
ENSMUSG00000018171	Vmp1	-0.140048287	0.0005627	ENSMUSG00000020978	Klhdc2	-0.127992316	0.0145276
ENSMUSG00000033799	Fam208b	-0.139820083	0.0211151	ENSMUSG00000049807	Arhgap23	-0.127894588	0.0463258
ENSMUSG00000028233	Tgs1	-0.139798839	0.0134023	ENSMUSG00000039703	Nploc4	-0.127815185	0.0064611
ENSMUSG00000018433	Nol11	-0.139637669	0.0009709	ENSMUSG00000055612	Cdca7	-0.127561108	0.0190798
ENSMUSG00000002602	Axl	-0.139508646	1.08E-10	ENSMUSG00000035898	Uba6	-0.127513189	0.0298651
ENSMUSG00000026867	Gapvd1	-0.13933117	0.0105004	ENSMUSG00000033149	Phldb2	-0.12749859	0.0367185
ENSMUSG00000020570	Sypl	-0.139258025	0.0123223	ENSMUSG00000035900	Gramd4	-0.12721566	0.0072044
ENSMUSG00000037855	Zfp365	-0.139225237	0.0275166	ENSMUSG00000027293	Ehd4	-0.126882036	0.0177459
ENSMUSG00000000399	Ndufa9	-0.139192152	0.0059353	ENSMUSG00000028557	Rnf11	-0.126759476	0.0156317
ENSMUSG00000028776	Tinagl1	-0.139167852	4.42E-05	ENSMUSG00000028468	Rgp1	-0.126734125	0.0346726
ENSMUSG00000035351	Nup37	-0.139004555	0.0147304	ENSMUSG00000022437	Samm50	-0.126722433	0.0032223
ENSMUSG00000024816	Frmd8	-0.138962053	0.0030263	ENSMUSG00000052397	Ezr	-0.126679114	0.0024077
ENSMUSG00000026280	Atg4b	-0.138918203	0.0284764	ENSMUSG00000032594	Ip6k1	-0.126614714	0.0208116
ENSMUSG00000042363	Lgalsl	-0.138764252	0.0238962	ENSMUSG00000030126	Tmcc1	-0.126469426	0.0263615
ENSMUSG00000031917	Nip7	-0.138741347	0.025854	ENSMUSG00000026037	Orc2	-0.126336559	0.0074999
ENSMUSG00000029334	Prkg2	-0.138662217	0.0001541	ENSMUSG00000021140	Pcnx	-0.126317809	0.0314112
ENSMUSG00000021102	Glrx5	-0.138421799	0.0211316	ENSMUSG00000026749	Nek6	-0.125931121	0.0107014
ENSMUSG00000033184	Tmed7	-0.138259352	0.0011333	ENSMUSG00000005813	Metap1	-0.125888772	0.0089382
ENSMUSG00000032244	Fem1b	-0.138188309	0.0068811	ENSMUSG00000087445	Gm14286	-0.125685165	0.0402795
ENSMUSG00000039105	Atp6v1g1	-0.137943722	0.0091278	ENSMUSG00000035754	Wdr18	-0.125656473	0.0249015
ENSMUSG00000029134	Plb1	-0.137916028	0.0361881	ENSMUSG00000048039	Isg20l2	-0.125570492	0.046923
ENSMUSG00000023004	Tuba1b	-0.137859704	6.02E-06	ENSMUSG00000071652	Ints5	-0.125495788	0.0228106
ENSMUSG00000031781	Ciapin1	-0.137806429	0.0311156	ENSMUSG00000041733	Coq5	-0.125237417	0.0385956
ENSMUSG00000039244	E130309D02Rik	-0.137725978	0.0284811	ENSMUSG00000040620	Dhx33	-0.125143205	0.0167795
ENSMUSG00000094627	Gm10182	-0.137706692	0.0338023	ENSMUSG00000035614	Fam179b	-0.125019253	0.0431155
ENSMUSG00000097346	Gm26619	-0.137610688	0.0358067	ENSMUSG00000020520	Galnt10	-0.125002045	0.001567
ENSMUSG00000045312	Lhfpl2	-0.137463728	0.0054799	ENSMUSG00000020388	Pdlim4	-0.124816278	0.0261341
ENSMUSG00000063317	Usp31	-0.13737167	0.0242052	ENSMUSG00000016664	Pacsin2	-0.124264156	0.000686
ENSMUSG00000052298	Cdc42se2	-0.137192548	0.0096837	ENSMUSG00000057497	Fam136a	-0.124197985	0.0442406
ENSMUSG00000068922	Msto1	-0.137165023	0.013935	ENSMUSG00000038485	Socs7	-0.123783484	0.0226383
ENSMUSG00000051391	Ywhag	-0.13703265	2.61E-06	ENSMUSG00000034612	Chst11	-0.123608914	0.0002098
ENSMUSG00000032773	Chrm1	-0.136790893	0.0372432	ENSMUSG00000020088	Sar1a	-0.123585012	0.0016364
ENSMUSG00000021608	Lpcat1	-0.136710014	0.0172757	ENSMUSG00000030505	Prmt3	-0.123264471	0.0119707
ENSMUSG00000028896	Rcc1	-0.136513983	0.0051385	ENSMUSG00000022538	Lsg1	-0.123167097	0.0145357
ENSMUSG00000066232	Ipo7	-0.136471827	1.70E-06	ENSMUSG00000062611	Rps3a2	-0.122553009	0.0213775
ENSMUSG00000020642	Rnf144a	-0.136372412	0.0329497	ENSMUSG00000033735	Spr	-0.122500127	0.0463086
ENSMUSG00000026087	Mrpl30	-0.136225592	0.0190921	ENSMUSG00000046756	Mrps7	-0.122475207	0.014212
ENSMUSG00000038683	Pak1ip1	-0.135912823	0.0260683	ENSMUSG00000060636	Rpl35a	-0.122437266	0.0011904
ENSMUSG00000046062	Ppp1r15b	-0.135849143	0.008475	ENSMUSG00000017715	Pgs1	-0.122212446	0.0197023
ENSMUSG00000028273	Pdlim5	-0.135677282	0.0016277	ENSMUSG00000070436	Serpinh1	-0.122090123	5.08E-06
ENSMUSG00000001521	Tulp3	-0.135561627	0.0042813	ENSMUSG00000055491	Pprc1	-0.121725338	0.0032802
ENSMUSG00000021939	Ctsb	-0.135491045	0.0003144	ENSMUSG00000042745	Id1	-0.121554338	0.0132837
ENSMUSG00000004054	Map3k11	-0.135386571	0.0428226	ENSMUSG00000022394	L3mbtl2	-0.121361841	0.0194494
ENSMUSG00000003518	Dusp3	-0.135369713	0.0285635	ENSMUSG00000040659	Efhd2	-0.121273744	0.0439167
ENSMUSG00000079104	Prps1l3	-0.134743289	0.0478722	ENSMUSG00000030753	Prkrir	-0.121254191	0.0025025
ENSMUSG00000022551	Cyc1	-0.134715479	0.0005178	ENSMUSG00000011096	Akt1s1	-0.121119358	0.0233222
ENSMUSG00000026667	Uhmk1	-0.134563712	0.0033405	ENSMUSG00000052144	Ppp4r2	-0.121072046	0.0010753
ENSMUSG00000023307	March5	-0.134159575	0.0097071	ENSMUSG00000050244	Heatr1	-0.120585713	0.0116945
ENSMUSG00000074746	Pdzd8	-0.134134778	0.0203952	ENSMUSG00000001627	Ifrd1	-0.119961356	0.0227351
ENSMUSG00000030327	Necap1	-0.134038005	0.0174061	ENSMUSG00000025995	Wdr75	-0.119821114	0.0082304
ENSMUSG00000028945	Rheb	-0.133916613	0.0069119	ENSMUSG00000047879	Usp14	-0.119489154	0.0047562
ENSMUSG00000051510	Mafg	-0.133863101	0.0197256	ENSMUSG00000025858	Get4	-0.119469938	0.0103866
ENSMUSG00000104222	Gm7292	-0.133839691	0.0375553	ENSMUSG00000001785	Pwp1	-0.11910573	0.0146397
ENSMUSG00000037458	Azin1	-0.133546638	2.16E-06	ENSMUSG00000048332	Lhfp	-0.119054374	0.0163771
ENSMUSG00000020592	Sdc1	-0.133534923	0.0029194	ENSMUSG00000020250	Txnrd1	-0.11904078	0.0002977
ENSMUSG00000022814	Umps	-0.133385927	0.0005364	ENSMUSG00000009614	Sardh	-0.11875328	0.04875
ENSMUSG00000071072	Ptges3	-0.133340279	2.87E-05	ENSMUSG00000019960	Dusp6	-0.118657957	0.006903
ENSMUSG00000044700	Tmem201	-0.132842202	0.02403	ENSMUSG00000062937	Mtap	-0.118565768	0.0120228
ENSMUSG00000018398	Sept8	-0.132565437	0.0056983	ENSMUSG00000025651	Uqcrc1	-0.118338673	0.0016391
ENSMUSG00000027465	Tbc1d20	-0.132555091	0.0095207	ENSMUSG00000027646	Src	-0.118272981	0.0363057
ENSMUSG00000028261	Ndufaf4	-0.132335812	0.024241	ENSMUSG00000022300	Dcaf13	-0.117972997	0.024108
ENSMUSG00000035342	Lzts2	-0.13186997	0.0078851	ENSMUSG00000054079	Utp18	-0.117822842	0.0205065
ENSMUSG00000028126	Pip5k1a	-0.131400722	0.0311239	ENSMUSG00000050567	Maml1	-0.117391747	0.0449877
ENSMUSG00000040152	Thbs1	-0.130917299	7.05E-06	ENSMUSG00000007659	Bcl2l1	-0.117332029	0.0032754
ENSMUSG00000022881	Rfc4	-0.130687411	0.0246478	ENSMUSG00000030660	Pik3c2a	-0.117148392	0.0099877
ENSMUSG00000020741	Cluh	-0.130269545	0.0006122	ENSMUSG00000021072	Tmx1	-0.117109367	0.0247625
ENSMUSG00000029152	Ociad1	-0.130086118	0.0015235	ENSMUSG00000027601	Mtfr1	-0.116807194	0.0380594
ENSMUSG00000031993	Snx19	-0.129982109	0.0333508	ENSMUSG00000034120	Srsf2	-0.116717357	0.0015042
ENSMUSG00000020840	Blmh	-0.129967496	0.0271283	ENSMUSG00000035770	Dync1li2	-0.116650282	0.0314069
ENSMUSG00000017831	Rab5a	-0.129883545	0.0391398	ENSMUSG00000043683	Fem1a	-0.116347292	0.0442234
ENSMUSG00000032058	Ppp2r1b	-0.129777031	0.0118021	ENSMUSG00000011877	Git1	-0.116338225	0.0003584
ENSMUSG00000012422	Tmem167	-0.129640481	0.0411134	ENSMUSG00000027823	Gmps	-0.116292861	0.0074904
ENSMUSG00000026374	Tsn	-0.129554582	0.0042659	ENSMUSG00000029578	Wipi2	-0.116277681	0.0132708
ENSMUSG00000032869	Psmf1	-0.129335048	0.0477553	ENSMUSG00000020472	Zkscan17	-0.116211719	0.0478961
ENSMUSG00000027502	Rtfdc1	-0.129155321	0.0240118	ENSMUSG00000029703	Lrwd1	-0.116068897	0.0356531
ENSMUSG00000031657	Heatr3	-0.129000823	0.0073352	ENSMUSG00000046032	Snx12	-0.116004583	0.0359741
ENSMUSG00000024997	Prdx3	-0.128661042	0.0120481	ENSMUSG00000023025	Larp4	-0.115237663	0.0015696
ENSMUSG00000027575	Arfgap1	-0.128511476	0.0365729	ENSMUSG00000020219	Timm13	-0.115234099	0.0260324
ENSMUSG00000025178	Pi4k2a	-0.128244406	0.0301042	ENSMUSG00000048029	Eno4	-0.115192652	0.0475703

Gene		Log_2 Fold Change	pValue	Gene		Log_2 Fold Change	pValue
ENSMUSG00000019795	Pcmt1	-0.115098315	0.0251025	ENSMUSG00000001228	Uhrf1	-0.094905262	0.0027189
ENSMUSG00000030275	Etnk1	-0.114767211	0.0359138	ENSMUSG00000022010	Tsc22d1	-0.094896602	0.043184
ENSMUSG00000040857	Erf	-0.114733958	0.0092886	ENSMUSG00000049553	Polr1a	-0.094621816	0.0118433
ENSMUSG00000039405	Prss23	-0.114732079	0.0237958	ENSMUSG00000056429	Tgoln1	-0.094614996	0.0256092
ENSMUSG00000017943	Gdap1l1	-0.114647977	0.0171253	ENSMUSG00000028955	Vamp3	-0.094460115	0.0491417
ENSMUSG00000000168	Dlat	-0.114360425	0.0150106	ENSMUSG00000018481	Appbp2	-0.094208543	0.0478042
ENSMUSG00000062929	Cfl2	-0.114320789	0.0353148	ENSMUSG00000026020	Nop58	-0.094030468	0.0052304
ENSMUSG00000024429	Gnl1	-0.114095801	0.0258822	ENSMUSG00000022438	Parvb	-0.093776608	0.0379334
ENSMUSG00000061904	Slc25a3	-0.113993599	5.54E-05	ENSMUSG00000009376	Met	-0.093134158	0.0159068
ENSMUSG00000093904	Tomm20	-0.113649844	0.0213977	ENSMUSG00000042506	Usp22	-0.092196314	0.0224898
ENSMUSG00000025856	Pdgfa	-0.113590329	0.0002013	ENSMUSG00000021024	Psma6	-0.092065561	0.0216038
ENSMUSG00000039682	Lap3	-0.113282569	0.0140761	ENSMUSG00000020473	Aebp1	-0.092004735	5.10E-05
ENSMUSG00000015733	Capza2	-0.112694683	0.003624	ENSMUSG00000032480	Dhx30	-0.092001745	0.0311886
ENSMUSG00000015653	Steap2	-0.1125454	0.0441694	ENSMUSG00000022255	Mtdh	-0.091838604	0.0141457
ENSMUSG00000025417	Pip4k2c	-0.112499499	0.0232783	ENSMUSG00000000740	Rpl13	-0.091388715	0.0013768
ENSMUSG00000017861	Mybl2	-0.112439595	0.0354705	ENSMUSG00000078652	Psme3	-0.091332867	0.0126915
ENSMUSG00000021877	Arf4	-0.111869818	0.0074697	ENSMUSG00000042079	Hnrnpf	-0.090964768	0.0008135
ENSMUSG00000023348	Trip6	-0.111732783	0.04265	ENSMUSG00000000753	Serpinf1	-0.090646449	0.0103571
ENSMUSG00000039001	Rps21	-0.111524622	0.0007374	ENSMUSG00000020114	Cand1	-0.090232555	0.0128528
ENSMUSG00000024120	Lrpprc	-0.111345094	0.006824	ENSMUSG00000025047	Pdcd11	-0.090199424	0.0369465
ENSMUSG00000016559	H3f3b	-0.111334125	6.26E-07	ENSMUSG00000029430	Ran	-0.090060431	0.0003925
ENSMUSG00000086704	Gm14582	-0.11114366	0.04575	ENSMUSG00000022962	Gart	-0.089640476	0.0410698
ENSMUSG00000066324	Impad1	-0.111025707	0.0041363	ENSMUSG00000020745	Pafah1b1	-0.089225592	0.0091326
ENSMUSG00000022295	Atp6v1c1	-0.110811472	0.016459	ENSMUSG00000026103	Gls	-0.088276096	0.0431755
ENSMUSG00000017776	Crk	-0.110798226	0.0018515	ENSMUSG00000036912	Piwil4	-0.088223476	0.0497369
ENSMUSG00000002059	Rab34	-0.11069879	0.020996	ENSMUSG00000104713	Gbp6	-0.087461771	0.0388856
ENSMUSG00000039804	Ncoa5	-0.110652089	0.0477481	ENSMUSG00000033813	Tcea1	-0.087368279	0.0237606
ENSMUSG00000025239	Limd1	-0.110638052	0.0251912	ENSMUSG00000024576	Csnk1a1	-0.086086148	0.0081217
ENSMUSG00000074656	Eif2s2	-0.110560423	0.0003055	ENSMUSG00000041459	Tardbp	-0.085814857	0.0052665
ENSMUSG00000002741	Ykt6	-0.110354803	0.0058424	ENSMUSG00000023068	Nus1	-0.085214337	0.0167379
ENSMUSG00000007029	Vars	-0.109775424	0.0006548	ENSMUSG00000039000	Ube3c	-0.084891209	0.0222623
ENSMUSG00000030180	Kdm5a	-0.109629635	0.0455916	ENSMUSG00000053332	Gas5	-0.08411424	0.029777
ENSMUSG00000018770	Atp5g3	-0.109494849	0.0018485	ENSMUSG00000005610	Eif4g2	-0.084032298	6.22E-05
ENSMUSG00000020097	Sgpl1	-0.109361493	0.0141563	ENSMUSG00000030884	Uqcrc2	-0.083350563	0.0163277
ENSMUSG00000051223	Bzw1	-0.109054439	0.0004063	ENSMUSG00000004356	Utp20	-0.083109876	0.0396398
ENSMUSG00000022629	Kif21a	-0.109034383	0.0432829	ENSMUSG00000020372	Gnb2l1	-0.082919396	0.000277
ENSMUSG00000028314	Toporsl	-0.109013537	0.0479056	ENSMUSG00000062825	Actg1	-0.081867184	0.0003025
ENSMUSG00000037857	Nufip2	-0.108907702	0.0312687	ENSMUSG00000046841	Ckap4	-0.081807042	0.0198611
ENSMUSG00000042747	Krtcap2	-0.108532136	0.0379323	ENSMUSG00000040945	Rcc2	-0.080408906	0.0031619
ENSMUSG00000020585	Laptm4a	-0.108022034	0.0006263	ENSMUSG00000018583	G3bp1	-0.080237724	0.0027266
ENSMUSG00000020238	Ncln	-0.107885083	0.0147157	ENSMUSG00000035242	Oaz1	-0.079640144	0.0110519
ENSMUSG00000021477	Ctsl	-0.107670832	0.0008717	ENSMUSG00000082976	Gm15056	-0.079511395	0.0494384
ENSMUSG00000036167	Pphln1	-0.107660268	0.0136845	ENSMUSG00000071646	Mta2	-0.079285563	0.0455381
ENSMUSG00000010048	Ifrd2	-0.107640681	0.0417553	ENSMUSG00000003131	Pafah1b2	-0.078576184	0.0280735
ENSMUSG00000021484	Lman2	-0.107134207	0.0089597	ENSMUSG00000040952	Rps19	-0.078315446	0.0049825
ENSMUSG00000013662	Atad1	-0.107134075	0.0215134	ENSMUSG00000012848	Rps5	-0.077405675	0.0014697
ENSMUSG00000038774	Ascc3	-0.106929312	0.0492864	ENSMUSG00000018446	C1qbp	-0.07531545	0.0222627
ENSMUSG00000022800	Fyttd1	-0.106286833	0.0171329	ENSMUSG00000026341	Actr3	-0.073993973	0.0247669
ENSMUSG00000017499	Cdc6	-0.106119409	0.0337388	ENSMUSG00000057863	Rpl36	-0.073343715	0.0279915
ENSMUSG00000014444	Piezo1	-0.105592672	0.0117319	ENSMUSG00000034993	Vat1	-0.073187222	0.0298837
ENSMUSG00000021039	Snw1	-0.105589505	0.0482032	ENSMUSG00000027404	Snrpb	-0.073124726	0.0252369
ENSMUSG00000027889	Ampd2	-0.105582688	0.0386014	ENSMUSG00000001440	Kpnb1	-0.072588467	0.0011917
ENSMUSG00000030224	Strap	-0.105526888	0.002135	ENSMUSG00000090862	Rps13	-0.072587282	0.0193257
ENSMUSG00000016487	Ppfibp1	-0.105470967	0.0001782	ENSMUSG00000022858	Tra2b	-0.072560563	0.044809
ENSMUSG00000036990	Otud4	-0.105431531	0.020196	ENSMUSG00000062006	Rpl34	-0.071506243	0.0301468
ENSMUSG00000018921	Pelp1	-0.105385625	0.0497257	ENSMUSG00000018379	Srsf1	-0.069025089	0.0215649
ENSMUSG00000036707	Cab39	-0.104672929	0.0131046	ENSMUSG00000001416	Cct3	-0.068440179	0.0171743
ENSMUSG00000029621	Arpc1a	-0.104555674	0.0083121	ENSMUSG00000028063	Lmna	-0.068223517	0.0068751
ENSMUSG00000037503	Fam168b	-0.104387124	0.0031958	ENSMUSG00000028234	Rps20	-0.066205216	0.0092201
ENSMUSG00000048852	Gm12185	-0.104332981	0.023365	ENSMUSG00000041734	Kirrel	-0.065825627	0.0273137
ENSMUSG00000028430	Nol6	-0.103892299	0.0157902	ENSMUSG00000037236	Matr3	-0.065624647	0.0450122
ENSMUSG00000027782	Kpna4	-0.103856547	0.0195024	ENSMUSG00000008683	Rps15a	-0.065323554	0.0135501
ENSMUSG00000020899	Pfas	-0.10340507	0.0112466	ENSMUSG00000032135	Mcam	-0.065054901	0.0388479
ENSMUSG00000032803	Cdv3	-0.102879184	0.0013471	ENSMUSG00000020361	Hspa4	-0.064101165	0.0156947
ENSMUSG00000056144	Trim34a	-0.102703346	0.0402025	ENSMUSG00000037331	Larp1	-0.064036492	0.0232094
ENSMUSG00000005204	Senp3	-0.102307909	0.0110681	ENSMUSG00000025351	Cd63	-0.059928081	0.0295175
ENSMUSG00000032867	Fbxw8	-0.10217449	0.0225946	ENSMUSG00000029622	Arpc1b	-0.056406833	0.0125219
ENSMUSG00000035885	Cox8a	-0.101784695	0.0104061	ENSMUSG00000029447	Cct6a	-0.052430118	0.0276991
ENSMUSG00000056537	Rlim	-0.101699034	0.0388563	ENSMUSG00000054808	Actn4	0.048750091	0.0398528
ENSMUSG00000091957	Rps2-ps10	-0.100691944	0.0062057	ENSMUSG00000020460	Rps27a	0.048849628	0.037112
ENSMUSG00000030007	Cct7	-0.100585039	0.0004993	ENSMUSG00000061983	Rps12	0.050853564	0.0257895
ENSMUSG00000020708	Psmc5	-0.100501784	0.0168449	ENSMUSG00000025809	Itgb1	0.051213084	0.0269067
ENSMUSG00000067851	Arfgef1	-0.100185464	0.0415371	ENSMUSG00000078812	Eif5a	0.051791296	0.0228381
ENSMUSG00000023150	Ivns1abp	-0.099948485	0.0022294	ENSMUSG00000074129	Rpl13a	0.054258971	0.0319998
ENSMUSG00000028455	Stoml2	-0.099902417	0.0397048	ENSMUSG00000062203	Gspt1	0.055086668	0.0437406
ENSMUSG00000030082	Sec61a1	-0.099706002	0.0031162	ENSMUSG00000034024	Cct2	0.05727966	0.0193269
ENSMUSG00000019132	BC005537	-0.099467373	0.0281471	ENSMUSG00000041841	Rpl37	0.061018163	0.0278106
ENSMUSG00000020598	Nrcam	-0.09884229	0.0134582	ENSMUSG00000019432	Ddx39b	0.061520957	0.0458675
ENSMUSG00000020664	Dld	-0.097803276	0.0092808	ENSMUSG00000032096	Arcn1	0.06173066	0.0399723
ENSMUSG00000025967	Eef1b2	-0.095986141	0.000245	ENSMUSG00000026478	Lamc1	0.062106586	0.0444485
ENSMUSG00000047180	Neurl3	-0.095984997	0.048494	ENSMUSG00000031167	Rbm3	0.062988191	0.007684

Gene		Log_2 Fold Change	pValue	Gene		Log_2 Fold Change	pValue
ENSMUSG00000024063	Lbh	0.063569182	0.0428576	ENSMUSG00000005698	Ctcf	0.089989562	0.0496204
ENSMUSG00000057113	Npm1	0.064722916	0.0021854	ENSMUSG00000015120	Ube2i	0.089990055	0.0074706
ENSMUSG00000048076	Arf1	0.06512033	0.0121262	ENSMUSG00000018160	Med1	0.090423747	0.0353455
ENSMUSG00000010277	2610507B11Rik	0.066393399	0.0241795	ENSMUSG00000025510	Cd151	0.09056356	0.0202898
ENSMUSG00000020917	Acly	0.066789313	0.0418318	ENSMUSG00000039953	Clstn1	0.090639013	0.0194159
ENSMUSG00000030062	Rpn1	0.067252681	0.0269704	ENSMUSG00000029718	Pcolce	0.09067208	0.0028615
ENSMUSG00000030835	Nomo1	0.067754623	0.0362596	ENSMUSG00000030603	Psmc4	0.091082135	0.0225196
ENSMUSG00000040385	Ppp1ca	0.06820549	0.046277	ENSMUSG00000027566	Psma7	0.091227487	0.0183648
ENSMUSG00000033047	Eif3l	0.068338583	0.0194943	ENSMUSG00000029364	Wsb2	0.091706121	0.0301793
ENSMUSG00000005683	Cs	0.068542021	0.0101174	ENSMUSG00000020994	Pnn	0.092095123	0.005506
ENSMUSG00000032115	Hyou1	0.068720947	0.0100274	ENSMUSG00000027455	Nsfl1c	0.09211347	0.0458216
ENSMUSG00000020719	Ddx5	0.069514712	0.0057523	ENSMUSG00000033006	Sox10	0.092380257	0.0026543
ENSMUSG00000055065	Ddx17	0.069692891	0.0390253	ENSMUSG00000040667	Nup88	0.092389539	0.0333342
ENSMUSG00000025508	Rplp2	0.069719908	0.0074817	ENSMUSG00000058230	Arhgap35	0.092930083	0.0195634
ENSMUSG00000027828	Ssr3	0.070932439	0.0152063	ENSMUSG00000003360	Ddx23	0.092994409	0.0083284
ENSMUSG00000027342	Pcna	0.071306559	0.0282915	ENSMUSG00000037029	Zfp146	0.093023343	0.0459726
ENSMUSG00000018707	Dync1h1	0.071815846	0.0305963	ENSMUSG00000058655	Eif4b	0.093305366	2.69E-05
ENSMUSG00000071644	Eef1g	0.071939754	0.0016354	ENSMUSG00000017760	Ctsa	0.093387017	0.0497951
ENSMUSG00000004891	Nes	0.072456934	0.0072467	ENSMUSG00000036309	Skp1a	0.093585551	0.009138
ENSMUSG00000003534	Ddr1	0.072594886	0.0384903	ENSMUSG00000040212	Emp3	0.0940296	0.0177664
ENSMUSG00000037608	Bclaf1	0.073105279	0.024922	ENSMUSG00000001525	Tubb5	0.094188976	1.29E-05
ENSMUSG00000025332	Kdm5c	0.074372383	0.0377673	ENSMUSG00000028809	Srrm1	0.094536852	0.0201499
ENSMUSG00000063511	Snrnp70	0.075035798	0.0175595	ENSMUSG00000002297	Dbf4	0.094753395	0.0490675
ENSMUSG00000018293	Pfn1	0.075965033	0.0086946	ENSMUSG00000038467	Chmp4b	0.095031462	0.0256695
ENSMUSG00000031078	Cttn	0.07615013	0.0110858	ENSMUSG00000038762	Abcf1	0.095128844	0.0064098
ENSMUSG00000026623	Lpgat1	0.076452997	0.0218094	ENSMUSG00000038084	Opa1	0.09522926	0.0189302
ENSMUSG00000034892	Rps29	0.076496163	0.0071989	ENSMUSG00000001517	Foxm1	0.09526755	0.0048101
ENSMUSG00000022234	Cct5	0.076747519	0.0034664	ENSMUSG00000028367	Txn1	0.095289986	0.0293437
ENSMUSG00000060166	Zdhhc8	0.077843013	0.049082	ENSMUSG00000011257	Pabpc4	0.095291733	0.0045487
ENSMUSG00000007891	Ctsd	0.078084481	0.0185397	ENSMUSG00000052752	Traf7	0.095424395	0.031799
ENSMUSG00000020929	Eftud2	0.078200817	0.0060933	ENSMUSG00000026837	Col5a1	0.095552499	0.0079296
ENSMUSG00000022285	Ywhaz	0.078676338	0.0031975	ENSMUSG00000003810	Mast2	0.095682468	0.0385259
ENSMUSG00000028691	Prdx1	0.07922751	0.0024872	ENSMUSG00000020181	Nav3	0.095751034	0.0206012
ENSMUSG00000014769	Psmb1	0.079393074	0.043285	ENSMUSG00000024661	Fth1	0.096228265	3.22E-05
ENSMUSG00000006333	Rps9	0.079467585	0.0012547	ENSMUSG00000027363	Usp8	0.09628846	0.0404469
ENSMUSG00000036606	Plxnb2	0.079623575	0.0200893	ENSMUSG00000029767	Calu	0.096526273	0.0002715
ENSMUSG00000032216	Nedd4	0.079700562	9.83E-05	ENSMUSG00000031865	Dctn1	0.096633735	0.0470176
ENSMUSG00000024054	Smchd1	0.079948592	0.045094	ENSMUSG00000036781	Rps27l	0.097353735	0.0281172
ENSMUSG00000094483	Purb	0.080074097	0.0279508	ENSMUSG00000047676	Rpsa-ps10	0.097587972	0.0064999
ENSMUSG00000033228	Scaf11	0.080199233	0.0162833	ENSMUSG00000040054	Baz2a	0.097875881	0.0485025
ENSMUSG00000028330	Ncbp1	0.080605791	0.0350357	ENSMUSG00000019471	Cdc37	0.097877834	0.0029039
ENSMUSG00000032178	Ilf3	0.081558268	0.0261257	ENSMUSG00000040479	Dgkz	0.097916611	0.0146643
ENSMUSG00000005514	Por	0.081575973	0.0455367	ENSMUSG00000032228	Tcf12	0.098559542	0.0085
ENSMUSG00000024981	Acsl5	0.081785479	0.0329498	ENSMUSG00000041355	Ssr2	0.098639597	0.0170533
ENSMUSG00000017057	Il13ra1	0.082513968	0.0493907	ENSMUSG00000026260	Ndufa10	0.098818466	0.0299286
ENSMUSG00000026042	Col5a2	0.083146991	9.87E-05	ENSMUSG00000032397	Tipin	0.098877128	0.0414074
ENSMUSG00000033295	Ptprf	0.083186118	0.0234748	ENSMUSG00000017548	Suz12	0.099008062	0.0073421
ENSMUSG00000027763	Mbnl1	0.083284217	0.0265487	ENSMUSG00000026457	Adipor1	0.099229631	0.0222417
ENSMUSG00000025364	Pa2g4	0.083315009	0.0049419	ENSMUSG00000038690	Atp5j2	0.09953458	0.0170397
ENSMUSG00000020349	Ppp2ca	0.083396858	0.0056096	ENSMUSG00000009013	Dynll1	0.099752004	0.003491
ENSMUSG00000024991	Eif3a	0.083696498	0.0003379	ENSMUSG00000047945	Marcksl1	0.099783608	0.0428924
ENSMUSG00000031256	Cstf2	0.083746393	0.0320732	ENSMUSG00000031059	Ndufb11	0.100009722	0.0352758
ENSMUSG00000022185	Acin1	0.083939204	0.0311652	ENSMUSG00000031060	Rbm10	0.100078131	0.0391391
ENSMUSG00000014959	Gorasp2	0.083976736	0.0454431	ENSMUSG00000001016	Ilf2	0.100244499	0.0117134
ENSMUSG00000059005	Hnrnpa3	0.084589374	0.0008861	ENSMUSG00000053565	Eif3k	0.100301131	0.026194
ENSMUSG00000020720	Psmd12	0.085167189	0.0319001	ENSMUSG00000025204	Ndufb8	0.100516621	0.0353895
ENSMUSG00000055204	Ankrd17	0.085272194	0.022603	ENSMUSG00000068823	Csde1	0.10062723	0.0005814
ENSMUSG00000060938	Rpl26	0.085361207	0.0014892	ENSMUSG00000061518	Cox5b	0.100628661	0.0318716
ENSMUSG00000024870	Rab1b	0.085925534	0.0312889	ENSMUSG00000010205	Raver1	0.100676192	0.0096317
ENSMUSG00000012535	Tnpo3	0.085965269	0.0221613	ENSMUSG00000024507	Hsd17b4	0.100677025	0.0249093
ENSMUSG00000021012	Zc3h14	0.086183489	0.0388723	ENSMUSG00000009073	Nf2	0.100750397	0.004447
ENSMUSG00000031503	Col4a2	0.086203492	0.004727	ENSMUSG00000028149	Rap1gds1	0.100899824	0.0370409
ENSMUSG00000003345	Csnk1g2	0.08626891	0.0342958	ENSMUSG00000020538	Srebf1	0.101157531	0.0339991
ENSMUSG00000028745	Capzb	0.086344263	0.0368838	ENSMUSG00000022607	Ptk2	0.10128319	0.0079786
ENSMUSG00000056342	Usp34	0.086413653	0.0445419	ENSMUSG00000014077	Chp1	0.101404302	0.0273922
ENSMUSG00000028284	Map3k7	0.086517976	0.0397104	ENSMUSG00000027523	Gnas	0.101445946	0.0079144
ENSMUSG00000094195	Gm6509	0.087348546	0.0491729	ENSMUSG00000053617	Sh3pxd2a	0.101507931	0.0060686
ENSMUSG00000019189	Rnf145	0.087358754	0.0175086	ENSMUSG00000032875	Arhgef17	0.101622504	0.0230068
ENSMUSG00000020737	Hn1	0.087533547	0.0126474	ENSMUSG00000024392	Bag6	0.101646075	0.0092504
ENSMUSG00000027201	Myef2	0.088382432	0.0341039	ENSMUSG00000069662	Marcks	0.101723271	0.0030698
ENSMUSG00000031715	Smarca5	0.08842211	0.0316154	ENSMUSG00000018286	Psmb6	0.101759903	0.0112959
ENSMUSG00000010608	Rbm25	0.088697094	0.0286138	ENSMUSG00000040824	Snrpd2	0.102102792	0.0298827
ENSMUSG00000021178	Psmc1	0.088761176	0.0158676	ENSMUSG00000024659	Anxa1	0.102266949	4.04E-05
ENSMUSG00000027479	Mapre1	0.088897275	0.0214773	ENSMUSG00000029148	Nrbp1	0.102406089	0.0371718
ENSMUSG00000038677	Scube3	0.088982186	0.0063423	ENSMUSG00000026176	Ctdsp1	0.102431665	0.026204
ENSMUSG00000058799	Nap1l1	0.088991015	0.0001394	ENSMUSG00000036256	Igfbp7	0.102450572	0.0401792
ENSMUSG00000025503	Taldo1	0.089125486	0.0064306	ENSMUSG00000025083	Afap1l2	0.102571848	0.0350453
ENSMUSG00000061477	Rps7	0.089268703	0.000851	ENSMUSG00000039220	Ppp1r10	0.102600981	0.0498029
ENSMUSG00000007670	Khsrp	0.089375431	0.0145664	ENSMUSG00000057278	Snrpg	0.102810946	0.045114
ENSMUSG00000008690	Ncaph2	0.089765644	0.0112464	ENSMUSG00000094690	1600014C23Rik	0.103251048	0.047266
ENSMUSG00000023110	Prmt5	0.089946375	0.0468704	ENSMUSG00000000751	Rpa1	0.10326747	0.0035189

Gene		Log_2 Fold Change	pValue	Gene		Log_2 Fold Change	pValue
ENSMUSG00000014226	Cacybp	0.103273877	0.0046474	ENSMUSG00000026083	Eif5b	0.114139503	0.000889
ENSMUSG00000041879	Ipo9	0.103478846	0.0025653	ENSMUSG00000027804	Ppid	0.114215586	0.0039846
ENSMUSG00000032458	Copb2	0.103512144	0.0089299	ENSMUSG00000020454	Eif4enif1	0.114276396	0.0121467
ENSMUSG00000029614	Rpl6	0.10395831	1.14E-05	ENSMUSG00000030852	Tacc2	0.11429381	0.0328231
ENSMUSG00000001833	Sept7	0.104099232	0.0010678	ENSMUSG00000046079	Lrrc8d	0.114325275	0.0263744
ENSMUSG00000056999	Ide	0.10413453	0.0151824	ENSMUSG00000047216	Cdh19	0.114496911	0.0325988
ENSMUSG00000031342	Gpm6b	0.10414494	0.0047294	ENSMUSG00000007564	Ppp2r1a	0.114541432	0.002455
ENSMUSG00000028343	Erp44	0.104344719	0.0457004	ENSMUSG00000023460	Rab12	0.114758664	0.0428433
ENSMUSG00000020392	Cdkn2aipnl	0.104419015	0.0494702	ENSMUSG00000008301	Phax	0.114822714	0.0394165
ENSMUSG00000039959	Hip1	0.104517666	0.0040628	ENSMUSG00000032399	Rpl4	0.114861967	1.51E-08
ENSMUSG00000033031	C330027C09Rik	0.104677268	0.0281568	ENSMUSG00000029613	Eif2ak1	0.114927269	0.0200831
ENSMUSG00000022378	Fam49b	0.10475083	0.0081771	ENSMUSG00000021377	Dek	0.115090927	0.0063161
ENSMUSG00000028937	Acot7	0.104836514	0.0151524	ENSMUSG00000044224	Dnajc21	0.115103901	0.0369496
ENSMUSG00000030216	Wbp11	0.104843511	0.0148493	ENSMUSG00000039148	Sart1	0.115277727	0.0260719
ENSMUSG00000057335	Cep170	0.104855387	0.0099699	ENSMUSG00000029550	Sppl3	0.115322565	0.0477297
ENSMUSG00000025132	Arhgdia	0.104928878	0.0003613	ENSMUSG00000001910	Nacc1	0.115354533	0.0063072
ENSMUSG00000020850	Prpf8	0.105353109	8.08E-06	ENSMUSG00000004937	Sgta	0.115456392	0.008598
ENSMUSG00000040785	Ttc3	0.106083518	0.0144981	ENSMUSG00000025935	Tram1	0.115687879	0.0298985
ENSMUSG00000029439	Sfswap	0.106171184	0.0250441	ENSMUSG00000060657	Marf1	0.11596481	0.0411613
ENSMUSG00000055319	Sec23ip	0.10628528	0.0241891	ENSMUSG00000034088	Hdlbp	0.116044475	2.03E-06
ENSMUSG00000037012	Hk1	0.106361376	0.0164059	ENSMUSG00000059273	Zc3h4	0.116054607	0.0106035
ENSMUSG00000028961	Pgd	0.106613911	0.0283895	ENSMUSG00000025027	Xpnpep1	0.116218662	0.0070541
ENSMUSG00000030605	Mfge8	0.106667603	0.0072556	ENSMUSG00000052146	Rps10	0.116466206	1.01E-05
ENSMUSG00000005161	Prdx2	0.106751794	0.0121816	ENSMUSG00000007041	Clic1	0.116496274	0.0144541
ENSMUSG00000026864	Hspa5	0.107312856	6.11E-06	ENSMUSG00000030654	Arl6ip1	0.116528305	0.0029392
ENSMUSG00000079487	Med12	0.107550301	0.0238476	ENSMUSG00000022148	Fyb	0.116606852	0.0137004
ENSMUSG00000001175	Calm1	0.107633518	0.0002079	ENSMUSG00000017721	Pigt	0.116664747	0.012011
ENSMUSG00000024083	Pja2	0.107649795	0.0369369	ENSMUSG00000000568	Hnrnpd	0.116691932	0.0009906
ENSMUSG00000045983	Eif4g1	0.10770643	2.27E-07	ENSMUSG00000031672	Got2	0.116745717	0.0036907
ENSMUSG00000001472	Tcf25	0.107740429	0.0096826	ENSMUSG00000057130	Txnl4a	0.116910089	0.045961
ENSMUSG00000022757	Tfg	0.107777775	0.0434445	ENSMUSG00000038664	Herc1	0.116998412	0.0489018
ENSMUSG00000028556	Dock7	0.107793545	0.0046572	ENSMUSG00000030557	Mef2a	0.117187147	0.0251975
ENSMUSG00000014606	Slc25a11	0.107917724	0.0412191	ENSMUSG00000027109	Sp3	0.117264955	0.0212342
ENSMUSG00000023106	Denr	0.107979463	0.0118593	ENSMUSG00000020922	Lsm12	0.117359357	0.0143913
ENSMUSG00000028790	Khdrbs1	0.10811385	0.0039551	ENSMUSG00000073838	Tufm	0.117371581	0.01446
ENSMUSG00000014195	Dnajc7	0.108141684	0.0045782	ENSMUSG00000029580	Actb	0.117373765	1.79E-10
ENSMUSG00000022912	Pros1	0.108144602	0.0102229	ENSMUSG00000049804	Armcx4	0.117499399	0.0334728
ENSMUSG00000006699	Cdc42	0.108399355	0.0022778	ENSMUSG00000007850	Hnrnph1	0.117529453	8.00E-05
ENSMUSG00000021546	Hnrnpk	0.108591186	5.76E-06	ENSMUSG00000040524	Zfp609	0.117663408	0.0194846
ENSMUSG00000024767	Otub1	0.10875085	0.0323244	ENSMUSG00000070544	Top1	0.117807988	0.0013315
ENSMUSG00000003099	Ppp5c	0.10875435	0.0203836	ENSMUSG00000030213	Atf7ip	0.117924255	0.0234636
ENSMUSG00000032418	Me1	0.109022856	0.0431936	ENSMUSG00000026728	Vim	0.11799488	1.49E-08
ENSMUSG00000052337	Immt	0.109023744	0.0010092	ENSMUSG00000021131	Erh	0.118000961	0.0055462
ENSMUSG00000071659	Hnrnpul2	0.109070458	0.001563	ENSMUSG00000056515	Rab31	0.118258074	0.0022338
ENSMUSG00000059552	Trp53	0.109202569	0.0070387	ENSMUSG00000023175	Bsg	0.118410663	6.01E-05
ENSMUSG00000030058	Copg1	0.109611969	0.0094091	ENSMUSG00000036241	Ube2r2	0.118422174	0.007201
ENSMUSG00000024941	Scyl1	0.109778197	0.0463381	ENSMUSG00000028960	Ube4b	0.11843411	0.023811
ENSMUSG00000027162	Lin7c	0.109841592	0.0116906	ENSMUSG00000019494	Cops6	0.118436111	0.0029517
ENSMUSG00000061315	Naca	0.110039786	8.05E-05	ENSMUSG00000004319	Clcn3	0.118694696	0.0475963
ENSMUSG00000029064	Gnb1	0.110080355	0.000108	ENSMUSG00000074797	Itpa	0.118728606	0.0267481
ENSMUSG00000054863	Fam19a5	0.110181419	0.0095188	ENSMUSG00000008475	Arpc5	0.118828954	0.0141761
ENSMUSG00000047675	Rps8	0.110257885	1.51E-05	ENSMUSG00000036087	Slain2	0.118836831	0.0303585
ENSMUSG00000022885	St6gal1	0.110343661	0.0480766	ENSMUSG00000043962	Thrap3	0.118879918	0.0022761
ENSMUSG00000013858	Tmem259	0.110528861	0.0299828	ENSMUSG00000061731	Ext1	0.119399473	0.0326471
ENSMUSG00000026509	Capn2	0.110850439	0.0022086	ENSMUSG00000027665	Pik3ca	0.119406233	0.0428123
ENSMUSG00000025982	Sf3b1	0.110855563	0.0002362	ENSMUSG00000022706	Mrpl40	0.119587006	0.0354764
ENSMUSG00000035227	Spcs2	0.111101043	0.0088257	ENSMUSG00000019969	Psen1	0.119621968	0.0436014
ENSMUSG00000022361	Zhx1	0.111184379	0.0254181	ENSMUSG00000001056	Nhp2	0.119705556	0.0005731
ENSMUSG00000027247	Arhgap1	0.11122457	0.0391068	ENSMUSG00000037933	Bicd2	0.119832219	0.0476666
ENSMUSG00000009035	Tmem184b	0.111318196	0.0104515	ENSMUSG00000040940	Arhgef1	0.119866521	0.0375635
ENSMUSG00000010663	Fads1	0.11135052	0.0121695	ENSMUSG00000022403	St13	0.120100116	2.34E-05
ENSMUSG00000021870	Slmap	0.111382631	0.0364604	ENSMUSG00000023932	Cdc5l	0.12026461	0.0076369
ENSMUSG00000062604	Srpk2	0.111394321	0.0356927	ENSMUSG00000004056	Akt2	0.120384161	0.0022756
ENSMUSG00000057363	Uxs1	0.111467368	0.032626	ENSMUSG00000001847	Rac1	0.120436861	2.38E-05
ENSMUSG00000039262	Prrc2b	0.111538392	0.0077301	ENSMUSG00000028081	Rps3a1	0.120504212	4.74E-07
ENSMUSG00000020716	Nf1	0.111559329	0.0269832	ENSMUSG00000018166	Erbb3	0.120519434	0.0023403
ENSMUSG00000028044	Cks1b	0.111599955	0.0172682	ENSMUSG00000000563	Atp5f1	0.120564922	0.000268
ENSMUSG00000036078	Sigmar1	0.111822502	0.0024095	ENSMUSG00000024533	Spire1	0.120616048	0.017033
ENSMUSG00000022710	Usp7	0.11191306	0.00114	ENSMUSG00000029822	Osbpl3	0.12061736	0.0415991
ENSMUSG00000028936	Rpl22	0.111928783	0.0012343	ENSMUSG00000036932	Aifm1	0.120628373	0.0098202
ENSMUSG00000002052	Supt6	0.111933373	0.0007545	ENSMUSG00000031703	Itfg1	0.120647836	0.0472727
ENSMUSG00000020368	Canx	0.112677816	1.68E-06	ENSMUSG00000052915	Msl1	0.120764565	0.0287595
ENSMUSG00000027198	Ext2	0.11268069	0.0109681	ENSMUSG00000024639	Gnaq	0.120863967	0.0412898
ENSMUSG00000078676	Casc3	0.112796951	0.0349984	ENSMUSG00000067367	Lyar	0.121155167	0.0068144
ENSMUSG00000054408	Spcs3	0.113220926	0.0433516	ENSMUSG00000048878	Hexim1	0.121175916	0.0114882
ENSMUSG00000028649	Macf1	0.113289573	0.0179517	ENSMUSG00000018042	Cyb5r3	0.12124552	6.45E-05
ENSMUSG00000029190	D5Ertd579e	0.113371406	0.0268276	ENSMUSG00000020358	Hnrnpab	0.121287438	1.17E-07
ENSMUSG00000006057	Atp5g1	0.113572112	0.0128383	ENSMUSG00000021756	Il6st	0.121317769	0.0006387
ENSMUSG00000032518	Rpsa	0.113727171	9.95E-09	ENSMUSG00000037364	Srrt	0.121334996	0.0003854
ENSMUSG00000024909	Efemp2	0.114019079	0.0191755	ENSMUSG00000029581	Fscn1	0.121868439	2.50E-05
ENSMUSG00000030663	1110004F10Rik	0.114073844	0.012821	ENSMUSG00000039128	Cdc123	0.121956321	0.035066

Gene		Log_2 Fold Change	pValue	Gene		Log_2 Fold Change	pValue
ENSMUSG00000038502	Ptov1	0.122021945	0.0316311	ENSMUSG00000038025	Phf2	0.13029185	0.0300048
ENSMUSG00000020640	Itsn2	0.122023599	0.0109844	ENSMUSG00000031347	Cetn2	0.13030462	0.0359164
ENSMUSG00000030824	Nucb1	0.122083926	0.0013374	ENSMUSG00000002524	Puf60	0.130450698	6.35E-05
ENSMUSG00000030583	Sipa1l3	0.122149901	0.0082717	ENSMUSG00000017119	Nbr1	0.130523218	0.0021266
ENSMUSG00000021556	Golm1	0.12217468	0.0180193	ENSMUSG00000031790	Mmp15	0.130549531	0.0351155
ENSMUSG00000021823	Vcl	0.122201149	0.0298917	ENSMUSG00000027699	Ect2	0.130618481	0.0003368
ENSMUSG00000020476	Dbnl	0.122551572	0.0038875	ENSMUSG00000066037	Hnrnpr	0.130841122	0.0022102
ENSMUSG00000042489	Clspn	0.122696005	0.0167699	ENSMUSG00000020402	Vdac1	0.130964694	7.95E-06
ENSMUSG00000002833	Hdgfrp2	0.122863157	0.011431	ENSMUSG00000065979	Cpped1	0.130997172	0.0324797
ENSMUSG00000024833	Pola2	0.122958494	0.0267976	ENSMUSG00000073497	AA792892	0.131131997	0.0249065
ENSMUSG00000050424	Pnma5	0.12311062	0.0268701	ENSMUSG00000079029	Gm5662	0.131191622	0.0419299
ENSMUSG00000020705	Ddx42	0.123326411	0.0064162	ENSMUSG00000025134	Alyref	0.131197219	0.0044569
ENSMUSG00000035325	Sec31a	0.123386465	0.0011224	ENSMUSG00000029610	Aimp2	0.131496577	0.0301929
ENSMUSG00000022307	Oxr1	0.123464596	0.0116056	ENSMUSG00000038845	Phb	0.131736429	0.0012257
ENSMUSG00000052727	Map1b	0.123654052	0.0031405	ENSMUSG00000015149	Sirt2	0.132113993	0.026127
ENSMUSG00000040711	Sh3pxd2b	0.123767268	0.0011777	ENSMUSG00000019961	Tmpo	0.132312362	2.21E-05
ENSMUSG00000032855	Pkd1	0.123826668	0.0147948	ENSMUSG00000010097	Nxf1	0.132492429	0.0030313
ENSMUSG00000008373	Prpf31	0.12404413	0.0061678	ENSMUSG00000017670	Elmo2	0.132594975	0.0160268
ENSMUSG00000037286	Stag1	0.12412254	0.0059475	ENSMUSG00000039414	Heatr5b	0.132632615	0.0246029
ENSMUSG00000037935	Smarce1	0.124359929	0.0043805	ENSMUSG00000020536	Llgl1	0.132663076	0.0070959
ENSMUSG00000036398	Ppp1r11	0.124425037	0.0253448	ENSMUSG00000040446	Rprd1a	0.1327191	0.0091017
ENSMUSG00000014498	Ankrd52	0.124535303	0.0075907	ENSMUSG00000032966	Fkbp1a	0.132755303	7.80E-06
ENSMUSG00000038766	Gabpb2	0.12454946	0.0137721	ENSMUSG00000006304	Arpc2	0.132981578	8.50E-05
ENSMUSG00000057133	Chd6	0.12456441	0.0338413	ENSMUSG00000000028	Cdc45	0.133161564	0.0050133
ENSMUSG00000031065	Cdk16	0.124684985	0.0013097	ENSMUSG00000020018	Snrpf	0.133258427	0.0049484
ENSMUSG00000037533	Rapgef6	0.124753773	0.0168401	ENSMUSG00000020235	Fzr1	0.133266488	0.0226965
ENSMUSG00000001729	Akt1	0.124769469	3.07E-06	ENSMUSG00000035726	Supt16	0.133320952	0.0005806
ENSMUSG00000022477	Aco2	0.124796829	6.46E-05	ENSMUSG00000036523	Greb1	0.133404378	0.0123274
ENSMUSG00000009927	Rps25	0.12512541	5.46E-07	ENSMUSG00000004455	Ppp1cc	0.133476592	8.03E-05
ENSMUSG00000022191	Drosha	0.125247839	0.0021791	ENSMUSG00000020608	Smc6	0.133844903	0.0015168
ENSMUSG00000027108	Ola1	0.125265675	0.00097	ENSMUSG00000051768	Xrcc1	0.133918688	0.0108662
ENSMUSG00000068744	Psrc1	0.125363793	0.0467496	ENSMUSG00000031392	Irak1	0.134012032	0.0096106
ENSMUSG00000026028	Trak2	0.125370657	0.0122314	ENSMUSG00000042133	Ppig	0.134158461	0.0031428
ENSMUSG00000027180	Fbxo3	0.125371052	0.045385	ENSMUSG00000006307	Kmt2b	0.134204949	0.0098714
ENSMUSG00000024902	Mrpl11	0.125388851	0.0498823	ENSMUSG00000027649	Ctnnbl1	0.134394828	0.0326906
ENSMUSG00000015092	Edf1	0.125446839	0.0316049	ENSMUSG00000020471	Pold2	0.134484763	0.0116886
ENSMUSG00000031592	Pcm1	0.125488818	0.0147502	ENSMUSG00000025794	Rpl14	0.13498303	1.28E-08
ENSMUSG00000020224	Llph	0.125684544	0.0303889	ENSMUSG00000048874	Phf3	0.135041128	0.0041596
ENSMUSG00000003038	Hmgn2	0.126120465	0.0069234	ENSMUSG00000034675	Dbn1	0.135219816	0.0477538
ENSMUSG00000020484	Xbp1	0.126129728	0.038761	ENSMUSG00000027379	Bub1	0.135238867	0.0031933
ENSMUSG00000024844	Banf1	0.126192172	0.0025974	ENSMUSG00000036323	Srp72	0.135322666	0.00029
ENSMUSG00000005575	Ube2m	0.126390188	0.0018812	ENSMUSG00000001761	Smo	0.135409617	0.0004287
ENSMUSG00000028309	Rnf20	0.126699447	0.0042551	ENSMUSG00000008429	Herpud2	0.135427553	0.0497853
ENSMUSG00000037300	Ttc13	0.126729837	0.0250781	ENSMUSG00000019777	Hdac2	0.135464353	0.0002396
ENSMUSG00000049327	Setd8	0.126813127	0.0001956	ENSMUSG00000076431	Sox4	0.135669129	0.0112557
ENSMUSG00000099835	Gm29668	0.126951537	0.0380828	ENSMUSG00000074305	Peak1	0.135795874	0.0390146
ENSMUSG00000039523	Cep104	0.127024173	0.0328123	ENSMUSG00000040043	Rbms2	0.135834585	0.0085927
ENSMUSG00000036199	Ndufa13	0.127080338	0.049446	ENSMUSG00000036371	Serbp1	0.135942146	1.31E-07
ENSMUSG00000019977	Hbs1l	0.127160367	0.0161994	ENSMUSG00000022201	Zfr	0.136035295	0.0001173
ENSMUSG00000032621	Srek1	0.127196238	0.0466077	ENSMUSG00000057177	Gsk3a	0.136357549	0.0118954
ENSMUSG00000079139	Gm4204	0.127302398	0.007611	ENSMUSG00000025266	Gnl3l	0.136474892	0.0013272
ENSMUSG00000037876	Jmjd1c	0.127406651	0.0170234	ENSMUSG00000036273	Lrrk2	0.136598265	0.006963
ENSMUSG00000027774	Gfm1	0.127505585	0.0023129	ENSMUSG00000002233	Rhoc	0.136681356	0.0007455
ENSMUSG00000026305	Lrrfip1	0.127632858	6.14E-05	ENSMUSG00000024290	Rock1	0.136705854	0.0152188
ENSMUSG00000026944	Abca2	0.127817779	0.0230512	ENSMUSG00000002010	Idh3g	0.136759461	0.0026909
ENSMUSG00000005609	Ctr9	0.127846903	0.0102166	ENSMUSG00000051586	Mical3	0.136777811	0.0429808
ENSMUSG00000039218	Srrm2	0.127910101	4.79E-06	ENSMUSG00000028496	Mllt3	0.136991982	0.0201445
ENSMUSG00000059208	Hnrnpm	0.127965233	1.29E-05	ENSMUSG00000006941	Eif1b	0.137270362	0.0270841
ENSMUSG00000029571	Tmem106b	0.128034286	0.0472484	ENSMUSG00000019841	Rev3l	0.137464319	0.0385201
ENSMUSG00000022141	Nipbl	0.128053209	0.0137965	ENSMUSG00000056091	St3gal5	0.137492606	0.0070791
ENSMUSG00000027104	Atf2	0.128058646	0.040428	ENSMUSG00000037013	Ss18	0.137537131	0.0015602
ENSMUSG00000029761	Cald1	0.128180758	0.000643	ENSMUSG00000027111	Itga6	0.137540927	5.14E-06
ENSMUSG00000021427	Ssr1	0.128401298	0.0002648	ENSMUSG00000023272	Creld2	0.137588475	0.0054145
ENSMUSG00000031502	Col4a1	0.12840472	1.21E-06	ENSMUSG00000049751	Rpl36al	0.137781617	0.0003016
ENSMUSG00000021244	Ylpm1	0.128428643	0.0166114	ENSMUSG00000002102	Psmc3	0.137936871	0.0001616
ENSMUSG00000050379	Sept6	0.128513043	0.0480417	ENSMUSG00000009575	Cbx5	0.137964363	5.69E-06
ENSMUSG00000007050	Lsm2	0.128733342	0.0351219	ENSMUSG00000041890	Git2	0.138020683	0.0098288
ENSMUSG00000031358	Msl3	0.128815196	0.0295537	ENSMUSG00000029422	Rsrc2	0.138036016	0.0031421
ENSMUSG00000061306	Slc38a10	0.128857107	0.0129105	ENSMUSG00000036752	Tubb4b	0.138464973	3.66E-05
ENSMUSG00000033623	Pcgf3	0.128885667	0.0104282	ENSMUSG00000095180	Rhox5	0.138764567	1.11E-06
ENSMUSG00000034210	Efcab14	0.129076485	0.0434964	ENSMUSG00000031393	Mecp2	0.138861794	0.0173217
ENSMUSG00000026490	Cdc42bpa	0.129128264	0.0157628	ENSMUSG00000001280	Sp1	0.139021714	0.0007734
ENSMUSG00000042487	Leo1	0.12930591	0.0267984	ENSMUSG00000068747	Sort1	0.139036413	0.0102469
ENSMUSG00000021215	Net1	0.12939562	0.0211326	ENSMUSG00000007080	Pole	0.1392423	0.0018596
ENSMUSG00000000605	Clcn4-2	0.129413625	0.0447158	ENSMUSG00000061665	Cd2ap	0.13935145	0.0035471
ENSMUSG00000038482	Tfdp1	0.129600293	0.0015243	ENSMUSG00000055320	Tead1	0.139411617	0.0043355
ENSMUSG00000036026	Tmem63b	0.12966142	0.0052959	ENSMUSG00000024908	Ppp6r3	0.13948439	0.0004241
ENSMUSG00000026965	Anapc2	0.129982995	0.0428731	ENSMUSG00000025743	Sdc3	0.139560675	3.28E-05
ENSMUSG00000039765	Cc2d2a	0.130222562	0.0467708	ENSMUSG00000025261	Huwe1	0.139676739	2.24E-06
ENSMUSG00000028759	Hp1bp3	0.130249844	0.0042839	ENSMUSG00000066406	Akap13	0.139700536	0.0087386
ENSMUSG00000094635	Gm7104	0.130278654	0.0255782	ENSMUSG00000071655	Ubxn1	0.139785804	0.0012969

Gene		Log_2 Fold Change	pValue	Gene		Log_2 Fold Change	pValue
ENSMUSG00000071054	Safb	0.139797979	0.0017282	ENSMUSG00000022186	Oxct1	0.148608104	1.17E-06
ENSMUSG00000027746	Ufm1	0.140016836	0.0271165	ENSMUSG00000022360	Atad2	0.14865109	4.33E-06
ENSMUSG00000025130	P4hb	0.140057756	8.33E-08	ENSMUSG00000035093	Secisbp2l	0.148745467	0.0004838
ENSMUSG00000022663	Atg3	0.140081806	0.0453487	ENSMUSG00000036372	Tmem258	0.148859094	0.0305125
ENSMUSG00000031221	Igbp1	0.140251433	0.0152769	ENSMUSG00000039108	Lsm14b	0.149109391	0.010006
ENSMUSG00000040322	Slc25a24	0.1402988	0.003533	ENSMUSG00000021500	Ddx46	0.14918462	0.0001154
ENSMUSG00000021760	Gpx8	0.140551759	0.0257509	ENSMUSG00000024393	Prrc2a	0.149248556	3.39E-10
ENSMUSG00000030779	Rbbp6	0.140829765	0.0015401	ENSMUSG00000056201	Cfl1	0.149646912	1.76E-11
ENSMUSG00000029657	Hsph1	0.140838784	4.53E-05	ENSMUSG00000003316	Glg1	0.1496816	0.0001691
ENSMUSG00000035493	Tgfbi	0.140997033	4.64E-05	ENSMUSG00000026730	Pter	0.14983529	0.039708
ENSMUSG00000022377	Asap1	0.141440126	0.0009305	ENSMUSG00000020823	Sec14l1	0.149843193	0.0091882
ENSMUSG00000022536	Glyr1	0.141523265	0.0003087	ENSMUSG00000025878	Uimc1	0.150095909	0.0343767
ENSMUSG00000048087	Gm4737	0.14154931	0.0417633	ENSMUSG00000001173	Ocrl	0.150099037	0.0182561
ENSMUSG00000030315	Vgll4	0.14171861	0.0151784	ENSMUSG00000006398	Cdc20	0.150115984	6.11E-05
ENSMUSG00000025224	Gbf1	0.141898639	0.0038872	ENSMUSG00000004099	Dnmt1	0.150146038	1.11E-06
ENSMUSG00000029552	Tes	0.142300145	0.0001813	ENSMUSG00000024302	Dtna	0.150163828	0.0298868
ENSMUSG00000041697	Cox6a1	0.142334178	0.0004916	ENSMUSG00000039585	Myo9a	0.15022653	0.0358941
ENSMUSG00000036591	Arhgap21	0.14237035	0.0216215	ENSMUSG00000037062	Sh3glb1	0.150855013	4.03E-05
ENSMUSG00000028873	Cdca8	0.142386151	0.0111093	ENSMUSG00000003458	Ncstn	0.150901038	0.0060215
ENSMUSG00000035851	Ythdc1	0.142568606	0.0067534	ENSMUSG00000030515	Tarsl2	0.150915136	0.0458389
ENSMUSG00000019179	Mdh2	0.142690931	1.56E-07	ENSMUSG00000029632	Ndufa4	0.150956818	0.0010878
ENSMUSG00000026134	Prim2	0.142924459	0.0146824	ENSMUSG00000027984	Hadh	0.151000062	0.0080388
ENSMUSG00000059495	Arhgef12	0.142949039	0.0007866	ENSMUSG00000067713	Prkag1	0.151027558	0.0407571
ENSMUSG00000004530	Coro1c	0.143024323	5.99E-05	ENSMUSG00000025781	Atp5c1	0.151036407	1.15E-05
ENSMUSG00000020321	Mdh1	0.143176309	0.0004871	ENSMUSG00000036550	Cnot1	0.151380243	8.71E-05
ENSMUSG00000032382	Snx1	0.143397551	0.0142677	ENSMUSG00000014551	Mrps25	0.151852365	0.0309716
ENSMUSG00000014504	Srp19	0.143774776	0.0258287	ENSMUSG00000004535	Tax1bp1	0.1521482	0.0002462
ENSMUSG00000028334	Nans	0.143908888	0.0061902	ENSMUSG00000039016	Timm8b	0.152216117	0.0263496
ENSMUSG00000023923	Tbc1d5	0.14394232	0.0183484	ENSMUSG00000043262	Uevld	0.152378505	0.038264
ENSMUSG00000042066	Tmcc2	0.14395877	0.0271136	ENSMUSG00000029017	Pmpcb	0.152550823	0.0022598
ENSMUSG00000018377	Vezf1	0.144454773	0.0197888	ENSMUSG00000055762	Eef1d	0.152681857	6.70E-07
ENSMUSG00000052539	Magi3	0.144539416	0.0488126	ENSMUSG00000005583	Mef2c	0.152892169	0.0076012
ENSMUSG00000055862	Izumo4	0.144606367	0.0423943	ENSMUSG00000050965	Prkca	0.152995945	0.0441183
ENSMUSG00000003039	Fam32a	0.144652109	0.0157117	ENSMUSG00000033565	Rbfox2	0.15305204	0.0014363
ENSMUSG00000003873	Bax	0.144783528	0.0014701	ENSMUSG00000028289	Epha7	0.153150067	0.0082868
ENSMUSG00000034109	Golim4	0.145113795	0.0019041	ENSMUSG00000006589	Aprt	0.153397266	0.00149
ENSMUSG00000022451	Twf1	0.145185546	0.0002876	ENSMUSG00000056050	Mia3	0.153512495	0.0088129
ENSMUSG00000000346	Dazap2	0.145258005	0.0002484	ENSMUSG00000020571	Pdia6	0.15360724	1.71E-08
ENSMUSG00000038708	Golga4	0.145390661	0.0029418	ENSMUSG00000060126	Tpt1	0.153657389	2.71E-08
ENSMUSG00000061119	Prcp	0.145659673	0.0418935	ENSMUSG00000042272	Sestd1	0.153750259	0.0468408
ENSMUSG00000020516	Rps6kb1	0.14572436	0.0022848	ENSMUSG00000004085	Zak	0.1538047	0.0395287
ENSMUSG00000034349	Smc4	0.145798221	5.17E-06	ENSMUSG00000030551	Nr2f2	0.153841283	0.0214851
ENSMUSG00000066979	Bub3	0.145808846	0.0002364	ENSMUSG00000057789	Bak1	0.154104697	0.0033584
ENSMUSG00000039298	Cdk5rap2	0.145800986	0.0202335	ENSMUSG00000025278	Flnb	0.154301211	6.04E-06
ENSMUSG00000024048	Myl12a	0.145829543	8.81E-06	ENSMUSG00000037400	Atp11b	0.154570817	0.0006201
ENSMUSG00000058407	Txndc9	0.145897288	0.0063802	ENSMUSG00000033307	Mif	0.154655989	0.039976
ENSMUSG00000004945	Tmem242	0.146016834	0.04236	ENSMUSG00000033671	Cep350	0.154736105	0.0403938
ENSMUSG00000039197	Adk	0.146196706	0.000828	ENSMUSG00000027533	Fabp5	0.154811838	0.0011716
ENSMUSG00000021156	Zmynd11	0.146343836	0.0053764	ENSMUSG00000034566	Atp5h	0.154812312	0.000493
ENSMUSG00000062353	Gm15772	0.146408074	0.0003895	ENSMUSG00000045039	Megf8	0.154831691	0.0003918
ENSMUSG00000025885	Myo5b	0.146438462	0.0001853	ENSMUSG00000048000	Gigyf2	0.154840719	0.0010994
ENSMUSG00000045180	Shroom2	0.146560874	0.0024172	ENSMUSG00000002778	Kdelr1	0.154872265	0.0032734
ENSMUSG00000029201	Ugdh	0.14674139	1.98E-05	ENSMUSG00000027010	Slc25a12	0.154878934	0.019799
ENSMUSG00000002885	Adgre5	0.146752213	0.0498719	ENSMUSG00000053931	Cnn3	0.155260551	7.46E-08
ENSMUSG00000024483	Ankhd1	0.146952316	0.0032249	ENSMUSG00000034254	Agpat1	0.155261196	0.0017065
ENSMUSG00000029106	Add1	0.146960678	0.001829	ENSMUSG00000037563	Rps16	0.15527597	1.95E-10
ENSMUSG00000027663	Zmat3	0.147035998	0.0150088	ENSMUSG00000027597	Ahcy	0.155323575	3.70E-05
ENSMUSG00000030342	Cd9	0.147152366	0.0016429	ENSMUSG00000052423	B4galt3	0.155425097	0.0439661
ENSMUSG00000020687	Cdc27	0.147352591	7.71E-05	ENSMUSG00000013698	Pea15a	0.155473065	1.27E-05
ENSMUSG00000027361	Gabpb1	0.147373373	0.0406741	ENSMUSG00000026039	Sgol2a	0.155655216	0.0467453
ENSMUSG00000042508	Dmtf1	0.147410007	0.0207219	ENSMUSG00000025810	Nrp1	0.155763166	0.0027075
ENSMUSG00000068284	Gm608	0.147461589	0.0473369	ENSMUSG00000027624	Epb4.1l1	0.155766732	0.0002819
ENSMUSG00000058318	Phf21a	0.147480973	0.0427727	ENSMUSG00000037712	Fermt2	0.155908928	0.0009265
ENSMUSG00000017485	Top2b	0.147491156	0.0021569	ENSMUSG00000028194	Ddah1	0.155972633	0.0008979
ENSMUSG00000041220	Elovl6	0.14757811	0.0194318	ENSMUSG00000038384	Setd1b	0.156021086	0.0400215
ENSMUSG00000034681	Rnps1	0.147610754	0.000268	ENSMUSG00000025758	Plk4	0.156225988	0.001323
ENSMUSG00000032582	Rbm6	0.147807327	0.0048627	ENSMUSG00000004364	Cul3	0.156239746	7.63E-05
ENSMUSG00000006931	P3h4	0.147962032	0.0033747	ENSMUSG00000038838	Vars2	0.156267905	0.0463054
ENSMUSG00000005374	Tbl2	0.14803112	0.0165107	ENSMUSG00000033788	Dysf	0.156386121	0.0348696
ENSMUSG00000040761	Spen	0.148049443	0.0073554	ENSMUSG00000030451	Herc2	0.156423865	0.0030312
ENSMUSG00000048668	Rhno1	0.148110208	0.0274508	ENSMUSG00000046574	Prr12	0.156697353	0.0090495
ENSMUSG00000041570	Camsap2	0.14811997	0.0090966	ENSMUSG00000008976	Gabpa	0.156744967	0.0057683
ENSMUSG00000026872	Zeb2	0.148149602	0.0006506	ENSMUSG00000028613	Lrp8	0.156838066	0.0054028
ENSMUSG00000022433	Csnk1e	0.148172345	0.0122521	ENSMUSG00000021830	Txndc16	0.156956064	0.0112712
ENSMUSG00000041702	Btbd7	0.148329785	0.0184095	ENSMUSG00000041235	Chd7	0.156971747	0.0326103
ENSMUSG00000058881	Zfp516	0.148356418	0.0169036	ENSMUSG00000024725	Ostf1	0.157112845	0.0269269
ENSMUSG00000028245	Nsmaf	0.148377487	0.0090967	ENSMUSG00000007815	Rhoa	0.157121229	1.92E-07
ENSMUSG00000068270	Shroom4	0.148459761	0.018685	ENSMUSG00000047547	Cltb	0.157318654	0.0067156
ENSMUSG00000020821	Kif1c	0.148483771	0.0001054	ENSMUSG00000030770	Parva	0.157319222	9.93E-05
ENSMUSG00000057000	Nxf3	0.14851507	0.0125335	ENSMUSG00000034902	Pip5k1c	0.157425935	0.0066964
ENSMUSG00000032570	Atp2c1	0.148565663	0.00212	ENSMUSG00000040204	2810417H13Rik	0.157772452	0.0002777

Gene		Log_2 Fold Change	pValue	Gene		Log_2 Fold Change	pValue
ENSMUSG00000028394	Pole3	0.157807015	0.0051704	ENSMUSG00000041258	Zfp236	0.167039653	0.0055949
ENSMUSG00000037742	Eef1a1	0.157935536	1.60E-18	ENSMUSG00000020190	Mknk2	0.167079701	0.0006427
ENSMUSG00000026547	Tagln2	0.157996949	4.33E-07	ENSMUSG00000082895	Rpsa-ps9	0.167102994	0.0286602
ENSMUSG00000058600	Rpl30	0.158162824	1.56E-07	ENSMUSG00000031812	Map1lc3b	0.167297302	0.0299668
ENSMUSG00000101625	Gm29371	0.158216944	0.0366892	ENSMUSG00000021578	Ccdc127	0.167301734	0.0234009
ENSMUSG00000026116	Tmem131	0.158248314	0.0009384	ENSMUSG00000032479	Map4	0.167372713	6.10E-08
ENSMUSG00000085208	Brip1os	0.158285835	0.0015885	ENSMUSG00000019978	Epb4.1l2	0.167410955	1.83E-08
ENSMUSG00000022338	Eny2	0.158350359	0.004184	ENSMUSG00000037234	Hook3	0.167444876	0.0149629
ENSMUSG00000006005	Tpr	0.158373017	2.67E-06	ENSMUSG00000075229	Ccdc58	0.167554866	0.009904
ENSMUSG00000026496	Parp1	0.158603601	2.93E-06	ENSMUSG00000038872	Zfhx3	0.167720828	0.0498327
ENSMUSG00000006705	Pknox1	0.158690553	0.0273195	ENSMUSG00000031540	Kat6a	0.167763294	0.0005077
ENSMUSG00000039952	Dag1	0.1589132	2.17E-07	ENSMUSG00000022889	Mrpl39	0.167894532	0.0335496
ENSMUSG00000045128	Rpl18a	0.158978826	2.53E-09	ENSMUSG00000037860	Aim2	0.168009197	0.0387454
ENSMUSG00000029153	Ociad2	0.158998171	0.03576	ENSMUSG00000038241	Cep250	0.168135401	0.0063948
ENSMUSG00000034485	Uaca	0.159060696	7.43E-08	ENSMUSG00000033373	Fntb	0.168322655	0.0261656
ENSMUSG00000020492	Ska2	0.159099806	0.013762	ENSMUSG00000032547	Ryk	0.168505529	0.0001535
ENSMUSG00000020580	Rock2	0.15924297	2.31E-06	ENSMUSG00000070923	Klhl9	0.168516441	0.0030845
ENSMUSG00000022261	Sdc2	0.159367259	0.0265675	ENSMUSG00000044155	Lsm8	0.16858891	0.0050945
ENSMUSG00000023921	Mut	0.159392575	0.0292684	ENSMUSG00000032301	Psma4	0.168793568	2.59E-05
ENSMUSG00000020982	Nemf	0.159395873	0.0021723	ENSMUSG00000024966	Stip1	0.168861119	1.00E-10
ENSMUSG00000024960	Plcb3	0.159448841	0.0001815	ENSMUSG00000062169	Cnih4	0.16896292	0.0018485
ENSMUSG00000041974	Spidr	0.159514044	0.0120108	ENSMUSG00000003352	Cacnb3	0.169054955	0.009231
ENSMUSG00000029672	Fam3c	0.159752506	0.027485	ENSMUSG00000021963	Sap18	0.169149744	0.0227836
ENSMUSG00000024777	Ppp2r5b	0.159756526	0.0473973	ENSMUSG00000052516	Robo2	0.169193869	0.0469522
ENSMUSG00000022771	Ppil2	0.159911147	0.0028433	ENSMUSG00000024853	Sf3b2	0.16934295	1.25E-08
ENSMUSG00000035674	Ndufa3	0.160023888	0.0219079	ENSMUSG00000018648	Dusp14	0.169371692	0.0454705
ENSMUSG00000057738	Sptan1	0.160134748	6.76E-08	ENSMUSG00000032280	Tle3	0.169404291	0.0007072
ENSMUSG00000000600	Krit1	0.160266572	0.0316144	ENSMUSG00000029156	Sgcb	0.169543586	0.0350431
ENSMUSG00000033676	Gabrb3	0.160447948	0.0004917	ENSMUSG00000027854	Sike1	0.169602719	0.0374117
ENSMUSG00000020074	Ccar1	0.160565477	0.0001178	ENSMUSG00000028837	Psmb2	0.16982445	0.0008071
ENSMUSG00000033105	Lss	0.160698136	0.0294356	ENSMUSG00000053477	Tcf4	0.169838694	0.0005209
ENSMUSG00000045482	Trrap	0.160708432	7.99E-05	ENSMUSG00000037343	Taf2	0.169889331	0.0003332
ENSMUSG00000041203	2310036O22Rik	0.161143572	0.0100954	ENSMUSG00000054405	Dnajc8	0.169898013	0.0006107
ENSMUSG00000031154	Otud5	0.161395193	0.0052362	ENSMUSG00000031328	Flna	0.169929779	1.30E-15
ENSMUSG00000069565	Dazap1	0.161416526	0.0003957	ENSMUSG00000038886	Man2a2	0.170177598	0.0001831
ENSMUSG00000024304	Cdh2	0.161522006	1.26E-07	ENSMUSG00000030560	Ctsc	0.170203547	0.0074577
ENSMUSG00000039536	Stau1	0.161648137	0.0006072	ENSMUSG00000069769	Msi2	0.170236194	0.0040264
ENSMUSG00000024560	Cxxc1	0.161843134	0.0111638	ENSMUSG00000038871	Bpgm	0.170245483	0.0411954
ENSMUSG00000032743	D430042O09Rik	0.162066212	0.0448313	ENSMUSG00000028800	Hdac1	0.170450396	0.0020339
ENSMUSG00000022641	Bbx	0.162071672	0.0108293	ENSMUSG00000025352	Gdf11	0.170513739	0.0277908
ENSMUSG00000084786	Ubl5	0.162073192	0.0108606	ENSMUSG00000035632	Cnot3	0.170530551	0.0004732
ENSMUSG00000031848	Lsm4	0.162088022	0.0077543	ENSMUSG00000062762	Ei24	0.170593421	0.0014577
ENSMUSG00000030987	Stim1	0.162166822	0.0278392	ENSMUSG00000031660	Brd7	0.170748537	0.0064714
ENSMUSG00000016253	Nelfcd	0.162222347	0.0119405	ENSMUSG00000037071	Scd1	0.170894788	2.18E-05
ENSMUSG00000002812	Flii	0.16229942	0.0008024	ENSMUSG00000029250	Polr2b	0.170940934	2.26E-05
ENSMUSG00000071176	Arhgef10	0.162511844	0.0253958	ENSMUSG00000035268	Pkig	0.1709808	0.0383725
ENSMUSG00000061755	Bod1l	0.16260485	0.0014773	ENSMUSG00000024807	Syvn1	0.171007729	0.0110918
ENSMUSG00000039156	Stim2	0.162779918	0.0219345	ENSMUSG00000063694	Cycs	0.171053173	3.18E-05
ENSMUSG00000032253	Phip	0.162850142	0.0045726	ENSMUSG00000009030	Pdcl	0.171074951	0.0457174
ENSMUSG00000053898	Ech1	0.162985972	0.0307481	ENSMUSG00000031400	G6pdx	0.171110996	0.0010276
ENSMUSG00000027936	Crtc2	0.16299098	0.022696	ENSMUSG00000021824	Ap3m1	0.171136017	0.0010782
ENSMUSG00000038463	Olfml2b	0.163063681	0.003469	ENSMUSG00000035107	Dcbld2	0.171250392	0.0069767
ENSMUSG00000024346	Pfdn1	0.1630876	0.0005298	ENSMUSG00000107176	RP23-263B18.4	0.171766633	0.0015497
ENSMUSG00000040850	Psme4	0.163145364	0.0001935	ENSMUSG00000022283	Pabpc1	0.171853664	6.57E-19
ENSMUSG00000039050	Osbpl2	0.163295502	0.0195734	ENSMUSG00000036980	Taf6	0.171861949	0.0075172
ENSMUSG00000055024	Ep300	0.163301651	0.0004833	ENSMUSG00000005442	Cic	0.171882141	5.22E-07
ENSMUSG00000027742	Cog6	0.163619447	0.0215556	ENSMUSG00000036023	Parp2	0.171897873	0.0437864
ENSMUSG00000069939	Gm12070	0.163838284	0.0013249	ENSMUSG00000054452	Aes	0.171902948	9.72E-07
ENSMUSG00000025395	Prim1	0.163897161	0.0023097	ENSMUSG00000028675	Pnrc2	0.171962503	0.0338615
ENSMUSG00000039159	Ube2h	0.164035661	0.025607	ENSMUSG00000028080	Lrba	0.172126827	0.007945
ENSMUSG00000033769	Exoc6b	0.164182345	0.0086411	ENSMUSG00000031954	Cfdp1	0.172131778	0.0004135
ENSMUSG00000041238	Rbbp8	0.164259931	0.0070562	ENSMUSG00000026238	Ptma	0.172181572	3.12E-11
ENSMUSG00000017466	Timp2	0.164366327	8.64E-05	ENSMUSG00000021134	Srsf5	0.17221561	1.04E-05
ENSMUSG00000042323	Pbrm1	0.164532556	0.0005842	ENSMUSG00000030726	Pold3	0.172375251	0.0078215
ENSMUSG00000050953	Gja1	0.16483811	7.58E-06	ENSMUSG00000022312	Eif3h	0.17239944	2.95E-08
ENSMUSG00000071708	Sms	0.164977915	0.0105262	ENSMUSG00000053119	Chmp3	0.172410762	0.0006223
ENSMUSG00000023015	Racgap1	0.16503218	9.08E-08	ENSMUSG00000022635	Zcrb1	0.172457521	0.000989
ENSMUSG00000003402	Prkcsh	0.165091789	4.63E-05	ENSMUSG00000022841	Ap2m1	0.172823832	2.75E-09
ENSMUSG00000030291	Med21	0.165290362	0.0235095	ENSMUSG00000038291	Snx25	0.172975385	0.0439131
ENSMUSG00000020964	Sel1l	0.165510264	0.0003576	ENSMUSG00000031479	Vps36	0.173018543	0.0146236
ENSMUSG00000003778	Brd8	0.165519213	0.0029291	ENSMUSG00000002997	Prkar2b	0.173221918	0.0005958
ENSMUSG00000027171	Prrg4	0.165664113	0.0454308	ENSMUSG00000012483	Rpa3	0.173252094	0.039959
ENSMUSG00000028161	Ppp3ca	0.166028749	0.0004817	ENSMUSG00000003865	Gys1	0.173370676	0.0099504
ENSMUSG00000034390	Cmip	0.166042805	0.0294169	ENSMUSG00000031226	Pbdc1	0.173611065	0.0001269
ENSMUSG00000070343	Gm10288	0.166059257	0.0218379	ENSMUSG00000019539	Rcn3	0.173748798	0.0109752
ENSMUSG00000002996	Hbp1	0.166128379	0.0341128	ENSMUSG00000039347	Atp6v0e2	0.173782057	0.0031866
ENSMUSG00000029185	Fam114a1	0.16618632	0.0229186	ENSMUSG00000031216	Stard8	0.173899692	0.0183224
ENSMUSG00000028246	Faxc	0.166496679	0.0395362	ENSMUSG00000054272	Zscan4c	0.173929517	0.0199295
ENSMUSG00000004096	Cwc15	0.166704963	0.0003793	ENSMUSG00000042670	Immp1l	0.173959299	0.0297571
ENSMUSG00000037679	Inf2	0.166909907	4.49E-06	ENSMUSG00000048930	Tada3	0.173986783	0.0485758
ENSMUSG00000028581	Laptm5	0.166971987	0.0270973	ENSMUSG00000020288	Ahsa2	0.174010157	0.0133272

Gene		Log_2 Fold Change	pValue	Gene		Log_2 Fold Change	pValue
ENSMUSG00000030516	Tjp1	0.174041682	5.35E-06	ENSMUSG00000078429	Ctdsp2	0.181899196	0.000152
ENSMUSG00000021248	Tmed10	0.174071848	3.05E-08	ENSMUSG00000041164	Zmiz2	0.182214922	7.84E-05
ENSMUSG00000063659	Zbtb18	0.174123953	0.0063556	ENSMUSG00000027883	Gpsm2	0.182297549	0.0043246
ENSMUSG00000040363	Bcor	0.174134015	0.014422	ENSMUSG00000018287	Spag7	0.182405877	0.0041874
ENSMUSG00000028821	Syf2	0.174420886	0.0176491	ENSMUSG00000035934	Pknox2	0.182500931	0.0105282
ENSMUSG00000000731	Aire	0.174453339	0.0495156	ENSMUSG00000027326	Casc5	0.182601157	0.0014858
ENSMUSG00000031278	Acsl4	0.174458051	1.16E-05	ENSMUSG00000029122	Evc	0.182609338	0.0171131
ENSMUSG00000042712	Wbp5	0.174482238	0.0017808	ENSMUSG00000040462	Os9	0.182678124	0.0002132
ENSMUSG00000030067	Foxp1	0.174526791	0.0039998	ENSMUSG00000023885	Thbs2	0.182689322	4.46E-11
ENSMUSG00000060206	Zfp462	0.174545926	3.57E-05	ENSMUSG00000022820	Ndufb4	0.182696642	0.0046303
ENSMUSG00000032512	Wdr48	0.174567384	0.0026689	ENSMUSG00000028433	Ubap2	0.183109955	8.73E-08
ENSMUSG00000025228	Actr1a	0.17460306	4.40E-05	ENSMUSG00000078453	Abracl	0.183286953	0.0146221
ENSMUSG00000021114	Atp6v1d	0.174695117	0.0032381	ENSMUSG00000043940	Wdfy3	0.183348422	0.0008608
ENSMUSG00000000759	Tubgcp3	0.174696671	0.0080468	ENSMUSG00000070733	Fryl	0.183514445	0.0176058
ENSMUSG00000064373	Sepp1	0.174697169	0.032478	ENSMUSG00000025040	Fundc1	0.183627004	0.0249915
ENSMUSG00000068184	Ndufaf2	0.174722418	0.0464055	ENSMUSG00000025260	Hsd17b10	0.183680998	0.0049212
ENSMUSG00000029993	Nfu1	0.174819741	0.0296409	ENSMUSG00000050668	Gpatch11	0.183837135	0.0477343
ENSMUSG00000039967	Zfp292	0.17487039	0.0086011	ENSMUSG00000026585	Kifap3	0.18384813	0.0063119
ENSMUSG00000035901	Dennd5a	0.17517495	3.87E-07	ENSMUSG00000027223	Mapk8ip1	0.183980332	0.0353867
ENSMUSG00000075232	Amd1	0.175227031	1.01E-06	ENSMUSG00000019362	D8Ertd738e	0.184377334	0.0065479
ENSMUSG00000027654	Fam83d	0.175341562	0.0268122	ENSMUSG00000024542	Cep192	0.184446963	0.0006791
ENSMUSG00000050148	Ubqln2	0.175376198	0.0098084	ENSMUSG00000034593	Myo5a	0.184474673	7.75E-09
ENSMUSG00000014402	Tsg101	0.175605246	0.0012201	ENSMUSG00000069729	Arid1b	0.184492637	0.0075474
ENSMUSG00000028849	Map7d1	0.17566786	0.0001652	ENSMUSG00000028998	Tomm7	0.184657335	0.0015214
ENSMUSG00000006390	Elovl1	0.175720025	0.003612	ENSMUSG00000027634	Ndrg3	0.184702916	0.0009835
ENSMUSG00000031668	Eif2ak3	0.175921804	0.0399451	ENSMUSG00000063077	Kif1b	0.184715924	0.0003384
ENSMUSG00000019813	Cep57l1	0.176202911	0.0322127	ENSMUSG00000028419	Chmp5	0.184819877	0.0005437
ENSMUSG00000017716	Birc5	0.176417635	9.40E-05	ENSMUSG00000049047	Armcx3	0.185037696	0.0114872
ENSMUSG00000018474	Chd3	0.176492897	1.47E-05	ENSMUSG00000019927	Ube2d1	0.18535066	0.0256758
ENSMUSG00000031441	Atp11a	0.176497895	0.0111106	ENSMUSG00000030591	Psmd8	0.185501857	3.49E-05
ENSMUSG00000038602	Slc35f1	0.176563609	2.69E-05	ENSMUSG00000036959	Bcorl1	0.186011872	0.0396159
ENSMUSG00000023050	Map3k12	0.176571583	0.0442507	ENSMUSG00000030417	Pdcd5	0.18618861	0.0002117
ENSMUSG00000042308	Setd1a	0.176580488	0.0175686	ENSMUSG00000019971	Cep290	0.186366234	0.0202265
ENSMUSG00000040990	Sh3kbp1	0.176635357	0.0005932	ENSMUSG00000028032	Papss1	0.186372095	6.80E-05
ENSMUSG00000035637	Grhpr	0.176726362	0.0405435	ENSMUSG00000039178	Tbc1d19	0.186424273	0.0408226
ENSMUSG00000039735	Fnbp1l	0.176747257	0.0002942	ENSMUSG00000028068	Iqgap3	0.186591872	0.0009383
ENSMUSG00000028034	Fubp1	0.176838388	1.05E-07	ENSMUSG00000032402	Smad3	0.186674405	0.0084644
ENSMUSG00000042918	Mamstr	0.177025071	0.0493836	ENSMUSG00000043154	Ppp2r3a	0.186762349	0.0320215
ENSMUSG00000040591	1110051M20Rik	0.177115271	0.0338044	ENSMUSG00000042978	Sbk1	0.18676571	0.0288262
ENSMUSG00000060743	H3f3a	0.177396098	3.13E-05	ENSMUSG00000033065	Pfkm	0.1868224	0.0019976
ENSMUSG00000041957	Pkp2	0.17779982	0.0020866	ENSMUSG00000060373	Hnrnpc	0.187027108	1.67E-10
ENSMUSG00000057841	Rpl32	0.177972354	1.05E-15	ENSMUSG00000021067	Sav1	0.187066614	0.0010822
ENSMUSG00000027187	Cat	0.178040609	0.0199224	ENSMUSG00000034621	Gpatch8	0.187384281	0.0003847
ENSMUSG00000060591	Ifitm2	0.178127988	0.0001623	ENSMUSG00000022205	Sub1	0.187492386	7.28E-06
ENSMUSG00000032481	Smarcc1	0.178265006	3.93E-08	ENSMUSG00000030718	Ppme1	0.187529013	0.0007128
ENSMUSG00000091625	Lsm5	0.178393476	0.029313	ENSMUSG00000017421	Zfp207	0.187655568	2.78E-08
ENSMUSG00000024099	Ndufv2	0.178440903	0.0001049	ENSMUSG00000031835	Mbtps1	0.187847923	2.70E-05
ENSMUSG00000021693	Kif2a	0.178444932	0.0033251	ENSMUSG00000060090	Rp2h	0.187911013	0.0134577
ENSMUSG00000001767	Crnkl1	0.178507542	0.0063121	ENSMUSG00000021318	Gli3	0.188066056	0.0084007
ENSMUSG00000048756	Foxo3	0.178559745	0.0187452	ENSMUSG00000061981	Flot2	0.188086238	0.0001826
ENSMUSG00000033589	Reep4	0.178670463	0.0223962	ENSMUSG00000042462	Dctpp1	0.18809863	0.0030496
ENSMUSG00000059409	Ppp2r5d	0.178714736	8.94E-05	ENSMUSG00000020111	Micu1	0.18828797	0.0096362
ENSMUSG00000030172	Erc1	0.179139494	0.0093204	ENSMUSG00000039031	Arhgap18	0.188296665	0.0285104
ENSMUSG00000028410	Dnaja1	0.17923424	2.35E-07	ENSMUSG00000004266	Ptpn6	0.188347757	0.010974
ENSMUSG00000012076	Brms1l	0.179272209	0.005722	ENSMUSG00000026239	Pde6d	0.188433856	0.009996
ENSMUSG00000017404	Rpl19	0.179318764	4.98E-15	ENSMUSG00000040481	Bptf	0.188450702	1.88E-06
ENSMUSG00000031229	Atrx	0.179341457	1.65E-05	ENSMUSG00000031996	Aplp2	0.188476851	9.99E-08
ENSMUSG00000041037	Irgq	0.17950209	0.0233176	ENSMUSG00000035696	Rnf38	0.18850429	0.0014152
ENSMUSG00000025151	Maged1	0.179553468	2.15E-09	ENSMUSG00000028538	St3gal3	0.18851307	0.0154037
ENSMUSG00000038374	Rbm8a	0.179698837	0.0001911	ENSMUSG00000027254	Map1a	0.188584164	0.0001057
ENSMUSG00000021366	Hivep1	0.180038281	0.0350503	ENSMUSG00000026571	Dcaf6	0.188593035	0.012219
ENSMUSG00000032231	Anxa2	0.180045818	8.46E-16	ENSMUSG00000061273	Mmgt1	0.188606482	9.69E-05
ENSMUSG00000001158	Snrnp27	0.180146436	0.0067745	ENSMUSG00000024942	Capn1	0.188699212	0.0315162
ENSMUSG00000033916	Chmp2a	0.18019421	0.0008654	ENSMUSG00000003037	Rab8a	0.188741429	0.0031234
ENSMUSG00000025745	Hadha	0.180218495	7.18E-06	ENSMUSG00000000197	Nalcn	0.189082122	0.0181187
ENSMUSG00000006498	Ptbp1	0.180221497	7.83E-11	ENSMUSG00000041219	Arhgap11a	0.189167358	4.24E-05
ENSMUSG00000030203	Dusp16	0.180300989	0.0268364	ENSMUSG00000021288	Klc1	0.189229455	1.87E-05
ENSMUSG00000029191	Rfc1	0.180340679	8.97E-06	ENSMUSG00000025103	Btbd1	0.189249368	0.004422
ENSMUSG00000022024	Sugt1	0.180356144	0.0497911	ENSMUSG00000024947	Men1	0.189265019	0.0014203
ENSMUSG00000068882	Ssb	0.180494415	2.57E-08	ENSMUSG00000035246	Pcyt1b	0.189338985	0.0021045
ENSMUSG00000032349	Elovl5	0.180623945	0.0001379	ENSMUSG00000033632	AW554918	0.189342372	0.0475065
ENSMUSG00000024666	Tmem138	0.180760247	0.0429302	ENSMUSG00000056073	Grik2	0.189505082	0.0475214
ENSMUSG00000054717	Hmgb2	0.180840515	1.50E-06	ENSMUSG00000005470	Asf1b	0.189649183	0.002962
ENSMUSG00000054196	Cthrc1	0.18085966	0.0037217	ENSMUSG00000028402	Mpdz	0.189670925	0.0104878
ENSMUSG00000021670	Hmgcr	0.180886865	0.0119638	ENSMUSG00000055053	Nfic	0.189683714	1.16E-07
ENSMUSG00000024283	Wac	0.181035795	0.0001705	ENSMUSG00000030246	Ldhb	0.189767074	0.0041886
ENSMUSG00000071533	Pcnp	0.181479627	0.0040311	ENSMUSG00000022322	Shcbp1	0.189824808	0.0067821
ENSMUSG00000038383	Pigu	0.181495025	0.0047334	ENSMUSG00000063787	Chchd1	0.189842602	0.0085032
ENSMUSG00000001985	Grik3	0.181584199	0.0452135	ENSMUSG00000031198	Fundc2	0.189998223	0.0011315
ENSMUSG00000002658	Gtf2f1	0.181653531	0.0001144	ENSMUSG00000021707	Dhfr	0.190439934	0.0053045
ENSMUSG00000021606	Ndufs6	0.181724084	0.0157905	ENSMUSG00000020803	Txndc17	0.190446446	0.0002165

Gene		Log_2 Fold Change	pValue	Gene		Log_2 Fold Change	pValue
ENSMUSG00000027165	B230118H07Rik	0.190559121	0.0449773	ENSMUSG00000021466	Ptch1	0.198771305	0.0020755
ENSMUSG00000039219	Arid4b	0.190583575	0.0169393	ENSMUSG00000041870	Ankrd13a	0.198924331	6.65E-05
ENSMUSG00000051579	Tceal8	0.190589208	0.0012062	ENSMUSG00000037058	Paip2	0.198970853	0.0004236
ENSMUSG00000025525	Apool	0.190608986	0.0472212	ENSMUSG00000060601	Nr1h2	0.199295319	0.0056383
ENSMUSG00000022808	Snx4	0.190637637	2.81E-05	ENSMUSG00000028248	Pnisr	0.199315556	0.000165
ENSMUSG00000071866	Ppia	0.190741252	2.57E-21	ENSMUSG00000023048	Prr13	0.199356502	0.0442097
ENSMUSG00000019066	Rab3d	0.190747716	0.0310356	ENSMUSG00000024914	Drap1	0.199491073	2.43E-05
ENSMUSG00000039234	Sec24d	0.191459564	0.0028387	ENSMUSG00000002250	Ppard	0.199517953	0.0127812
ENSMUSG00000019738	Polr2i	0.191466669	0.0263976	ENSMUSG00000041431	Ccnb1	0.199631459	2.07E-05
ENSMUSG00000037020	Wdr62	0.191734306	0.0270724	ENSMUSG00000022329	Stk3	0.199883307	0.0037001
ENSMUSG00000074457	S100a16	0.191786582	0.0146409	ENSMUSG00000068036	Mllt4	0.199993109	0.0002736
ENSMUSG00000032580	Rbm5	0.191821957	0.0004576	ENSMUSG00000030323	Ift122	0.200127425	0.0425508
ENSMUSG00000046138	9930021J03Rik	0.192060404	0.0047856	ENSMUSG00000021957	Tkt	0.200232014	5.56E-07
ENSMUSG00000032060	Cryab	0.192067627	1.07E-07	ENSMUSG00000036599	Chst12	0.200331303	0.0069438
ENSMUSG00000042548	Asxl1	0.192270352	2.14E-05	ENSMUSG00000030868	Dctn5	0.200345719	0.0036431
ENSMUSG00000020462	Cfap36	0.192276504	0.000699	ENSMUSG00000031134	Rbmx	0.200357305	5.93E-06
ENSMUSG00000042606	Hirip3	0.192388378	8.04E-05	ENSMUSG00000036561	Ppp6r2	0.200377408	0.0201388
ENSMUSG00000091337	Eid1	0.192390995	0.0002419	ENSMUSG00000031626	Sorbs2	0.200421352	0.040608
ENSMUSG00000013033	Adgrl1	0.192549068	0.0153545	ENSMUSG00000024052	Lpin2	0.200478485	0.0029369
ENSMUSG00000025823	Pdia4	0.192561363	1.71E-08	ENSMUSG00000025757	Hspa4l	0.200527025	0.0004291
ENSMUSG00000020009	Ifngr1	0.193046795	0.044466	ENSMUSG00000039844	Rapgef1	0.200529492	1.24E-06
ENSMUSG00000007987	Ift22	0.193066071	0.0284197	ENSMUSG00000025736	Jmjd8	0.200571193	0.011766
ENSMUSG00000039117	Taf4a	0.193088863	0.0075345	ENSMUSG00000033938	Ndufb7	0.200658613	0.004824
ENSMUSG00000031295	Phka2	0.19318442	0.0142605	ENSMUSG00000048922	Cdca2	0.200750381	0.0161974
ENSMUSG00000038206	Fbxo8	0.193356973	0.0408826	ENSMUSG00000047248	C2cd3	0.200782672	0.0008387
ENSMUSG00000037622	Wdtc1	0.193444349	0.0239859	ENSMUSG00000030978	Rrm1	0.201189534	2.79E-12
ENSMUSG00000022817	Itgb5	0.19344863	5.85E-05	ENSMUSG00000058558	Rpl5	0.201222668	7.73E-18
ENSMUSG00000026853	Crat	0.19345882	0.0088351	ENSMUSG00000032047	Acat1	0.201333648	0.0006945
ENSMUSG00000018501	Ncor1	0.193573461	6.92E-09	ENSMUSG00000026043	Col3a1	0.201338096	0.0003052
ENSMUSG00000005871	Apc	0.193636323	1.71E-06	ENSMUSG00000030409	Dmpk	0.201416119	0.0097724
ENSMUSG00000066551	Hmgb1	0.193718415	1.08E-09	ENSMUSG00000073702	Rpl31	0.201439662	2.89E-13
ENSMUSG00000046111	Cep295	0.193803181	0.0014156	ENSMUSG00000029762	Akr1b8	0.201506123	4.99E-05
ENSMUSG00000024220	Zfp523	0.19405209	0.0072527	ENSMUSG00000002477	Snrpd1	0.201537115	1.27E-05
ENSMUSG00000060739	Nsa2	0.194121298	0.0001646	ENSMUSG00000015478	Rnf5	0.201625604	0.0053119
ENSMUSG00000045095	Magi1	0.194291142	0.001247	ENSMUSG00000031756	Cenpn	0.201729045	0.0173607
ENSMUSG00000047003	Zfp41	0.194305585	0.0372231	ENSMUSG00000020315	Sptbn1	0.201994274	3.35E-11
ENSMUSG00000053317	Sec61b	0.194368871	0.001005	ENSMUSG00000075470	Alg10b	0.202012528	4.93E-06
ENSMUSG00000014601	Strip1	0.194466866	0.0003612	ENSMUSG00000032551	1110059G10Rik	0.202045286	0.0492019
ENSMUSG00000014767	Tbp	0.194488437	0.0096793	ENSMUSG00000036968	Cnpy4	0.202331197	0.0063482
ENSMUSG00000038119	Cdon	0.19456562	0.0419839	ENSMUSG00000024913	Lrp5	0.202493139	6.37E-05
ENSMUSG00000045671	Spred2	0.19457692	0.0001047	ENSMUSG00000046435	Gm13078	0.202496337	0.0078333
ENSMUSG00000070047	Fat1	0.194627943	0.0003948	ENSMUSG00000024758	Rtn3	0.202535095	7.02E-08
ENSMUSG00000037815	Ctnna1	0.194656699	6.70E-11	ENSMUSG00000041444	Arhgap32	0.202677343	0.0008345
ENSMUSG00000021585	Cast	0.194735718	0.001144	ENSMUSG00000031146	Plp2	0.202688974	5.71E-07
ENSMUSG00000040359	Ufl1	0.194926271	0.0041252	ENSMUSG00000024810	Il33	0.202763301	0.0066757
ENSMUSG00000049916	2610318N02Rik	0.195310427	0.0415055	ENSMUSG00000010110	Stx5a	0.202859062	0.0089342
ENSMUSG00000006276	Eps15l1	0.195397081	0.0091941	ENSMUSG00000016427	Ndufa1	0.202898337	0.0028425
ENSMUSG00000026469	Xpr1	0.195521266	0.0010095	ENSMUSG00000015291	Gdi1	0.203233953	0.0001919
ENSMUSG00000021359	Tfap2a	0.195889261	0.0048489	ENSMUSG00000020738	Sumo2	0.203318899	1.80E-10
ENSMUSG00000031168	Ebp	0.195937068	0.0034492	ENSMUSG00000028495	Rps6	0.203534598	6.65E-16
ENSMUSG00000030077	Chl1	0.196258671	9.19E-07	ENSMUSG00000037628	Cdkn3	0.203788334	0.0370617
ENSMUSG00000020747	2310067B10Rik	0.1963163	0.0096586	ENSMUSG00000037361	Sf3b6	0.204082912	0.0004283
ENSMUSG00000015937	H2afy	0.196427737	0.0006254	ENSMUSG00000020827	Mink1	0.204178302	2.92E-06
ENSMUSG00000063410	Stk24	0.196428747	0.0058713	ENSMUSG00000020140	Lgr5	0.204240966	0.0466675
ENSMUSG00000022450	Ndufa6	0.196507901	0.0005203	ENSMUSG00000034544	Rsrc1	0.204392401	0.0009929
ENSMUSG00000045962	Wnk1	0.196508516	9.65E-10	ENSMUSG00000094973	Gm8994	0.204395248	0.0180948
ENSMUSG00000031516	Dctn6	0.196553554	0.0271238	ENSMUSG00000033306	Lpp	0.204479411	0.0010484
ENSMUSG00000039716	Dock3	0.197018689	0.0153469	ENSMUSG00000036955	Kif1bp	0.205012244	0.0029556
ENSMUSG00000008859	Rala	0.197029236	0.0015671	ENSMUSG00000004798	Ulk2	0.205104867	0.0043428
ENSMUSG00000037270	4932438A13Rik	0.197462723	0.0004129	ENSMUSG00000037221	Mospd3	0.205145196	0.0327861
ENSMUSG00000032330	Cox7a2	0.197471628	6.09E-05	ENSMUSG00000093760	Gm20678	0.205363335	0.0103023
ENSMUSG00000027679	Dnajc19	0.197495711	0.0058886	ENSMUSG00000049504	Proser1	0.205395005	0.0303592
ENSMUSG00000027074	Slc43a3	0.197505997	0.0013338	ENSMUSG00000033985	Tesk2	0.20543267	0.0428804
ENSMUSG00000039741	Bahcc1	0.19757399	0.0119239	ENSMUSG00000042605	Atxn2	0.205535402	2.49E-05
ENSMUSG00000030335	Mrpl51	0.197629842	6.59E-05	ENSMUSG00000023919	Cenpq	0.205594403	0.0063267
ENSMUSG00000021807	2700060E02Rik	0.197728861	7.62E-05	ENSMUSG00000027248	Pdia3	0.20566041	2.86E-20
ENSMUSG00000068917	Clk2	0.197762324	0.0155244	ENSMUSG00000027303	Ptpra	0.205731393	7.24E-06
ENSMUSG00000042557	Sin3a	0.197768753	0.0002606	ENSMUSG00000030120	Mlf2	0.205855207	5.13E-08
ENSMUSG00000040767	Snrnp25	0.197865435	0.0362772	ENSMUSG00000024002	Brd4	0.206091726	1.21E-06
ENSMUSG00000028576	Ift74	0.19787637	0.029633	ENSMUSG00000023170	Gps2	0.206132992	0.0174095
ENSMUSG00000025144	Stra13	0.197902022	0.0487231	ENSMUSG00000032562	Gnai2	0.20616603	4.24E-11
ENSMUSG00000039828	Wdr70	0.197931867	0.0045654	ENSMUSG00000043866	Taf10	0.206278276	4.14E-05
ENSMUSG00000010376	Nedd8	0.197950794	7.00E-05	ENSMUSG00000040407	Akap9	0.20630242	4.23E-05
ENSMUSG00000031153	Gripap1	0.19806504	0.0066258	ENSMUSG00000025571	Tnrc6c	0.206656248	0.0069678
ENSMUSG00000024949	Sf1	0.198142522	3.37E-08	ENSMUSG00000055538	Zcchc24	0.206843854	0.0001874
ENSMUSG00000020572	Nampt	0.19829133	3.96E-05	ENSMUSG00000020721	Helz	0.207005565	0.0003756
ENSMUSG00000032187	Smarca4	0.198304596	5.82E-10	ENSMUSG00000022385	Gtse1	0.207022421	1.78E-05
ENSMUSG00000048154	Kmt2d	0.198386091	0.034345	ENSMUSG00000000127	Fer	0.207118061	0.0189664
ENSMUSG00000031157	Pqbp1	0.198526407	0.0018732	ENSMUSG00000049288	Lix1l	0.207156614	1.13E-05
ENSMUSG00000032740	Ccdc88a	0.198715585	0.0054507	ENSMUSG00000024974	Smc3	0.207623479	4.89E-09
ENSMUSG00000015222	Map2	0.198738164	0.0002501	ENSMUSG00000032383	Ppib	0.207941124	9.96E-06

Gene		Log_2 Fold Change	pValue	Gene		Log_2 Fold Change	pValue
ENSMUSG00000086151	Gm5698	0.208174796	0.0019242	ENSMUSG00000028832	Stmn1	0.21817378	4.67E-11
ENSMUSG00000028312	Smc2	0.208199543	1.50E-10	ENSMUSG00000025474	Tubgcp2	0.218182507	0.0028935
ENSMUSG00000020808	Fam64a	0.20835471	9.15E-05	ENSMUSG00000040084	Bub1b	0.218185723	3.97E-08
ENSMUSG00000029472	Anapc5	0.208569853	1.77E-12	ENSMUSG00000000282	Mnt	0.218255983	0.0209518
ENSMUSG00000030774	Pak1	0.208571976	0.0008157	ENSMUSG00000032186	Tmod2	0.218821011	0.006469
ENSMUSG00000034709	Ppp1r21	0.20870688	0.0051928	ENSMUSG00000014813	Stc1	0.219054618	0.0180299
ENSMUSG00000008200	Fnbp4	0.208731302	0.0017523	ENSMUSG00000074280	Gm6166	0.219102086	5.05E-06
ENSMUSG00000004667	Polr2e	0.208740527	2.76E-05	ENSMUSG00000040225	Prrc2c	0.219113553	7.44E-14
ENSMUSG00000018395	Kif3a	0.208970158	0.0023454	ENSMUSG00000045215	Asxl3	0.219122474	0.0020988
ENSMUSG00000000957	Mmp14	0.208997122	2.45E-09	ENSMUSG00000036572	Upf3b	0.219457785	0.0019561
ENSMUSG00000025574	Tk1	0.209392543	0.0002195	ENSMUSG00000001441	Npepps	0.219504261	4.20E-06
ENSMUSG00000040746	Rnf167	0.209472259	0.0242834	ENSMUSG00000058603	Rpl28-ps1	0.21951133	0.0010396
ENSMUSG00000029554	Mad1l1	0.209614746	0.0001393	ENSMUSG00000037703	Lzts3	0.219644598	0.0127908
ENSMUSG00000025868	Higd2a	0.20980854	0.020842	ENSMUSG00000029096	Htra3	0.219812405	0.0136047
ENSMUSG00000071415	Rpl23	0.209837481	2.32E-20	ENSMUSG00000066306	Numa1	0.219978255	2.57E-10
ENSMUSG00000036002	Fam214b	0.209879131	0.042213	ENSMUSG00000005198	Polr2a	0.220024162	7.73E-12
ENSMUSG00000031149	Praf2	0.210023216	0.0062038	ENSMUSG00000003228	Grk5	0.220100075	0.0320472
ENSMUSG00000020864	Ankrd40	0.210246632	6.82E-08	ENSMUSG00000039607	Rbms3	0.220140369	0.0119996
ENSMUSG00000017781	Pitpna	0.21025211	1.63E-07	ENSMUSG00000034295	Fhod3	0.220370392	0.0035657
ENSMUSG00000043456	Zfp536	0.210309185	0.0205994	ENSMUSG00000031378	Abcd1	0.220487228	0.0064756
ENSMUSG00000040151	Hs2st1	0.210337129	1.81E-10	ENSMUSG00000022428	Cby1	0.220663741	0.0197456
ENSMUSG00000034761	Map4k5	0.210950613	9.05E-05	ENSMUSG00000020935	Dcakd	0.220703723	0.0002441
ENSMUSG00000029623	Pdap1	0.211094896	7.71E-13	ENSMUSG00000036427	Gpi1	0.220729495	0.0023394
ENSMUSG00000037217	Syn1	0.211315237	0.0280901	ENSMUSG00000073434	Wdr90	0.220738598	0.0193598
ENSMUSG00000020986	Sec23a	0.211319359	0.0005078	ENSMUSG00000020173	Cobl	0.220750799	0.015926
ENSMUSG00000019942	Cdk1	0.211325603	3.04E-10	ENSMUSG00000070639	Lrrc8b	0.220844806	6.39E-05
ENSMUSG00000001151	Pcnt	0.211392759	3.25E-05	ENSMUSG00000035024	Ncapd3	0.220944243	8.59E-06
ENSMUSG00000005371	Fbxo11	0.211532717	0.000309	ENSMUSG00000019194	Scn1b	0.221105915	0.0279264
ENSMUSG00000045160	Bola3	0.211548394	0.0090646	ENSMUSG00000000804	Usp32	0.221200402	0.0002439
ENSMUSG00000044285	Gm1821	0.211581549	0.0469344	ENSMUSG00000021273	Fdft1	0.221255993	0.0169041
ENSMUSG00000041911	Dlx1	0.211670348	0.0102318	ENSMUSG00000002055	Spag5	0.221318882	3.94E-06
ENSMUSG00000028878	Fam76a	0.211678862	0.0390144	ENSMUSG00000024588	Fech	0.221336557	0.0005757
ENSMUSG00000034021	Pds5b	0.211766465	1.51E-07	ENSMUSG00000020814	Mxra7	0.221389839	0.0086989
ENSMUSG00000083670	Gm6829	0.211768587	0.0379806	ENSMUSG00000028484	Psip1	0.221470346	2.60E-08
ENSMUSG00000023904	Hcfc1r1	0.211895983	0.0072161	ENSMUSG00000009687	Fxyd5	0.221559154	1.33E-07
ENSMUSG00000028671	Gale	0.211960114	0.0451893	ENSMUSG00000028378	Ptgr1	0.221585192	0.0331902
ENSMUSG00000004698	Hdac9	0.212049325	0.0190367	ENSMUSG00000025357	Dgka	0.222042585	0.021509
ENSMUSG00000029461	Fam168a	0.212236408	0.0006876	ENSMUSG00000013367	Iglon5	0.222323521	0.0312556
ENSMUSG00000037621	Atoh8	0.212266474	0.0405854	ENSMUSG00000033282	Rpgrip1l	0.222443532	0.0279034
ENSMUSG00000061607	Mdc1	0.212330554	4.13E-07	ENSMUSG00000063065	Mapk3	0.222503258	2.08E-08
ENSMUSG00000030587	2200002D01Rik	0.212397118	0.0104034	ENSMUSG00000026779	Mastl	0.222645594	0.0053099
ENSMUSG00000035198	Tubg1	0.212443967	0.000171	ENSMUSG00000080893	Gm15920	0.222690839	0.0249453
ENSMUSG00000078180	Gm20900	0.212523984	0.0089695	ENSMUSG00000022139	Mbnl2	0.222715577	7.16E-05
ENSMUSG00000023072	Cep89	0.212800628	0.0038352	ENSMUSG00000056394	Lig1	0.22330003	9.18E-09
ENSMUSG00000049517	Rps23	0.212947439	2.96E-15	ENSMUSG00000031604	Msmo1	0.22338013	0.0025185
ENSMUSG00000042520	Ubap2l	0.212950237	1.24E-11	ENSMUSG00000022314	Rad21	0.223387866	1.65E-17
ENSMUSG00000056763	Cspp1	0.213496563	0.0119527	ENSMUSG00000027115	Kif18a	0.223676827	0.0008878
ENSMUSG00000020241	Col6a2	0.213542606	0.010767	ENSMUSG00000033278	Ptprm	0.223803332	0.0060957
ENSMUSG00000039270	Megf9	0.213748439	0.0031052	ENSMUSG00000022678	Nde1	0.223970871	1.97E-06
ENSMUSG00000024277	Mapre2	0.213970981	0.0020122	ENSMUSG00000063445	Nmral1	0.224030317	0.010259
ENSMUSG00000096284	Tcstv1	0.213973339	0.0039191	ENSMUSG00000070619	Gm13119	0.224032203	0.0085956
ENSMUSG00000024556	Me2	0.214112155	5.13E-06	ENSMUSG00000036295	Lrrn3	0.224128543	0.0311276
ENSMUSG00000040549	Ckap5	0.214126393	1.24E-10	ENSMUSG00000042331	Specc1	0.22424927	1.92E-07
ENSMUSG00000028718	Stil	0.214447235	0.0174344	ENSMUSG00000081406	Rps6-ps4	0.224315472	0.0002612
ENSMUSG00000024590	Lmnb1	0.214651051	1.28E-06	ENSMUSG00000024925	Rnaseh2c	0.224353271	0.0187051
ENSMUSG00000038648	Creb3l2	0.21474352	0.000267	ENSMUSG00000028134	Ptbp2	0.225087654	0.0006023
ENSMUSG00000001794	Capns1	0.214795232	2.32E-07	ENSMUSG00000027012	Dync1i2	0.225111336	3.60E-07
ENSMUSG00000031386	Hcfc1	0.215260408	1.03E-14	ENSMUSG00000030693	Klk10	0.225135511	1.35E-05
ENSMUSG00000008450	Nutf2	0.215403515	0.0002336	ENSMUSG00000025404	R3hdm2	0.225188878	2.48E-06
ENSMUSG00000070808	Gltscr1	0.215524004	0.0362421	ENSMUSG00000057388	Mrpl18	0.225208346	9.32E-06
ENSMUSG00000030035	Wbp1	0.215553201	0.0057626	ENSMUSG00000031762	Mt2	0.225323115	0.0032148
ENSMUSG00000027797	Dclk1	0.21566699	0.0026955	ENSMUSG00000024260	Sap130	0.225458575	8.49E-05
ENSMUSG00000105868	RP24-223I19.6	0.215740273	0.0404511	ENSMUSG00000032410	Xrn1	0.225525378	0.0001732
ENSMUSG00000090841	Myl6	0.216080843	0.0140356	ENSMUSG00000048118	Arid4a	0.225528826	0.0201613
ENSMUSG00000035357	Pdzrn3	0.216167571	5.84E-05	ENSMUSG00000026797	Stxbp1	0.225573966	0.0022613
ENSMUSG00000042284	Itga1	0.216259832	4.56E-05	ENSMUSG00000027330	Cdc25b	0.225652678	2.03E-05
ENSMUSG00000019302	Atp6v0a1	0.216280911	0.0123062	ENSMUSG00000029135	Fosl2	0.225656279	5.01E-05
ENSMUSG00000005447	Pafah1b3	0.216601308	0.0018952	ENSMUSG00000053137	Mapk11	0.225749528	0.0221475
ENSMUSG00000077450	Rab11b	0.216994367	5.74E-05	ENSMUSG00000029101	Rgs12	0.225812169	0.0135588
ENSMUSG00000018750	Zbtb4	0.217077144	0.0132726	ENSMUSG00000020485	Supt4a	0.226069874	0.0015494
ENSMUSG00000062933	Gm10123	0.217137163	0.0137926	ENSMUSG00000028412	Slc44a1	0.226319123	1.33E-07
ENSMUSG00000038072	Galnt11	0.217168043	0.0066522	ENSMUSG00000038065	Mturn	0.226608817	0.0490654
ENSMUSG00000021127	Zfp36l1	0.217170359	0.00999	ENSMUSG00000032355	Mlip	0.226817906	0.0246526
ENSMUSG00000021068	Nin	0.217365354	0.0001586	ENSMUSG00000007817	Zmiz1	0.227041332	6.03E-06
ENSMUSG00000039686	Zer1	0.217422227	0.0487613	ENSMUSG00000030701	Plekhb1	0.227373949	0.0002542
ENSMUSG00000025374	Nabp2	0.217609592	0.0023644	ENSMUSG00000031391	L1cam	0.227736947	6.32E-07
ENSMUSG00000024989	Cep55	0.217726864	4.35E-05	ENSMUSG00000058239	Usf2	0.227746318	5.47E-05
ENSMUSG00000020859	Spag9	0.217737005	2.93E-06	ENSMUSG00000067288	Rps28	0.22776661	2.96E-13
ENSMUSG00000020776	Fbf1	0.217899361	0.0061611	ENSMUSG00000054199	Gon4l	0.227861084	0.0003324
ENSMUSG00000013236	Ptprs	0.217946134	2.23E-05	ENSMUSG00000061533	Cep128	0.227909486	0.009047
ENSMUSG00000021196	Pfkp	0.218170064	0.0376001	ENSMUSG00000020932	Gfap	0.227910576	1.31E-11

Gene		Log_2 Fold Change	pValue	Gene		Log_2 Fold Change	pValue
ENSMUSG00000046364	Rpl27a	0.228227576	7.98E-24	ENSMUSG00000064351	mt-Co1	0.243465525	5.36E-47
ENSMUSG00000073987	Ggh	0.22830973	0.0464787	ENSMUSG00000001383	Zmat2	0.243550077	1.50E-06
ENSMUSG00000026879	Gsn	0.228643703	0.000691	ENSMUSG00000035683	Melk	0.243560135	1.33E-05
ENSMUSG00000040725	Hnrnpul1	0.228972542	2.10E-11	ENSMUSG00000020375	Rufy1	0.243634465	0.0012085
ENSMUSG00000046753	Ccdc66	0.229052848	0.0196496	ENSMUSG00000032575	Manf	0.243647149	1.06E-09
ENSMUSG00000056211	R3hdm1	0.229053127	4.43E-07	ENSMUSG00000040721	Zfhx2	0.243835504	0.0455284
ENSMUSG00000061028	Clasrp	0.229263755	0.0046102	ENSMUSG00000067925	Cxx1a	0.243864707	0.0322663
ENSMUSG00000024646	Cyb5a	0.229271665	0.0438815	ENSMUSG00000034401	Spata6	0.244381686	0.0094976
ENSMUSG00000057963	Itpk1	0.22960994	0.0005295	ENSMUSG00000078193	Gm2000	0.244460623	0.0032062
ENSMUSG00000035051	Dhx57	0.230158787	0.0094364	ENSMUSG00000028969	Cdk5	0.244589964	0.0005559
ENSMUSG00000043987	Cep164	0.230281486	0.0012596	ENSMUSG00000028799	Zfp362	0.24520216	0.0139232
ENSMUSG00000039477	Tnrc18	0.23032416	8.58E-08	ENSMUSG00000026851	BC005624	0.245261769	0.0008992
ENSMUSG00000017843	Ppp2r5c	0.230876834	1.96E-06	ENSMUSG00000075590	Nrbp2	0.245366973	0.0409819
ENSMUSG00000024269	Tpgs2	0.231147601	0.0017374	ENSMUSG00000024018	Ccdc167	0.245847838	0.0432777
ENSMUSG00000008575	Nfib	0.231614844	0.0066145	ENSMUSG00000000711	Rab5b	0.246059344	3.71E-06
ENSMUSG00000038717	Atp5l	0.231689653	1.56E-05	ENSMUSG00000033460	Armcx1	0.246152123	0.0351686
ENSMUSG00000019370	Calm3	0.231729469	5.51E-12	ENSMUSG00000031879	Fam96b	0.246287925	0.007922
ENSMUSG00000078695	Cisd3	0.231736077	0.0305246	ENSMUSG00000062691	Cebpzos	0.246324099	0.0307114
ENSMUSG00000026074	Map4k4	0.231928707	3.47E-10	ENSMUSG00000034520	Gjc1	0.246344719	0.0025158
ENSMUSG00000058325	Dock1	0.231979777	5.93E-07	ENSMUSG00000024498	Tcerg1	0.246366846	9.18E-09
ENSMUSG00000064302	Clasp1	0.232247138	1.33E-06	ENSMUSG00000063382	Bcl9l	0.246585749	1.71E-05
ENSMUSG00000027994	Ccdc109b	0.232298889	0.0325719	ENSMUSG00000030867	Plk1	0.246606328	5.47E-11
ENSMUSG00000041997	Tlk1	0.232400042	6.39E-06	ENSMUSG00000019804	Snx3	0.246664472	4.50E-08
ENSMUSG00000105388	Rpl36a-ps2	0.232896582	0.0036423	ENSMUSG00000024056	Ndc80	0.246713214	8.61E-05
ENSMUSG00000044674	Fzd1	0.232952215	0.0002818	ENSMUSG00000052331	Ankrd44	0.246878007	0.006619
ENSMUSG00000028760	Eif4g3	0.233196204	3.12E-08	ENSMUSG00000026790	Odf2	0.247081066	9.53E-05
ENSMUSG00000010751	Tnfrsf22	0.233346422	7.33E-05	ENSMUSG00000061288	Taok3	0.247539741	0.0138362
ENSMUSG00000021262	Evl	0.233350702	0.0013566	ENSMUSG00000064193	Gm4735	0.24764698	0.0112492
ENSMUSG00000037313	Tacc3	0.23364818	1.86E-06	ENSMUSG00000022013	Dnajc15	0.247678539	0.0218744
ENSMUSG00000020185	E2f7	0.233863873	0.0049733	ENSMUSG00000020024	Cep83	0.247744615	0.0006686
ENSMUSG00000005233	Spc25	0.233940267	0.0006321	ENSMUSG00000058056	Palld	0.247755677	0.0353383
ENSMUSG00000026473	Glul	0.234125453	0.0016474	ENSMUSG00000031708	Tecr	0.247857552	2.63E-06
ENSMUSG00000023067	Cdkn1a	0.234234224	1.42E-06	ENSMUSG00000078427	Sarnp	0.247910691	5.34E-07
ENSMUSG00000027940	Tpm3	0.234980966	2.50E-08	ENSMUSG00000062248	Cks2	0.248261053	4.38E-05
ENSMUSG00000028609	Magoh	0.235409385	0.0004841	ENSMUSG00000039781	Cep131	0.248355628	0.0120294
ENSMUSG00000020849	Ywhae	0.235453926	5.03E-23	ENSMUSG00000002546	Golga2	0.248432562	5.53E-05
ENSMUSG00000072594	Gm16439	0.2354691	0.0402839	ENSMUSG00000034205	Loxl2	0.24848243	0.0454574
ENSMUSG00000078923	Ube2v1	0.235490156	0.0343649	ENSMUSG00000073177	Gm773	0.248609183	1.57E-06
ENSMUSG00000020163	Uqcr11	0.235910213	9.79E-06	ENSMUSG00000068923	Syt11	0.24903653	0.0001959
ENSMUSG00000027997	Casp6	0.235963239	0.0088946	ENSMUSG00000006800	Sulf2	0.249244957	9.11E-11
ENSMUSG00000032238	Rora	0.236192345	0.0432607	ENSMUSG00000038379	Ttk	0.249441542	2.81E-05
ENSMUSG00000031207	Msn	0.236275065	1.74E-26	ENSMUSG00000031232	Magt1	0.249490027	1.54E-05
ENSMUSG00000003031	Cdkn1b	0.236434813	0.0030427	ENSMUSG00000034341	Wbp2	0.249547178	2.13E-06
ENSMUSG00000003437	Paf1	0.236618003	1.90E-05	ENSMUSG00000018449	Rpain	0.249571249	0.0186755
ENSMUSG00000063229	Ldha	0.237201879	0.0160158	ENSMUSG00000051154	Commd3	0.249724439	1.95E-05
ENSMUSG00000029705	Cux1	0.23734647	1.10E-05	ENSMUSG00000031683	Lsm6	0.249729027	0.0001726
ENSMUSG00000030096	Slc6a6	0.237789189	1.14E-12	ENSMUSG00000029512	Ulk1	0.249732857	0.0011243
ENSMUSG00000058454	Dhcr7	0.237907018	0.0054902	ENSMUSG00000038332	Sesn1	0.250180895	0.030253
ENSMUSG00000038256	Bcl9	0.238070712	2.88E-05	ENSMUSG00000021591	Glrx	0.250342162	0.0392698
ENSMUSG00000059518	Znhit1	0.238132048	0.0002785	ENSMUSG00000009418	Nav1	0.250345839	3.90E-05
ENSMUSG00000053580	Tanc2	0.238142476	4.07E-05	ENSMUSG00000041559	Fmod	0.250456702	0.0201014
ENSMUSG00000028843	Sh3bgrl3	0.238187763	0.0035557	ENSMUSG00000085289	Gm15337	0.25049557	0.0430977
ENSMUSG00000037960	1110007C09Rik	0.238187935	0.0019735	ENSMUSG00000035545	Leng8	0.250671293	0.0001549
ENSMUSG00000057110	Cntrl	0.238387363	0.0007811	ENSMUSG00000068740	Celsr2	0.25077704	0.0313736
ENSMUSG00000058258	Idi1	0.238923614	0.0007946	ENSMUSG00000018567	Gabarap	0.250814897	6.24E-07
ENSMUSG00000063457	Rps15	0.23939081	1.64E-20	ENSMUSG00000074884	Serf2	0.250819474	2.60E-08
ENSMUSG00000028647	Mycbp	0.239406471	0.0105516	ENSMUSG00000006191	Cdkal1	0.251046574	0.0173307
ENSMUSG00000027304	Rtf1	0.239545886	1.04E-05	ENSMUSG00000039849	Pcif1	0.251154396	0.0001043
ENSMUSG00000024795	Kif20b	0.239550536	4.05E-06	ENSMUSG00000031558	Slit2	0.251302976	9.29E-12
ENSMUSG00000027860	Vangl1	0.239637632	0.0019396	ENSMUSG00000005732	Ranbp1	0.251311902	2.16E-19
ENSMUSG00000004270	Lpcat3	0.239655639	0.0034618	ENSMUSG00000026492	Tfb2m	0.25140345	0.0014604
ENSMUSG00000025154	Arhgap19	0.239857569	0.0147666	ENSMUSG00000044022	Pcdhb21	0.251567229	0.0428181
ENSMUSG00000032064	Dixdc1	0.239860911	0.0021266	ENSMUSG00000054942	Fam73a	0.251672883	7.03E-08
ENSMUSG00000024067	Dpy30	0.239925563	0.0001233	ENSMUSG00000056962	Jmjd6	0.251965632	1.67E-05
ENSMUSG00000031311	Nono	0.240078463	1.86E-23	ENSMUSG00000074637	Sox2	0.252145009	1.91E-08
ENSMUSG00000041133	Smc1a	0.240240886	1.94E-12	ENSMUSG00000100005	B130024G19Rik	0.252184281	0.0245927
ENSMUSG00000039542	Ncam1	0.240468847	1.76E-06	ENSMUSG00000046519	Golph3l	0.252255269	0.0068466
ENSMUSG00000027966	Col11a1	0.240701372	2.91E-15	ENSMUSG00000040621	Gemin8	0.252455169	0.0104851
ENSMUSG00000007880	Arid1a	0.240763808	6.40E-08	ENSMUSG00000070890	Gm12794	0.252597379	0.0095018
ENSMUSG00000038518	Jarid2	0.241001542	0.0344177	ENSMUSG00000015668	Pdzd11	0.252942212	7.31E-06
ENSMUSG00000022174	Dad1	0.241030166	8.69E-05	ENSMUSG00000032249	Anp32a	0.253034875	4.11E-11
ENSMUSG00000045679	Pqlc3	0.241188903	0.043055	ENSMUSG00000058135	Gstm1	0.253088683	0.0421121
ENSMUSG00000037111	Setd7	0.241278823	6.19E-07	ENSMUSG00000022957	Itsn1	0.253172792	2.62E-05
ENSMUSG00000022449	Adamts20	0.241717982	0.0135744	ENSMUSG00000020091	Eif4ebp2	0.253329962	6.58E-05
ENSMUSG00000038967	Pdk2	0.241886237	0.0497932	ENSMUSG00000083261	Gm7816	0.253726695	0.0282792
ENSMUSG00000024201	Kdm4b	0.241910447	0.0020812	ENSMUSG00000020048	Hsp90b1	0.25403545	4.10E-39
ENSMUSG00000064127	Med14	0.242428368	2.24E-08	ENSMUSG00000031314	Taf1	0.254149652	7.19E-08
ENSMUSG00000027993	Trim2	0.243048233	0.0020369	ENSMUSG00000036678	Aaas	0.254212696	2.85E-08
ENSMUSG00000028678	Kif2c	0.243116598	6.53E-08	ENSMUSG00000055200	Sertad3	0.254277633	0.0412842
ENSMUSG00000053333	Dis3l2	0.243152845	0.0066978	ENSMUSG00000026147	Col9a1	0.254310599	0.0108954
ENSMUSG00000037426	Depdc5	0.243307488	0.0007859	ENSMUSG00000105263	RP24-230J14.5	0.254530192	2.81E-11

Gene		Log_2 Fold Change	pValue	Gene		Log_2 Fold Change	pValue
ENSMUSG00000017314	Mpp2	0.255001001	0.032157	ENSMUSG00000026032	Ndufb3	0.272361306	0.0005949
ENSMUSG00000061079	Zfp143	0.255005989	0.001188	ENSMUSG00000031839	Hsbp1	0.272541631	3.69E-05
ENSMUSG00000025558	Dock9	0.255417534	0.0003232	ENSMUSG00000038369	Ncoa6	0.272649045	1.55E-08
ENSMUSG00000024968	Rcor2	0.255474765	3.20E-06	ENSMUSG00000041498	Kif14	0.272735661	2.73E-05
ENSMUSG00000036777	Anln	0.255607659	1.54E-18	ENSMUSG00000029661	Col1a2	0.272926378	2.83E-38
ENSMUSG00000009828	Ick	0.255608633	0.0031584	ENSMUSG00000020267	Hint1	0.272954388	8.16E-13
ENSMUSG00000020180	Snrpd3	0.255808965	6.26E-10	ENSMUSG00000044927	H1fx	0.273069731	8.02E-05
ENSMUSG00000030541	Idh2	0.25581591	9.55E-15	ENSMUSG00000073590	3222401L13Rik	0.273164631	0.0282059
ENSMUSG00000031634	Ufsp2	0.255818852	0.0018656	ENSMUSG00000027641	Rbl1	0.273173651	3.71E-06
ENSMUSG00000030095	Tmem43	0.256060557	1.57E-05	ENSMUSG00000095339	Zscan4b	0.273219537	0.0026656
ENSMUSG00000026708	Cenpl	0.256256403	0.0081421	ENSMUSG00000024660	Incenp	0.273674267	3.12E-12
ENSMUSG00000018965	Ywhah	0.256326341	1.05E-11	ENSMUSG00000079435	Rpl36a	0.274753123	9.12E-23
ENSMUSG00000097439	Gm16754	0.256525148	0.0304088	ENSMUSG00000062380	Tubb3	0.275181593	0.0001088
ENSMUSG00000039599	Fam149b	0.256569996	0.007425	ENSMUSG00000034243	Golgb1	0.275434415	4.25E-06
ENSMUSG00000020456	Ogdh	0.257090855	1.56E-14	ENSMUSG00000032845	Alpk2	0.275983005	0.0126415
ENSMUSG00000027985	Lef1	0.257162182	0.0197575	ENSMUSG00000090247	Bloc1s1	0.27629903	0.000723
ENSMUSG00000071653	1810009A15Rik	0.257364834	0.0046321	ENSMUSG00000035401	2210018M11Rik	0.276348537	1.79E-05
ENSMUSG00000010830	Kdelr3	0.25738486	0.0327527	ENSMUSG00000024474	Ik	0.276592547	2.26E-11
ENSMUSG00000081007	Gm11543	0.257413385	0.0014159	ENSMUSG00000062070	Pgk1	0.276651999	0.0051369
ENSMUSG00000026727	Rsu1	0.257693827	6.35E-08	ENSMUSG00000025066	Sfr1	0.276966789	3.33E-10
ENSMUSG00000001025	S100a6	0.257833679	8.34E-14	ENSMUSG00000011884	Gltp	0.277407073	1.23E-06
ENSMUSG00000005774	Rfx5	0.257865884	0.024448	ENSMUSG00000072235	Tuba1a	0.277695012	1.04E-16
ENSMUSG00000001120	Pcbp3	0.258137857	0.0024754	ENSMUSG00000048108	Tmem72	0.277916406	0.0249756
ENSMUSG00000020277	Pfkl	0.258453335	0.0272931	ENSMUSG00000025212	Sfxn3	0.278227446	1.09E-05
ENSMUSG00000015932	Dstn	0.258492257	1.62E-10	ENSMUSG00000084304	Gm6142	0.278443609	0.0247004
ENSMUSG00000020758	Itgb4	0.258814083	2.14E-07	ENSMUSG00000032316	Clk3	0.278501191	0.0008635
ENSMUSG00000029436	Mmp17	0.258986591	1.89E-09	ENSMUSG00000030555	Ttc23	0.278571965	0.0014913
ENSMUSG00000020593	Lpin1	0.259204558	0.024272	ENSMUSG00000021975	Ints9	0.279090618	0.0101151
ENSMUSG00000035835	Lppr3	0.259705715	2.23E-05	ENSMUSG00000048747	E130114P18Rik	0.279289174	0.0234125
ENSMUSG00000042510	AA986860	0.259828521	0.0368713	ENSMUSG00000027605	Acss2	0.279361648	0.0249812
ENSMUSG00000003779	Kif20a	0.260242946	2.70E-09	ENSMUSG00000033429	Mcee	0.279382157	0.0189026
ENSMUSG00000007721	Ccdc124	0.260305135	7.80E-05	ENSMUSG00000051989	Smim11	0.279686926	0.00608
ENSMUSG00000101970	1810026B05Rik	0.261012984	0.0172439	ENSMUSG00000022956	Atp5o	0.279782735	8.99E-11
ENSMUSG00000066456	Hmgn3	0.261033516	1.22E-05	ENSMUSG00000006567	Atp7b	0.280076045	0.021926
ENSMUSG00000067279	Ppp1r3c	0.261088405	0.0199366	ENSMUSG00000021643	Serf1	0.280140226	0.0196943
ENSMUSG00000027977	Ndst3	0.261147991	0.0078273	ENSMUSG00000027715	Ccna2	0.280575217	9.52E-21
ENSMUSG00000008398	Elk3	0.261551856	1.38E-07	ENSMUSG00000032294	Pkm	0.280612147	5.09E-09
ENSMUSG00000021537	Cetn3	0.261687209	0.0002362	ENSMUSG00000040048	Ndufb10	0.28064006	3.34E-06
ENSMUSG00000026817	Ak1	0.262036986	2.46E-06	ENSMUSG00000059291	Rpl11	0.280671424	1.80E-21
ENSMUSG00000054428	Atpif1	0.262251843	2.35E-05	ENSMUSG00000028639	Ybx1	0.281582475	2.40E-27
ENSMUSG00000039943	Plcb4	0.262291337	0.0081192	ENSMUSG00000019873	Reep3	0.281704601	8.91E-09
ENSMUSG00000030695	Aldoa	0.262543379	0.0025579	ENSMUSG00000009569	Mkl2	0.281737738	3.24E-06
ENSMUSG00000049775	Tmsb4x	0.262653627	6.26E-18	ENSMUSG00000019124	Scrn1	0.282065341	2.34E-10
ENSMUSG00000025207	Sema4g	0.262696084	0.0265896	ENSMUSG00000031125	3830403N18Rik	0.28236488	1.91E-05
ENSMUSG00000009739	Pou6f1	0.26273438	0.0218424	ENSMUSG00000036854	Hspb6	0.282588296	0.0009614
ENSMUSG00000031166	Wdr13	0.263112095	0.0006509	ENSMUSG00000022982	Sod1	0.282670709	2.23E-11
ENSMUSG00000003033	Ap1m1	0.264443276	3.45E-05	ENSMUSG00000046711	Hmga1	0.282708828	1.37E-24
ENSMUSG00000019883	Echdc1	0.264616516	0.0047322	ENSMUSG00000020801	Med31	0.282976912	0.0088419
ENSMUSG00000063524	Eno1	0.265247663	0.0011753	ENSMUSG00000048764	Tmprss11f	0.283460808	0.0128079
ENSMUSG00000067924	Cxx1b	0.265534701	0.0086973	ENSMUSG00000024206	Rfx2	0.283770618	0.0226774
ENSMUSG00000035048	Anapc13	0.265645685	0.0060081	ENSMUSG00000036223	Ska1	0.283855074	0.0009605
ENSMUSG00000030847	Bag3	0.26585153	5.24E-08	ENSMUSG00000028398	Tmem261	0.284198676	0.0023907
ENSMUSG00000034413	Neurl1b	0.266278923	0.0103855	ENSMUSG00000019055	Plod1	0.284545235	8.55E-10
ENSMUSG00000031590	Frg1	0.266306805	0.0016559	ENSMUSG00000026578	Ccdc181	0.284657451	0.0109588
ENSMUSG00000028040	Efna4	0.266400272	0.0318559	ENSMUSG00000002732	Fkbp7	0.284716415	0.0206708
ENSMUSG00000029763	Exoc4	0.266469871	1.64E-07	ENSMUSG00000022051	Bnip3l	0.284741227	5.90E-05
ENSMUSG00000033237	Arid2	0.266667437	5.06E-08	ENSMUSG00000031666	Rbl2	0.284809987	0.0089215
ENSMUSG00000047123	Ticam1	0.266768173	0.0191061	ENSMUSG00000018909	Arrb1	0.285481617	0.0114858
ENSMUSG00000029231	Pdgfra	0.266775995	0.0319479	ENSMUSG00000038252	Ncapd2	0.285596274	2.27E-12
ENSMUSG00000038965	Ube2l3	0.266921342	9.22E-15	ENSMUSG00000030677	Kif22	0.286196598	1.52E-08
ENSMUSG00000022280	Rnf19a	0.267563683	0.0004542	ENSMUSG00000022321	Cdh10	0.286270968	0.0020652
ENSMUSG00000051550	Zfp579	0.26820358	0.0254569	ENSMUSG00000039168	Dap	0.286507284	1.46E-06
ENSMUSG00000069910	Spdl1	0.268311476	9.20E-06	ENSMUSG00000037544	Dlgap5	0.286998627	2.76E-07
ENSMUSG00000032220	Myo1e	0.268393916	4.21E-10	ENSMUSG00000096210	H1f0	0.287039009	1.28E-39
ENSMUSG00000003814	Calr	0.268526787	9.06E-30	ENSMUSG00000062901	Klhl24	0.287260269	0.0021519
ENSMUSG00000020897	Aurkb	0.268819213	5.47E-08	ENSMUSG00000006476	Nsmf	0.287363532	2.02E-06
ENSMUSG00000037605	Adgrl3	0.269215592	1.13E-05	ENSMUSG00000100967	Gm29666	0.288078988	0.004153
ENSMUSG00000042312	S100a13	0.269462318	0.0295646	ENSMUSG00000026932	Nacc2	0.288474879	1.48E-07
ENSMUSG00000056671	Prelid2	0.269812526	0.0293559	ENSMUSG00000013921	Clip3	0.28884044	2.41E-06
ENSMUSG00000097055	Gm4419	0.27005326	0.0089676	ENSMUSG00000056629	Fkbp2	0.289227731	0.0004266
ENSMUSG00000037890	Wdr19	0.270183564	0.0144001	ENSMUSG00000079480	Pin4	0.289270408	0.0006868
ENSMUSG00000034818	Celf5	0.270390197	0.0070566	ENSMUSG00000030432	Rpl28	0.289370294	3.28E-26
ENSMUSG00000022034	Esco2	0.270993695	0.008932	ENSMUSG00000041959	S100a10	0.290227836	5.41E-21
ENSMUSG00000051378	Kif18b	0.271348175	3.02E-07	ENSMUSG00000021838	Samd4	0.290562922	1.04E-05
ENSMUSG00000037325	Bbs7	0.271416248	0.008127	ENSMUSG00000027160	Ccdc34	0.291392082	3.86E-05
ENSMUSG00000082908	Gm13736	0.271428211	0.0253162	ENSMUSG00000019230	Lhx9	0.291658533	0.0192075
ENSMUSG00000047534	Mis18bp1	0.271445857	3.99E-06	ENSMUSG00000036438	Calm2	0.291933774	7.32E-26
ENSMUSG00000027102	Hoxd8	0.271680069	0.0005222	ENSMUSG00000050908	Tvp23a	0.292146919	0.0001862
ENSMUSG00000046330	Rpl37a	0.271869238	2.84E-19	ENSMUSG00000027130	Slc12a6	0.293039356	0.002683
ENSMUSG00000029516	Cit	0.27197219	0.0002889	ENSMUSG00000022707	Gbe1	0.293161305	0.0009884
ENSMUSG00000004032	Gstm5	0.272261824	0.0212682	ENSMUSG00000028218	Fam92a	0.293198941	1.84E-09

Gene		Log_2 Fold Change	pValue	Gene		Log_2 Fold Change	pValue
ENSMUSG00000021485	Mxd3	0.293277052	0.0015618	ENSMUSG00000020493	Prr11	0.319301183	5.71E-12
ENSMUSG00000041895	Wipi1	0.2934047	0.000548	ENSMUSG00000031231	Cox7b	0.319660843	1.50E-13
ENSMUSG00000036565	Ttyh3	0.293478959	1.24E-07	ENSMUSG00000056055	Sag	0.319751558	0.0017632
ENSMUSG00000023055	Calcoco1	0.293771012	0.0002308	ENSMUSG00000032527	Pccb	0.319782918	0.0007733
ENSMUSG00000015656	Hspa8	0.29453256	1.69E-37	ENSMUSG00000022351	Sqle	0.319871127	7.78E-09
ENSMUSG00000102700	Gm38312	0.294658681	1.75E-05	ENSMUSG00000048388	Fam171b	0.320063696	0.0006662
ENSMUSG00000079884	Gm10698	0.294937878	0.0010848	ENSMUSG00000078566	Bnip3	0.320635134	0.0078187
ENSMUSG00000066043	Phactr4	0.294963842	0.0002544	ENSMUSG00000004151	Etv1	0.320640792	0.0069356
ENSMUSG00000012609	Ttll5	0.295466472	0.0001528	ENSMUSG00000026987	Baz2b	0.320705655	0.0001489
ENSMUSG00000021486	Prelid1	0.295529949	4.20E-14	ENSMUSG00000022421	Nptxr	0.321403908	9.59E-10
ENSMUSG00000001467	Cyp51	0.29592032	1.40E-05	ENSMUSG00000038481	Cdk19	0.321788097	0.000251
ENSMUSG00000038126	Mphosph9	0.296337649	3.41E-05	ENSMUSG00000038371	Sbf2	0.322405778	2.30E-11
ENSMUSG00000069601	Ank3	0.297018661	7.94E-10	ENSMUSG00000028645	Slc2a1	0.322995835	0.0068067
ENSMUSG00000003153	Slc2a3	0.297383259	0.0147251	ENSMUSG00000064339	mt-Rnr2	0.323134179	8.70E-12
ENSMUSG00000023505	Cdca3	0.297625124	1.91E-07	ENSMUSG00000071547	Nt5dc2	0.323391036	1.05E-11
ENSMUSG00000036667	Tcaf1	0.297680297	4.25E-05	ENSMUSG00000092166	Gm7942	0.323863362	0.0001614
ENSMUSG00000071528	Usmg5	0.298037783	2.02E-06	ENSMUSG00000083773	Gm13394	0.324398533	0.0048234
ENSMUSG00000041126	H2afv	0.298257352	4.87E-05	ENSMUSG00000041064	Pif1	0.32504649	8.44E-05
ENSMUSG00000032883	Acsl3	0.298501583	1.68E-06	ENSMUSG00000021754	Map3k1	0.325637168	0.0015537
ENSMUSG00000032218	Ccnb2	0.298668246	2.47E-10	ENSMUSG00000063450	Syne2	0.325932548	1.53E-08
ENSMUSG00000030321	Efcab12	0.29873109	0.0157075	ENSMUSG00000023089	Ndufa5	0.326029543	3.24E-07
ENSMUSG00000001289	Pfdn5	0.298958953	6.06E-09	ENSMUSG00000025203	Scd2	0.32624725	4.55E-10
ENSMUSG00000027496	Aurka	0.29951365	6.73E-11	ENSMUSG00000044627	Swi5	0.327013954	4.38E-14
ENSMUSG00000029910	Mad2l1	0.299520614	3.86E-11	ENSMUSG00000021520	Uqcrb	0.327092277	5.55E-08
ENSMUSG00000037725	Ckap2	0.299645013	3.71E-08	ENSMUSG00000026193	Fn1	0.327353138	1.32E-42
ENSMUSG00000068391	Chrac1	0.299874196	4.94E-05	ENSMUSG00000034192	Lsm3	0.327680875	4.38E-09
ENSMUSG00000033685	Ucp2	0.300249394	1.40E-11	ENSMUSG00000032377	Plscr4	0.328162169	0.0047656
ENSMUSG00000032782	Cntrob	0.300394543	1.45E-05	ENSMUSG00000047604	Frat2	0.328405664	0.0075744
ENSMUSG00000001403	Ube2c	0.301103522	1.48E-13	ENSMUSG00000093674	Rpl41	0.328886329	2.80E-43
ENSMUSG00000022463	Srebf2	0.302135922	4.48E-13	ENSMUSG00000036242	3632451O06Rik	0.32959721	0.0081648
ENSMUSG00000018678	Sp2	0.30315056	4.77E-06	ENSMUSG00000039771	Polr2j	0.329941752	1.31E-10
ENSMUSG00000036985	Zdhhc9	0.303617428	0.000223	ENSMUSG00000066553	Gm6969	0.330620791	0.0028718
ENSMUSG00000050334	C130071C03Rik	0.303755099	0.0148044	ENSMUSG00000091537	Tma7	0.331862413	5.92E-08
ENSMUSG00000029465	Arpc3	0.304230435	1.25E-11	ENSMUSG00000018593	Sparc	0.331920833	1.87E-45
ENSMUSG00000027952	Pmvk	0.304453484	0.0020009	ENSMUSG00000029022	Miip	0.332088931	0.0003292
ENSMUSG00000056904	Gm5620	0.304507418	0.013595	ENSMUSG00000024376	Epb4.1l4a	0.33221461	1.62E-05
ENSMUSG00000048644	Ctxn1	0.304575546	0.0120504	ENSMUSG00000002409	Dyrk1b	0.332360745	0.0075152
ENSMUSG00000042116	Vwa1	0.306188672	0.0031083	ENSMUSG00000015944	Gatsl2	0.332520393	1.73E-05
ENSMUSG00000053470	Kdm3a	0.306206107	0.0058631	ENSMUSG00000030103	Bhlhe40	0.333629513	0.0027743
ENSMUSG00000062647	Rpl7a	0.306278414	1.11E-29	ENSMUSG00000068397	Gm10240	0.333895411	6.03E-10
ENSMUSG00000084159	Gm12696	0.306510358	0.0028593	ENSMUSG00000025369	Smarcc2	0.333929435	1.99E-18
ENSMUSG00000083563	Gm13340	0.306686885	0.0099458	ENSMUSG00000068220	Lgals1	0.334801987	2.28E-48
ENSMUSG00000031155	Pim2	0.307577653	0.0026456	ENSMUSG00000104413	Gm37065	0.335228552	0.0045837
ENSMUSG00000027331	Knstrn	0.307612758	3.84E-15	ENSMUSG00000005125	Ndrg1	0.335888969	0.0070241
ENSMUSG00000001119	Col6a1	0.307818456	1.03E-11	ENSMUSG00000035919	Bbs9	0.33613089	0.0025346
ENSMUSG00000033276	Stk36	0.308163913	0.0116408	ENSMUSG00000072214	Sept5	0.336261201	2.30E-05
ENSMUSG00000037573	Tob1	0.308659618	4.23E-05	ENSMUSG00000030022	Adamts9	0.33630205	0.0003137
ENSMUSG00000001131	Timp1	0.308720579	2.52E-14	ENSMUSG00000035834	Polr3g	0.337330563	9.78E-05
ENSMUSG00000025035	Arl3	0.309169842	0.0004527	ENSMUSG00000027469	Tpx2	0.33777417	5.88E-26
ENSMUSG00000042804	Gpr153	0.309443891	0.0045315	ENSMUSG00000042541	Shfm1	0.33842989	5.30E-13
ENSMUSG00000015217	Hmgb3	0.30946547	2.27E-09	ENSMUSG00000036768	Kif15	0.338696573	2.85E-10
ENSMUSG00000034771	Tle2	0.309526754	0.0110363	ENSMUSG00000004267	Eno2	0.339574748	0.0062039
ENSMUSG00000048148	Nwd1	0.309550394	0.0116003	ENSMUSG00000031799	Tpm4	0.339931856	8.50E-28
ENSMUSG00000031843	Mphosph6	0.309567258	0.0012134	ENSMUSG00000005682	Pan2	0.340075085	7.47E-05
ENSMUSG00000019837	Gtf3c6	0.309865617	5.94E-05	ENSMUSG00000085787	Gm13092	0.340395535	0.0059356
ENSMUSG00000081128	Gm13328	0.310196067	0.0127408	ENSMUSG00000018906	P4ha2	0.340652834	0.0004954
ENSMUSG00000024975	Pdcd4	0.310365315	0.0052437	ENSMUSG00000020022	Ndufa12	0.341328026	1.56E-10
ENSMUSG00000046179	E2f8	0.310517768	2.28E-07	ENSMUSG00000034906	Ncaph	0.34340848	2.32E-11
ENSMUSG00000019820	Utrn	0.31058429	2.14E-13	ENSMUSG00000050555	Hyls1	0.343843863	0.0004379
ENSMUSG00000051285	Pcmtd1	0.310588642	0.0011027	ENSMUSG00000012443	Kif11	0.344296791	4.20E-17
ENSMUSG00000020109	Dnajb12	0.310956168	5.41E-07	ENSMUSG00000028211	Trp53inp1	0.344327383	0.000142
ENSMUSG00000047146	Tet1	0.311829144	0.0118695	ENSMUSG00000046432	Ngfrap1	0.344419365	1.63E-12
ENSMUSG00000034868	Myl12b	0.312180097	2.13E-12	ENSMUSG00000062981	Mrpl42	0.34455256	1.38E-13
ENSMUSG00000037060	Prkcdbp	0.313319679	2.00E-09	ENSMUSG00000020949	Fkbp3	0.34488777	1.02E-12
ENSMUSG00000061887	Ssbp3	0.313770667	2.72E-05	ENSMUSG00000025791	Pgm2	0.345154054	4.47E-08
ENSMUSG00000037706	Cd81	0.314095712	6.25E-12	ENSMUSG00000021697	Depdc1b	0.345281885	0.0025632
ENSMUSG00000096472	Cdkn2d	0.314337455	0.0001455	ENSMUSG00000018362	Kpna2	0.345735646	9.29E-27
ENSMUSG00000028463	Car9	0.315360711	0.0108251	ENSMUSG00000037235	Mxd4	0.345799398	0.000134
ENSMUSG00000027778	Ift80	0.31561182	3.14E-05	ENSMUSG00000045294	Insig1	0.346508635	3.83E-07
ENSMUSG00000025978	Rftn2	0.315713137	0.0038775	ENSMUSG00000032254	Kif23	0.346862803	1.16E-19
ENSMUSG00000036882	Arhgap33	0.315753067	0.0112797	ENSMUSG00000028943	Espn	0.347801096	4.61E-10
ENSMUSG00000040624	Plekhg1	0.315771524	0.0007659	ENSMUSG00000021097	Clmn	0.348550964	0.0007696
ENSMUSG00000025006	Sorbs1	0.315877304	1.94E-14	ENSMUSG00000055675	Kbtbd11	0.348983389	2.85E-05
ENSMUSG00000026131	Dst	0.316163527	0.0006105	ENSMUSG00000023456	Tpi1	0.349022004	8.21E-05
ENSMUSG00000078300	Gm2606	0.316678003	0.0027418	ENSMUSG00000051517	Arhgef39	0.349087272	4.55E-05
ENSMUSG00000023064	Sncg	0.316892606	0.006334	ENSMUSG00000097796	Gm16702	0.349155201	0.0025691
ENSMUSG00000026335	Pam	0.317447584	6.19E-22	ENSMUSG00000059401	Mamld1	0.349387053	0.0002954
ENSMUSG00000054626	Xlr	0.31769859	9.97E-06	ENSMUSG00000020330	Hmmr	0.349632224	2.17E-20
ENSMUSG00000043073	Usp17le	0.318009324	0.0009516	ENSMUSG00000050856	Atp5k	0.350000706	1.06E-06
ENSMUSG00000062328	Rpl17	0.318206705	2.10E-40	ENSMUSG00000031617	Tmem184c	0.353362269	8.98E-07
ENSMUSG00000090394	4930523C07Rik	0.31899104	0.0020543	ENSMUSG00000019916	P4ha1	0.3535996	0.0005502

Gene		Log_2 Fold Change	pValue
ENSMUSG00000032398	Snapc5	0.353789174	0.0003863
ENSMUSG00000074802	Gas2l3	0.355625885	1.77E-18
ENSMUSG00000060429	Sntb1	0.356408527	3.59E-11
ENSMUSG00000097554	Gm26825	0.358727649	9.48E-20
ENSMUSG00000075610	Tmem92	0.359367821	0.0004082
ENSMUSG00000090714	Zscan4d	0.359718958	0.0009232
ENSMUSG00000074506	Gm10705	0.36113103	0.0023395
ENSMUSG00000020150	Gamt	0.361957224	4.82E-05
ENSMUSG00000025290	Rps24	0.362065618	4.92E-45
ENSMUSG00000046329	Slc25a23	0.362160502	7.37E-10
ENSMUSG00000034311	Kif4	0.362490148	1.88E-14
ENSMUSG00000025362	Rps26	0.362920399	1.01E-51
ENSMUSG00000032332	Col12a1	0.362927729	0.0009663
ENSMUSG00000055415	Atp10b	0.363184312	0.0001647
ENSMUSG00000029209	Gnpda2	0.363190913	0.0001711
ENSMUSG00000064372	mt-Tp	0.365154709	0.0002125
ENSMUSG00000026768	Itga8	0.367569433	0.0010103
ENSMUSG00000074968	Ano3	0.368033564	0.0030136
ENSMUSG00000031765	Mt1	0.368310958	1.20E-11
ENSMUSG00000031987	Egln1	0.369542348	1.26E-10
ENSMUSG00000090137	Uba52	0.369573648	6.60E-18
ENSMUSG00000037613	Tnfrsf23	0.369726707	6.62E-14
ENSMUSG00000004558	Ndrg2	0.370226578	0.0027983
ENSMUSG00000048327	Ckap2l	0.370248939	6.85E-19
ENSMUSG00000036977	Anapc10	0.37085065	0.0004041
ENSMUSG00000027210	Meis2	0.371528424	9.70E-05
ENSMUSG00000095677	Dynlt1f	0.371914674	0.0006645
ENSMUSG00000079627	Rhox2h	0.372368393	0.0001236
ENSMUSG00000070729	Gm12966	0.374608464	0.0006875
ENSMUSG00000030122	Ptms	0.37614749	9.15E-18
ENSMUSG00000041189	Chrnb1	0.376894829	0.0001707
ENSMUSG00000104022	Gm37214	0.37904391	1.34E-06
ENSMUSG00000024985	Tcf7l2	0.379523985	0.0009452
ENSMUSG00000003955	Fam162a	0.379586661	6.55E-06
ENSMUSG00000078776	9530053A07Rik	0.379743761	0.0019591
ENSMUSG00000078974	Sec61g	0.380371249	2.14E-10
ENSMUSG00000029253	Cenpc1	0.383353442	3.88E-07
ENSMUSG00000051855	Mest	0.387511788	1.19E-05
ENSMUSG00000019647	Sema6a	0.388682126	0.0007253
ENSMUSG00000047459	Dynlrb1	0.389049555	8.67E-15
ENSMUSG00000029427	Zcchc8	0.389568014	1.65E-10
ENSMUSG00000047888	Tnrc6b	0.392591046	1.28E-08
ENSMUSG00000020914	Top2a	0.393094024	1.39E-66
ENSMUSG00000038943	Prc1	0.393413406	1.04E-38
ENSMUSG00000024044	Epb4.1l3	0.393794306	0.0008556
ENSMUSG00000056888	Glipr1	0.393957949	5.60E-06
ENSMUSG00000098183	Gm27010	0.395801534	0.0006558
ENSMUSG00000025656	Arhgef9	0.397049786	4.98E-05
ENSMUSG00000057092	Fxyd3	0.399702281	1.59E-06
ENSMUSG00000031349	Nsdhl	0.400383816	1.37E-09
ENSMUSG00000032374	Plod2	0.400491564	7.02E-07
ENSMUSG00000028175	Depdc1a	0.402929565	6.50E-08
ENSMUSG00000039114	Nrn1	0.402955163	1.02E-07
ENSMUSG00000072082	Ccnf	0.403209167	2.54E-13
ENSMUSG00000035847	Ids	0.404588608	2.54E-12
ENSMUSG00000026683	Nuf2	0.405005768	5.22E-16
ENSMUSG00000022639	5330426P16Rik	0.40689475	0.0002952
ENSMUSG00000020644	Id2	0.407336986	1.64E-14
ENSMUSG00000039396	Neil3	0.410945333	0.0003526
ENSMUSG00000017446	C1qtnf1	0.41258478	1.33E-12
ENSMUSG00000058546	Rpl23a	0.415723483	1.61E-72
ENSMUSG00000032363	Adamts7	0.416249386	1.96E-06
ENSMUSG00000043192	Gm1840	0.417346846	0.0001074
ENSMUSG00000093930	Hmgcs1	0.421279341	1.36E-08
ENSMUSG00000028551	Cdkn2c	0.424319663	2.45E-08
ENSMUSG00000042109	Csdc2	0.424926795	5.59E-09
ENSMUSG00000054312	Mrps21	0.426103859	7.14E-11
ENSMUSG00000025025	Mxi1	0.426215588	0.0001703
ENSMUSG00000065947	mt-Nd4l	0.427825495	0.0005936
ENSMUSG00000049299	Trappc1	0.428124938	1.63E-07
ENSMUSG00000045328	Cenpe	0.429416053	1.20E-24
ENSMUSG00000079523	Tmsb10	0.431501666	5.23E-37
ENSMUSG00000036751	Cox6b1	0.432353848	1.70E-25
ENSMUSG00000024038	Ndufv3	0.434669524	2.30E-07
ENSMUSG00000041577	Prelp	0.436170813	0.000191
ENSMUSG00000078784	1810022K09Rik	0.437231675	2.88E-11
ENSMUSG00000029004	Kmt2e	0.437644656	1.09E-14
ENSMUSG00000046794	Ppp1r3b	0.439659808	0.000295
ENSMUSG00000029309	Sparcl1	0.440029525	1.49E-12
ENSMUSG00000100215	Gm8292	0.441965852	1.60E-07
ENSMUSG00000026385	Dbi	0.446568121	7.43E-31
ENSMUSG00000020427	Igfbp3	0.450255365	2.63E-23
ENSMUSG00000031245	Hmgn5	0.451586868	3.76E-14
ENSMUSG00000100801	Gm15459	0.451889317	9.74E-26
ENSMUSG00000028464	Tpm2	0.452450625	5.16E-12
ENSMUSG00000047557	Lxn	0.45495059	2.26E-13
ENSMUSG00000020601	Trib2	0.45614354	2.10E-05
ENSMUSG00000037010	Apln	0.456986438	0.000202
ENSMUSG00000001870	Ltbp1	0.457888604	5.65E-11
ENSMUSG00000020263	Appl2	0.458760223	1.80E-08
ENSMUSG00000050914	Ankrd37	0.462803241	0.0001273
ENSMUSG00000033952	Aspm	0.463333419	2.07E-26
ENSMUSG00000021253	Tgfb3	0.467246627	6.58E-05
ENSMUSG00000087687	Pet100	0.468238267	6.40E-05
ENSMUSG00000020326	Ccng1	0.470461284	3.04E-32
ENSMUSG00000000056	Narf	0.470944481	8.73E-05
ENSMUSG00000029385	Ccng2	0.474152871	1.41E-08
ENSMUSG00000029304	Spp1	0.47931031	3.99E-89
ENSMUSG00000106334	WI1-49P9.2	0.480495257	5.77E-57
ENSMUSG00000055435	Maf	0.480744667	2.11E-07
ENSMUSG00000032193	Ldlr	0.483947608	1.05E-20
ENSMUSG00000062997	Rpl35	0.491120144	5.06E-46
ENSMUSG00000041453	Rpl21	0.498354569	2.14E-20
ENSMUSG00000081455	Hmgb1-ps3	0.507663957	1.38E-05
ENSMUSG00000035105	Egln3	0.513738146	1.32E-05
ENSMUSG00000048758	Rpl29	0.516669545	3.48E-24
ENSMUSG00000038375	Trp53inp2	0.52545131	8.37E-14
ENSMUSG00000063882	Uqcrh	0.542199773	8.78E-25
ENSMUSG00000079685	Ulbp1	0.543396072	1.74E-17
ENSMUSG00000027306	Nusap1	0.54792867	3.63E-27
ENSMUSG00000003541	Ier3	0.553296509	6.23E-14
ENSMUSG00000057666	Gapdh	0.557001188	7.62E-17
ENSMUSG00000031561	Tenm3	0.557206543	9.20E-46
ENSMUSG00000064367	mt-Nd5	0.565834364	2.24E-131
ENSMUSG00000031004	Mki67	0.568434196	4.58E-137
ENSMUSG00000026605	Cenpf	0.569979866	4.29E-49
ENSMUSG00000001020	S100a4	0.576591039	8.55E-39
ENSMUSG00000038776	Ephx1	0.58659428	2.13E-22
ENSMUSG00000027907	S100a11	0.588540773	8.19E-73
ENSMUSG00000081049	Rps24-ps3	0.591188478	6.43E-09
ENSMUSG00000021185	9030617O03Rik	0.600343835	9.59E-09
ENSMUSG00000064368	mt-Nd6	0.618043075	1.17E-79
ENSMUSG00000070828	Zscan4f	0.618413883	1.16E-07
ENSMUSG00000039601	Rcan2	0.628762927	6.52E-14
ENSMUSG00000064363	mt-Nd4	0.644745122	1.43E-164
ENSMUSG00000091618	H60c	0.651164026	4.09E-08
ENSMUSG00000064370	mt-Cytb	0.672783511	0
ENSMUSG00000040128	Pnrc1	0.6878621	1.80E-10
ENSMUSG00000064337	mt-Rnr1	0.691784944	4.44E-36
ENSMUSG00000064341	mt-Nd1	0.722884839	1.68E-293
ENSMUSG00000064345	mt-Nd2	0.73108998	6.87E-276
ENSMUSG00000097352	C920009B18Rik	0.769834513	8.33E-18
ENSMUSG00000075297	H60b	0.793052386	3.55E-12
ENSMUSG00000064356	mt-Atp8	0.812613327	2.25E-164

APPENDIX D:

COPYRIGHT PERMISSIONS

NATURE PUBLISHING GROUP LICENSE
TERMS AND CONDITIONS

Oct 12, 2017

This Agreement between James B Case ("You") and Nature Publishing Group ("Nature Publishing Group") consists of your license details and the terms and conditions provided by Nature Publishing Group and Copyright Clearance Center.

License Number	4206621287308
License date	Oct 12, 2017
Licensed Content Publisher	Nature Publishing Group
Licensed Content Publication	Nature Reviews Microbiology
Licensed Content Title	Coronaviruses post-SARS: update on replication and pathogenesis
Licensed Content Author	Stanley Perlman and Jason Netland
Licensed Content Date	Jun 1, 2009
Licensed Content Volume	7
Licensed Content Issue	6
Type of Use	reuse in a dissertation / thesis
Requestor type	academic/educational
Format	print and electronic
Portion	figures/tables/illustrations
Number of figures/tables/illustrations	1
High-res required	no
Figures	2b
Author of this NPG article	no
Your reference number	
Title of your thesis / dissertation	Roles of the Coronavirus 3'-to-5' Exoribonuclease and N7-Methyltransferase in Counteracting Innate Immunity
Expected completion date	May 2018
Estimated size (number of pages)	180
Requestor Location	James B Case Vanderbilt University Medical Center MCN D-6221 1161 21st Avenue South NASHVILLE, TN 37232 United States Attn: James Case
Billing Type	Invoice
Billing Address	James Case Vanderbilt University Medical Center MCN D-6221 1161 21st Avenue South NASHVILLE, TN 37232 United States Attn: James B Case

Total 0.00 USD

Terms and Conditions

Terms and Conditions for Permissions

Nature Publishing Group hereby grants you a non-exclusive license to reproduce this material for this purpose, and for no other use,subject to the conditions below:

1. NPG warrants that it has, to the best of its knowledge, the rights to license reuse of this material. However, you should ensure that the material you are requesting is original to Nature Publishing Group and does not carry the copyright of another entity (as credited in the published version). If the credit line on any part of the material you have requested indicates that it was reprinted or adapted by NPG with permission from another source, then you should also seek permission from that source to reuse the material.

2. Permission granted free of charge for material in print is also usually granted for any electronic version of that work, provided that the material is incidental to the work as a whole and that the electronic version is essentially equivalent to, or substitutes for, the print version.Where print permission has been granted for a fee, separate permission must be obtained for any additional, electronic re-use (unless, as in the case of a full paper, this has already been accounted for during your initial request in the calculation of a print run).NB: In all cases, web-based use of full-text articles must be authorized separately through the 'Use on a Web Site' option when requesting permission.

3. Permission granted for a first edition does not apply to second and subsequent editions and for editions in other languages (except for signatories to the STM Permissions Guidelines, or where the first edition permission was granted for free).

4. Nature Publishing Group's permission must be acknowledged next to the figure, table or abstract in print. In electronic form, this acknowledgement must be visible at the same time as the figure/table/abstract, and must be hyperlinked to the journal's homepage.

5. The credit line should read:
   Reprinted by permission from Macmillan Publishers Ltd: [JOURNAL NAME] (reference citation), copyright (year of publication)
   For AOP papers, the credit line should read:
   Reprinted by permission from Macmillan Publishers Ltd: [JOURNAL NAME], advance online publication, day month year (doi: 10.1038/sj.[JOURNAL ACRONYM].XXXXX)

   Note: For republication from the *British Journal of Cancer,* the following credit lines apply.
   Reprinted by permission from Macmillan Publishers Ltd on behalf of Cancer Research UK: [JOURNAL NAME] (reference citation), copyright (year of publication)For AOP papers, the credit line should read:
   Reprinted by permission from Macmillan Publishers Ltd on behalf of Cancer Research UK: [JOURNAL NAME], advance online publication, day month year (doi: 10.1038/sj.[JOURNAL ACRONYM].XXXXX)

6. Adaptations of single figures do not require NPG approval. However, the adaptation should be credited as follows:

   Adapted by permission from Macmillan Publishers Ltd: [JOURNAL NAME] (reference citation), copyright (year of publication)

   Note: For adaptation from the *British Journal of Cancer,* the following credit line applies.
   Adapted by permission from Macmillan Publishers Ltd on behalf of Cancer Research UK: [JOURNAL NAME] (reference citation), copyright (year of publication)

7. Translations of 401 words up to a whole article require NPG approval. Please visit http://www.macmillanmedicalcommunications.com for more information.Translations of up to a 400 words do not require NPG approval. The translation should be credited as follows:

Translated by permission from Macmillan Publishers Ltd: [JOURNAL NAME] (reference citation), copyright (year of publication).

Note: For translation from the *British Journal of Cancer,* the following credit line applies.
Translated by permission from Macmillan Publishers Ltd on behalf of Cancer Research UK: [JOURNAL NAME] (reference citation), copyright (year of publication)

We are certain that all parties will benefit from this agreement and wish you the best in the use of this material. Thank you.
Special Terms:
v1.1

Questions? customercare@copyright.com or +1-855-239-3415 (toll free in the US) or +1-978-646-2777.

Microbiology Society LICENSE TERMS AND CONDITIONS

Oct 30, 2017

This is a License Agreement between James B Case ("You") and Microbiology Society ("Microbiology Society") provided by Copyright Clearance Center ("CCC"). The license consists of your order details, the terms and conditions provided by Microbiology Society, and the payment terms and conditions.

All payments must be made in full to CCC. For payment instructions, please see information listed at the bottom of this form.

License Number	4218920508768
License date	Oct 30, 2017
Licensed content publisher	Microbiology Society
Licensed content title	The Journal of general virology
Licensed content date	Jan 1, 1967
Type of Use	Thesis/Dissertation
Requestor type	Academic institution
Format	Print, Electronic
Portion	image/photo
Number of images/photos requested	1
The requesting person/organization is:	James Case
Title or numeric reference of the portion(s)	Figure 1
Title of the article or chapter the portion is from	The Morphological and Biological Effects of Various Antisera on Avian Infectious Bronchitis Virus
Editor of portion(s)	N/A
Author of portion(s)	D.M. Berry and June D. Almeida
Volume of serial or monograph.	3
Issue, if republishing an article from a serial	1
Page range of the portion	Plate 1
Publication date of portion	February 12, 1968
Rights for	Main product
Duration of use	Current edition and up to 5 years
Creation of copies for the disabled	no
With minor editing privileges	no
For distribution to	Worldwide
In the following language(s)	Original language of publication
With incidental promotional	no

use	
The lifetime unit quantity of new product	Up to 499
Title	Roles of the Coronavirus 3'-to-5' Exoribonuclease and N7-Methyltransferase in Counteracting Innate Immunity
Instructor name	n/a
Institution name	n/a
Expected presentation date	May 2018
Total (may include CCC user fee)	0.00 USD

Terms and Conditions

TERMS AND CONDITIONS
The following terms are individual to this publisher:

None

Other Terms and Conditions:
STANDARD TERMS AND CONDITIONS

1. Description of Service; Defined Terms. This Republication License enables the User to obtain licenses for republication of one or more copyrighted works as described in detail on the relevant Order Confirmation (the "Work(s)"). Copyright Clearance Center, Inc. ("CCC") grants licenses through the Service on behalf of the rightsholder identified on the Order Confirmation (the "Rightsholder"). "Republication", as used herein, generally means the inclusion of a Work, in whole or in part, in a new work or works, also as described on the Order Confirmation. "User", as used herein, means the person or entity making such republication.

2. The terms set forth in the relevant Order Confirmation, and any terms set by the Rightsholder with respect to a particular Work, govern the terms of use of Works in connection with the Service. By using the Service, the person transacting for a republication license on behalf of the User represents and warrants that he/she/it (a) has been duly authorized by the User to accept, and hereby does accept, all such terms and conditions on behalf of User, and (b) shall inform User of all such terms and conditions. In the event such person is a "freelancer" or other third party independent of User and CCC, such party shall be deemed jointly a "User" for purposes of these terms and conditions. In any event, User shall be deemed to have accepted and agreed to all such terms and conditions if User republishes the Work in any fashion.

3. Scope of License; Limitations and Obligations.

3.1 All Works and all rights therein, including copyright rights, remain the sole and exclusive property of the Rightsholder. The license created by the exchange of an Order Confirmation (and/or any invoice) and payment by User of the full amount set forth on that document includes only those rights expressly set forth in the Order Confirmation and in these terms and conditions, and conveys no other rights in the Work(s) to User. All rights not expressly granted are hereby reserved.

3.2 General Payment Terms: You may pay by credit card or through an account with us payable at the end of the month. If you and we agree that you may establish a standing account with CCC, then the following terms apply: Remit Payment to: Copyright Clearance Center, 29118 Network Place, Chicago, IL 60673-1291. Payments Due: Invoices are payable upon their delivery to you (or upon our notice to you that they are available to you for downloading). After 30 days, outstanding amounts will be subject to a service charge of 1-1/2% per month or, if less, the maximum rate allowed by applicable law. Unless otherwise specifically set forth in the Order Confirmation or in a separate written agreement signed by CCC, invoices are due and payable on "net 30" terms. While User may exercise the rights licensed immediately upon issuance of the Order Confirmation, the license is automatically revoked and is null and void, as if it had never been issued, if complete payment for the

6. Limited Warranties. THE WORK(S) AND RIGHT(S) ARE PROVIDED “AS IS”. CCC HAS THE RIGHT TO GRANT TO USER THE RIGHTS GRANTED IN THE ORDER CONFIRMATION DOCUMENT. CCC AND THE RIGHTSHOLDER DISCLAIM ALL OTHER WARRANTIES RELATING TO THE WORK(S) AND RIGHT(S), EITHER EXPRESS OR IMPLIED, INCLUDING WITHOUT LIMITATION IMPLIED WARRANTIES OF MERCHANTABILITY OR FITNESS FOR A PARTICULAR PURPOSE. ADDITIONAL RIGHTS MAY BE REQUIRED TO USE ILLUSTRATIONS, GRAPHS, PHOTOGRAPHS, ABSTRACTS, INSERTS OR OTHER PORTIONS OF THE WORK (AS OPPOSED TO THE ENTIRE WORK) IN A MANNER CONTEMPLATED BY USER; USER UNDERSTANDS AND AGREES THAT NEITHER CCC NOR THE RIGHTSHOLDER MAY HAVE SUCH ADDITIONAL RIGHTS TO GRANT.
7. Effect of Breach. Any failure by User to pay any amount when due, or any use by User of a Work beyond the scope of the license set forth in the Order Confirmation and/or these terms and conditions, shall be a material breach of the license created by the Order Confirmation and these terms and conditions. Any breach not cured within 30 days of written notice thereof shall result in immediate termination of such license without further notice. Any unauthorized (but licensable) use of a Work that is terminated immediately upon notice thereof may be liquidated by payment of the Rightsholder's ordinary license price therefor; any unauthorized (and unlicensable) use that is not terminated immediately for any reason (including, for example, because materials containing the Work cannot reasonably be recalled) will be subject to all remedies available at law or in equity, but in no event to a payment of less than three times the Rightsholder's ordinary license price for the most closely analogous licensable use plus Rightsholder's and/or CCC's costs and expenses incurred in collecting such payment.
8. **Miscellaneous.**
8.1 User acknowledges that CCC may, from time to time, make changes or additions to the Service or to these terms and conditions, and CCC reserves the right to send notice to the User by electronic mail or otherwise for the purposes of notifying User of such changes or additions; provided that any such changes or additions shall not apply to permissions already secured and paid for.
8.2 Use of User-related information collected through the Service is governed by CCC’s privacy policy, available online here:
http://www.copyright.com/content/cc3/en/tools/footer/privacypolicy.html.
8.3 The licensing transaction described in the Order Confirmation is personal to User. Therefore, User may not assign or transfer to any other person (whether a natural person or an organization of any kind) the license created by the Order Confirmation and these terms and conditions or any rights granted hereunder; provided, however, that User may assign such license in its entirety on written notice to CCC in the event of a transfer of all or substantially all of User’s rights in the new material which includes the Work(s) licensed under this Service.
8.4 No amendment or waiver of any terms is binding unless set forth in writing and signed by the parties. The Rightsholder and CCC hereby object to any terms contained in any writing prepared by the User or its principals, employees, agents or affiliates and purporting to govern or otherwise relate to the licensing transaction described in the Order Confirmation, which terms are in any way inconsistent with any terms set forth in the Order Confirmation and/or in these terms and conditions or CCC's standard operating procedures, whether such writing is prepared prior to, simultaneously with or subsequent to the Order Confirmation, and whether such writing appears on a copy of the Order Confirmation or in a separate instrument.
8.5 The licensing transaction described in the Order Confirmation document shall be governed by and construed under the law of the State of New York, USA, without regard to the principles thereof of conflicts of law. Any case, controversy, suit, action, or proceeding arising out of, in connection with, or related to such licensing transaction shall be brought, at CCC's sole discretion, in any federal or state court located in the County of New York, State

ELSEVIER LICENSE
TERMS AND CONDITIONS

Oct 11, 2017

This Agreement between James Case ("You") and Elsevier ("Elsevier") consists of your license details and the terms and conditions provided by Elsevier and Copyright Clearance Center.

License Number	4206121184493
License date	Oct 11, 2017
Licensed Content Publisher	Elsevier
Licensed Content Publication	The American Journal of Pathology
Licensed Content Title	Pathology and Pathogenesis of Severe Acute Respiratory Syndrome
Licensed Content Author	Jiang Gu,Christine Korteweg
Licensed Content Date	Apr 1, 2007
Licensed Content Volume	170
Licensed Content Issue	4
Licensed Content Pages	12
Start Page	1136
End Page	1147
Type of Use	reuse in a thesis/dissertation
Intended publisher of new work	other
Portion	figures/tables/illustrations
Number of figures/tables/illustrations	1
Format	both print and electronic
Are you the author of this Elsevier article?	No
Will you be translating?	No
Original figure numbers	Figure 2
Title of your thesis/dissertation	Roles of the Coronavirus 3'-to-5' Exoribonuclease and N7-Methyltransferase in Counteracting Innate Immunity
Expected completion date	May 2018
Estimated size (number of pages)	180
Requestor Location	James Case Vanderbilt University Medical Center MCN D-6221 1161 21st Avenue South NASHVILLE, TN 37232 United States Attn: James Case
Publisher Tax ID	98-0397604
Total	0.00 USD

11. No Transfer of License: This license is personal to you and may not be sublicensed, assigned, or transferred by you to any other person without publisher's written permission.
12. No Amendment Except in Writing: This license may not be amended except in a writing signed by both parties (or, in the case of publisher, by CCC on publisher's behalf).
13. Objection to Contrary Terms: Publisher hereby objects to any terms contained in any purchase order, acknowledgment, check endorsement or other writing prepared by you, which terms are inconsistent with these terms and conditions or CCC's Billing and Payment terms and conditions. These terms and conditions, together with CCC's Billing and Payment terms and conditions (which are incorporated herein), comprise the entire agreement between you and publisher (and CCC) concerning this licensing transaction. In the event of any conflict between your obligations established by these terms and conditions and those established by CCC's Billing and Payment terms and conditions, these terms and conditions shall control.
14. Revocation: Elsevier or Copyright Clearance Center may deny the permissions described in this License at their sole discretion, for any reason or no reason, with a full refund payable to you. Notice of such denial will be made using the contact information provided by you. Failure to receive such notice will not alter or invalidate the denial. In no event will Elsevier or Copyright Clearance Center be responsible or liable for any costs, expenses or damage incurred by you as a result of a denial of your permission request, other than a refund of the amount(s) paid by you to Elsevier and/or Copyright Clearance Center for denied permissions.

LIMITED LICENSE

The following terms and conditions apply only to specific license types:
15. **Translation**: This permission is granted for non-exclusive world **English** rights only unless your license was granted for translation rights. If you licensed translation rights you may only translate this content into the languages you requested. A professional translator must perform all translations and reproduce the content word for word preserving the integrity of the article.
16. **Posting licensed content on any Website**: The following terms and conditions apply as follows: Licensing material from an Elsevier journal: All content posted to the web site must maintain the copyright information line on the bottom of each image; A hyper-text must be included to the Homepage of the journal from which you are licensing at http://www.sciencedirect.com/science/journal/xxxxx or the Elsevier homepage for books at http://www.elsevier.com; Central Storage: This license does not include permission for a scanned version of the material to be stored in a central repository such as that provided by Heron/XanEdu.
Licensing material from an Elsevier book: A hyper-text link must be included to the Elsevier homepage at http://www.elsevier.com . All content posted to the web site must maintain the copyright information line on the bottom of each image.

Posting licensed content on Electronic reserve: In addition to the above the following clauses are applicable: The web site must be password-protected and made available only to bona fide students registered on a relevant course. This permission is granted for 1 year only. You may obtain a new license for future website posting.
17. **For journal authors:** the following clauses are applicable in addition to the above:
Preprints:
A preprint is an author's own write-up of research results and analysis, it has not been peer-reviewed, nor has it had any other value added to it by a publisher (such as formatting, copyright, technical enhancement etc.).
Authors can share their preprints anywhere at any time. Preprints should not be added to or enhanced in any way in order to appear more like, or to substitute for, the final versions of articles however authors can update their preprints on arXiv or RePEc with their Accepted Author Manuscript (see below).

If accepted for publication, we encourage authors to link from the preprint to their formal publication via its DOI. Millions of researchers have access to the formal publications on ScienceDirect, and so links will help users to find, access, cite and use the best available version. Please note that Cell Press, The Lancet and some society-owned have different preprint policies. Information on these policies is available on the journal homepage.
Accepted Author Manuscripts: An accepted author manuscript is the manuscript of an article that has been accepted for publication and which typically includes author-incorporated changes suggested during submission, peer review and editor-author communications.
Authors can share their accepted author manuscript:

- immediately
    - via their non-commercial person homepage or blog
    - by updating a preprint in arXiv or RePEc with the accepted manuscript
    - via their research institute or institutional repository for internal institutional uses or as part of an invitation-only research collaboration work-group
    - directly by providing copies to their students or to research collaborators for their personal use
    - for private scholarly sharing as part of an invitation-only work group on commercial sites with which Elsevier has an agreement
- After the embargo period
    - via non-commercial hosting platforms such as their institutional repository
    - via commercial sites with which Elsevier has an agreement

In all cases accepted manuscripts should:

- link to the formal publication via its DOI
- bear a CC-BY-NC-ND license - this is easy to do
- if aggregated with other manuscripts, for example in a repository or other site, be shared in alignment with our hosting policy not be added to or enhanced in any way to appear more like, or to substitute for, the published journal article.

Published journal article (JPA): A published journal article (PJA) is the definitive final record of published research that appears or will appear in the journal and embodies all value-adding publishing activities including peer review co-ordination, copy-editing, formatting, (if relevant) pagination and online enrichment.
Policies for sharing publishing journal articles differ for subscription and gold open access articles:
Subscription Articles: If you are an author, please share a link to your article rather than the full-text. Millions of researchers have access to the formal publications on ScienceDirect, and so links will help your users to find, access, cite, and use the best available version.
Theses and dissertations which contain embedded PJAs as part of the formal submission can be posted publicly by the awarding institution with DOI links back to the formal publications on ScienceDirect.
If you are affiliated with a library that subscribes to ScienceDirect you have additional private sharing rights for others' research accessed under that agreement. This includes use for classroom teaching and internal training at the institution (including use in course packs and courseware programs), and inclusion of the article for grant funding purposes.
Gold Open Access Articles: May be shared according to the author-selected end-user license and should contain a CrossMark logo, the end user license, and a DOI link to the formal publication on ScienceDirect.
Please refer to Elsevier's posting policy for further information.
18. **For book authors** the following clauses are applicable in addition to the above:
Authors are permitted to place a brief summary of their work online only. You are not

allowed to download and post the published electronic version of your chapter, nor may you scan the printed edition to create an electronic version. **Posting to a repository:** Authors are permitted to post a summary of their chapter only in their institution's repository.
19. **Thesis/Dissertation**: If your license is for use in a thesis/dissertation your thesis may be submitted to your institution in either print or electronic form. Should your thesis be published commercially, please reapply for permission. These requirements include permission for the Library and Archives of Canada to supply single copies, on demand, of the complete thesis and include permission for Proquest/UMI to supply single copies, on demand, of the complete thesis. Should your thesis be published commercially, please reapply for permission. Theses and dissertations which contain embedded PJAs as part of the formal submission can be posted publicly by the awarding institution with DOI links back to the formal publications on ScienceDirect.

Elsevier Open Access Terms and Conditions
You can publish open access with Elsevier in hundreds of open access journals or in nearly 2000 established subscription journals that support open access publishing. Permitted third party re-use of these open access articles is defined by the author's choice of Creative Commons user license. See our open access license policy for more information.
Terms & Conditions applicable to all Open Access articles published with Elsevier:
Any reuse of the article must not represent the author as endorsing the adaptation of the article nor should the article be modified in such a way as to damage the author's honour or reputation. If any changes have been made, such changes must be clearly indicated.
The author(s) must be appropriately credited and we ask that you include the end user license and a DOI link to the formal publication on ScienceDirect.
If any part of the material to be used (for example, figures) has appeared in our publication with credit or acknowledgement to another source it is the responsibility of the user to ensure their reuse complies with the terms and conditions determined by the rights holder.
Additional Terms & Conditions applicable to each Creative Commons user license:
CC BY: The CC-BY license allows users to copy, to create extracts, abstracts and new works from the Article, to alter and revise the Article and to make commercial use of the Article (including reuse and/or resale of the Article by commercial entities), provided the user gives appropriate credit (with a link to the formal publication through the relevant DOI), provides a link to the license, indicates if changes were made and the licensor is not represented as endorsing the use made of the work. The full details of the license are available at http://creativecommons.org/licenses/by/4.0.
CC BY NC SA: The CC BY-NC-SA license allows users to copy, to create extracts, abstracts and new works from the Article, to alter and revise the Article, provided this is not done for commercial purposes, and that the user gives appropriate credit (with a link to the formal publication through the relevant DOI), provides a link to the license, indicates if changes were made and the licensor is not represented as endorsing the use made of the work. Further, any new works must be made available on the same conditions. The full details of the license are available at http://creativecommons.org/licenses/by-nc-sa/4.0.
CC BY NC ND: The CC BY-NC-ND license allows users to copy and distribute the Article, provided this is not done for commercial purposes and further does not permit distribution of the Article if it is changed or edited in any way, and provided the user gives appropriate credit (with a link to the formal publication through the relevant DOI), provides a link to the license, and that the licensor is not represented as endorsing the use made of the work. The full details of the license are available at http://creativecommons.org/licenses/by-nc-nd/4.0.
Any commercial reuse of Open Access articles published with a CC BY NC SA or CC BY NC ND license requires permission from Elsevier and will be subject to a fee.
Commercial reuse includes:

- Associating advertising with the full text of the Article
- Charging fees for document delivery or access

- Article aggregation
- Systematic distribution via e-mail lists or share buttons

Posting or linking by commercial companies for use by customers of those companies.

20. **Other Conditions**:

v1.9

Questions? customercare@copyright.com or +1-855-239-3415 (toll free in the US) or +1-978-646-2777.

NATURE PUBLISHING GROUP LICENSE TERMS AND CONDITIONS

Oct 11, 2017

This Agreement between James Case ("You") and Nature Publishing Group ("Nature Publishing Group") consists of your license details and the terms and conditions provided by Nature Publishing Group and Copyright Clearance Center.

License Number	4206110969024
License date	Oct 11, 2017
Licensed Content Publisher	Nature Publishing Group
Licensed Content Publication	Nature Reviews Microbiology
Licensed Content Title	SARS and MERS: recent insights into emerging coronaviruses
Licensed Content Author	Emmie de Wit, Neeltje van Doremalen, Darryl Falzarano, Vincent J. Munster
Licensed Content Date	Jun 27, 2016
Licensed Content Volume	14
Licensed Content Issue	8
Type of Use	reuse in a dissertation / thesis
Requestor type	academic/educational
Format	print and electronic
Portion	figures/tables/illustrations
Number of figures/tables/illustrations	1
High-res required	no
Figures	Figure 1b
Author of this NPG article	no
Your reference number	
Title of your thesis / dissertation	Roles of the Coronavirus 3'-to-5' Exoribonuclease and N7-Methyltransferase in Counteracting Innate Immunity
Expected completion date	May 2018
Estimated size (number of pages)	180
Requestor Location	James Case Vanderbilt University Medical Center MCN D-6221 1161 21st Avenue South NASHVILLE, TN 37232 United States Attn: James Case
Billing Type	Invoice
Billing Address	James Case Vanderbilt University Medical Center MCN D-6221 1161 21st Avenue South NASHVILLE, TN 37232

United States
Attn: James B Case

Total 0.00 USD

Terms and Conditions

Terms and Conditions for Permissions

Nature Publishing Group hereby grants you a non-exclusive license to reproduce this material for this purpose, and for no other use,subject to the conditions below:

1. NPG warrants that it has, to the best of its knowledge, the rights to license reuse of this material. However, you should ensure that the material you are requesting is original to Nature Publishing Group and does not carry the copyright of another entity (as credited in the published version). If the credit line on any part of the material you have requested indicates that it was reprinted or adapted by NPG with permission from another source, then you should also seek permission from that source to reuse the material.

2. Permission granted free of charge for material in print is also usually granted for any electronic version of that work, provided that the material is incidental to the work as a whole and that the electronic version is essentially equivalent to, or substitutes for, the print version.Where print permission has been granted for a fee, separate permission must be obtained for any additional, electronic re-use (unless, as in the case of a full paper, this has already been accounted for during your initial request in the calculation of a print run).NB: In all cases, web-based use of full-text articles must be authorized separately through the 'Use on a Web Site' option when requesting permission.

3. Permission granted for a first edition does not apply to second and subsequent editions and for editions in other languages (except for signatories to the STM Permissions Guidelines, or where the first edition permission was granted for free).

4. Nature Publishing Group's permission must be acknowledged next to the figure, table or abstract in print. In electronic form, this acknowledgement must be visible at the same time as the figure/table/abstract, and must be hyperlinked to the journal's homepage.

5. The credit line should read:
   Reprinted by permission from Macmillan Publishers Ltd: [JOURNAL NAME] (reference citation), copyright (year of publication)
   For AOP papers, the credit line should read:
   Reprinted by permission from Macmillan Publishers Ltd: [JOURNAL NAME], advance online publication, day month year (doi: 10.1038/sj.[JOURNAL ACRONYM].XXXXX)

   Note: For republication from the *British Journal of Cancer,* the following credit lines apply.
   Reprinted by permission from Macmillan Publishers Ltd on behalf of Cancer Research UK: [JOURNAL NAME] (reference citation), copyright (year of publication)For AOP papers, the credit line should read:
   Reprinted by permission from Macmillan Publishers Ltd on behalf of Cancer Research UK: [JOURNAL NAME], advance online publication, day month year (doi: 10.1038/sj.[JOURNAL ACRONYM].XXXXX)

6. Adaptations of single figures do not require NPG approval. However, the adaptation should be credited as follows:

   Adapted by permission from Macmillan Publishers Ltd: [JOURNAL NAME] (reference citation), copyright (year of publication)

   Note: For adaptation from the *British Journal of Cancer,* the following credit line applies.
   Adapted by permission from Macmillan Publishers Ltd on behalf of Cancer Research UK: [JOURNAL NAME] (reference citation), copyright (year of publication)

7. Translations of 401 words up to a whole article require NPG approval. Please visit http://www.macmillanmedicalcommunications.com for more information.Translations of up

to a 400 words do not require NPG approval. The translation should be credited as follows:

Translated by permission from Macmillan Publishers Ltd: [JOURNAL NAME] (reference citation), copyright (year of publication).

Note: For translation from the *British Journal of Cancer,* the following credit line applies.
Translated by permission from Macmillan Publishers Ltd on behalf of Cancer Research UK: [JOURNAL NAME] (reference citation), copyright (year of publication)

We are certain that all parties will benefit from this agreement and wish you the best in the use of this material. Thank you.
Special Terms:
v1.1

NATURE PUBLISHING GROUP LICENSE TERMS AND CONDITIONS

Oct 12, 2017

This Agreement between James B Case ("You") and Nature Publishing Group ("Nature Publishing Group") consists of your license details and the terms and conditions provided by Nature Publishing Group and Copyright Clearance Center.

License Number	4206600479276
License date	Oct 12, 2017
Licensed Content Publisher	Nature Publishing Group
Licensed Content Publication	Nature Reviews Microbiology
Licensed Content Title	Conventional and unconventional mechanisms for capping viral mRNA
Licensed Content Author	Etienne Decroly, François Ferron, Julien Lescar and Bruno Canard
Licensed Content Date	Jan 1, 2012
Licensed Content Volume	10
Licensed Content Issue	1
Type of Use	reuse in a dissertation / thesis
Requestor type	academic/educational
Format	print and electronic
Portion	figures/tables/illustrations
Number of figures/tables/illustrations	1
High-res required	no
Figures	1a
Author of this NPG article	no
Your reference number	
Title of your thesis / dissertation	Roles of the Coronavirus 3'-to-5' Exoribonuclease and N7-Methyltransferase in Counteracting Innate Immunity
Expected completion date	May 2018
Estimated size (number of pages)	180
Requestor Location	James B Case Vanderbilt University Medical Center MCN D-6221 1161 21st Avenue South NASHVILLE, TN 37232 United States Attn: James Case
Billing Type	Invoice
Billing Address	James Case Vanderbilt University Medical Center MCN D-6221 1161 21st Avenue South NASHVILLE, TN 37232

United States
Attn: James B Case

Total 0.00 USD

Terms and Conditions

Terms and Conditions for Permissions

Nature Publishing Group hereby grants you a non-exclusive license to reproduce this material for this purpose, and for no other use,subject to the conditions below:

1. NPG warrants that it has, to the best of its knowledge, the rights to license reuse of this material. However, you should ensure that the material you are requesting is original to Nature Publishing Group and does not carry the copyright of another entity (as credited in the published version). If the credit line on any part of the material you have requested indicates that it was reprinted or adapted by NPG with permission from another source, then you should also seek permission from that source to reuse the material.

2. Permission granted free of charge for material in print is also usually granted for any electronic version of that work, provided that the material is incidental to the work as a whole and that the electronic version is essentially equivalent to, or substitutes for, the print version.Where print permission has been granted for a fee, separate permission must be obtained for any additional, electronic re-use (unless, as in the case of a full paper, this has already been accounted for during your initial request in the calculation of a print run).NB: In all cases, web-based use of full-text articles must be authorized separately through the 'Use on a Web Site' option when requesting permission.

3. Permission granted for a first edition does not apply to second and subsequent editions and for editions in other languages (except for signatories to the STM Permissions Guidelines, or where the first edition permission was granted for free).

4. Nature Publishing Group's permission must be acknowledged next to the figure, table or abstract in print. In electronic form, this acknowledgement must be visible at the same time as the figure/table/abstract, and must be hyperlinked to the journal's homepage.

5. The credit line should read:
   Reprinted by permission from Macmillan Publishers Ltd: [JOURNAL NAME] (reference citation), copyright (year of publication)
   For AOP papers, the credit line should read:
   Reprinted by permission from Macmillan Publishers Ltd: [JOURNAL NAME], advance online publication, day month year (doi: 10.1038/sj.[JOURNAL ACRONYM].XXXXX)

   Note: For republication from the *British Journal of Cancer,* the following credit lines apply.
   Reprinted by permission from Macmillan Publishers Ltd on behalf of Cancer Research UK: [JOURNAL NAME] (reference citation), copyright (year of publication)For AOP papers, the credit line should read:
   Reprinted by permission from Macmillan Publishers Ltd on behalf of Cancer Research UK: [JOURNAL NAME], advance online publication, day month year (doi: 10.1038/sj.[JOURNAL ACRONYM].XXXXX)

6. Adaptations of single figures do not require NPG approval. However, the adaptation should be credited as follows:

   Adapted by permission from Macmillan Publishers Ltd: [JOURNAL NAME] (reference citation), copyright (year of publication)

   Note: For adaptation from the *British Journal of Cancer,* the following credit line applies.
   Adapted by permission from Macmillan Publishers Ltd on behalf of Cancer Research UK: [JOURNAL NAME] (reference citation), copyright (year of publication)

7. Translations of 401 words up to a whole article require NPG approval. Please visit http://www.macmillanmedicalcommunications.com for more information.Translations of up

to a 400 words do not require NPG approval. The translation should be credited as follows:

Translated by permission from Macmillan Publishers Ltd: [JOURNAL NAME] (reference citation), copyright (year of publication).

Note: For translation from the *British Journal of Cancer,* the following credit line applies.
Translated by permission from Macmillan Publishers Ltd on behalf of Cancer Research UK: [JOURNAL NAME] (reference citation), copyright (year of publication)

We are certain that all parties will benefit from this agreement and wish you the best in the use of this material. Thank you.
Special Terms:
v1.1

REFERENCES

Acheson, N.H. (2011). Fundamentals of Molecular Virology, 2nd Edition (Wiley Global Education).

Adedeji, A.O., Marchand, B., Velthuis, te, A.J.W., Snijder, E.J., Weiss, S., Eoff, R.L., Singh, K., and Sarafianos, S.G. (2012). Mechanism of nucleic acid unwinding by SARS-CoV helicase. PLoS ONE *7*, e36521.

Almeida, J.D., Berry, D.M., Cunningham, C.H., Hamre, D., Hofstad, M.S., Mallucci, L., McIntosh, K., and Tyrrell, D.A.J. (1968). Coronaviruses. Nature *3*, NP–470.

Annamalai, T., Saif, L.J., Lu, Z., and Jung, K. (2015). Age-dependent variation in innate immune responses to porcine epidemic diarrhea virus infection in suckling versus weaned pigs. Veterinary Immunology and Immunopathology *168*, 193–202.

Azhar, E.I., El-Kafrawy, S.A., Farraj, S.A., Hassan, A.M., Al-Saeed, M.S., Hashem, A.M., and Madani, T.A. (2014). Evidence for Camel-to-Human Transmission of MERS Coronavirus. N Engl J Med *370*, 2499–2505.

Baker, M.L., Schountz, T., and Wang, L.-F. (2013). Antiviral immune responses of bats: a review. Zoonoses Public Health *60*, 104–116.

Barretto, N., Jukneliene, D., Ratia, K., Chen, Z., Mesecar, A.D., and Baker, S.C. (2005). The Papain-Like Protease of Severe Acute Respiratory Syndrome Coronavirus Has Deubiquitinating Activity. Journal of Virology *79*, 15189–15198.

Baum, A., and García-Sastre, A. (2009). Induction of type I interferon by RNA viruses: cellular receptors and their substrates. Amino Acids *38*, 1283–1299.

Becares, M., Pascual-Iglesias, A., Nogales, A., Sola, I., Enjuanes, L., and Zuñiga, S. (2016). Mutagenesis of Coronavirus nsp14 Reveals Its Potential Role in Modulation of the Innate Immune Response. Journal of Virology *90*, 5399–5414.

Becker, M.M., Graham, R.L., Donaldson, E.F., Rockx, B., Sims, A.C., Sheahan, T., Pickles, R.J., Corti, D., Johnston, R.E., Baric, R.S., et al. (2008). Synthetic recombinant bat SARS-like coronavirus is infectious in cultured cells and in mice. Proceedings of the National Academy of Sciences *105*, 19944–19949.

Birdwell, L.D., Zalinger, Z.B., Li, Y., Wright, P.W., Elliott, R., Rose, K.M., Silverman, R.H., and Weiss, S.R. (2016). Activation of RNase L by Murine Coronavirus in Myeloid Cells Is Dependent on Basal OasGene Expression and Independent of Virus-Induced Interferon. Journal of Virology *90*, 3160–3172.

Boonyaratanakornkit, J.B., Bartlett, E.J., Amaro-Carambot, E., Collins, P.L., Murphy, B.R., and Schmidt, A.C. (2009). The C proteins of human parainfluenza virus type 1 (HPIV1) control the

transcription of a broad array of cellular genes that would otherwise respond to HPIV1 infection. Journal of Virology *83*, 1892–1910.

Bouvet, M., Imbert, I., Subissi, L., Gluais, L., Canard, B., and Decroly, E. (2012). RNA 3'-end mismatch excision by the severe acute respiratory syndrome coronavirus nonstructural protein nsp10/nsp14 exoribonuclease complex. Proceedings of the National Academy of Sciences *109*, 9372–9377.

Bouvet, M., Debarnot, C., Imbert, I., Selisko, B., Snijder, E.J., Canard, B., and Decroly, E. (2010). In Vitro Reconstitution of SARS-Coronavirus mRNA Cap Methylation. PLoS Pathog *6*, e1000863.

Bradwell, K., Combe, M., Domingo-Calap, P., and Sanjuan, R. (2013). Correlation Between Mutation Rate and Genome Size in Riboviruses: Mutation Rate of Bacteriophage Q. Genetics *195*, 243–251.

Brierley, I., Boursnell, M.E., Binns, M.M., Bilimoria, B., Blok, V.C., Brown, T.D., and Inglis, S.C. (1987). An efficient ribosomal frame-shifting signal in the polymerase-encoding region of the coronavirus IBV. Embo J. *6*, 3779–3785.

Brubaker, S.W., Bonham, K.S., Zanoni, I., and Kagan, J.C. (2015). Innate Immune Pattern Recognition: A Cell Biological Perspective. Annu. Rev. Immunol. *33*, 257–290.

Calisher, C.H., Childs, J.E., Field, H.E., Holmes, K.V., and Schountz, T. (2006). Bats: important reservoir hosts of emerging viruses. Clin. Microbiol. Rev. *19*, 531–545.

Case, J.B., Ashbrook, A.W., Dermody, T.S., and Denison, M.R. (2016). Mutagenesis of S-Adenosyl-l-Methionine-Binding Residues in Coronavirus nsp14 N7-Methyltransferase Demonstrates Differing Requirements for Genome Translation and Resistance to Innate Immunity. Journal of Virology *90*, 7248–7256.

Case, J.B., Li, Y., Elliott, R., Lu, X., Graepel, K.W., Sexton, N.R., Smith, E.C., Weiss, S.R., and Denison, M.R. (2017). Murine hepatitis virus nsp14 exoribonuclease activity is required for resistance to innate immunity. Journal of Virology JVI.01531–17.

Cavanagh, D. (2007). Coronavirus avian infectious bronchitis virus. Vet. Res. *38*, 281–297.

Chan, K.H., Poon, L.L.L.M., Cheng, V.C.C., Guan, Y., Hung, I.F.N., Kong, J., Yam, L.Y.C., Seto, W.H., Yuen, K.Y., and Peiris, J.S.M. (2004). Detection of SARS Coronavirus in Patients with Suspected SARS. Emerg. Infect. Dis. *10*, 294–299.

Chen, W., and Baric, R.S. (1996). Molecular anatomy of mouse hepatitis virus persistence: coevolution of increased host cell resistance and virus virulence. Journal of Virology *70*, 3947–3960.

Chen, Y., Cai, H., Pan, J., Xiang, N., Tien, P., Ahola, T., and Guo, D. (2009). Functional screen reveals SARS coronavirus nonstructural protein nsp14 as a novel cap N7 methyltransferase. Proceedings of the National Academy of Sciences *106*, 3484–3489.

Chen, Y., Tao, J., Sun, Y., Wu, A., Su, C., Gao, G., Cai, H., Qiu, S., Wu, Y., Ahola, T., et al. (2013). Structure-Function Analysis of Severe Acute Respiratory Syndrome Coronavirus RNA Cap Guanine-N7-Methyltransferase. Journal of Virology *87*, 6296–6305.

Chen, Y., Su, C., Ke, M., Jin, X., Xu, L., Zhang, Z., Wu, A., Sun, Y., Yang, Z., Tien, P., et al. (2011). Biochemical and Structural Insights into the Mechanisms of SARS Coronavirus RNA Ribose 2′-O-Methylation by nsp16/nsp10 Protein Complex. PLoS Pathog *7*, e1002294.

Cheung, C.Y., Poon, L.L.M., Ng, I.H.Y., Luk, W., Sia, S.-F., Wu, M.H.S., Chan, K.-H., Yuen, K.-Y., Gordon, S., Guan, Y., et al. (2005). Cytokine responses in severe acute respiratory syndrome coronavirus-infected macrophages in vitro: possible relevance to pathogenesis. Journal of Virology *79*, 7819–7826.

Crossley, B., Mock, R., Callison, S., and Hietala, S. (2012). Identification and Characterization of a Novel Alpaca Respiratory Coronavirus Most Closely Related to the Human Coronavirus 229E. Viruses *4*, 3689–3700.

Daffis, S., Szretter, K.J., Schriewer, J., Li, J., Youn, S., Errett, J., Lin, T.-Y., Schneller, S., Züst, R., Dong, H., et al. (2010). 2′-O methylation of the viral mRNA cap evades host restriction by IFIT family members. Nature *468*, 452–456.

Darnell, J.E. (1979). Transcription units for mRNA production in eukaryotic cells and their DNA viruses. Progress in Nucleic Acid Research and Molecular Biology *22*, 327–353.

de Wit, E., van Doremalen, N., Falzarano, D., and Munster, V.J. (2016). SARS and MERS: recent insights into emerging coronaviruses. Nat Rev Micro *14*, 523–534.

Decroly, E., Debarnot, C., Ferron, F., Bouvet, M., Coutard, B., Imbert, I., Gluais, L., Papageorgiou, N., Sharff, A., Bricogne, G., et al. (2011a). Crystal Structure and Functional Analysis of the SARS-Coronavirus RNA Cap 2′-O-Methyltransferase nsp10/nsp16 Complex. PLoS Pathog *7*, e1002059.

Decroly, E., Ferron, F., Lescar, J., and Canard, B. (2011b). Conventional and unconventional mechanisms for capping viral mRNA. Nat Rev Micro *9*, 645–665.

Decroly, E., Imbert, I., Coutard, B., Bouvet, M., Selisko, B., Alvarez, K., Gorbalenya, A.E., Snijder, E.J., and Canard, B. (2008). Coronavirus nonstructural protein 16 is a cap-0 binding enzyme possessing (nucleoside-2'O)-methyltransferase activity. Journal of Virology *82*, 8071–8084.

Devaraj, S.G., Wang, N., Chen, Z., Chen, Z., Tseng, M., Barretto, N., Lin, R., Peters, C.J., Tseng, C.-T.K., Baker, S.C., et al. (2007). Regulation of IRF-3-dependent Innate Immunity by the Papain-like Protease Domain of the Severe Acute Respiratory Syndrome Coronavirus. J. Biol. Chem. *282*, 32208–32221.

Diamond, M.S., and Farzan, M. (2012). The broad-spectrum antiviral functions of IFIT and IFITM proteins. Nat Rev Immunol *13*, 46–57.

Dominguez, S.R., O'Shea, T.J., Oko, L.M., and Holmes, K.V. (2007). Detection of Group 1 Coronaviruses in Bats in North America. Emerg. Infect. Dis. *13*, 1295–1300.

Donaldson, E.F., Donaldson, E.F., Sims, A.C., Sims, A.C., Graham, R.L., Graham, R.L., Denison, M.R., Denison, M.R., Baric, R.S., and Baric, R.S. (2007). Murine Hepatitis Virus Replicase Protein nsp10 Is a Critical Regulator of Viral RNA Synthesis. Journal of Virology *81*, 6356–6368.

Drappier, M., and Michiels, T. (2015). Inhibition of the OAS/RNase L pathway by viruses. Current Opinion in Virology *15*, 19–26.

Drexler, J.F., Corman, V.M., and Drosten, C. (2014). Ecology, evolution and classification of bat coronaviruses in the aftermath of SARS. Antiviral Res. *101*, 45–56.

Drosten, C., Günther, S., Preiser, W., van der Werf, S., Brodt, H.-R., Becker, S., Rabenau, H., Panning, M., Kolesnikova, L., Fouchier, R.A.M., et al. (2003). Identification of a novel coronavirus in patients with severe acute respiratory syndrome. N. Engl. J. Med. *348*, 1967–1976.

Eckerle, L.D., Lu, X., Sperry, S.M., Choi, L., and Denison, M.R. (2007). High Fidelity of Murine Hepatitis Virus Replication Is Decreased in nsp14 Exoribonuclease Mutants. Journal of Virology *81*, 12135–12144.

Eckerle, L.D., Becker, M.M., Halpin, R.A., Li, K., Venter, E., Lu, X., Scherbakova, S., Graham, R.L., Baric, R.S., Stockwell, T.B., et al. (2010). Infidelity of SARS-CoV Nsp14-Exonuclease Mutant Virus Replication Is Revealed by Complete Genome Sequencing. PLoS Pathog *6*, e1000896.

Egloff, M.-P., Ferron, F., Campanacci, V., Longhi, S., Rancurel, C., Dutartre, H., Snijder, E.J., Gorbalenya, A.E., Cambillau, C., and Canard, B. (2004). The severe acute respiratory syndrome-coronavirus replicative protein nsp9 is a single-stranded RNA-binding subunit unique in the RNA virus world. Proceedings of the National Academy of Sciences *101*, 3792–3796.

Eigen, M. (1971). Selforganization of matter and the evolution of biological macromolecules. Die Naturwissenschaften *58*, 465–523.

Fernald, G.H., Knott, S., Pachner, A., Caillier, S.J., Narayan, K., Oksenberg, J.R., Mousavi, P., and Baranzini, S.E. (2007). Genome-wide network analysis reveals the global properties of IFN-beta immediate transcriptional effects in humans. J. Immunol. *178*, 5076–5085.

Filipowicz, W., Furuichi, Y., Sierra, J.M., Muthukrishnan, S., Shatkin, A.J., and Ochoa, S. (1976). A protein binding the methylated 5'-terminal sequence, m7GpppN, of eukaryotic messenger RNA. Proceedings of the National Academy of Sciences *73*, 1559–1563.

Fouchier, R.A.M., Hartwig, N.G., Bestebroer, T.M., Niemeyer, B., de Jong, J.C., Simon, J.H., and Osterhaus, A.D.M.E. (2004). A previously undescribed coronavirus associated with respiratory disease in humans. Proceedings of the National Academy of Sciences *101*, 6212–6216.

Freeman, M.C., Graham, R.L., Lu, X., Peek, C.T., and Denison, M.R. (2014). Coronavirus Replicase-Reporter Fusions Provide Quantitative Analysis of Replication and Replication Complex Formation. Journal of Virology *88*, 5319–5327.

Frieman, M., Heise, M., and Baric, R. (2008). SARS coronavirus and innate immunity. Virus Research *133*, 101–112.

Furuichi, Y., and Shatkin, A.J. (2000). Viral and cellular mRNA capping: past and prospects. Adv. Virus Res. *55*, 135–184.

Garbino, J., Crespo, S., Aubert, J.D., Rochat, T., Ninet, B., Deffernez, C., Wunderli, W., Pache, J.-C., Soccal, P.M., and Kaiser, L. (2006). A Prospective Hospital-Based Study of the Clinical Impact of Non–Severe Acute Respiratory Syndrome (Non-SARS)–Related Human Coronavirus Infection. Clin Infect Dis *43*, 1009–1015.

Ge, X.-Y., Li, J.-L., Yang, X.-L., Chmura, A.A., Zhu, G., Epstein, J.H., Mazet, J.K., Hu, B., Zhang, W., Peng, C., et al. (2013). Isolation and characterization of a bat SARS-like coronavirus that uses the ACE2 receptor. Nature *503*, 535–538.

Gebauer, F., Gebauer, F.A.T., and Hentze, M.W. (2004). Molecular mechanisms of translational control. Nat Rev Mol Cell Biol *5*, 827–835.

Gloza-Rausch, F., Ipsen, A., Seebens, A., Göttsche, M., Panning, M., Drexler, J.F., Petersen, N., Annan, A., Grywna, K., Müller, M., et al. (2008). Detection and Prevalence Patterns of Group I Coronaviruses in Bats, Northern Germany. Emerg. Infect. Dis. *14*, 626–631.

Gorbalenya, A.E., Enjuanes, L., Ziebuhr, J., and Snijder, E.J. (2006). Nidovirales: Evolving the largest RNA virus genome. Virus Research *117*, 17–37.

Graepel, K., Lu, X., Case, J.B., Sexton, N.R., Smith, E.C., and Denison, M.R. (2017). Proofreading-deficient coronaviruses adapt for increased fitness over long-term passage without reversion of exoribonuclease-inactivating mutations.

Graham, R.L., Becker, M.M., Eckerle, L.D., Bolles, M., Denison, M.R., and Baric, R.S. (2012). A live, impaired-fidelity coronavirus vaccine protects in an aged, immunocompromised mouse model of lethal disease. Nat Med *18*, 1820–1826.

Grotthuss, von, M., Wyrwicz, L.S., and Rychlewski, L. (2003). mRNA cap-1 methyltransferase in the SARS genome. Cell *113*, 701–702.

Gu, J., and Korteweg, C. (2007). Pathology and pathogenesis of severe acute respiratory syndrome. Am. J. Pathol. *170*, 1136–1147.

Guan, Y., Zheng, B., He, Y., Liu, X., and Zhuang, Z. (2003). Isolation and characterization of viruses related to the SARS coronavirus from animals in southern China. Science *302*, 276–278.

Haagmans, B.L., Dhahiry, Al, S.H.S., Reusken, C.B.E.M., Raj, V.S., Galiano, M., Myers, R., Godeke, G.-J., Jonges, M., Farag, E., Diab, A., et al. (2014). Middle East respiratory syndrome

coronavirus in dromedary camels: an outbreak investigation. The Lancet Infectious Diseases *14*, 140–145.

Habjan, M., Hubel, P., Lacerda, L., Benda, C., Holze, C., Eberl, C.H., Mann, A., Kindler, E., Gil-Cruz, C., Ziebuhr, J., et al. (2013). Sequestration by IFIT1 Impairs Translation of 2′O-unmethylated Capped RNA. PLoS Pathog *9*, e1003663.

Hastie, K.M., Kimberlin, C.R., Zandonatti, M.A., MacRae, I.J., and Saphire, E.O. (2011). Structure of the Lassa virus nucleoprotein reveals a dsRNA-specific 3“ to 5” exonuclease activity essential for immune suppression. Proceedings of the National Academy of Sciences *108*, 2396–2401.

Hayashi, J., Stoyanova, R., and Seeger, C. (2005). The transcriptome of HCV replicon expressing cell lines in the presence of alpha interferon. Virology *335*, 264–275.

He, R., Leeson, A., Andonov, A., Li, Y., Bastien, N., Cao, J., Osiowy, C., Dobie, F., Cutts, T., Ballantine, M., et al. (2003). Activation of AP-1 signal transduction pathway by SARS coronavirus nucleocapsid protein. Biochemical and Biophysical Research Communications *311*, 870–876.

Hemida, M.G., Chu, D.K.W., Poon, L.L.M., Perera, R.A.P.M., Alhammadi, M.A., Ng, H.-Y., Siu, L.Y., Guan, Y., Alnaeem, A., and Peiris, M. (2014). MERS Coronavirus in Dromedary Camel Herd, Saudi Arabia. Emerg. Infect. Dis. *20*, 1231–1234.

Hemmila, E., Turbide, C., Olson, M., Jothy, S., Holmes, K.V., and Beauchemin, N. (2004). Ceacam1a-/- Mice Are Completely Resistant to Infection by Murine Coronavirus Mouse Hepatitis Virus A59. Journal of Virology *78*, 10156–10165.

Hornung, V., Ellegast, J., Kim, S., Brzozka, K., Jung, A., Kato, H., Poeck, H., Akira, S., Conzelmann, K.K., Schlee, M., et al. (2006). 5'-Triphosphate RNA Is the Ligand for RIG-I. Science *314*, 994–997.

Hrecka, K., Hao, C., Gierszewska, M., Swanson, S.K., Kesik-Brodacka, M., Srivastava, S., Florens, L., Washburn, M.P., and Skowronski, J. (2011). Vpx relieves inhibition of HIV-1 infection of macrophages mediated by the SAMHD1 protein. Nature *474*, 658–661.

Huynh, J., Huynh, J., Li, S., Li, S., Yount, B., Yount, B., Smith, A., Smith, A., Sturges, L., Sturges, L., et al. (2012). Evidence Supporting a Zoonotic Origin of Human Coronavirus Strain NL63. Journal of Virology *86*, 12816–12825.

Indraccolo, S., Pfeffer, U., Minuzzo, S., Esposito, G., Roni, V., Mandruzzato, S., Ferrari, N., Anfosso, L., Dell'Eva, R., Noonan, D.M., et al. (2007). Identification of genes selectively regulated by IFNs in endothelial cells. J. Immunol. *178*, 1122–1135.

Ivanov, K.A., Hertzig, T., Rozanov, M., Bayer, S., Thiel, V., Gorbalenya, A.E., and Ziebuhr, J. (2004a). Major genetic marker of nidoviruses encodes a replicative endoribonuclease. Proceedings of the National Academy of Sciences *101*, 12694–12699.

Ivanov, K.A., Thiel, V., Dobbe, J.C., van der Meer, Y., Snijder, E.J., and Ziebuhr, J. (2004b). Multiple enzymatic activities associated with severe acute respiratory syndrome coronavirus helicase. Journal of Virology *78*, 5619–5632.

Kamitani, W., Narayanan, K., Huang, C., Lokugamage, K., Ikegami, T., Ito, N., Kubo, H., and Makino, S. (2006). Severe acute respiratory syndrome coronavirus nsp1 protein suppresses host gene expression by promoting host mRNA degradation. Proceedings of the National Academy of Sciences *103*, 12885–12890.

Kanjanahaluethai, A., Chen, Z., Jukneliene, D., and Baker, S.C. (2007). Membrane topology of murine coronavirus replicase nonstructural protein 3. Virology *361*, 391–401.

Katze, M.G., He, Y., and Gale, M. (2002). Viruses and interferon: a fight for supremacy. Nat Rev Immunol *2*, 675–687.

Kindler, E., and Thiel, V. (2014). To sense or not to sense viral RNA--essentials of coronavirus innate immune evasion. Curr. Opin. Microbiol. *20*, 69–75.

Kindler, E., Gil-Cruz, C., Spanier, J., Li, Y., Wilhelm, J., Rabouw, H.H., Züst, R., Hwang, M., V'kovski, P., Stalder, H., et al. (2017). Early endonuclease-mediated evasion of RNA sensing ensures efficient coronavirus replication. PLoS Pathog *13*, e1006195.

Knoops, K., Kikkert, M., Worm, S.H.E.V.D., Zevenhoven-Dobbe, J.C., van der Meer, Y., Koster, A.J., Mommaas, A.M., and Snijder, E.J. (2008). SARS-Coronavirus Replication Is Supported by a Reticulovesicular Network of Modified Endoplasmic Reticulum. PLoS Biol *6*, e226.

Kopecky-Bromberg, S.A., Martinez-Sobrido, L., Frieman, M., Baric, R.A., and Palese, P. (2006). Severe Acute Respiratory Syndrome Coronavirus Open Reading Frame (ORF) 3b, ORF 6, and Nucleocapsid Proteins Function as Interferon Antagonists. Journal of Virology *81*, 548–557.

Ksiazek, T.G., Erdman, D., Goldsmith, C.S., Zaki, S.R., Peret, T., Emery, S., Tong, S., Urbani, C., Comer, J.A., Lim, W., et al. (2003). A Novel Coronavirus Associated with Severe Acute Respiratory Syndrome. N Engl J Med *348*, 1953–1966.

Lahouassa, H., Daddacha, W., Hofmann, H., Ayinde, D., Logue, E.C., Dragin, L., Bloch, N., Maudet, C., Bertrand, M., Gramberg, T., et al. (2012). SAMHD1 restricts the replication of human immunodeficiency virus type 1 by depleting the intracellular pool of deoxynucleoside triphosphates. Nat Immunol *13*, 223–228.

Lai, M.M., and Stohlman, S.A. (1981). Comparative analysis of RNA genomes of mouse hepatitis viruses. Journal of Virology *38*, 661–670.

Lai, M.M., Patton, C.D., and Stohlman, S.A. (1982). Further characterization of mRNA"s of mouse hepatitis virus: presence of common 5-"end nucleotides. Journal of Virology *41*, 557–565.

Lau, S.K.P., Woo, P.C.Y., Li, K.S.M., Huang, Y., Tsoi, H.W., Wong, B.H.L., Wong, S.S.Y.,

Leung, S.Y., Chan, K.H., and Yuen, K.Y. (2005). Severe acute respiratory syndrome coronavirus-like virus in Chinese horseshoe bats. Proceedings of the National Academy of Sciences *102*, 14040–14045.

Lauber, C., Goeman, J.J., Parquet, M.D.C., Nga, P.T., Thi Nga, P., Snijder, E.J., Morita, K., and Gorbalenya, A.E. (2013). The Footprint of Genome Architecture in the Largest Genome Expansion in RNA Viruses. PLoS Pathog *9*, e1003500.

Lehmann, K.C., Gulyaeva, A., Zevenhoven-Dobbe, J.C., Janssen, G.M.C., Ruben, M., Overkleeft, H.S., van Veelen, P.A., Samborskiy, D.V., Kravchenko, A.A., Leontovich, A.M., et al. (2015). Discovery of an essential nucleotidylating activity associated with a newly delineated conserved domain in the RNA polymerase-containing protein of all nidoviruses. Nucleic Acids Research *43*, 8416–8434.

Leibowitz, J., Kaufman, G., and Liu, P. (2011). Coronaviruses: Propagation, Quantification, Storage, and Construction of Recombinant Mouse Hepatitis Virus. Curr. Protoc. Mircrobiol. 21:15E.1.1-15E.1.46.

Li, J., Ding, S.C., Cho, H., Chung, B.C., Gale, M., Chanda, S.K., and Diamond, M.S. (2013). A short hairpin RNA screen of interferon-stimulated genes identifies a novel negative regulator of the cellular antiviral response. mBio *4*, e00385–13.

Li, J., Li, J., Fontaine-Rodriguez, E.C., Fontaine-Rodriguez, E.C., Whelan, S.P.J., and Whelan, S.P.J. (2005). Amino Acid Residues within Conserved Domain VI of the Vesicular Stomatitis Virus Large Polymerase Protein Essential for mRNA Cap Methyltransferase Activity. Journal of Virology *79*, 13373–13384.

Li, W. (2005). Bats Are Natural Reservoirs of SARS-Like Coronaviruses. Science *310*, 676–679.

Li, W., Moore, M.J., Vasilieva, N., Sui, J., Wong, S.K., Berne, M.A., Somasundaran, M., Sullivan, J.L., Luzuriaga, K., Greenough, T.C., et al. (2003). Angiotensin-converting enzyme 2 is a functional receptor for the SARS coronavirus. Nature *426*, 450–454.

Li, Y., Banerjee, S., Goldstein, S.A., Dong, B., Gaughan, C., Rath, S., Donovan, J., Korennykh, A., Silverman, R.H., and Weiss, S.R. (2017). Ribonuclease L mediates the cell-lethal phenotype of double-stranded RNA editing enzyme ADAR1 deficiency in a human cell line. Elife *6*, e25687.

Li, Y., Banerjee, S., Wang, Y., Goldstein, S.A., Dong, B., Gaughan, C., Silverman, R.H., and Weiss, S.R. (2016). Activation of RNase L is dependent on OAS3 expression during infection with diverse human viruses. Proceedings of the National Academy of Sciences *113*, 2241–2246.

Ma, Y., Wu, L., Shaw, N., Gao, Y., Wang, J., Sun, Y., Lou, Z., Yan, L., Zhang, R., and Rao, Z. (2015). Structural basis and functional analysis of the SARS coronavirus nsp14–nsp10 complex. Proceedings of the National Academy of Sciences *112*, 9436–9441.

Malathi, K., Dong, B., Gale, M., and Silverman, R.H. (2007). Small self-RNA generated by RNase L amplifies antiviral innate immunity. Nature *448*, 816–819.

Mannion, N.M., Greenwood, S.M., Young, R., Cox, S., Brindle, J., Read, D., Nellåker, C., Vesely, C., Ponting, C.P., McLaughlin, P.J., et al. (2014). The RNA-Editing Enzyme ADAR1 Controls Innate Immune Responses to RNA. Cell Reports *9*, 1482–1494.

Marcotrigiano, J., Gingras, A.-C., Sonenberg, N., and Burley, S.K. (1997). Cocrystal Structure of the Messenger RNA 5′ Cap-Binding Protein (eIF4E) Bound to 7-methyl-GDP. Cell *89*, 951–961.

Marcus, P.I., and Sekellick, M.J. (2001). Combined Sequential Treatment with Interferon and dsRNA Abrogates Virus Resistance to Interferon Action. Journal of Interferon & Cytokine Research *21*, 423–429.

Masters, P.S. (2006). The molecular biology of coronaviruses. Adv. Virus Res. *66*, 193–292.

Menachery, V.D., Yount, B.L., Josset, L., Gralinski, L.E., Scobey, T., Agnihothram, S., Katze, M.G., and Baric, R.S. (2014). Attenuation and Restoration of Severe Acute Respiratory Syndrome Coronavirus Mutant Lacking 2'-O-Methyltransferase Activity. Journal of Virology *88*, 4251–4264.

Minskaia, E., Hertzig, T., Gorbalenya, A.E., Campanacci, V., Cambillau, C., Canard, B., and Ziebuhr, J. (2006). Discovery of an RNA virus 3“->5” exoribonuclease that is critically involved in coronavirus RNA synthesis. Proceedings of the National Academy of Sciences *103*, 5108–5113.

Müller, M.A., Corman, V.M., Jores, J., Meyer, B., Younan, M., Liljander, A., Bosch, B.J., Lattwein, E., Hilali, M., Musa, B.E., et al. (2014). MERS Coronavirus Neutralizing Antibodies in Camels, Eastern Africa, 1983–1997. Emerg. Infect. Dis. *20*, 2093–2095.

Neil, S., and Bieniasz, P. (2009). Human Immunodeficiency Virus, Restriction Factors, and Interferon. Journal of Interferon & Cytokine Research *29*, 569–580.

Oostra, M., Lintelo, te, E.G., Deijs, M., Verheije, M.H., Rottier, P.J.M., and de Haan, C.A.M. (2007). Localization and Membrane Topology of Coronavirus Nonstructural Protein 4: Involvement of the Early Secretory Pathway in Replication. Journal of Virology *81*, 12323–12336.

Peiris, J.S.M., Yuen, K.Y., Osterhaus, A.D.M.E., and Stöhr, K. (2003). The Severe Acute Respiratory Syndrome. N Engl J Med *349*, 2431–2441.

Perlman, S., and Netland, J. (2009). Coronaviruses post-SARS: update on replication and pathogenesis. Nat Rev Micro *7*, 439–450.

Pfeffer, L.M., Kim, J.-G., Pfeffer, S.R., Carrigan, D.J., Baker, D.P., Wei, L., and Homayouni, R. (2004). Role of nuclear factor-kappaB in the antiviral action of interferon and interferon-regulated gene expression. J. Biol. Chem. *279*, 31304–31311.

Pfefferle, S., Oppong, S., Drexler, J.F., Gloza-Rausch, F., Ipsen, A., Seebens, A., Müller, M.A., Annan, A., Vallo, P., Adu-Sarkodie, Y., et al. (2009). Distant Relatives of Severe Acute Respiratory Syndrome Coronavirus and Close Relatives of Human Coronavirus 229E in Bats,

Ghana. Emerg. Infect. Dis. *15*, 1377–1384.

Piontkivska, H., Frederick, M., Miyamoto, M.M., and Wayne, M.L. (2017). RNA editing by the host ADAR system affects the molecular evolution of the Zika virus. Ecology and Evolution *7*, 4475–4485.

Plant, E.P., Pérez-Alvarado, G.C., Jacobs, J.L., Mukhopadhyay, B., Hennig, M., and Dinman, J.D. (2005). A Three-Stemmed mRNA Pseudoknot in the SARS Coronavirus Frameshift Signal. PLoS Biol *3*, e172.

Qi, X., Lan, S., Wang, W., Schelde, L.M., Dong, H., Wallat, G.D., Ly, H., Liang, Y., and Dong, C. (2010). Cap binding and immune evasion revealed by Lassa nucleoprotein structure. Nature *468*, 779–783.

Raj, V.S., Farag, E.A.B.A., Reusken, C.B.E.M., Lamers, M.M., Pas, S.D., Voermans, J., Smits, S.L., Osterhaus, A.D.M.E., Al-Mawlawi, N., Al-Romaihi, H.E., et al. (2014). Isolation of MERS Coronavirus from a Dromedary Camel, Qatar, 2014. Emerg. Infect. Dis. *20*, 1339–1342.

Raj, V.S., Mou, H., Smits, S.L., Dekkers, D.H.W., Müller, M.A., Dijkman, R., Muth, D., Demmers, J.A.A., Zaki, A., Fouchier, R.A.M., et al. (2013). Dipeptidyl peptidase 4 is a functional receptor for the emerging human coronavirus-EMC. Nature *495*, 251–254.

Ren, W., Qu, X., Li, W., Han, Z., Yu, M., Zhou, P., Zhang, S.Y., Wang, L.-F., Deng, H., and Shi, Z. (2008). Difference in Receptor Usage between Severe Acute Respiratory Syndrome (SARS) Coronavirus and SARS-Like Coronavirus of Bat Origin. Journal of Virology *82*, 1899–1907.

Reusken, C.B.E.M., Haagmans, B.L., Müller, M.A., Gutierrez, C., Godeke, G.-J., Meyer, B., Muth, D., Raj, V.S., Smits-De Vries, L., Corman, V.M., et al. (2013). Middle East respiratory syndrome coronavirus neutralising serum antibodies in dromedary camels: a comparative serological study. The Lancet Infectious Diseases *13*, 859–866.

Rose, K.M., Rose, K.M., Elliott, R., Elliott, R., Martínez-Sobrido, L., Martinez-Sobrido, L., Garcia-Sastre, A., García-Sastre, A., Weiss, S.R., and Weiss, S.R. (2010). Murine Coronavirus Delays Expression of a Subset of Interferon-Stimulated Genes. Journal of Virology *84*, 5656–5669.

Rose, K.M., and Weiss, S.R. (2009). Murine Coronavirus Cell Type Dependent Interaction with the Type I Interferon Response. Viruses *1*, 689–712.

Roth-Cross, J.K., Martinez-Sobrido, L., Scott, E.P., Garcia-Sastre, A., and Weiss, S.R. (2007). Inhibition of the Alpha/Beta Interferon Response by Mouse Hepatitis Virus at Multiple Levels. Journal of Virology *81*, 7189–7199.

Russier, M., Reynard, S., Carnec, X., and Baize, S. (2014). The Exonuclease Domain of Lassa Virus Nucleoprotein Is Involved in Antigen-Presenting-Cell-Mediated NK Cell Responses. Journal of Virology *88*, 13811–13820.

Saif, L.J. (2010). Bovine Respiratory Coronavirus. Veterinary Clinics of North America: Food Animal Practice *26*, 349–364.

Samuel, C.E. (2011). Adenosine deaminases acting on RNA (ADARs) are both antiviral and proviral. Virology *411*, 180–193.

Sanjuan, R., Nebot, M.R., Chirico, N., Mansky, L.M., and Belshaw, R. (2010). Viral Mutation Rates. Journal of Virology *84*, 9733–9748.

Sanjuán, R., and Domingo-Calap, P. (2016). Mechanisms of viral mutation. Cell. Mol. Life Sci. *73*, 4433–4448.

Sawicki, S.G., and Sawicki, D.L. (1998). A new model for coronavirus transcription. Adv. Exp. Med. Biol. *440*, 215–219.

Sawicki, S.G., and Sawicki, D.L. (2005). Coronavirus transcription: a perspective. Current Topics in Microbiology and Immunology *287*, 31–55.

Schibler, U., and Perry, R.P. (1977). The 5′-termini of heterogeneous nuclear RNA: a comparison among molecules of different sizes and ages. Nucleic Acids Research *4*, 4133–4150.

Schneider, W.M., Chevillotte, M.D., and Rice, C.M. (2014). Interferon-Stimulated Genes: A Complex Web of Host Defenses. Annu. Rev. Immunol. *32*, 513–545.

Schoggins, J.W., MacDuff, D.A., Imanaka, N., Gainey, M.D., Shrestha, B., Eitson, J.L., Mar, K.B., Richardson, R.B., Ratushny, A.V., Litvak, V., et al. (2014). Pan-viral specificity of IFN-induced genes reveals new roles for cGAS in innate immunity. Nature *505*, 691–695.

Schoggins, J.W., Wilson, S.J., Panis, M., Murphy, M.Y., Jones, C.T., Bieniasz, P., and Rice, C.M. (2011). A diverse range of gene products are effectors of the type I interferon antiviral response. Nature *472*, 481–485.

Sexton, N.R., Smith, E.C., Blanc, H., Vignuzzi, M., Peersen, O.B., and Denison, M.R. (2016). Homology-Based Identification of a Mutation in the Coronavirus RNA-Dependent RNA Polymerase That Confers Resistance to Multiple Mutagens. Journal of Virology *90*, 7415–7428.

Shatkin, A.J. (1976). Capping of eucaryotic mRNAs. Cell *9*, 645–653.

Silverman, R.H. (2007). Viral Encounters with 2“,5-”Oligoadenylate Synthetase and RNase L during the Interferon Antiviral Response. Journal of Virology *81*, 12720–12729.

Smith, E.C., and Denison, M.R. (2012). Implications of altered replication fidelity on the evolution and pathogenesis of coronaviruses. Current Opinion in Virology *2*, 519–524.

Smith, E.C., and Denison, M.R. (2013). Coronaviruses as DNA wannabes: a new model for the regulation of RNA virus replication fidelity. PLoS Pathog *9*, e1003760.

Smith, E.C., Blanc, H., Vignuzzi, M., and Denison, M.R. (2013). Coronaviruses Lacking

Exoribonuclease Activity Are Susceptible to Lethal Mutagenesis: Evidence for Proofreading and Potential Therapeutics. PLoS Pathog *9*, e1003565.

Smith, E.C., Case, J.B., Blanc, H., Isakov, O., Shomron, N., Vignuzzi, M., and Denison, M.R. (2015). Mutations in Coronavirus Nonstructural Protein 10 Decrease Virus Replication Fidelity. Journal of Virology *89*, 6418–6426.

Smith, E.C., Sexton, N.R., and Denison, M.R. (2014). Thinking Outside the Triangle: Replication Fidelity of the Largest RNA Viruses. Annu. Rev. Virol. *1*, 111–132.

Snijder, E.J., van der Meer, Y., Zevenhoven-Dobbe, J., Onderwater, J.J.M., van der Meulen, J., Koerten, H.K., and Mommaas, A.M. (2006). Ultrastructure and Origin of Membrane Vesicles Associated with the Severe Acute Respiratory Syndrome Coronavirus Replication Complex. Journal of Virology *80*, 5927–5940.

Snijder, E.J., Bredenbeek, P.J., Dobbe, J.C., Thiel, V., Ziebuhr, J., Poon, L.L.M., Guan, Y., Rozanov, M., Spaan, W.J.M., and Gorbalenya, A.E. (2003). Unique and conserved features of genome and proteome of SARS-coronavirus, an early split-off from the coronavirus group 2 lineage. Journal of Molecular Biology *331*, 991–1004.

Subissi, L., Posthuma, C.C., Collet, A., Zevenhoven-Dobbe, J.C., Gorbalenya, A.E., Decroly, E., Snijder, E.J., Canard, B., and Imbert, I. (2014). One severe acute respiratory syndrome coronavirus protein complex integrates processive RNA polymerase and exonuclease activities. Proc. Natl. Acad. Sci. U.S.a. *111*, E3900–E3909.

Sun, J., Wei, Y., Rauf, A., Zhang, Y., Ma, Y., Zhang, X., Shilo, K., Yu, Q., Saif, Y.M., Lu, X., et al. (2014). Methyltransferase-defective avian metapneumovirus vaccines provide complete protection against challenge with the homologous Colorado strain and the heterologous Minnesota strain. Journal of Virology *88*, 12348–12363.

Tomaselli, S., Galeano, F., Locatelli, F., and Gallo, A. (2015). ADARs and the Balance Game between Virus Infection and Innate Immune Cell Response. Current Issues in Molecular Biology *17*, 37–51.

Tong, S., Conrardy, C., Ruone, S., Kuzmin, I.V., Guo, X., Tao, Y., Niezgoda, M., Haynes, L., Agwanda, B., Breiman, R.F., et al. (2009). Detection of Novel SARS-like and Other Coronaviruses in Bats from Kenya. Emerg. Infect. Dis. *15*, 482–485.

van der Hoek, L., Pyrc, K., Jebbink, M.F., Vermeulen-Oost, W., Berkhout, R.J.M., Wolthers, K.C., Wertheim-van Dillen, P.M.E., Kaandorp, J., Spaargaren, J., and Berkhout, B. (2004). Identification of a new human coronavirus. Nat Med *10*, 368–373.

Velthuis, te, A.J.W., van den Worm, S.H.E., and Snijder, E.J. (2011). The SARS-coronavirus nsp7+nsp8 complex is a unique multimeric RNA polymerase capable of both de novo initiation and primer extension. Nucleic Acids Research *40*, 1737–1747.

Vijgen, L., Keyaerts, E., Moes, E., Thoelen, I., Wollants, E., Lemey, P., Vandamme, A.M., and Van Ranst, M. (2005). Complete Genomic Sequence of Human Coronavirus OC43: Molecular

Clock Analysis Suggests a Relatively Recent Zoonotic Coronavirus Transmission Event. Journal of Virology *79*, 1595–1604.

Wang, L.-F., Shi, Z., Zhang, S., Field, H., Daszak, P., and Eaton, B. (2006). Review of Bats and SARS. Emerg. Infect. Dis. *12*, 1834–1840.

Wei, C.M., Gershowitz, A., and Moss, B. (1975). Methylated nucleotides block 5' terminus of HeLa cell messenger RNA. Cell *4*, 379–386.

Woo, P.C.Y., Lau, S.K.P., Chu, C.M., Chan, K.H., Tsoi, H.W., Huang, Y., Wong, B.H.L., Poon, R.W.S., Cai, J.J., Luk, W.K., et al. (2004). Characterization and Complete Genome Sequence of a Novel Coronavirus, Coronavirus HKU1, from Patients with Pneumonia. Journal of Virology *79*, 884–895.

Woo, P.C.Y., Wang, M., Lau, S.K.P., Xu, H., Poon, R.W.S., Guo, R., Wong, B.H.L., Gao, K., Tsoi, H.W., Huang, Y., et al. (2007). Comparative Analysis of Twelve Genomes of Three Novel Group 2c and Group 2d Coronaviruses Reveals Unique Group and Subgroup Features. Journal of Virology *81*, 1574–1585.

Xiao, Y., Dolan, P.T., Goldstein, E.F., Li, M., Farkov, M., Brodsky, L., and Andino, R. (2017). Poliovirus intrahost evolution is required to overcome tissue-specific innate immune responses. Nature Communications *8*, 375.

Ye, Y., Hauns, K., Langland, J.O., Jacobs, B.L., and Hogue, B.G. (2007). Mouse Hepatitis Coronavirus A59 Nucleocapsid Protein Is a Type I Interferon Antagonist. Journal of Virology *81*, 2554–2563.

Yount, B., Denison, M.R., Weiss, S.R., and Baric, R.S. (2002). Systematic Assembly of a Full-Length Infectious cDNA of Mouse Hepatitis Virus Strain A59. Journal of Virology *76*, 11065–11078.

Zaki, A., and van Boheemen, S. (2012). Isolation of a novel coronavirus from a man with pneumonia in Saudi Arabia. N Engl J Med *367*, 1814-1820.

Zhai, Y., Sun, F., Li, X., Pang, H., Xu, X., Bartlam, M., and Rao, Z. (2005). Insights into SARS-CoV transcription and replication from the structure of the nsp7–nsp8 hexadecamer. Nat Struct Mol Biol *12*, 980–986.

Zhang, G., Cowled, C., Shi, Z., Huang, Z., Bishop-Lilly, K.A., Fang, X., Wynne, J.W., Xiong, Z., Baker, M.L., Zhao, W., et al. (2013). Comparative analysis of bat genomes provides insight into the evolution of flight and immunity. Science *339*, 456–460.

Zhang, R., Li, Y., Cowley, T.J., Steinbrenner, A.D., Phillips, J.M., Yount, B.L., Baric, R.S., and Weiss, S.R. (2015). The nsp1, nsp13, and M Proteins Contribute to the Hepatotropism of Murine Coronavirus JHM.WU. Journal of Virology *89*, 3598–3609.

Zhao, H., Lin, W., and Chung, R.T. (2012a). A functional genomic screen reveals novel host genes that mediate interferon-alpha's effects against hepatitis C virus. Journal of Hepatology *56*,

326–333.

Zhao, L., Birdwell, L.D., Wu, A., Elliott, R., Rose, K.M., Phillips, J.M., Li, Y., Grinspan, J., Silverman, R.H., and Weiss, S.R. (2013). Cell-Type-Specific Activation of the Oligoadenylate Synthetase-RNase L Pathway by a Murine Coronavirus. Journal of Virology *87*, 8408–8418.

Zhao, L., Jha, B.K., Wu, A., Elliott, R., Ziebuhr, J., Gorbalenya, A.E., Silverman, R.H., and Weiss, S.R. (2012b). Antagonism of the Interferon-Induced OAS-RNase L Pathway by Murine Coronavirus ns2 Protein Is Required for Virus Replication and Liver Pathology. Cell Host & Microbe *11*, 607–616.

Zhao, L., Zhao, L., Rose, K.M., Rose, K.M., Elliott, R., Elliott, R., Van Rooijen, N., Van Rooijen, N., Weiss, S.R., and Weiss, S.R. (2011). Cell-Type-Specific Type I Interferon Antagonism Influences Organ Tropism of Murine Coronavirus. Journal of Virology *85*, 10058–10068.

Zhou, P., Tachedjian, M., Wynne, J.W., Boyd, V., Cui, J., Smith, I., Cowled, C., Ng, J.H.J., Mok, L., Michalski, W.P., et al. (2016). Contraction of the type I IFN locus and unusual constitutive expression of IFN-αin bats. Proceedings of the National Academy of Sciences *113*, 2696–2701.

Züst, R., Cervantes-Barragan, L., Habjan, M., Maier, R., Neuman, B.W., Ziebuhr, J., Szretter, K.J., Baker, S.C., Barchet, W., Diamond, M.S., et al. (2011). Ribose 2′-O-methylation provides a molecular signature for the distinction of self and non-self mRNA dependent on the RNA sensor Mda5. Nat Immunol *12*, 137–143.

(2017a). WHO | Middle East respiratory syndrome coronavirus (MERS-CoV). Who. http://www.who.int/mediacentre/factsheets/mers-cov/en/

(2017b). WHO | Middle East respiratory syndrome coronavirus (MERS-CoV) – Saudi Arabia. Who. http://www.who.int/csr/don/17-august-2017-mers-saudi-arabia/en/